Universitat Autònoma de Barcelona

Quantum transport with Bohmian mechanics: application to graphene devices

Enrique Colomés Capón

Universidad Autònoma de Barcelona
Departamento de Ingeniería Electrónica

Doctoral Thesis in Electrical Engineering

and Telecommunications, 2018

Quantum transport with Bohmian mechanics: application to graphene devices

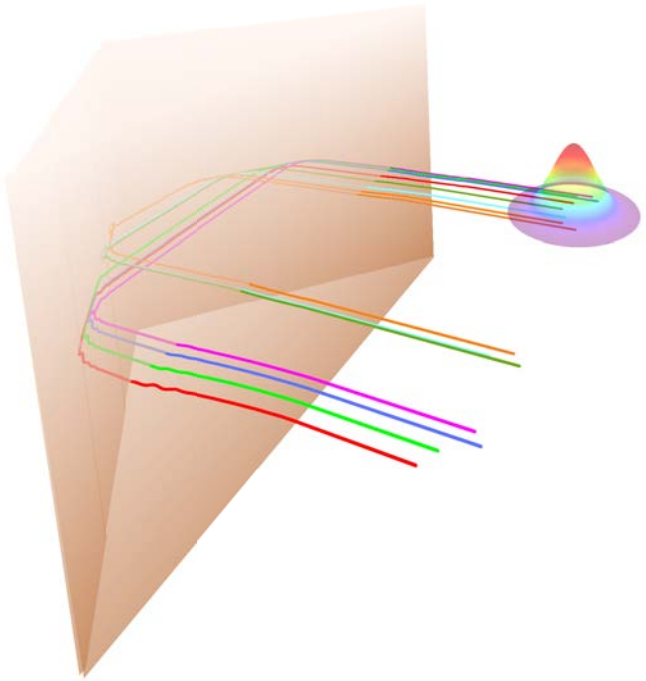

Author: Enrique Colomés Capón *Supervisor:* Prof. Xavier Oriols Pladevall

Quantum transport with Bohmian mechanics: application to graphene devices

Abstract:

Moore's law has been the milestone for electronics improvement, and the cause for the exponential growth in our computational abilities and for reaching nanoscale electron devices. At such dimensions, classical simulation tools must be substituted by quantum ones. Such substitution implies to tackle new fundamental problems. First, the many-body problem makes (almost) impossible the exact simulation of many particles scenarios. Second, the measurement problem is especially relevant in high-frequency scenarios where multi-time measurements are mandatory.

Alternatively to the orthodox theory, Bohmian mechanics emerges as a quantum theory which is specially well-equipped for the simulation of high-frequency characteristic of quantum electron devices. The Bohmian theory provides the conditional wave function that guides particles with well-defined positions.

In this thesis, I explored quantum transport using Bohmian mechanics, putting special emphasis to graphene, a 2D material with linear bandstructure, which is expected to play an important role in the next future electronics. Differently from other materials, graphene obeys the bispinor Dirac equation, electrons behave as massless particles, exhibiting exotic behaviors, such as the Klein Tunneling effect.

During the thesis, the quantum BITLLES simulator has been improved to correctly model electron nanodevices with either linear (by the inclusion of the complex bispinor Dirac equation) or parabolic bandstructures in either ballistic or dissipative (by the inclusion of the complete positive Bohmian scattering approach) systems. Thus, the BITLLES has become the candidate for substituting the versatile semiclassical Monte Carlo approach in the quantum regime, while keeping the versatility to predict DC, AC and noise performances.

As practical applications, during the thesis, unexpected scattering probabilities in a Hong-Ou-Mandel experiment were predicted. In addition, different current-voltage characteristics were analyzed. Finally, a new limit (due to the discrete nature of charge) for ultra-small logic applications working at THz frequencies was predicted.

Transporte cuántico con mecánica Bohmiana: aplicación a dispositivos de grafeno

Resumen: La ley de Moore ha sido una piedra fundamental en la mejora de la electónica y la causa del aumento de nuestra capacidad computacional y de la existencia de la electónica. En estas dimensiones, herramientas de simulación clásica deben ser sustituidas por cuánticas. Dicha substitución implica enfrentarse a nuevos problemas fundamentales. Primero, el problema de muchos cuerpos imposibilita la exacta simulación de sistemas con muchas partículas. Por otra parte, el problema de la medida, que es especialmente relevante en escenarios de alta frequencia donde se debe medir muchas veces.

Alternativamente a la teoría ortodoxa, la mecánica cuántica Bohmiana emerge como una teoría cuántica especialmente bien equipada para simular parámetros de alta frecuencia en dispositivos electrónicos cuánticos, gracias a la función de onda condicional que guía a las partículas con posiciones bien definidas.

En esta tesis, el transporte cuántico fue explorado bajo la mecánica cuántica Bohmiana, poniendo especial atención en grafeno, un novedoso material con estructura de bandas lineal, del que se espera que ocupe una posición central en el futuro próximo de la electrónica. Difiere de otros materiales en que obedece la ecuación biespinor de Dirac y el electrón se comporta entonces como una partícula sin masa, exhibiendo efectos como el Klein tunneling.

Durante la tesis, el simulador cuántico BITLLES fue mejorado y ahora es capaz de simular correctamente nanodispositivos con materials de banda parabólica o linear (gracias a la inclusión de la ecuación de Dirac) en sistemas balísticos o con disipación (gracias a la inclusión del método completamente positivo de scattering Bohmiano). Por tanto, el BITLLES se ha convertido en un excelente candidato a ocupar el lugar del versátil método Monte Carlo en el régimen cuántico, manteniendo su versatibilidad para calcular parámetros de DC, AC y ruido.

Como aplicaciones prácticas, durante la tesis se predijeron probabilidades (no esperadas) de encontrar dos electrones en el mismo lugar. También se obtuvieron curvas IV en diferentes escenarios. Finalmente, se encontró un nuevo límite (debido a la naturaleza discreta de los electrones) para nanodispositivos para aplicaciones lógicas trabajando a altas frecuencias.

Dedicado a mis abuelos y a Soledad.

"Conquistadors of the useless"

Lionel Terray

Acknowledgments

¡Gracias! Thanks! Merci! Eso es lo que tendría que decirle a tanta gente por haberme acompañado durante esta aventura que es el doctorado que no se ni cómo empezar.

En primer lugar, a mi supervisor Xavier Oriols. Sin él, esta tesis simplemene no existiría. Gracias por contagiarme toda esa pasión que emanas. Agradezco infinitimente, que dentro de este gran espacio de configuración, mi "time-dependent trajectory" me haya hecho pasar tanto tiempo discutiendo en tu despacho. No he acabado y ya hecho de menos esos momentos.

También agradecer a todas las personas de la universidad que han llenado estos años de buenos recuerdos. Gracias Pol por todo el tiempo compartido. Gracias Yepes por esas innumerables sesiones de gym y las tardías comidas. Finalmente, gracias Damiano por todas tus enseñanzas iniciales Bohmianas en casa y todos los años vividos juntos.

Quiero dar las gracias a todos los amigos de Barcelona, a toda la Résistance, especialmente a Sergio. También a Alberto y su familia por poder contar siempre con ellos. Mención aparte merece Samira, que me ha soportado a diario durante cuatro años sin hartarse de mi, así como al resto de compañeros de piso.

Quiero dar las gracias a mi familia. Mis padres (Enrique y Carmen María) simplemente me lo han dado todo, siempre me dejásteis claro que no existen límites. También me dieron la cosa de la que más orgullosa estoy en mi vida, mi hermana Carmen. Gracias por todo enana, eres genial.

Gracias a mi otra familia (Bartos), y es que esté donde esté, nunca me siento sólo. Sois una fuente de fuerza e inspiración todos y cada uno de vosotros. Gracias por hacerme mejor persona.

Finalmente, gracias a todos los compañeros de cordada y traveseros (VOC included). Muchas horas (y penurias) he compartido con vosotros. Sin más de uno esta tesis tampoco existiría.

Contents

Part I

PART ONE: INTRODUCTION

Chapter 1

Introduction to electron devices

This first Chapter is dedicated to introduce electronics and which are the challenges for new generation of devices. In this framework, trustful quantum simulators are needed to model the new physics and effects that the new generation electron devices require. I will focus on the simulation techniques developed until now, which are their requirements to successfully model electron transport and which are their mathematical formalisms.

1.1 Electronics history

Electronics is the field in science that studies the flow of electrons in different materials (gases, semiconductors, metals, etc.). It can be discussed when electronics was born as a scientific discipline, but probably we can talk about the last years of the 19^{th} century, since many relevant events occurred. For instance, in 1883 Edison observed for the first time the thermionic emission, named later "Edison effect"). He has different experimental lamp bulbs, which have a filament as well as a metal plate inside the bulb. He observed a certain blackening of the light bulbs. He was trying to understand this phenomenon when he realized that, as soon as he applied a negative potential relative to the filament in the metal plate -which acted as an electrode, a metallic material with free electrons inside- there was not flow of current[1], while current was able to flow when it was positive. This was the first milestone to create a diode. Another relevant fact happened in 1897, when Thomson showed that cathode rays were composed by a negatively charged particle, named *electron*[2]. Later, in 1904, Fleming improved Edison's set-up and applied the thermionic emission to create the first vacuum diode. Next, De Forest improved Fleming's original invention by creating the triode with an additional

[1] At that time, electrons were not called as such.

[2] In fact, the name electron (*elecktron*) was first used by the Greeks to refer to amber, which acquires the property of attracting other objects when rubbed. This process is called *frictional electrification*.

third terminal, the grid. So, the flux of electrons from the filament to the electrode was controlled by the voltage applied in the grid [1]. A particular voltage was used to define an *On* state with a net current through the triode and another voltage for the *Off* state without current.

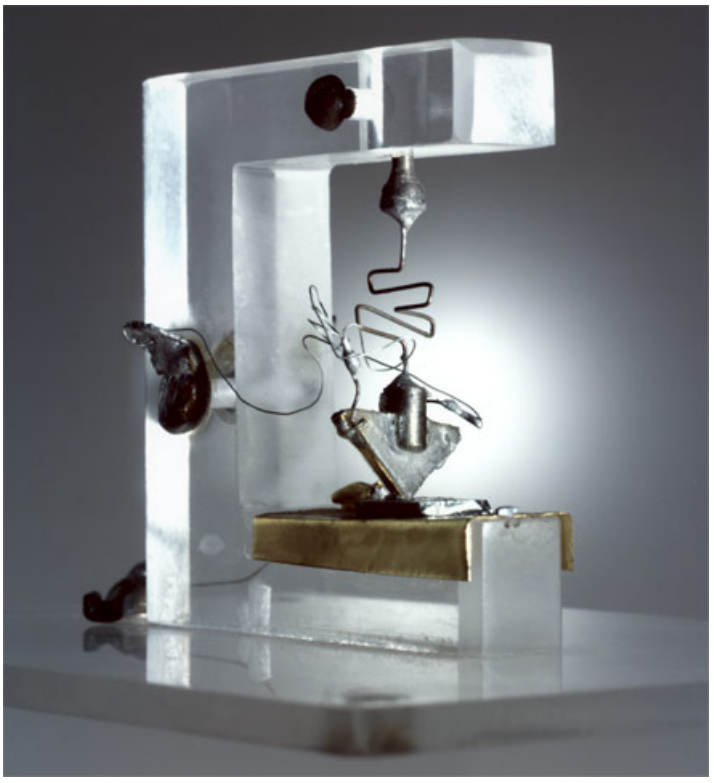

FIGURE 1.1: Replica of the first transistor designed in the Bell labs by Bardeen, Brattain and Shockley in 1947.

Definitively, electronics was born with the diode and triode vacuum tubes, and during half a century spectacular electronic applications were developed. However, the appearance of Alan Turing computation required more powerful and smaller electronic devices. The short life and high power consumption of the vacuum tubes made the Bell laboratories establish a research group focused on investigating the possibility of using semiconductor solid-state electron devices. In 1947, Bardeen, Brattain and Shockley created the first solid-state transistor at Bell laboratories[3]. Although the functionality of the solid-state transistor was quite similar to that of the triode, the former was much smaller, faster, cheaper and more reliable. Thus, it became the fundamental element of the electronic technology in the second half of the 20^{th} century. In the 60's, the previous solid-state transistor was improved by using a Metal-Oxide-Semiconductor (MOS) solid-state capacitor. A third terminal, the (metal) gate, separated from the (semiconductor)

[3]In fact, they all three jointly shared the Nobel Prize in Physics in 1956 for this discovery.

channel by an (oxide) dielectric, controlled the *On* and *Off* states of the transistor by means of a simple electrostatic force between gate and channel electrons. Because of the importance of the electric field in defining the behaviour of such MOS transistor, it was also called Field-Effect-Transistor (FET)[4]. For years, transistor improvements occurred but without any fundamental modification.

Regarding the improvement of transistors, in 1965 Gordon E. Moore stated that: "The complexity for minimum component costs has increased at a rate of roughly a factor of two per year. Certainly over the short term this rate can be expected to continue, if not to increase. Over the longer term, the rate of increase is a bit more uncertain, although there is no reason to believe it will not remain nearly constant for at least 10 years.". The truth is that this statement, known as "Moore's law" has been fulfilled until now (see Figure 1.2), and it is the milestone of electronics improvement and the cause for the exponential growth in our computational abilities.

In the recent years, however, the future perspectives have changed and the miniaturization of electronic devices has reached the quantum regime. For that reason a different strategy should be followed. The ITRS (International Technology Roadmap for Semiconductors [2]) established in 2013 that, until 2022, the best strategy was the so called "more Moore" domain, which consists in a trade-off between the traditional CMOS scaling and the introduction of new technological solutions (such as high-κ dielectric, multiple gate transistors, strained silicon, metal gates, etc.). Notwithstanding, after 2022 Moore's law would require 4 nm channel length transistors, that in principle will be technologically and economically unattainable. The scientific community is also searching for completely different alternatives to CMOS valid after this year, something which is known as "Beyond CMOS". In 2017, the ITRS morphed to the IRDS (International Roadmap of Devices and Systems [3]). It emphasizes the necessity of "more Moore" and "Beyond CMOS".

In this sense, the "Beyond CMOS" domain explores emerging devices based on different physical principles (spintronics, resonant tunnelling, band-to-band tunnelling, single-electron, etc.) and on different materials (graphene, MoS_2, etc.), which should improve the power consumption, the performance and the scaling of current transistors. Although it is unclear if any of these proposals may replace the conventional silicon MOSFET, what is unquestionable is that a proper treatment of the quantum phenomena is a mandatory requirement to understand them, i.e., accounting for the particles wave

[4]It was also named MOSFET by combining both previous acronyms.

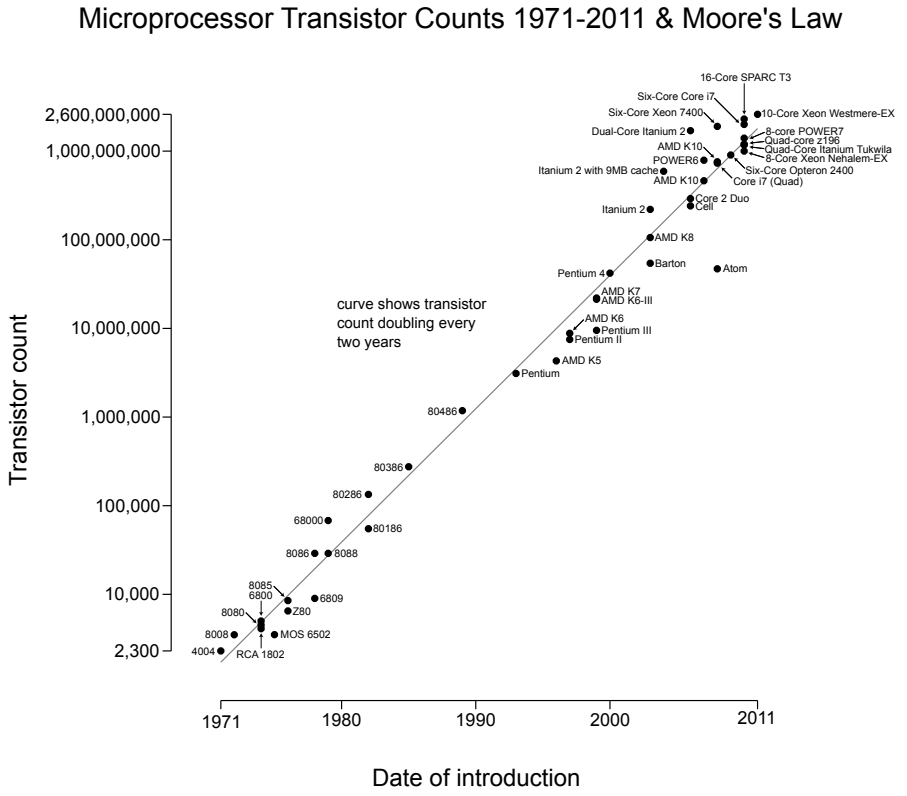

FIGURE 1.2: Since 1970, Moore's law predictions have been followed and the transistor density has been growing according to it. Because of that, computing power goes up, while costs and energy consumption go down.

nature is unavoidable. Furthermore, when device size is scaled down, approaching the few-atom limit, electronic current modelling becomes more and more interwoven with band-structure modelling, and the traditional distinction between these two fields starts to fade.

As it will be show in next section, simulation techniques have always been highly desirable. But, since "Beyond CMOS" devices explore new designs and different physic effects (different from the used currently), before the realization of the devices, a good comprehension of the devices that are wanted to build is needed. In that framework, new trustful simulation techniques are completely mandatory. In this sense, the scientific community involved in device simulation is, step by step, migrating from traditional semi-classical tools, such as Monte Carlo (MC) based on the Boltzmann Transport Equation (BTE), towards new completely quantum ones.

1.2 Simulator's Evolution

1.2.1 What is a simulator?

Before explaining which has been the evolution of the simulator in the electron devices field, I would like to answer the following question: What is a simulator? The definition of "simulate" is *the action of imitate the appearance or character of a system*. Since old times simulation tools were developed. The trial and error method is both costly and time consuming. For that reasons, since the antiquity, simulate a system in order to get information for future applications has been extremely useful. Simulators are instruments which have improved our knowledge of the world and have allowed the developing of new technologies.

From a current scientific point of view, mathematical models and theories have been usually developed inspired by real experiments and observations. Since the last centuries, new phenomena required mathematical models which were analytically not solvable. Then, numerical simulators are completely needed to check the accuracy and the validity of such mathematical models.

In that sense, it is a cyclic process. New phenomena requires the construction of new mathematical model, which needs in turns to be tested through comparison between numerical results performed with simulators and experiments. Once we trust the model and the simulators, it allows us to go beyond the current set ups, and then explore and imagine new and more sophisticated devices and experiments which could lead us to improve the actual technologies.

1.2.2 Classical Simulators

The first reality which we (as human beings) are able to appreciate is what is called "classical world". It studies the movements of bodies, where relativity and quantum laws have no role in it, and therefore their effects have no relevance, or at least we cannot directly appreciate them.

Many different fields has used classical simulators.

It is very relevant the appearance of Monte Carlo methods. Nowadays, we understand by Monte Carlo methods, a wide class of algorithms which obtain and predict results

from random initial samplings [5]. The first first appearance was due to Jon Von Neumann and Stanislaw Ulam, who worked in the Manhattan Project during world war II [4]. They used the first Monte Carlo method to study the neutron multiplication rates in order to estimate the explosive behavior of fission weapons. Since then, Monte Carlo methods has been widely used in all scientific fields, including physics, mathematics, economics, chemistry or biology.

If we turn our mind to electron devices simulating tools, classical drift-diffusion model[5] simulators have played an important role [6, 7]. Hydrodynamic models has also been developed [8, 9] as well as energy transport models [10, 11]. The use of Monte Carlo methods has also been successfully used for modeling electron transport phenomena in semiconductors, the first appearance in the literature corresponds to 1966 [12]. For future purposes, I will make a longer introduction to electronic Monte Carlo algorithms.

The basic Monte Carlo methods used random initial conditions to study electron transport in different materials. Since the beginnings, more complex and sophisticated methods has been developed in order to incorporate more interactions, such as scattering, lattice defects, impurities, many-body interactions, etc. [13, 14]. The main idea of the method is as follows. Firstly, from a domain of possible inputs, an initial multi-electron state is chosen, defined mainly by their positions and velocities. Then, electrons are time evolved following a equation of motion. These electrons describes trajectories. Finally, the properties of the system we are interested are computed from the final state of these trajectories. The experiment is repeated until the average of these properties converge and therefore we are satisfied with the result obtained. An important point is that semi classical Monte Carlo methods are time-dependent, allowing in a easy way the computation of properties and scenarios where one cannot easily avoid time. This is the case for example of AC scenarios. Interestingly, Monte Carlo methods are able to obtain the electron probability distribution obtained from the Boltzmann transport equation, but since there is a stochastic injection of electrons, more information about the system can be obtained, such as fluctuations.

For years, Monte Carlo methods were widely used in both research and the industrial electronic engineering, without significantly modifications. There was a clear necessity: to model electron devices in several scenarios, both DC and AC, transients, and obtain the expected transport properties such as currents, noise, cut-off frequencies... For that

[5] Curiously, the name of these methods, *Monte Carlo* is not by chance. It reflects the similarities with gambling games, and since Monte Carlo casino in Monaco was the center of gambling at that times, this name was given.

purpose, Monte Carlo methods, where electrons were injected randomly following certain statistics (such as the Fermi distribution), allowed to compute electron trajectories from classical laws, whereas interacting terms, such scattering rates, were obtained from the Quantum Fermi Golden rule. For that reason, it was treated as a semi-classical method. From these time-dependent methods, electron trajectories enabled to compute all transport properties.

Nowadays, all these classical simulation tools are becoming obsoletes. when trying to describe the small present electron devices. In the last decades, the miniaturization of electronic devices (due to Moore's law as stated in Section 1.1) has reached the nanoscopic regime, quantum effects appear. Conventional (classical) models started to fail and quantum corrections were needed to be incorporated, the wave nature of particles, cannot longer be neglected. Differently from classical mechanics, in the quantum regime, particles are described by wave function $\psi(\vec{r}, t)$, and the system under study by a global wave function $\Psi(\vec{r}, t)$ which is a combination of the former $\psi(\vec{r}, t)$ wave functions[6] and whose modulus square represent the probability of finding a particle at each spatial point.

The first attempts were to introduce quantum corrections (such as the Wigner-based correction or the Schrödinger-based correction). However, these corrections were unable to account for all quantum effects (such as resonant tunnelling) or nowadays the Klein Tunneling effect in 2D linear band structures materials (such as graphene), since these effects are wave interference, and classical models fails. For that reason, fully quantum methods are currently required [15].

1.2.3 Quantum simulators and their formalism

Apart from reflecting the quantum behaviour, the new quantum simulators must predict the realistic performance of electronic devices, for that reason they must include dissipation effects, such as scattering with the atom lattice, described by the interaction with (the quasi-particle) phonons.

The usual next step when constructing a quantum simulator is to analyze the different available quantum formalisms (such as the Wigner function, density matrix... [16]) and then develop the simulator. In the literature, we can find different quantum simulators (from my knowledge, all of them based on formalisms which comes from the orthodox

[6] Depending on the nature of particles, fermions or bosons, this combinations must follow some rules, such as being symmetric or antisymmetric.

theory as we will see in Section 2.1). A quantum simulator must be able to analyse (in a full quantum way) systems out of equilibrium, made by different material structures, and obtain reasonably good results of transport properties (such as DC and AC current, noise, transients, etc.). Here I refer to the main used ones:

1.2.3.1 Density matrix

The density matrix corresponding to a pure state of a system $\Psi(\vec{r},t)$ is $\hat{\rho} = \Psi(\vec{r},t)^*\Psi(\vec{r},t)$. The evolution for the density matrix is given by the quantum Liouville equation. It is very interesting when studying statistics because its formulation allows to work easily with mixed states. A mixed state describe a system which we do not exactly its composition, but we know with certain probability that it is in one certain state.

When one wants to include any additional interaction with the environment, such as dissipation, one has to trace the density matrix of the full system, obtaining a reduced density matrix, where there is an and extra term [17]. This term is usually added in phenomenological way (such as the Boltzmann Collision operator which will be discussed in Section 5.2.3) and the rates are governed by the Fermi Golden Rule. In principle, it does not guarantee to obtain a positive dynamical way, unless it fulfills the Lindbland equation (discussed in Chapter 5). Examples where the density matrix is used are Refs.[18–20].

1.2.3.2 Wigner Function

The Wigner function is a phase space function. It is obtained by a Wigner-Weyl transformation of the Liouville equation for the density matrix, and the kinetic equation (Wigner transport equation) which governs its dynamics is very similar to the classical Boltzmann equation[7]. For that reason it is intuitively very insightful. It is quite simple to transfer intuition and knowledge from the well known semiclassical Monte Carlo methods to this quantum formalism [21, 22]. However, since it is based on the orthodox theory some contradiction appears. If in the theory there is no space for defining simultaneously positions and momenta, how can you build a phase space map? The distribution function in the Boltzmann equation describes the probability of finding electrons in a particular point of the phase space, it is a probability function. However, in the Wigner function negative values may appear. For that reason it is just considered as a quasi probability function. This problem is enhanced when we include dissipation (via either a relaxation time or a collision operator [23, 24]). I emphasize that this is a clear example where the formalism is not in agreement with the quantum theory.

[7] In fact, if one takes the classical limit, the Boltzmann transport equation is obtained.

Within this formalism, the Wigner–Boltzmann Monte Carlo device simulation is constructed and when coupled with the Poisson equation, successfully used in several scenarios[25–27].

1.2.3.3 Non Equilibrium Green Functions

NEGF emerged as a good method to study non equilibrium problems. It was first used by Schwinger [28], Kadanoff, and Baym [29] in the early 1960s. Since then, the method has been adapted to the new necessities and new devices, as well as it incorporates many interactions, such as phonon and impurity scattering[30, 31]. The Hamiltonian is split in several parts, the one containing the device, the leads, the one coupling both parts and the one which accounts for the different interactions. Thanks to the Keldysh formulas, and solving the Dyson's equation it obtains transport quantities. This Hamiltonian is usually obtained with other transport models, such as DFT. NanoTCAD ViDES[32] is an example of quantum simulator using NEGF which is able to solve many different situations [33–35]. TranSIESTA [36] is another simulator which combines NEGF with DFT by means of SIESTA(Simulation Environment for Semiconductor Technology Analysis[37]).

1.2.3.4 Landauer-Büttiker formalism

A very useful formalism for quantum transport is the so called Landauer-Büttiker formalism. In this formalism the device is sandwiched between (at least) two reservoirs (where there is no dissipation), connected to the device (where there may be dissipation) through the leads. By taking some reasonable assumptions, such as reflectionless contacts and thermodynamical equilibrium in the contacts, it can be shown [38] that most quantum properties, such as conductance, are mainly deduced from the transmission probability of one electron crossing the whole device and the number of transverse (left and right) moving modes available in the reservoirs. Under this formalism, Landauer proved that conductance is quantized. After that, Büttiker realized that when treating with multichannel devices, the Landauer formula was still valid as far as the different currents coming from each reservoir was considered[39, 40]. It was also Büttiker who introduced the second quantization operators in this framework, where electrons are created and annihilated[39, 41]. These operators were extremely useful to understand and compute quantum noise. Quantum noise will be deeply discussed in Chapter 6, but I anticipate that it is interesting and surprising how second quantization, a tool belonging to quantum field theory, appears in a non-relativistic scenario. This is a consequence of the understanding of *the measurement problem* in the orthodox quantum theory, which

in turns I will discuss in Chapter 2. For computing current, we could just use the wave nature of the electron, i.e., the wave function, but when computing noise, we need to collapse, and then the orthodox theory suffers. For that reason, Büttiker introduced in a elegant way this second quantization method (whose validity for predicting results is completely out of doubt), which naturally collapses the electron by splitting the full Hilbert space in two different ones.

1.2.3.5 Density Functional Theory

DFT beginnings were done in 1964 by Walter Kohn and Pierre Hohenberg with their well known theorems Hohenberg–Kohn theorems[42]. These theorems demonstrates that the ground state of a many-body electron system are determined by the three real space coordinates of an electron density. Therefore, avoiding to work in the complex (3N dimensional, being N the number of particles in the system) configuration space and working in the (3D) real space. They also proof that there is a correct electron density that minimizes an energy functional. Two problems appear immediately: this functional is unknown and it only works for the ground state of a system. After the work of Kohn and Hohenberg many other theorems and additional tools have developed inside DFT, but the cornerstone are these theorems.

When applied to electronics, there are mainly two limitations. First, they are applicable to finite or periodic systems and an electron device is definitively none of these cases, since obviously it is not a finite object (unless we consider the whole device, cables, something which is computationally impossible) and it is not periodic since there is no translational symmetry. Secondly, DFT studies ground states and electron devices are in a non equilibrium state. TranSIESTA (Simulation Environment for Semiconductor Technology Analysis[37])is an example of TCAD software which uses DFT.

1.2.3.6 Bohmian formalism

Finally, I present the Bohmian formalism. Since it is the one used during the thesis, Chapter 3 will be dedicated just to it. But let me explain me briefly the reasons why it is very interesting to explore this path and how it can help the electronics field.

Previously, I have presented the main objectives and requirements of the electronics simulation field and the most used formalisms used and developed until now. I anticipate

that these methods come from the orthodox quantum theory, while the Bohmian formalism comes from the Bohmian theory, which allows the existence of definite particle positions and velocities simultaneously. Therefore, the Bohmian formalism is without doubts one candidate to convert classical Monte Carlo method in a fully quantum method. The similarities between both methods are undeniable. Both are time-dependent methods where electrons describe trajectories and from them, transport properties are computed. It is clear that time-independent methods have advantages, specially because these methods involve less computational burden and it simplifies many computations, however time-dependent models are a convenient characteristic, specially when modeling transport, whose definition involves the movement of something, and therefore *time*. This fact allows to compute the total (not only particle, but also displacement) AC current. The time-dependent injection model also allows to compute shot and thermal noise in a simple way.

Another property which makes the Bohmian theory appropriate for studying quantum transport is that (as it will be seen in Chapter 3 and contrarily to the standard theory) it allows to study subsystems. This is a very important point, since the study of a full electronic device (cables, leads, active region, atoms...) is computationally unapproachable (many-body problem). Therefore, one has just to focus on a simpler system, called subsystem, which is affected by its environment.

Finally, apart from these practical considerations which make completely necessary to explore the tools and facilities that the Bohmian formalism provide us, (and this is my personal opinion), Bohmian mechanics also presents a more intuitive way of understanding the quantum world. As it will be shown in Chapter 3, collapse appears as a consequence of the interaction between the measuring apparatus and the system and is not an additional postulate. It also recuperates the concept of particles which describe (following quantum laws) trajectories.

1.3 Thesis Structure

The thesis is structured in three different parts. In the first part is dedicated to make an introduction to the thesis framework. In Chapter 1, I made an introduction to the state-of-the-art of quantum electron devices simulators and the main available formalisms. In Chapter 2, I will make a brief introduction to quantum mechanics. I will show that quantum mechanics ontology is not as well established as it is in classical mechanics and I will describe the main different theories of quantum mechanics. Since through the thesis

the Bohmian formalism will be used, I will make an introduction to Bohmian mechanics theory and its formalism in Chapter 3. I will present the useful conditional wave function (unique for this formalism), how Bohmian mechanics faces the measurement problem and also the BITLLES quantum simulator, which was developed as well as used to obtain numerical results during the thesis. In the second part, present results obtained during the thesis. In Chapter 4 it is presented how the Dirac equation was introduced in the BITLLES simulator to be able of capturing the physics of the new 2D materials with linear band structure, such as graphene. During this thesis, a scattering method was developed and it will be presented in Chapter 5. It will be also discussed why it is interesting to develop completely positive methods (as the one presented) and not the opposite. In Chapter 6, I will show how the use of the Bohmian time dependent formalism simplifies enormously the study of AC quantum current and its fluctuations in different scenarios. A novel source of noise and the time dependent model injection of the BITLLES will be showed. It will be also presented how the discreteness nature of electrons leads to an intrinsic noise limit for the miniaturization of electron devices. In part three, I present the conclusions.

Chapter 2

Different theories of the quantum world

In this Chapter, I present different theories of the quantum world. In many physic research fields, it is assumed that the only explanation of the quantum world is the Copenhagen theory[1], but it is not the only one. In this Chapter, I present other quantum theories which are nowadays still being discussed by fundamental physicist and science philosophers[43, 44]. They try to answer question such as: Is the wave function a real object? Do we comprehend what is really happening in quantum systems? Regarding the quantum measurement problem, does the observer have an important role? What about the ontology of the theory? In this Chapter, firstly, I will introduce what are the requirements and components of a theory. Afterwards, I will present briefly different quantum theories. Nowadays, since there is not a feasible experiment which can reject any of them, still they are just theories.

2.1 Realism and experiments

When trying to understand Nature, scientists constructs theories which tries to anticipate and predict experimental outcomes. When constructing a theory, we can distinguish two different main branches: rationalism and empiricism. Rationalists believe that there is an innate and fundamental knowledge. They believe that knowledge can be gained by reasoning, independently of experiments. Experiments are just a manifestation and our perception of this fundamental and deep reality, which is formed by (usually) abstract

[1]For that reason, when speaking about quantum theory or quantum mechanics, it is assumed that we refer to the Copenhagen or orthodox theory. However, this is not true, and as I will shown, more quantum theories also exist.

objects and entities. On the other hand, empiricists believes that the only source of knowledge is experience.

For rationalists, it is important to know what is beyond the perception. When constructing a theory, they care about the ontology of that theory, i.e., *what is in it?*, *what entities are there in the universe?*. On the other hand, empiricists affirms that there is nothing beyond our epistemic perception. One should just take care of reproducing correctly experimental results, since there is nothing beyond this knowledge.

The formalisms[2] that can be constructed from a theory will be different if they come from a rationalist theory or an empirical theory (obviously, theories can be a mix, there is not a sharp line defining empirical theories or rationalist ones), because they handle different objects and entities.

It is interesting how some theories are constructed in a empirical way, and how after some time, they are deeper understood and constructed in a more rationalist way, until a consensus is achieved. A good example of how a theory develops is classical mechanics. The ontology of classical mechanics was discussed during years, and there has always been some minority groups which have tried to convince a majority that the understanding of Nature is not as it was believed at this point. For instance, in the 5^{th} century B.C., when all realities were attributed to some God, Empedocles proposed that the world was made by four ultimate elements, which he called "roofs", fire, air, water and earth. From these materials, all structures in the world were constructed. In the next century, Democrito and Leucipo broke with this belief and proposed the atomistic theory, where they proposed that the most basic structure of matter are small particles, called atoms. Many centuries later, Kepler, Galileo, Descartes, and Newton among others made a radical break between the intuitive and common sense ideas of the previous Greek philosophers, with models based in experimental results and installed the essential pillars of what is currently understood as the scientific method. During this period, some minor groups have always "transgressed" the establishment to propose novel alternatives to the current knowledge[3]. Nowadays, nobody discusses the primitive ontology of classical mechanics which has been established through a long ripening time: matter is described by particles, which evolves describing trajectories, defined by positions and velocities, in a three dimensional space. Nobody denies that the classical ontology are the particle positions, it is a special parameter, since it is the one we perceive.

[2] I understand a formalism as the mathematical tools that a theory can provide to predict experimental outcomes

[3] For instance, notice all problems that Galileo Galilei had for supporting Nicolaus Copernicus heliocentrism, even if this idea was already in the Greeks mind in 6^{th} century B.C.

Therefore, its validity is out of doubt in the classical regime, and different formalisms have been constructed according to it. Classical laws were initially developed by Newton and Leibniz in the 17^{th} century. In 1788 J. L. introduced the Lagrangian mechanics formalism. Later, the Hamiltonian formalism, formulated by W. R. Hamilton in 1933. These different formalisms has something in common: their ontology. Nowadays, when exploring new regions in the classical world, nobody brings up the ontology of the theory.

A similar thing occurs in quantum mechanics. Several formalisms has been developed as seen in Section 1.2.3, most of them under the orthodox theory. These models reproduce without doubts experiments, and in that sense they are extremely useful and allows the discovery of many new effects and the modeling of new devices which are improving our daily life. Even if they have to deal with the quantum measurement problem which will be described in the next Chapter 3, it is out of doubt that the different algorithms have extremely contributed to the scientific progress, achieving numerical results very accurate and close to real experiments.

However, some questions have been disregarded in some research communities: *Is the ontology of the quantum world as well established as in classical mechanics? Do we really understand the quantum world? What are the different theories and ontologies of quantum mechanics theories? Under which quantum theory do we construct the quantum simulating methods?*

These questions were already discussed in the beginning of the 20^{th} century. In that sense, when Einstein considered that the aim of physics is "the complete description of any (individual) real situation (as it supposedly exists irrespective) of any act of observation or substantiation)" [45] he was expressing that there must be a fundamental reality, whereas when Bohr asserted that "It is wrong to think that the task of physics is to find out how Nature is. Physics concerns what we say about Nature" [46], Bohr was being more empiricist.

Since these times, it is commonly accepted that these question are meaningless, because the orthodox version was accepted by majority and taught at the universities. However, still many researchers are not convinced by the usual answers and try to explore another alternatives[43, 44]. In fact, there do exist other quantum theories and they provide additional tools which lead to different quantum formulations[16].

Even if these questions may seem useless from a practical point of view, they are not. When constructing a formalism, it is very relevant under which theory is constructed. Even if we have achieved a high knowledge from the techniques developed until now, still

they could be improved. Different theories do not only provide different kind of intuition and orientation, but they can help when solving different quantum problems (such as the *many-body problem*), since they can contribute with different mathematical tools, approximations and way of facing the same problem. Clearly, in order to be correct, all theories must reproduce the experimental results, but as stated before, choosing one theory or other will allow us to develop different formalisms on which different approximations can be done.

2.2 Different Quantum theories: the measurement problem

Measurements has always been determinant in the development of physics: a theory cannot be accepted as true if it is not supported by experiments. In classical mechanics, since we deal with massive particles, the act of measuring does not affect (or at least nor crucially) the measured system, and this discussion does not appear. However, when studying small and light particles, to measure implies to disturb the system under study. This is the well known *measurement problem* - which will be deeply discussed in the following Chapter- and this problem has a very narrow relationship with the appearance of the different theories of the quantum world. Each theory faces and explains the problem in a different way. In some of them, the observer plays no role, while in others (such as the most used and known one, the orthodox theory) it plays and essential role. In 1995, Maudlin [47] explained the measurement problem in the following way. Assume these three assertions:

- a) "The wave-function specifies (directly or indirectly) all of the physical properties of a system.
- b) The wave-function always evolves in accord with a linear dynamical equation (e.g. the Schrödinger equation).
- c) Measurements of, e.g., the spin of an electron always (or at least usually) have determinate outcomes, i.e., at the end of the measurement the measuring device is either in a state which indicates spin up (and not down) or spin down (and not up)."

Although these sentences seem to be true and consistent, they are not. One of them must be rejected to develop a consistent theory. The Schrödinger cat paradox illustrates why the three cannot be true simultaneously [48]. If we assume that the wave

function specifies the cat configuration, and we assume that it evolves according to the Schrödinger equation, the wave function will consist in a superposition of a state where the cat is alive and a state where the cat is dead. Since there is no additional laws, when measuring we should obtain this entangled state, and not a projective measurement where the cat is either alive or dead. Therefore, depending on which assertion we choose to reject, we will reach a different quantum theory.

2.2.1 Removal of the linear dynamics equation

In this case, I will explain two different theories. One (the Copenhaguen) where the observer has a relevant role in the theory, and another one which tries to remove this importance.

Copenhagen (or orthodox) theory

In this theory, assertion b) does not hold anymore. There is a dynamical equation, such as the Schrödinger or the Dirac equation. However, once the (strong or projective[4]) measurement occurs, there is an extra law: *the collapse*. Once we measure the wave function collapses to one of the possible eigenstates of the system, with a probability given by Born's rule.

This theory depends crucially on the measurement (for a more detailed discussion, see Section 6.1.3). Particles behave differently if they are measured or not. When particles are not measured, they are not longer point-particles, but a wave. When we measure, the point-particle nature appears again. Many scientists have argues against this theories which gives such a big power to the act of measuring.

One of them was Albert Einstein, when he said "Such an theory is certainly by no means absurd from a purely logical standpoints; yet there is hardly likely to be anyone who would consider it seriously." [49]

Also Richard Feynmann "This is all very confusing, especially when we consider that even tough we may consistently consider ourselves always to be the outside observer when we look at the rest of the world, the rest of the world is at the same time observing us, and that often we agree on what we see in each other. Does this mean that my observations become real only when I observe an observer observing something as it happens? This

[4]Even if they are also usually ignored, weak measurements also exist. This kind of measurement disturb softly the wave function. The price to pay is that one cannot obtain the same amount of information of the system compared to strong measurements.

is an horrible viewpoint. Do you seriously entertain the thought without the observer there is no reality? Which observer? Any observer? Is a fly an observer? Is a star an observer? Was there no reality in the universe before 109 B.C. when life began? Or are you the observer? Then there is no reality to the world after you are dead? I know a number of otherwise respectable physicists who have bought life insurance." [50]

In my opinion, John Bell was one of the best who summarized the problem in his work entitled "Against measurement" [51]. In it, he cited some Dirac assertions from Ref.[52] and concludes:

"It would seem that the theory is exclusively concerned about 'results of measurement', and has nothing to say about anything else. What exactly qualifies some physical systems to play the role of 'measurer'? Was the wavefunction of the world waiting to jump for thousands of millions of years until a singlecelled living creature appeared? Or did it have to wait a little longer, for some better qualified system ... with a PhD? If the theory is to apply to anything but highly idealized laboratory operations, are we not obliged to admit that more or less "measurement-like" processes are going on more or less all the time, more or less everywhere? Do we not have jumping then all the time?"

GRW theory

The orthodox theory is not the only one abandoning b). In that path, the Ghirardi-Rimini-Weber (GRW) theory [53, 54] adds an additional non-lineal term to the dynamic equation. This extra term provokes that the wave function collapse spontaneously. The probability of collapse for single particles is extremely low, for that reason spontaneous collapse is not observed. However, when more particles are involved and entangled (as in a measuring process), the collapse probability (given by the additional term) increases enormously, and then the system collapses. It is important to emphasize that differently to the the orthodox theory, in GRW there is not an extra collapse law. This theory tries to get rid of the importance of the observer. Similarly to the orthodox theory, the collapse of the wave function exists, but in a random way, not just when measuring. However, how is this collapse term? In principle it is a universal term. Usually a Gaussian term is a assumed with a certain dispersion, which follows a Poisson distribution in order to obtain the occurrences of the mentioned random collapses. However, the Gaussian and Poisson parameters have different constrains to reproduce correctly results, and these constrains makes difficult to find compatible values. This theory predicts different results from the Copenhaguen theory, but such results belong to experiments which are nowadays technically inaccessible[55].

2.2.2 Removal of determinate outcomes

Many-worlds (or Everett) theory

Many-worlds theories[56, 57] rejects c). It denies in any way the collapse of the wave function. According to Everett there is not only a real world, but different story lines. Every time a measurement is performed, a story line is split in different story lines, each one corresponding to every possible output result of the performed experiment. For instance, in the scenario where an electron wave function impinges on a potential barrier and part of the electron wave function is reflected and part transmitted, if we measure (at least) two different stories of line will appear: in one of them the electron has been transmitted and in the other one the electron has been reflected. This theory also gets rid of the importance of the observer. The wave function never collapses and it just keeps branching. However, this quantum theory has also an inconvenient to fulfill Born's law, which is evident in the next example. Imagine a particle impinging in a barrier, part of the wave function is transmitted (let's say with probability 0.1 and reflected with probability 0.9. Then, the world cannot split just in two different worlds, but at least in 10 different ones, to reconstruct properly the outcomes probability.

2.2.3 Removal of the wave function

Bohmian mechanics (or the pilot-wave) theory

There are theories which abandon a) and state that there is some other parameters, called hidden variables, apart from the wave function. Bohmian mechanics is one of these non-local hidden variables theories and the most popular one. I anticipate that this theory will be the one used along the thesis and that next chapter will be dedicated just to explain the theory. For that reason, here I will just mention which are the main characteristics of that theory. In the ontology of Bohmian mechanics, apart from the wave function, there are the particle positions, which are the (non well called)hidden variables of that theory[5]. In Bohmian mechanics when we say particles, we mean real particles, similar to classical mechanics, but whose trajectories follows quantum laws, instead of Newton law. These trajectories are guided by the wave function, and we cannot measure them directly because of the system perturbation when measuring, also called Heisenberg uncertainty principle[58]. Differently from the other previous theories, it is the only one deterministic. If we knew the initial positions of all the particles, we

[5]Hidden in the sense that we cannot see them and measure them continuously, but the same occurs with the wave function, which in an object which we cannot measure (only its square modulus after many different measures). In fact, most scientist accept that positions are real, but non agreement has been achieved about the reality or not of the wave function

would be able to determine their future positions. However, the impossibility of knowing this information, makes it empirically non deterministic, and then the typical quantum randomness is obtained.

From all the theories I feel clearly more comfortable with any of the theories where the observer has no role. My mind cannot conceive that nature gave us such a huge power. Among the non-observers theories, from my point of view Bohmian offers the most intuitive and understandable sight of quantum mechanics. I really appreciate how the world is conceived in a elegant way, without totally abandoning the classical ontology (particles are still particles describing trajectories) but describing totally the quantum world (thanks to the wave function, since it guides the particles). Obviously, Bohmian mechanics is not the last theory, in the sense that it has problems (similarly to the other theories) when trying to include relativistic effects and then moving to quantum field theory. But as said in Section 1.2, each theory has its own regime and limits. In that sense, the physics of the world could be separated in different layers, each one containing another one (similar to an onion), where classical mechanics would be the most internal one. Obviously, the laws describing the most exterior one must fulfill the laws of the inner ones. But not the opposite. A clear an correct understanding of the internal layers are mandatory and necessary to move to the next one. In that sense, I believe that quantum mechanics is still not completely understood, a clear example is that still many researchers ask themselves and think about quantum mechanics ontology. So, even if any of these theories are not the definitively theory since they do not include relativistic effects, it is worth the effort to understand and put some clearance in quantum mechanics.

Chapter 3

Introduction to Bohmian mechanics

3.1 A bit of Bohmian History

Since the 5^{th} Solvay conference in October 1927, the standard and most accepted quantum theory is the orthodox one. This conference is usually presented as a key event in the history of quantum mechanics. Many well known physicist participated in it[1]. The well known phrase of Einstein, who disliked the Heisenber's Uncertainty Principle "God does not play dice" happened there, followed by Böhr answer, "Einstein, stop telling God what to do". According to Bacciagaluppi and Valentini [59], "the Broglie's theory was one of the sharply conflicting points of view presented at the meeting (matrix mechanics, wave mechanics and pilot-wave theory)". But, where was this discussion coming from?

After some unexpected experimental results, such as the black-body radiation, where Max Planck proposed that light is emitted in discrete quanta of energy [60], or the photoelectric effect, where Einstein proposed that light is propagated and absorbed in quanta[61], a new theory able to explain these non classical (and not continuous but quantized) effects was required. In his thesis in 1924[62], De Broglie suggested that matter, apart from its particle behaviour also behaves as a wave. It is what is known currently as wave-particle duality. But he never abandoned the particle behaviour. After that, in 1926 Schrödinger (following De-Broglie's ideas) described [63] particles in terms of a wave solution of the following (nowadays called Schrödinger) equation:

[1] Among others: P. Ehrenfest, E. Schrödinger, W. Pauli, W. Heisenberg, L. Brillouin, P. A. M. Dirac, W. L. Bragg,M. Born, M. Planck, M. Curie, A. Einstein, V. de Broglie and N. Böhr.

$$i\hbar\frac{\partial\Psi(\vec{x},t)}{\partial t} = \left[-\frac{\hbar^2}{2m}\nabla^2 + V(\vec{x},t)\right]\psi(\vec{x},t) \tag{3.1}$$

where $V(\vec{x},t)$ is the potential energy seen by the electron and m its mass. In the beginning, $|\Psi(\vec{x},t)|^2$ was interpreted as the electron charge by Schrödinger. Later on Born interpreted it as the probability density of finding the electron. There was no longer the idea of particle as a point-particle describing a trajectory. This idea was replaced by the idea of a particle behaving sometimes as a wave, and as a point-particle when measuring it. The question about where is the particle is a nonsense without measuring. Related to this point, Einstein did not like this point of view, as it reflects this affirmation: "I like to think the moon is there even if I am not looking at it.". On the other hand, De Broglie's theory was the following: the particle behaves always as a particle, whose trajectory is guided by the solution of Equation (3.1). The first theory deals with *waves or particles*, i.e., the orthodox theory, and the latter is a theory about *waves and particles*, i.e., Bohmian mechanics.

At this point, the Solvay conference occurred. There, De Broglie was alone to defend his theory. The other scientists were strongly collaborating and his ideas were not received strong acceptance in the conference. He did not keep defending his ideas and abandoned this *fight*. Since then, the orthodox theory, where the observer has an enormous role in the story, is the most popular theory and the one students learn. Since then, when a student reads the double slit experiment and asks to the teacher if the electron passes one slit or the other and why there is an interference pattern, the answer is "the electron passes through both slits at the same time and then we see the interference pattern because of its own interference" (orthodox answer) and the answer is not "just by one, but we do not know which one. The interference pattern occurs because the wave function, which is the one guiding the particle has the information of the whole system (quantum wholeness)" (bohmian answer).

Regarding this issue, let me quote the enlightening affirmation of Bell [64]:

"Is it not clear from the smallness of the scintillation on the screen that we have to do with a particle? And is it not clear, the diffraction and interference patterns, that the motion of the particle is directed by a wave? De Broglie showed in detail how the motion of a particle, passing through just one of two holes in screen, could be influenced by waves propagating through both holes. And so influenced that the particle does not go where the waves cancel out, but is attracted to where they cooperate. This

idea seems to me so natural and simple, to resolve the waveparticle dilemma in such a clear and ordinary way, that it is a great mystery to me that it was so generally ignored."

Afterwards, in the early 50's, David Bohm was not very convinced about the orthodox theory and, in his book [65], he tried to avoid the collapse and find a way to explain the measurement just with the wave function. Later, in 1952 he published two works [66, 67] where he proposed a theory with trajectories, Bohmian mechanics was again dug up. Instead of using De Broglie's formulation, he obtained the guidance and velocities equations in a different way.

From Equation (3.1), it can be derived the following continuity equation by straightforward mathematical manipulations:

$$\frac{\partial|\Psi(\vec{x},t)|^2}{\partial t} + \vec{\nabla}\vec{j}(\vec{x},t) = 0 \tag{3.2}$$

where $\vec{j}(\vec{x},t) = |\Psi(\vec{x},t)|^2 \frac{\hbar}{m}\mathrm{Im}\frac{\nabla\Psi}{\Psi}$ is the particle current density and $|\Psi(\vec{x},t)|^2$ the particle probability density. The particle current density can also be understood as $\vec{j}(\vec{x},t) = |\Psi(\vec{x},t)|^2\vec{v}(\vec{x},t)$ where $\vec{v}(\vec{x},t)$ is a velocity field. From here we can derive this velocity field:

$$\vec{v}(\vec{x},t) = \frac{\vec{j}(\vec{x},t)}{|\Psi(\vec{x},t)|^2} = \frac{\hbar}{m}\mathrm{Im}\frac{\nabla\Psi(\vec{x},t)}{\Psi(\vec{x},t)} \tag{3.3}$$

By integrating Equation (3.3) we can obtain a set of trajectories, each one having a different initial position $\vec{x}(t_0)$:

$$\vec{x}(t) = \vec{x}(t_0) + \int_{t_0}^{t} \vec{v}(\vec{x},t')dt' \tag{3.4}$$

Therefore, in a very natural and easy way, electron trajectories can be obtained directly from the Schrödinger Equation (3.1). Therefore, electrons recover a very fundamental property, its positions. Perhaps they cannot be measured, but even that, particles have definite positions. In that sense, Bohmian mechanics is deterministic. If we were able to know the particle position $\vec{x}(t_0)$ at time t_0, we could know its future trajectory. However,

because initial positions are not known, empirically it is not deterministic, and it can be proved that it predicts the same outcomes as the orthodox theory due to the Quantum Equilibrium Hypothesis[2][68]. The trajectories from Equation (3.4) have information from all other particles and the system, since their velocity (Equation (3.3)) depends on the total wave function $\Psi(\vec{x}, t)$. This is why the Bohmian theory is an holistic and non-local theory (the parts of any whole cannot exist and cannot be understood except in their relation to the whole).

Why has it been mostly ignored during these years? Probably because Bohm's papers appeared almost 25 years after the orthodox theory was established. Another reason is that the orthodox theory predicts the same results, so why to care if in addition there are more parameters (the trajectories)? In this thesis (as already stated in Chapter 2), I argue and prove that apart from the intuitive insight, it can provide extra tools and approximations which the orthodox theory cannot give. In section Section 3.3, one of the main tools, *the conditional wave function*, is explained and used continuously in Chapter 5 and Chapter 6. Finally, I want to remark that, as stated in Section 2.2, Bohmian mechanics (as any other non relativistic theory) is not the ultimate theory able to account for all physical levels. It accounts for classical as well as quantum outcomes, but it does not include relativistic effects. In any case, understanding the quantum regime and knowing which is its ontology and what is actually happening in quantum systems is, at least, strongly recommended before moving to the following and larger "onion layer", i.e., quantum field theory.

3.2 Many Body Problem

Before presenting the conditional wave function and its dynamical evolution, I want to briefly introduce the many-body problem, which is a technical problem in the sense that it makes impossible to have analytic solution for many-particle problems and strongly obstructs numerical results. For that reason, approximations are mandatory. In quantum mechanics, the particle configuration is no longer described in a $\mathbb{R}^d$ (where d is the dimension of the system) space, but in a $\mathbb{R}^{dN}$ dimensional space, where N is the number of particles in the system that we are interested in. This means that each particle we are considering contributes with d degrees of freedom. Obviously, this exponential growth

[2]This hypothesis states that particles are distributed according to the modulus square of the wave function since the initial time. When saying initial time, I mean the Big Bang. After that the evolution of the total universe wave function evolved according to the Schrödinger equation and the distribution of particles have always reproduced the modulus square of the wave function.

has a direct impact in the computational cost of the system. This is the so called *many-body problem*. There are many famous sentences related to this problem. For example, in 1929 Dirac stated[69]:

"The general theory of quantum mechanics is now almost complete. The underlying physical laws necessary for the mathematical theory of a large part of physics and the entire chemistry are thus completely known, and the difficulty is only that the exact application of these laws leads to equations much too complicated to be soluble."

Another example is the next Born affirmation[70]:

"It would indeed be remarkable if Nature fortified herself against further advances in knowledge behind the analytic difficulties of the many-body problem."

Currently, with nowadays computers, it is impossible to simulate more than a few particle systems. For example, in a 2 dimensional system with $N = 10$ particles of $10nm^2$, discretized with a spatial step of $\Delta x = 1$ nm, a grid of 10^2 points is obtained. Then, the total number of points in the configuration space for the 10 particles is 100^{10}. If we use 4 bytes to store the (complex) value of the wave function at each grid point, the information would require more than 10^8 Terabytes. For that reason, approximations are necessary in order to decrease the computational burden. As already mentioned, depending on the theory we are using, it will provide us different mathematical objects, which allow us to tackle this problem in different ways. For example, the orthodox theory, uses (among other) the Hartree and Hartree-Fock methods, as well as Density Functional Theory or Quantum Monte Carlo methods. In the case of Bohmian mechanics, this theory allows to define the conditional wave function of a subsystem which is unique to study and face many body problems, as it will be shown in next section.

3.3 The Conditional Wave Function

3.3.1 Definition of the Conditional Wave Function

As stated previously, in the ontology of Bohmian mechanics, in addition to the wave function there is also the position of particles. Positions are very important and especial in this theory. It is a property from all particles, even if one does not measure it, Bohmian mechanics affirms that particles has definite positions. Other properties, such as spin, does not have value unless being measured, but this is not the case of particle positions.

This fact allows the appearance of trajectories (Equation (3.4)) and an object which has not been discussed until now: *the conditional wave function*. It is a unique tool of Bohmian mechanics. Since all particles in the world are entangled with others (many-body problem), in principle, strictly speaking, there is only one wave function $\Psi(\tilde{\mathbf{x}}_\mathbf{N}, t)$[3], which corresponds to the wave function of the whole universe and that cannot be split. Obviously, we do not know this wave function and we can just obtain information from a subsystem formed by M particles when measuring it. However, if we assume the current positions of the rest $N - M$ particles, we can define the conditional wave function $\psi(\tilde{\mathbf{x}}_\mathbf{M}, t)$ of that subsystem as:

$$\psi(\tilde{\mathbf{x}}_\mathbf{M}, t) \equiv \Psi(\tilde{\mathbf{x}}_\mathbf{N}, t)|_{\vec{x_i}=\vec{X_i(t)}} \equiv \Psi(\tilde{\mathbf{x}}_\mathbf{M}, \vec{X}_i(t), t) \quad where\ i \notin M \tag{3.5}$$

It corresponds to the wave function of the mentioned M particle subsystem conditioned to the actual positions $\vec{X(t)}$ of the $N - M$ particles of the rest of the universe. In this way, what we are really doing is to make slides of the total, complex and unknown universe wave function (see Figure 3.1). Since in the orthodox theory, the current positions of particles is not in the ontology of theory, it is impossible to construct in any way the wave function of a subsystem, which as we will see is extremely useful. For that reason, strictly speaking, orthodox physicists cannot use the wave function of a subsystem and use the reduced density matrix to study subsystems.

With the conditional wave function, the *many-body problem* can be tackled in a very elegant way as we will see below. In fact, the *measurement problem*, which leads to the orthodox collapse law, can be reinterpreted and easily understood.

In the orthodox theory, the dynamics of the wave function are given firstly by Equation (3.1), which is a deterministic and has a unitary evolution. Once we measure, an additional postulate (the collapse postulate) is required, and then the wave function collapses randomly in one of the eigenstates[71]. Let me give an example, an electron impinges in a potential barrier. Part of the wave function is reflected and part is transmitted. Once we measure, the electron collapses and appears in one side of the barrier. At this time, the wave function belonging to the side where the electron is not is removed. From here, a new evolution given again by Equation (3.1) begins.

[3]Hereafter I will use the following notation: $\tilde{\mathbf{x}}_\mathbf{N}$ corresponds to a point in the $3N$ (or $2N$ in 2D materials) dimensional configuration space, $\tilde{\mathbf{x}}_\mathbf{N} = (\vec{x_1}, ..., \vec{x_N})$. On the other hand, $\vec{x}_i$ corresponds to the 3D space of the $i-th$ particle, i.e $\vec{x}_i = (x_i, y_i, z_i)$ (or 2D when talking about 2D materials, $\vec{x}_i = (x_i, z_i)$. Finally, when considering a particular (conditioned) position of the $i-th$ particle at time t in a 3D material, $\vec{X}_i(t) = (X_i(t), Y_i(t), Z_i(t))$ or $\vec{X_i(t)} = (X_i(t), Z_i(t))$ in a 2D material

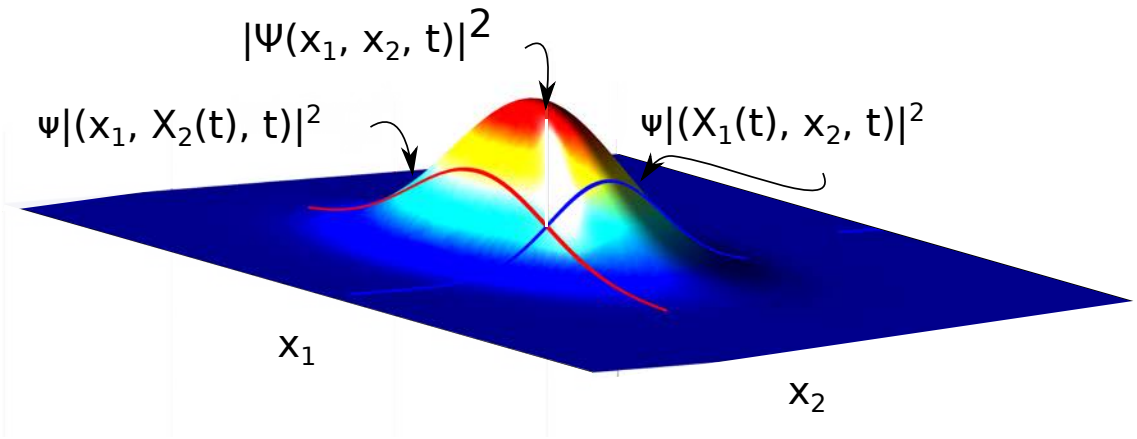

FIGURE 3.1: The total wave function for two particles in a one dimensional system. The space configuration x_1x_2 is plotted. Two different conditional wave functions (one for each particle) are also shown. They correspond to slices of the total wave function. By summing all possible conditional wave function, the total wave function can be recovered.

In Bohmian mechanics, there is nothing special about measuring. The measuring apparatus is composed by particles. As any other particles which are coupled to the system under study, they must be included in the wave function of the system $\Psi(\tilde{\mathbf{x}}_\mathbf{s}, \tilde{\mathbf{x}}_\mathbf{a}, t)$ where $\tilde{\mathbf{x}}_\mathbf{s}$ refers to the degrees of freedom of the particles we are interested to measure and $\tilde{\mathbf{x}}_\mathbf{a}$ the particles composing the macroscopic measuring apparatus. By evolving the wave function of that system with Equation (3.1), we would see how the macroscopic pointer selects one outcome or other. I emphasize that the final outcome depends on the initial position configuration of the system, which is not known. Otherwise we could have known the output before measuring.

The differences are clear, in the orthodox theory the observer has a big role, without it, there would not be any collapse. Randomness appears exactly when measuring. This is why the observer plays and important role, and where questions such as *what is to measure?* appear. On the other hand, in Bohmian mechanics, to measure is just another way of disturbing the system which should be taken into account, and therefore measuring is just a kind of distortion of the system and the observer plays no role. Randomness appears because our ignorance on the initial positions of the system, which were determined in the Big Bang.

However, to include the apparatus (composed by contacts, leads, cables, pointer...) in the wave function and make computations is clearly impossible, as I mentioned previously we are only able to solve numerically problems of a few particles. Here it is where

the conditional wave function is very useful. We can obtain the wave function of the subsystem without including the apparatus, and evolve it according to a similar equation as Equation (3.1), but now including two additional (in general non-linear) terms. This what I call hereafter a pseudo-dynamical equation. For linear band structures it corresponds to a pseudo-Dirac equation and in parabolic band structures it corresponds to a pseudo-Schrödinger equation.

3.3.2 Wave equation for the Conditional Wave Function

The idea to obtain the dynamical equation for the conditional wave function is to find a similar equation as the Schrödinger equation, but just for the few degrees of freedom that we are interested in [72]. Here, for simplicity, I will consider that we are just interested in one particle, the $a-th$ one.

We start from the many particle Schrödinger equation:

$$i\hbar\frac{\partial\Psi(\tilde{\mathbf{x}}_{\mathbf{N}},t)}{\partial t}=\left[-\sum_i\frac{\hbar^2}{2m_i^*}\nabla_i+V(\tilde{\mathbf{x}}_{\mathbf{N}},t)\right]\Psi(\tilde{\mathbf{x}}_{\mathbf{N}},t) \tag{3.6}$$

where m_i^* is the effective mass of the $i-th$ electron, $V(\tilde{\mathbf{x}}_{\mathbf{N}},t))$ the many-body potential and $\Psi(\tilde{\mathbf{x}}_{\mathbf{N}},t)$ is the many body wave function. From here, if we put the wave function in the polar form:

$$\Psi(\tilde{\mathbf{x}}_{\mathbf{N}},t)=R(\tilde{\mathbf{x}}_{\mathbf{N}},t)e^{\frac{i}{\hbar}S(\tilde{\mathbf{x}}_{\mathbf{N}},t)} \tag{3.7}$$

and I introduce this Equation (3.7) in Equation (3.6) and split it in the real and complex part, I obtain the quantum Hamilton-Jacobi equation as well as a continuity equation:

$$\frac{\partial S(\tilde{\mathbf{x}}_{\mathbf{N}},t)}{\partial t}+U(\tilde{\mathbf{x}}_{\mathbf{N}},t)+\sum_i^N\left(\frac{(\nabla_i S(\tilde{\mathbf{x}}_{\mathbf{N}},t))^2}{2m_i^*}-\frac{\hbar^2}{2m_i^*}\frac{\triangle_i R(\tilde{\mathbf{x}}_{\mathbf{N}},t)}{R(\tilde{\mathbf{x}}_{\mathbf{N}},t)}\right)=0 \tag{3.8}$$

$$\frac{\partial R^2(\tilde{\mathbf{x}}_{\mathbf{N}},t)}{\partial t}+\sum_i^N\nabla_i\left(R^2(\tilde{\mathbf{x}}_{\mathbf{N}},t)\frac{\nabla_i S(\tilde{\mathbf{x}}_{\mathbf{N}},t)}{m_i^*}\right)=0 \tag{3.9}$$

From here, the velocity field of the $i-th$ particle is identified as:

$$\vec{v_i}(\tilde{\mathbf{x}}_{\mathbf{N}},t)=\frac{\nabla_i S(\tilde{\mathbf{x}}_{\mathbf{N}},t)}{m_i^*} \tag{3.10}$$

Now, I will search similar equations as Equation (3.6), but this time corresponding for the evolution of the conditional wave function of the $a-th$ electron, i.e., $\psi(\vec{x_a},t)=\Psi(\tilde{\mathbf{x}}_{\mathbf{N}},t)|_{\vec{x_2}=\vec{X_2}(t),\ldots,\vec{x_N}=\vec{X_N}(t)}$ and then I will find similar equations as Equation (3.8) and Equation (3.9). So, let me write:

$$i\hbar\frac{\partial\psi(\vec{x_a},t)}{\partial t} = \left[-\frac{\hbar^2}{2m_a^*}\frac{\partial}{\partial\vec{x}_a}+u(\vec{x_a},t)\right]\psi(\vec{x_a},t) \tag{3.11}$$

where the only different term compared to Equation (3.6) is $u(\vec{x_a},t)$. This potential term can be decomposed as:

$$u(\vec{x_a},t)=V(\vec{x_a},t)+A(\vec{x_a},t)+iB(\vec{x_a},t) \tag{3.12}$$

Let me explain a bit more this term. The $A(\vec{x_a},t)$ and $B(\vec{x_a},t)$ terms are some terms whose shape I will determine below. The total many-body potential $V(\tilde{\mathbf{x}}_{\mathbf{N}},t)$ has been decomposed in two terms, one containing the degrees of freedom of the first particle, and the other without it, i.e., $V(\tilde{\mathbf{x}}_{\mathbf{N}},t)=V(x_a,\vec{X}_i(t),t)|_{i\neq 1}+V(\tilde{\mathbf{x}}_{\mathbf{N-1}},t)=V(\vec{x_a},t)+V(\tilde{\mathbf{x}}_{\mathbf{N-1}},t)$. The term $V(\tilde{\mathbf{x}}_{\mathbf{N-1}},t)$ is included in $A(\vec{x_a},t)$.

In a similar way as done for obtaining Equation (3.8) and Equation (3.9), i.e., writing the conditional wave function in the polar form:

$$\psi(\vec{x_a},t)=\Psi(\vec{x_a},\vec{X}_i(t),t)|_{i\neq 1}=R((\vec{x_a},\vec{X}_i(t),t)e^{\frac{i}{\hbar}S(\vec{x_a},\vec{X}_i(t),t)}|_{i\neq 1}=r(\vec{x_a},t)e^{\frac{i}{\hbar}S(\vec{x_a},t)} \tag{3.13}$$

and substituting it in Equation (3.11) and splitting the real and complex part I can find the two following equations:

$$\frac{\partial s(\vec{x_a},t)}{\partial t}+\left(\frac{(\nabla_a s(\vec{x_a},t),t))^2}{2m_i^*}-\frac{\hbar^2}{2m_i^*}\frac{\triangle_a\, r(\vec{x_a},t)}{r(\vec{x_a},t)}\right)+V(\vec{x_a},t)+V(\tilde{\mathbf{x}}_{\mathbf{N-1}},t)$$
$$+\quad\sum_{i,i\neq 1}^{N}\left(\frac{(\nabla_i S(\tilde{\mathbf{x}}_{\mathbf{N}},t))^2}{2m_i^*}-\frac{\hbar^2}{2m_i^*}\frac{\triangle_i\, R(\tilde{\mathbf{x}}_{\mathbf{N}},t)}{R(\tilde{\mathbf{x}}_{\mathbf{N}},t)}-\frac{(\nabla_i S(\tilde{\mathbf{x}}_{\mathbf{N}},t))^2}{m_i^*}\right)=0 \tag{3.14}$$

$$\frac{\partial r^2(\vec{x_a},t),t)}{\partial t}+\nabla_a\left(r^2(\vec{x_a},t),t)\frac{\nabla_a s(\vec{x_a},t),t)}{m_i^*}\right) \tag{3.15}$$
$$+\quad\sum_{i\neq 1}^{N}\left[\nabla_i\left(R^2(\tilde{\mathbf{x}}_{\mathbf{N}},t),t)\frac{\nabla_i S(\tilde{\mathbf{x}}_{\mathbf{N}},t)}{m_i^*}\right)-\nabla_i\left(R^2(\tilde{\mathbf{x}}_{\mathbf{N}},t)\frac{\nabla_i S(\tilde{\mathbf{x}}_{\mathbf{N}},t)}{m_i^*}\right)\right]=0$$

From here, once again I can define a velocity field for the $a-th$ electron:

$$\vec{v_a}(\tilde{\mathbf{x}}_{\mathbf{N}},t)=\frac{\nabla_a s(\vec{x}_a,t)}{m_a^*} \tag{3.16}$$

The first requirement for Equation (3.11) is that it reproduces the same physics and results as Equation (3.6). In Bohmian mechanics, this assertion is the same as saying that both equations Equation (3.6) and Equation (3.11) reproduces the same particle velocities. It is straightforward to notice that since the derivatives in Equation (3.16) only depends on $\vec{x}_a$, the velocities obtained from Equation (3.6) and Equation (3.11) are exactly the same ones.

In addition, from Equation (3.14) and Equation (3.16) and comparing them with Equation (3.8) and Equation (3.9), one can identify the exact shape of the $u(\vec{x_a},t)$ potential terms in Equation (3.12):

$$A(\vec{x_a},t)=V(\tilde{\mathbf{x}}_{\mathbf{N-1}},t)+\sum_{i,i\neq 1}^{N}\left(\frac{(\nabla_i S(\tilde{\mathbf{x}}_{\mathbf{N}},t))^2}{2m_i^*}-\frac{\hbar^2}{2m_i^*}\frac{\triangle_i\, R(\tilde{\mathbf{x}}_{\mathbf{N}},t)}{R(\tilde{\mathbf{x}}_{\mathbf{N}},t)}-\frac{(\nabla_i S(\tilde{\mathbf{x}}_{\mathbf{N}},t))^2}{m_i^*}\right) \tag{3.17}$$

$$B(\vec{x_a},t)=\frac{\hbar^2}{m_i^*}\sum_{i\neq 1}^{N}\left[\nabla_i\left(R^2(\tilde{\mathbf{x}}_{\mathbf{N}},t),t)\frac{\nabla_i S(\tilde{\mathbf{x}}_{\mathbf{N}},t)}{m_i^*}\right)-\nabla_i\left(R^2(\tilde{\mathbf{x}}_{\mathbf{N}},t)\frac{\nabla_i S(\tilde{\mathbf{x}}_{\mathbf{N}},t)}{m_i^*}\right)\right] \tag{3.18}$$

Obviously, we have just moved the many-body problem into the $A(\vec{x_a}, t)$ and $B(\vec{x_a}, t)$ terms, but if we were able (something impossible in general) to know these two terms, the Schrödinger equation (which has 3N degrees of freedom) would have been decomposed in 3N equations (with just one degree of freedom each one).

The existence of a dynamical equation for the conditional wave function is very important, even if in principle it is not possible to know its exact value. With educated guesses, it is possible to estimate these terms, and then it allows to make approximations which are not possible in the orthodox theory.

3.4 Measurement problem

As I showed in Chapter 2, there are several quantum theories available in the literature that, by construction, are empirically equivalent when explaining all quantum phenomena. Among others, the so-called Copenhagen or orthodox theory [73, 74], Bohmian mechanics [66, 67, 75, 76] or the many-worlds theory [57]. I also discussed in Chapter 3 that different theories provide different formalisms, a set of mathematical rules (using elements such as wave functions, operators, trajectories) that allow us to make practical computations that reproduce experimental results. Theories also provide different interpretations about the reality. Interpretations try to provide a deep connection on how the mathematical rules and its elements explain how nature works.

Many people argue that the only important part of a quantum theory (once we know it is empirically valid) is its formalism because it is the only part we need to make computations. Certainly, one can make computations using any of the available formalisms without worrying about its interpretation. At the end of the day, by construction, each theory should give the same predictions (otherwise it is not a correct theory). Other people argue that even when one is only interested in computations, a correct understanding of the interpretation issues of each theory is fruitful because it provides an enlarged vision about how correctly apply the theory in unsolved problems (abandoning the *shut up and calculate* [77]).

In Section 3.4.1 I present the orthodox understanding of the measuring problem from the orthodox and Bohmian point of view respectively. In 3.4.2 I discuss the Bohmian understanding, and how the conditional wave function can help us. Since in Chapter 6 I will discuss quantum fluctuations in electron devices, where consecutive measurements occur, I will analyze the measurement problem with a noise example.

3.4.1 Orthodox perspective: Multi-time measurement with operators

A common scenario when discussing quantum noise in electrical devices is a flux of electrons impinging upon a partially transparent barrier (located in the middle of the active region). Electron transport through the barrier takes place by tunnelling. Electron is either transmitted or reflected, but not both! [78–80] The electron probability of being transmitted is T, while being reflected is $R = 1 - T$. To simplify the discussion, I consider a constant injection of electrons (at zero temperature), one by one. Each electron, after measurement at time t_1, will appear randomly at the left or the right of the barrier. The time averaged number of transmitted electrons will be proportional to T, but the number of transmitted electrons fluctuates instantaneously because of the randomness of the transmission. These fluctuations on the number of transmitted electrons (when compared with the DC signal) are named partition noise [80–82][4].

I consider a very simple example, but with a detailed discussion of the role played by the measuring apparatus (the ammeter). The Copenhagen interpretation associates a wave function $\Psi(\tilde{\mathbf{x}}_\mathbf{N}, t)$ to a system of N particles. In principle, such wave function *lives* in a $3N+1$ dimensional configuration space. Within the first non-relativistic quantization language, the evolution of this wave function is defined by two laws [71]. The first law, known as Schrödinger equation, states that (when the system is not measured) the wave function evolves unitarily and deterministically according to the following equation

$$i\hbar \frac{\partial \Psi(\tilde{\mathbf{x}}_\mathbf{N}, t)}{\partial t} = H\Psi(\tilde{\mathbf{x}}_\mathbf{N}, t) \tag{3.19}$$

where $H = \left[\sum_i -\frac{\hbar^2}{2m_i}\nabla_i^2 + U(\vec{x}_N, t)\right]$. With $U(\vec{x}_N, t)$ we denote a generic interaction potential in the position representation, with m_i the mass of the i-th particle and with $\tilde{\mathbf{x}}_\mathbf{N} = (x_1, x_2, ..., x_N)$ the multidimensional vector in the configuration space.

To provide a simple discussion of the partition noise in a tunnelling barrier, let me assume that each electron in the experiment can be described by a single-particle wave function (I neglect the exchange and the Coulomb interaction among electrons). In Figure 3.2 the (unitary) evolution of such wave function solution of Equation (3.19) is plotted. However, the (unitary) Schrödinger equation alone depicted in Figure 3.2 is not enough to understand quantum noise. The orthodox theory has a second law, known as the *collapse* of the wave function, that takes into account the effects of the interaction of a measuring apparatus with the quantum (sub)system [71]. It requires a new non-unitary operator A. This operator is different from the Hamiltonian seen below Equation (3.19)

[4] There are many other sources of noise in electrical devices, for example, the $1/f$ noise which become very relevant at low frequencies [41, 81]. Here, I will only deal with partition noise due to a tunnelling barrier.

and it must be able to encapsulate all the interactions of the quantum systems with the rest of the particles (including the ammeter, the cables, the environment, etc). This new operator A is the only tool provided by the theory to determine the possible results of a measurement. In principle we do not know anything about this operator except that it is a (hermitian $A = A^\dagger$) function whose (real) eigenvalues a_n of its spectral decomposition are the possible results of the measurement. Once the system in Figure 3.3 is measured (and not before), the wave function is projected to one of the eigenstates of the mentioned operator in a non-unitary evolution.[5] After the collapse, the *new* wave packet evolves again according to the time-dependent Schrödinger equation until a new measurement is done.

For simplicity, in the present conceptual discussion let me assume a reasonable (but ad-hoc) operator (why this operator is reasonable will be clarified in Section 3.4.2). Such operator provides the following perturbation of the wave function. If the electron is *randomly* measured as a reflected electron at t_1, the transmitted part of the wave function is eliminated. This measuring process corresponds to Figure 3.3 (c) and (d) where only the reflected wave function survives after t_1. Equivalently, the measurement process associated to *randomly* getting a transmitted electron corresponds to eliminating the reflected part, as seen in Figure 3.3 (g) and (h).

Now, by comparing the evolutions of the wave functions in Figure 3.2 and Figure 3.3, it is obvious that the former is wrong. Consider that I make a two time measurement (this is the case when measuring quantum fluctuations as it will be shown in Chapter 6). By looking at Figure 3.2, it could be the case that an electron found at time t_1 on the right (transmitted) can be found in a later time t_2 on the left as a reflected electron (see the evolution of the probability density in Figure 3.2). This sequence of possibilities is wrong. Experimental results confirm that once, say time t_1, the electron is detected at one side, in a later time t_2 it is always found at the same side. Then, it is obtained a very valuable lesson from the Copenhagen explanation: the (unitary) Schrödinger equation alone is not able to explain completely quantum noise. It is necessary to include the collapse of the wave function to understand properly what is quantum noise (temporal correlations). The popular arguments that *"Shot noise is a consequence of quantization of charge"* [41] or *"This is the noise that arises from the graininess of the current"* [80] emphasize exactly this very point.

All mentioned orthodox formalisms dealing with quantum noise reproduce experimental results successfully because they include the measurement process inside [78–83, 170]. Most of them do not discuss explicitly which is the operator associated with the ammeter.

[5] The measurement described in most textbooks is called "projective" (*strong*) measurement. There exists, for example, another type of measurement known as *weak* measurement, which is useful to describe situations where the effects of the apparatus on the measured system is just a small perturbation.

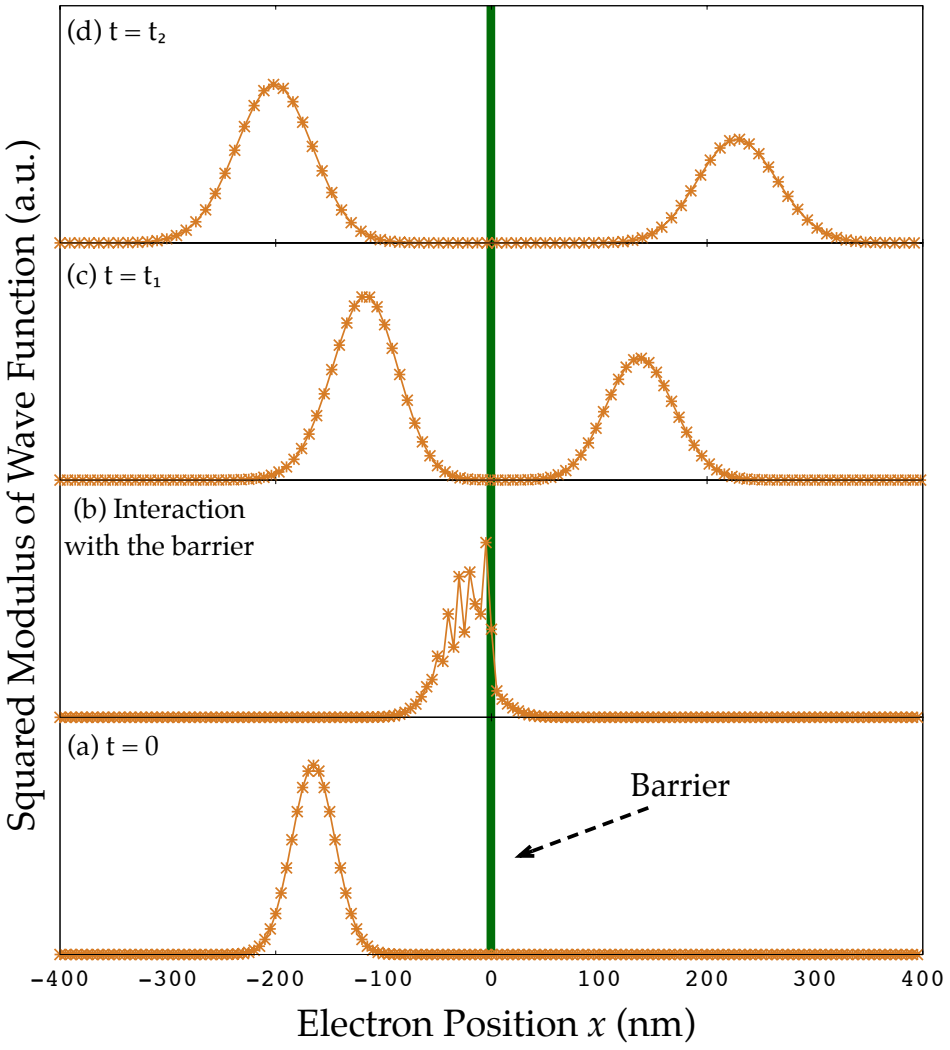

FIGURE 3.2: Evolution of the squared modulus of the wave function of an electron impinging on a tunneling barrier (green solid line). We plot four different times corresponding to (a) initial time, (b) the moment when the wave function interacts with the barrier, (c) the time t_1 when it occurs the first measurement and (d) time t_2 corresponding to the second measurement. At time t_1 and t_2, because of the unitary evolution, the electron can be detected at both sides of the barrier (Color figure online)

Over the years, physicists have identified the operators, by developing instincts on which are the effects of measurements on the wave function. There are scenarios (as the one depicted in Figure 3.3) where is quite obvious which operator is the *right* one. On the contrary, for example, when measuring the total (conduction plus displacement) current it is not at all obvious which are the relevant operators. Is this measurement process *continuous* or *instantaneous*? Does it provide a *strong* or a *weak* perturbation of the wave function? The answers to these questions are certainly not simple. The Copenhagen theory itself does not answer these *technical* questions on how to find the *right* operator. These questions will appear again in Chapter 6.

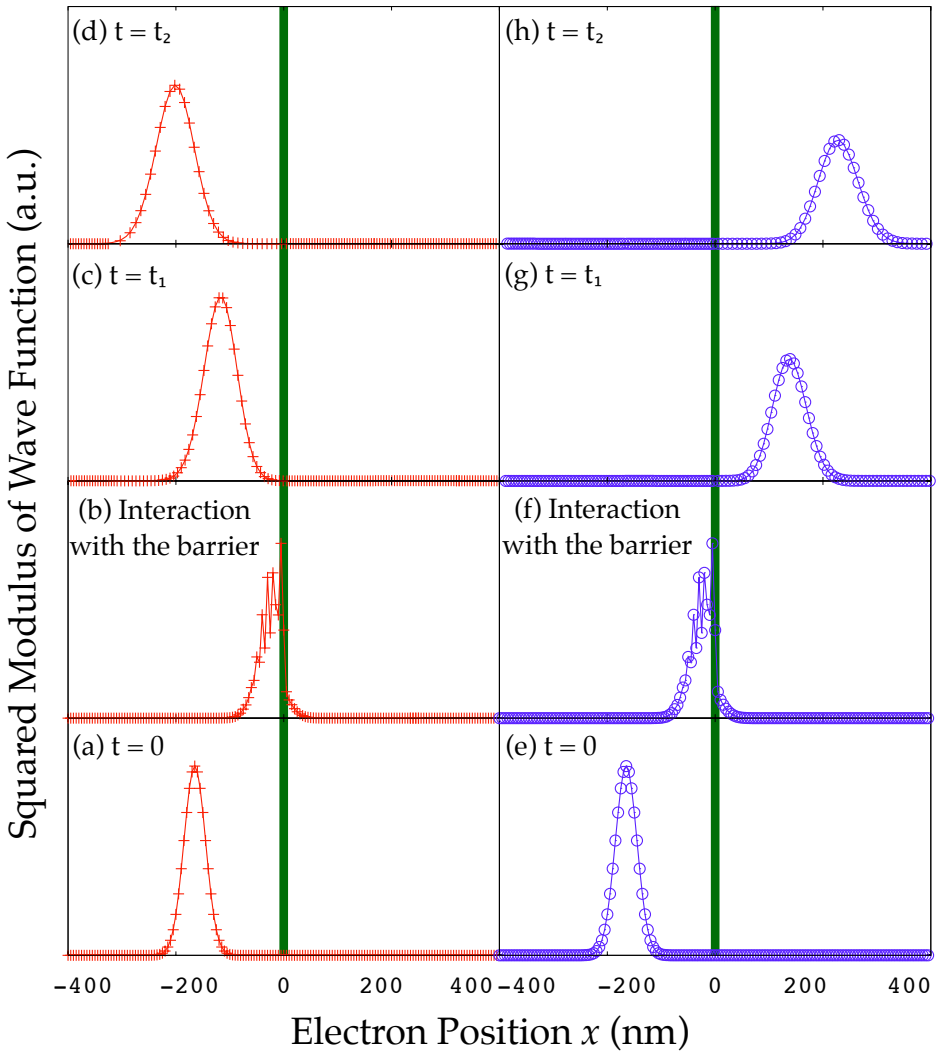

FIGURE 3.3: (a), (b), (c) and (d) Non unitary evolution of the wave function for a reflected electron detected at time t_1 on the left side. (e), (f), (g) and (h) Non unitary evolution of the wave function for a transmitted electron detected at time t_1 on the right side. Symbols are the same of Figure 3.2 (Color figure online)

3.4.2 Bohmian perspective: Multi-time measurement without operators

I have previously discussed how the Copenhagen theory can be used to understand quantum noise in electrical devices. One technical difficulty with this theory is the proper definition of the *right* operator that determines the collapse of the wave function when, for example, the total (conduction plus displacement) current is measured.

In the Bohmian theory, the complete description of a quantum system of N particles is given by the (same) wave function, $\tilde{\mathbf{x}}_\mathbf{N}$ mentioned in Section 3.4.1, and by the actual positions of the point-like particles, $\vec{X}_N(t) = (X_1(t), X_2(t), ..., X_N(t))$.

A proper ensemble of the Bohmian trajectories (proper means that the initial position of each trajectory of the ensemble is selected according to the initial squared modulus of the wave function, see Chapter 3) reproduces the time-evolution of the many particle wave function, at any later time.

In Section 3.4.1, I showed that in order to reproduce the experimental results, I have used the notion of operators to describe how the wave function of a measured system is modified under the measurement process. In the Bohmian theory, I simply consider the apparatus as another (big and complex) quantum system interacting with our measured system. The interaction among them is then included in the Hamiltonian of Equation (3.19) as any other interaction. Then from the unitary evolution of the many-particle wave function (system plus apparatus) I can look at the behavior of the wave function of the measured system (Equation (3.11)).

Let me provide a quite realistic (in particular, non-instantaneous, but in some ways schematic) example in which I can numerically track the behavior of the conditional wave function during the measurement process of the partition noise discussed in Section 3.4.1. The quantum system is an electron labeled as X_1 impinging on an external tunneling barrier. Behind the barrier there is a measuring device, that I call "transmitted charge detector" modeled as a single degree of freedom X_2 (thought as the center of mass of a complex system), which can detect the successful transmission of an electron[6]. First, there is an interaction of the electron with the potential barrier and, subsequently, an interaction with the transmitted charge detector. It is important to stress that both interactions are regarded at the very same level within Bohmian mechanics. The measurement interaction introduces a channeling of the wave function in the configuration space such that the desired property of the "quantum system" (here, whether the electron is reflected or transmitted) can be read off from the final position X_2 of a particle, thought of as the pointer of the apparatus. The interaction between the electron and the pointer can be modeled as:

$$H_{int} = \lambda Q(x_1) P_{x_2} = -i\hbar\lambda Q(x_1)\frac{\partial}{\partial x_2}, \tag{3.20}$$

where $P_{x_2} = -i\hbar\partial/\partial x_2$ is the momentum operator of the detector and $\lambda = 50\ nm/ps$ is the interaction constant. $Q(x_1)$ is a function that is equal to zero when the electron is outside the detector, ($x_1 < 75\ nm$ in Figure 3.4), and is equal to one when the particle

[6]Obviously, a pointer is not just a particle, but this fact has no relevance in this discussion.

is inside the detector ($x_1 > 75\ nm$).[7] In Figure 3.4 the region in the configuration space in which this function is different from zero is represented by a rectangle. The many-particle Schrödinger equation reads:

$$i\hbar\frac{\partial\Psi(x_1,x_2,t)}{\partial t}=\Big(-\frac{\hbar^2}{2m}\frac{\partial^2}{\partial x_1^2}-\frac{\hbar^2}{2M}\frac{\partial^2}{\partial x_2^2}+U(x_1)-i\hbar\lambda Q(x_1)\frac{\partial}{\partial x_2}\Big)\Psi(x_1,x_2,t) \quad (3.21)$$

where m is the effective mass of the electron, M is the mass of the apparatus pointer and $U(x_1)$ is the external potential energy barrier.

The main feature of a transmitted charge detector is that the center of mass of the wave function in the x_2 direction has to move if the electron is transmitted and it has to be at rest if the electron is reflected. I solved Equation (3.21) numerically considering as initial wave function the products of two Gaussian wave packets, i.e., $\Psi(x_1,x_2,0) = \psi(x_1,0)\phi(x_2,0)$. In particular we are considering $M = 75000\ m$. In Figure 3.4 the numerical solution of the squared modulus of $\Psi(x_1,x_2,t)$ is plotted at four different times. At the initial time $t = 0$, Figure 3.4 (a), the entire wave function is at the left of the barrier. At a later time t_0 the wave function has split up into reflected and transmitted parts due to the barrier, see Figure 3.4 (b). Then, because the electron has not yet arrived at the transmitted charge detector, the wave function has the following form:

$$\Psi(x_1,x_2,t_0) = [\psi_T(x_1,t_0) + \psi_R(x_1,t_0)]\,\phi(x_2,t_0) \quad (3.22)$$

After that, Figure 3.4 (c) and (d), the interaction of the detector with the transmitted part of the wave function appears. For time $t > t_0$ the transmitted part of the wave function is shifted up in the x_2 direction while the reflected part does not move. The interaction with the apparatus thus produces two channels in the configuration space, one corresponding to the electron being transmitted and the other corresponding to the electron being reflected, getting an entangled superposition among the electron and the apparatus.

In Figure 3.4 I also plot the actual positions of the system and detector $\{X_1(t), X_2(t)\}$ for four different possible initial positions $\{X_1(0), X_2(0)\}$, corresponding (say) to four distinct runs of the experiment (labelled by $\alpha = 1, ..., 4$). Of the four possible evolutions shown, three show the electron being transmitting ($\alpha = 2, 3, 4$) and one being reflecting ($\alpha = 1$). While the pointer position $X_2(t)$ does not move for the reflected particle, its evolution for the transmitted ones clearly shows a movement. In conclusion, looking at

[7] The transition of $Q(x_1)$, from zero to one, is done softly in order to minimize the perturbation of the "quantum system" as explained in [84].

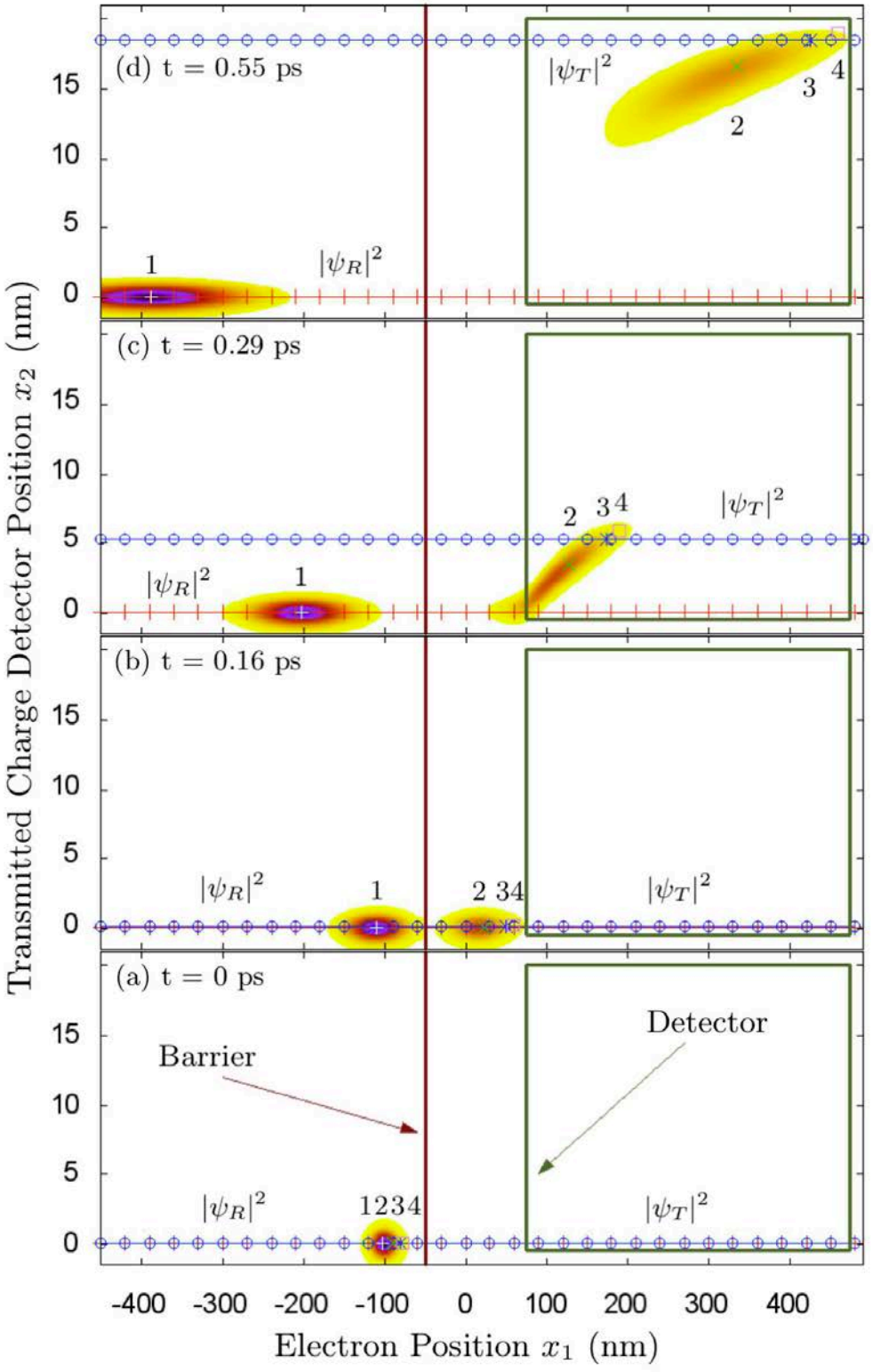

FIGURE 3.4: Time evolution of the squared modulus of $\Psi(x_1, x_2, t)$ at four different times. The configuration space region where the *transmitted charge detector* is present is indicated by a rectangle and the barrier by a solid line. The + line indicates the modulus of the conditional wave function $|\psi_R|^2 = |\Psi(x_1, X_2^{\alpha=1}(t), t)|^2$, while the $\odot$ line corresponds to $|\psi_T|^2 = |\Psi(x_1, X_2^{\alpha=3}(t), t)|^2$. Four trajectories $\{X_1^\alpha(t), X_2^\alpha(t)\}$ with different initial positions are presented with $\square$, $*$, $\times$ and $+$. The actual detector position associated with the reflected trajectory (+) with $\alpha = 1$ does not move because there is no interaction between this trajectory and the detector

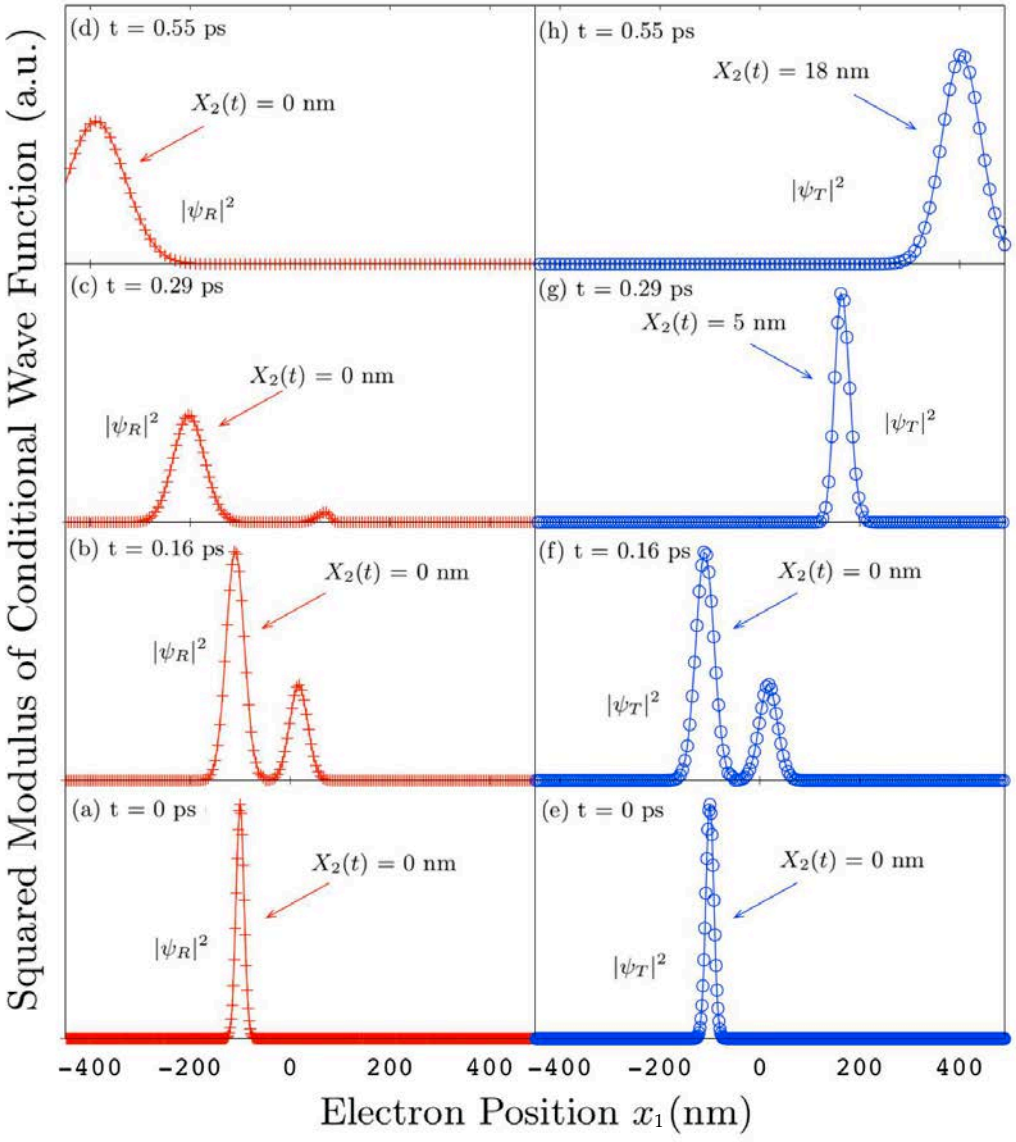

FIGURE 3.5: The + line in (a), (b), (c) and (d) is the time evolution of the squared modulus of the conditional wave function associated to the trajectory $\alpha = 1$ in Figure 3.4, i.e., $\psi_R = |\Psi(x_1, X_2^{\alpha=1}(t), t)|$. The $\odot$ line in (e), (f), (g) and (h) is the squared modulus of the conditional wave function associated to the trajectory $\alpha = 3$ in Figure 3.4. i.e., $\psi_T = |\Psi(x_1, X_2^{\alpha=3}(t), t)|$. The actual detector position $X_2(t)$ is plotted at each time in order to compare these results with those in Figure 3.4 (Color figure online)

the *detector* position I can perfectly certify if the particle has been reflected ($X_1(t) < -50\ nm$ and $X_2(t) = 0\ nm$) or transmitted ($X_1(t) > -50\ nm$ and $X_2(t) \approx 15\ nm$). I hope the reader will realize how trivially we have been able to explain the measurement, using only a *channelized* (unitary) time-evolution of 2D wave function plus two Bohmian trajectories, one for the system and another for the measuring apparatus.

Once the complete problem of the measurement has been solved in (2D) configuration space, I can describe the same measurement in (1D) physical space with the help of the conditional wave function. The key point illustrated here is that the collapse of the one-particle wave function for the electron arises naturally and automatically in Bohmian mechanics, opposite to the orthodox theory, where a second postulate is needed. It is simply a consequence of slicing the unitary-evolving (2D) wave function Ψ along the (moving) line $x_2 = X_2(t)$, resulting $\psi_1(x_1, t) = \Psi(x_1, X_2(t), t)$. In Figure 3.4 I have plotted two solid horizontal lines corresponding to a slice of the wave function at two different values of $X_2(t)$. In Figure 3.5 I report the evolution of these (time-dependent) slices of the many-particle wave function, the *conditional wave function* for the electron, for the trajectories $\alpha = 1$ and $\alpha = 3$ from Figure 3.4. We clearly see that if the particle is reflected, as it is the case for $\alpha = 1$, the position of the pointer does not change with time and, after the interaction with the detector has been performed, the electron's *conditional wave function* includes only a reflected part. See Figs. 3.5 (c) and (d). On the other hand, when the particle is transmitted (e.g., $\alpha = 3$), it is the reflected part of the *conditional wave function* which collapses away, leaving only the transmitted packet. See Figure 3.5 (g) and (h). Note in particular that the evolution of $\psi_1(x_1, t)$ (the electron's *conditional wave function*) is not unitary, even though the evolution of Ψ is.

While a wave function formulation of quantum mechanics provides only statistical information about the experimental results, with the help of the Bohmian trajectories I have been able to recover the individual result of each experiment. In fact for each experiment the pointer of the detector is either moving (corresponding to a transmitted electron) or not (reflected electron), while an ensemble of repeated experiments (where the initial positions of the particles, both the electron $X_1(0)$ and the detector $X_2(0)$, are selected according to the squared modulus of the wave function at the initial time $|\Psi(x_1, x_2, 0)|^2$) reproduce the same statistical results.

Thus with the previous numerical example I have reproduced the collapse-behaviour of the wave function of a transmitted (or reflected) electron. This fact allows me to conclude that the same results of standard formalism (I explained them in Section 3.4.1) are obtained within Bohmian mechanics (see [75, 85] for a formal derivation of the empirical

equivalence of the two theories). Apart from irrelevant technicalities (related to how we define the measuring apparatus) the results in Figure 3.3 and Figure 3.5 are identical.

3.5 The BITLLES simulator

All the formalism explained previously has been introduced in the BITLLES. The simulator has been developed for years by Prof. Xavier Oriols and his research group, in the University Autonoma of Barcelona. Its name is not a coincidence, The acronym BITLLES is also, in the catalan language, the name of bowling pins, which are solid pieces of plastic or wood situated in a periodic structure (similar to a solid-state structure), waiting for a ball (an electron) to impinge on them. It is the only electron device simulator (from my knowledge) using the Bohmian formalism. In a natural way, it is the Monte Carlo simulator heir in the quantum regime. As a brief description it works in the following way: electrons (described initially by a Gaussian wave function and a position) are continuously attempting to enter from the contacts in the electronic device and they injected randomly following the Fermi-Dirac distribution (the injection model will be deeply discussed in Chapter 6). Each electron that successfully enters in the active region has its own pseudo-dynamical equation and evolves according to it while it is inside the active region. Trajectories are obtained from this wave function evolution and quantities such as total current (particle and displacement) or noise are computed from these trajectories.

The most special and relevant characteristic of the BITLLES simulator which makes it so unique is precisely the use of the conditional wave function. When facing the many-body problem, if we have N electrons in the system, in principle we would have to deal with a $\mathbb{R}^{Nd}$ dimensional configuration space and one dynamical equation with $Nd+1$ degrees of freedom. Instead, with the conditional wave function we are able to split the problem ("divide and rule") in N pseudo equations with $d+1$ degrees of freedom. These pseudo equations are coupled through the A and B terms explained before in Section 3.3. This coupling is very important since it allows to introduce different correlations, such as electron-electron interaction beyond mean field. The BITLLES simulator also computes the Poisson equation, and both the Poisson equation and the pseudo-dynamical equations are self-consistently solved.

One of the main goals during my thesis was to improve the simulator. Even if it was highly developed, two important points to be completed and useful for real simulations nowadays were missing. Firstly, it was just thought for ballistic transport. Dissipation was not considered in the simulator, and as it will be seen in Chapter 5, during the thesis a completely positive[86] Bohmian method for scattering was developed and

implemented in the BITLLES [87]. On the other hand, the BITLLES was only conceived for parabolic band structures materials, i.e., the dynamical equation which was solved was always a pseudo-Schrödinger one. During the thesis, the Dirac equation was included, allowing the performance of simulations with linear band structures, such as graphene (this point will be discussed in next Chapter 4. These two additional tools convert nowadays the BITLLES in a extremely versatile and powerful simulator for current electronic devices. Specifically, its time-dependent behaviour makes it an excellent candidate to study all kind of AC properties and parameters.

Part II

PART TWO: DEVELOPMENT OF NUMERICAL RESULTS

Chapter 4

Graphene with trajectories

In Chapter 1, it was described why graphene and other 2D materials are very important for the electronic industry and why it is expected that they make a revolution in the electronics field. In this Chapter I discuss more deeply what are the differences between graphene and other materials (with some numerical examples), how Bohmian trajectories are obtained and how the Dirac equation was introduced in the BITLLES simulator.

4.1 Graphene Structure

Graphene is a two dimensional material (its thickness is one atom) with a hexagonal structure. It is made of carbon atoms, alternating single bonds with double bonds. It exhibits sp2 hybridization, while p_z orbitals are free and are the responsible for the electronic transport[88, 89].

The unit cell of graphene is the one seen in Figure 4.1. It consists of a triangular lattice with a basis of two atoms, named A and B. The distance among two consecutive atoms is $a_C = 1.42$ Å and the vector which links two atoms of the same unit cell is $\vec{\tau} = a\,(0, -1)$, where $a = \sqrt{3}a_C = 2.46$ Å.
The lattice vectors are the following:

$$\vec{a}_1 = a\left(-\frac{\sqrt{3}}{2}, \frac{3}{2}\right) \; and \; \vec{a_2} = a\left(\frac{\sqrt{3}}{2}, \frac{3}{2}\right) \tag{4.1}$$

The first Brillouin zone is a primitive cell in the reciprocal lattice [90]. All the reciprocal vectors are equivalent to one that lies in this zone by a combination of the reciprocal lattice vectors, which are:

$$\vec{G_1} = \left(\frac{2\pi}{3a}, -\frac{2\sqrt{3}\pi}{a}\right) \; and \; \vec{G_2} = \left(-\frac{2\pi}{\sqrt{3}a}, \frac{2\pi}{3a}\right) \tag{4.2}$$

There are two non-equivalent points in the reciprocal space, the so called K and K' points (also called Dirac points). As it will be seen after, these points are of extremely importance because all the relevant electronic properties of graphene occurs at these points. Their coordinates are:

$$\vec{K} = \left(\frac{4\pi}{3\sqrt{3}a}, 0\right) \; and \; \vec{K'} = \left(-\frac{4\pi}{3\sqrt{3}a}, 0\right) \tag{4.3}$$

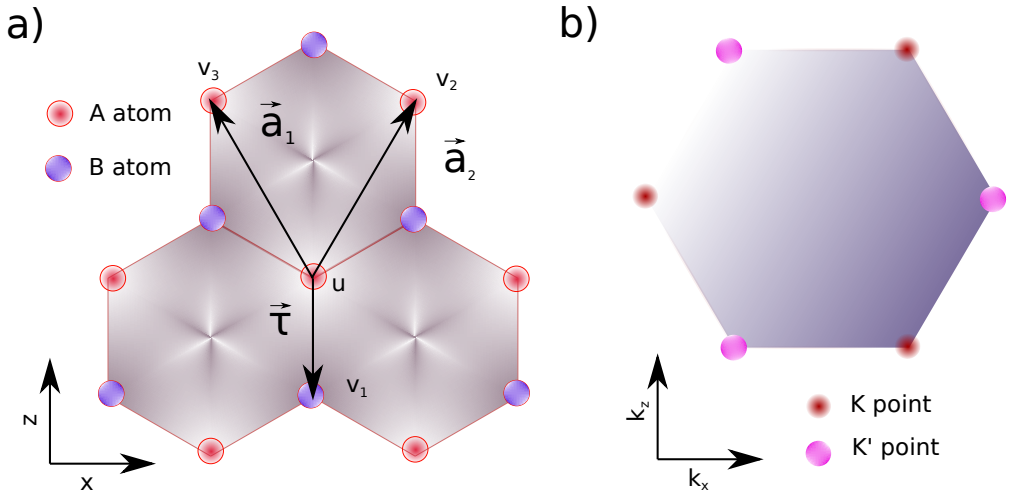

FIGURE 4.1: Graphene structure. a) $\vec{a_1}$ and $\vec{a_2}$ are the lattice vectors. The vector that links the two atoms of the same unit cell is $\vec{\tau}$. b) First Brillouin zone in graphene, the well known Dirac cones lie in the corners (K and K' points).

This K and K' points in the momentum space are special, since at is it is well known, electrons with similar momentum behave as massless relativistic carriers, exhibiting for example the Klein Tunnelling effect. But how can this conclusion be reached? I explain it in the following sections.

4.2 From a Graphene Tight Binding towards the Dirac equation

4.2.1 Towards a Tight Binding equation

As mentioned before, graphene is a 2D periodic structure, with two atoms in its unit cell (A and B). Then, the most general expression to write a time-dependent wave packet is the following:

$$\psi(\vec{r},t) = \sum_{\vec{R}_A} u(\vec{R}_A,t)\phi(\vec{r}-\vec{R}_A) + \sum_{\vec{R}_B} v(\vec{R}_B,t)\phi(\vec{r}-\vec{R}_B) \tag{4.4}$$

where $\phi(\vec{r})$ are a set of "atomic orbitals" (in fact, I can chose any set of single particle wave functions that form a base of the Hilbert space which are enough localized) in the position representation, and therefore orthogonal between them:

$$\int_{-\infty}^{\infty} \phi^*(\vec{r}-\vec{R}_i)\phi^*(\vec{r}-\vec{R}_j)d\vec{r} = \delta_{i,j} \tag{4.5}$$

The sums in Equation (4.4) runs over all atoms positions ($\vec{R}_A$ and $\vec{R}_B$). By construction, u and v are defined as:

$$u(\vec{R}_A,t) = \int_{-\infty}^{\infty} \phi^*(\vec{r}-\vec{R}_A)\psi(\vec{r},t)d\vec{r} \tag{4.6}$$

$$v(\vec{R}_B,t) = \int_{-\infty}^{\infty} \phi^*(\vec{r}-\vec{R}_B)\psi(\vec{r},t)d\vec{r} \tag{4.7}$$

Next, I will consider the following Schrödinger equation:

$$i\hbar\frac{\partial\psi(\vec{r},t)}{\partial t} = \left(H_0 + V(\vec{r},t)\right)\psi(\vec{r},t) \tag{4.8}$$

where H_0 is the kinetic part of the Hamiltonian and $V(\vec{r},t)$ is a time-dependent potential which includes the conditional potential terms from Equation (3.11).

Now, I can multiply Equation (4.8) multiplying by a specific atomic orbital $\phi^*(r-\vec{R}_i)$, where $i = A, B$ and then I obtain:

$$i\hbar\int_{-\infty}^{\infty} \phi^*(\vec{r}-\vec{R}_i)\frac{\partial\psi(\vec{r},t)}{\partial t}d\vec{r} = \int_{-\infty}^{\infty} \phi^*(\vec{r}-\vec{R}_i)\left(H_0 + V(\vec{r},t)\right)\psi(\vec{r},t)d\vec{r} \tag{4.9}$$

Now, I will make the first neighbors tight-binding approximation, i.e., each atom will just interact with itself and with its three nearest neighbors. Then, the terms appearing in Equation (4.9) are the following:

$$\int_{-\infty}^{\infty} \phi^*(\vec{r} - \vec{R}_i) H_0 \phi(\vec{r} - \vec{R}_i) d\vec{r} = \epsilon_i \tag{4.10}$$

Since all atoms are identical, hereafter I will assume $\epsilon_i = 0$, since it is just an energy offset.

$$\int_{-\infty}^{\infty} \phi^*(\vec{r} - \vec{R}_i) H_0 \phi(\vec{r} - \vec{R}_j) d\vec{r} = -t \tag{4.11}$$

where the $-$ sign is used for convention.

$$\int_{-\infty}^{\infty} \phi^*(\vec{r} - \vec{R}_i) V(\vec{r}, t) \phi(\vec{r} - \vec{R}_i) d\vec{r} \approx V(\vec{R}_i) \tag{4.12}$$

$$\int_{-\infty}^{\infty} \phi^*(\vec{r} - \vec{R}_i) V(\vec{r}, t) \phi(\vec{r} - \vec{R}_j) d\vec{r} \approx V(\vec{R}_j) \int_{-\infty}^{\infty} \phi^*(\vec{r} - \vec{R}_i) \phi(\vec{r} - \vec{R}_j) d\vec{r} = 0 \tag{4.13}$$

where i, j are always first neighbors atoms. The approximation performed in Equation (4.12) and Equation (4.13) means that the potential term is smooth (almost constant) along a unit cell. With the above equations we can split Equation (4.9) in two equations, one for u and the other for v:

$$i\hbar \frac{\partial u(\vec{R}_A, t)}{\partial t} = -t \left(v_1(\vec{R}_B, t) + v_2(\vec{R}_B, t) + v_3(\vec{R}_B, t) \right) + V(\vec{R}_A) u(\vec{R}_A, t) \tag{4.14}$$

$$i\hbar \frac{\partial v(\vec{R}_B, t)}{\partial t} = -t \left(u_1(\vec{R}_A, t) + u_2(\vec{R}_A, t) + u_3(\vec{R}_A, t) \right) + V(\vec{R}_B) v(\vec{R}_B, t) \tag{4.15}$$

where the terms in the left hand side of Equation (4.14) (Equation (4.15)) v_1, v_2, v_3 (u_1, u_2, u_3) correspond to the three neighbours of the A (B) atom chosen, see Figure 4.1a). Now, I can define the following Fourier series for $u(\vec{R}_A, t)$ and $v(\vec{R}_B, t)$:

$$u(\vec{R}_A, t) = \sum_{\vec{k}} e^{i\vec{k}\vec{R}_A} a_u(\vec{k}, t) \tag{4.16}$$

$$v(\vec{R}_B, t) = \sum_{\vec{k}} e^{i\vec{k}\vec{R}_B} a_v(\vec{k}, t) \tag{4.17}$$

I mention that the $\vec{k}$ vectors appearing in the expressions above, are the same one appearing in the graphene Bloch functions, since all expressions (Bloch function and Equation (4.16) and Equation (4.17)) are Fourier series of the same system with the same number of atoms and therefore the same discrete $\vec{k}$ values.

Then, the terms v_1, v_2, v_3 (see Figure 4.1a)), u_1, u_2 and u_3 appearing in Equation (4.14) and Equation (4.15) are:

$$v_1(\vec{R}_B, t) = \sum_{\vec{k}} e^{i\vec{k}\vec{R}_B} a_v(\vec{k}, t) \tag{4.18}$$

$$v_2(\vec{R}_B, t) = \sum_{\vec{k}} e^{i\vec{k}(\vec{R}_B - \vec{a}_2)} a_v(\vec{k}, t) \tag{4.19}$$

$$v_3(\vec{R}_B, t) = \sum_{\vec{k}} e^{i\vec{k}(\vec{R}_B - \vec{a}_1)} a_v(\vec{k}, t) \tag{4.20}$$

$$u_1(\vec{R}_A, t) = \sum_{\vec{k}} e^{i\vec{k}\vec{R}_A} a_u(\vec{k}, t) \tag{4.21}$$

$$u_2(\vec{R}_A, t) = \sum_{\vec{k}} e^{i\vec{k}(\vec{R}_A + \vec{a}_2)} a_u(\vec{k}, t) \tag{4.22}$$

$$u_3(\vec{R}_A, t) = \sum_{\vec{k}} e^{i\vec{k}(\vec{R}_A + \vec{a}_1)} a_u(\vec{k}, t) \tag{4.23}$$

$$\tag{4.24}$$

Then I can rewrite Equation (4.14) and Equation (4.15) as:

$$i\hbar\frac{\partial u(\vec{R}_A,t)}{\partial t} = -t\sum_{\vec{k}}\left(1+e^{i\vec{k}\vec{a}_1}+e^{i\vec{k}\vec{a}_2}\right)e^{i\vec{k}\vec{R}_B}a_v(\vec{k},t)+V(\vec{R}_A)u(\vec{R}_A,t)$$
$$= -t\sum_{\vec{k}} f(\vec{k})e^{i\vec{k}\vec{R}_B}a_v(\vec{k},t)+V(\vec{R}_A)u(\vec{R}_A,t) \tag{4.25}$$

$$i\hbar\frac{\partial v(\vec{R}_B,t)}{\partial t} = -t\sum_{\vec{k}}\left(1+e^{-i\vec{k}\vec{a}_1}+e^{-i\vec{k}\vec{a}_2}\right)e^{i\vec{k}\vec{R}_A}a_u(\vec{k},t)+V(\vec{R}_B)v(\vec{R}_B,t)$$
$$= -t\sum_{\vec{k}} f^*(\vec{k})e^{i\vec{k}\vec{R}_A}a_u(\vec{k},t)+V(\vec{R}_B)v(\vec{R}_B,t) \tag{4.26}$$

where $f(\vec{k}) = \left(1+e^{-i\vec{k}\vec{a}_1}+e^{-i\vec{k}\vec{a}_2}\right)$. Equation (4.25) and Equation (4.26) can be written in a matrix way:

$$i\hbar\frac{\partial}{\partial t}\begin{pmatrix} u(\vec{R}_A,t)\\ v(\vec{R}_B,t)\end{pmatrix} = \begin{pmatrix} V(\vec{R}_A) & -tf(\vec{k})\\ -tf^*(\vec{k}) & V(\vec{R}_B)\end{pmatrix}\begin{pmatrix} u(\vec{R}_A,t)\\ v(\vec{R}_B,t)\end{pmatrix} \tag{4.27}$$

Equation (4.27) is all we could need in order to evolve a wave packet in graphene. However, with this equation, we cannot directly understand why electrons in graphene behaves (under some circumstances) as relativistic carriers.

4.2.2 Towards the Dirac equation

For that purpose, we can realize that $f(\vec{k})$ is equal to zero in the Brillouin corners, i.e., $f(K) = f(K') = 0$. By doing a Taylor expansion around momenta close to these points ($\vec{k} = \vec{K}_\alpha + \vec{q}$), we can obtain that (see Appendix A for a detailed derivation):

$$f(\vec{K}_\alpha+\vec{q}) = -\frac{3a}{2}(\alpha q_x - iq_z) \tag{4.28}$$
$$f^*(\vec{K}_\alpha+\vec{q}) = -\frac{3a}{2}(\alpha q_x + iq_z) \tag{4.29}$$

where $\alpha = \pm 1$, being $\vec{K}_1 = K$ and $\vec{K}_{-1}$ the K' point. Therefore, if the momentum of our wave packet (Equation (4.4)) is close to one of these Dirac points, we can rewrite a

new set of u' and v' functions, which are the old ones but translated to a momentum close to the K or K' Dirac points.

$$u'(\vec{R}_A, t) = e^{-iK_\alpha \vec{R}_A} u(\vec{R}_A, t) \tag{4.30}$$

$$v'(\vec{R}_B, t) = e^{-iK_\alpha \vec{R}_B} v(\vec{R}_B, t) \tag{4.31}$$

Then, defining $\vec{q} = \vec{k} - \vec{K}_\alpha$ and using the Fourier translation property, the new Fourier transforms are:

$$u'(\vec{R}_A, t) = e^{-iK_\alpha \vec{R}_A} \sum_{\vec{k}} e^{i\vec{k}\vec{R}_A} a_u(\vec{k}, t) = \sum_{\vec{q}} e^{i\vec{q}\vec{R}_A} a_u(\vec{q}, t) \tag{4.32}$$

$$v'(\vec{R}_B, t) = e^{-iK_\alpha \vec{R}_B} \sum_{\vec{k}} e^{i\vec{k}\vec{R}_B} a_v(\vec{k}, t) = \sum_{\vec{q}} e^{i\vec{q}\vec{R}_B} a_v(\vec{q}, t) \tag{4.33}$$

With Equation (4.32) and Equation (4.33), I can rewrite Equation (4.25) and Equation (4.26) for momenta $\vec{q}$ close to the Dirac points as:

$$\begin{aligned} i\hbar \frac{\partial u'(\vec{R}_A, t)}{\partial t} &= i\frac{3at}{2} \sum_{\vec{q}} (q_x + i\alpha q_z) e^{i\vec{q}\vec{R}_B} a_v(\vec{q}, t) + V(\vec{R}_A) u'(\vec{R}_A, t) \\ = \quad & i\hbar v_f \sum_{\vec{q}} (q_x + i\alpha q_z) e^{i\vec{q}\vec{R}_B} a_v(\vec{q}, t) + V(\vec{R}_A) u'(\vec{R}_A, t) \end{aligned} \tag{4.34}$$

$$\begin{aligned} i\hbar \frac{\partial v'(\vec{R}_B, t)}{\partial t} &= i\frac{3at}{2} \sum_{\vec{q}} (-q_x + i\alpha q_z) e^{i\vec{q}\vec{R}_A} a_u(\vec{q}, t) + V(\vec{R}_B) v'(\vec{R}_B, t) \\ = \quad & i\hbar v_f \sum_{\vec{q}} (-q_x + i\alpha q_z) e^{i\vec{q}\vec{R}_A} a_u(\vec{q}, t) + V(\vec{R}_B) v(\vec{R}_B, t) \end{aligned} \tag{4.35}$$

where I have defined the Fermi velocity as $v_f = -\frac{3ta}{2\hbar} \approx 10^6 \, \frac{m}{s}$. Next step is to realize that (see Appendix A for a detailed derivation):

$$\frac{\partial w(\vec{R}_j,t)}{\partial x} = \frac{\partial}{\partial x} w(\vec{R}_j,t) = i\sum_{\vec{k}} q_x e^{i\vec{k}\vec{R}_j} a_w(\vec{k},t) \tag{4.36}$$
$$\frac{\partial w(\vec{R}_j,t)}{\partial z} = \frac{\partial}{\partial z} w(\vec{R}_j,t) = i\sum_{\vec{k}} q_z e^{i\vec{k}\vec{R}_j} a_w(\vec{k},t)$$

where $(w,j) = (u',A)$ or $(w,j) = (v',B)$. Then we can obtain from Equation (4.34) and Equation (4.35):

$$i\hbar\frac{\partial u(\vec{R}_A,t)}{\partial t} = -i\hbar v_f(\alpha\frac{\partial}{\partial x} - i\frac{\partial}{\partial z})v(\vec{R}_B,t) + V(\vec{R}_A)u(\vec{R}_A,t) \tag{4.37}$$

$$i\hbar\frac{\partial v(\vec{R}_B,t)}{\partial t} = -i\hbar v_f(\alpha\frac{\partial}{\partial x} + i\alpha\frac{\partial}{\partial z})u(\vec{R}_A,t) + V(\vec{R}_B)v(\vec{R}_B,t) \tag{4.38}$$

Finally, Equation (4.37) and Equation (4.38) can be written with a matrix notation:

$$\begin{aligned} i\hbar\frac{\partial}{\partial t}\begin{pmatrix} u(\vec{R}_A,t) \\ v(\vec{R}_B,t)\end{pmatrix} &= -i\hbar v_f \begin{pmatrix} V(\vec{R}_A) & \alpha\frac{\partial}{\partial x} - i\frac{\partial}{\partial z}\frac{\partial}{\partial z} \\ \alpha\frac{\partial}{\partial x} + i\frac{\partial}{\partial z}\frac{\partial}{\partial z} & V(\vec{R}_B)\end{pmatrix}\begin{pmatrix} u(\vec{R}_A,t) \\ v(\vec{R}_B,t)\end{pmatrix} \\ \equiv\ & -i\hbar v_f\left(\vec{\sigma}\cdot\vec{\nabla} + V\right)\begin{pmatrix} u(\vec{R}_A,t) \\ v(\vec{R}_B,t)\end{pmatrix} \end{aligned} \tag{4.39}$$

which is the bispinor Dirac equation. I remark that it acts differently in each valley K or K' (because of α). Unless high momenta values appear, there are not intervalley transitions.

In Equation (4.39), $\vec{\sigma}$ are the Pauli matrices[1]:

$$\vec{\sigma} = (\sigma_x,\sigma_z) = \left(\begin{pmatrix} 0 & 1 \\ 1 & 0\end{pmatrix}, \begin{pmatrix} 0 & -i \\ i & 0\end{pmatrix}\right) \tag{4.40}$$

[1]Usually, in the literature, one finds σ_z as σ_y, however, since I defined the graphene plane as the XZ one, the notation here is different.

4.2.3 Graphene energy dispersion and eigenvectors

4.2.3.1 Energy dispersion

In order to obtain the energy dispersion, I will analyze the time-independent equation version of Equation (4.27) when there is no potential ($V = 0$):

$$E \begin{pmatrix} u(\vec{R}_A) \\ v(\vec{R}_B) \end{pmatrix} = \hbar v_f \begin{pmatrix} 0 & f(\vec{k}) \\ f^*(\vec{k}) & 0 \end{pmatrix} \begin{pmatrix} u(\vec{R}_A) \\ v(\vec{R}_B) \end{pmatrix} \tag{4.41}$$

From here, I can obtain the band structure by solving $|H - EI| = 0$ and I obtain:

$$E = \pm t \left[3 + 2cos(ak_z) + 4cos(\frac{k_z a}{2}) cos(\frac{\sqrt{3}k_x a}{2}) \right]^{\frac{1}{2}} = \pm t |f(\vec{k})| \tag{4.42}$$

This energy dispersion, which is shown in Figure 4.2a), is valid at any $\vec{k}$-point for graphene.

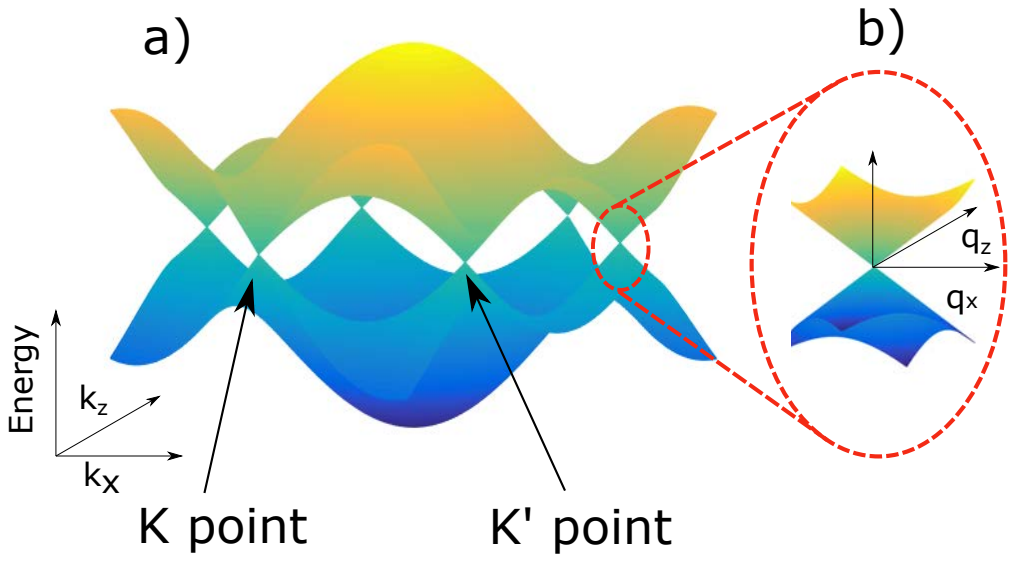

FIGURE 4.2: a) Graphene energy dispersion. b) Graphene energy dispersion around the K and K' points.

Again, if I do a Taylor expansion around the Dirac points, I will obtain the energy dispersion for a massless relativistic particle:

$$E(\vec{q}) = \pm\hbar v_f |\vec{q}| \tag{4.43}$$

It can be clearly seen from Equation (4.43) that we obtain a linear band (see Figure 4.2b)), opposite to the Schrödinger Hamiltonian where we get parabolic bands. Positive energies in Equation (4.43) correspond to electrons in the conduction band, whereas negative energies correspond to electrons in the valence band[2]. The same energy dispersion (Equation (4.43)) could have been also obtained directly by solving the time-independent equation in Equation (4.39).

4.2.3.2 Eigenvectors

Now, let me finally calculate the corresponding eigenfunctions. From Equation (4.43) and Equation (4.41) I get:

$$\pm\hbar v_f |\vec{q}| \begin{pmatrix} u(\vec{R}_A) \\ v(\vec{R}_B) \end{pmatrix} = \hbar v_f \begin{pmatrix} 0 & f(\vec{k}) \\ f^*(\vec{k}) & 0 \end{pmatrix} \begin{pmatrix} u(\vec{R}_A) \\ v(\vec{R}_B,) \end{pmatrix} \tag{4.44}$$

By solving Equation (4.44), two set of eigenfunctions are obtained, one for positive energies and other for negative ones. In the case of positive ones (electrons in the conduction band) I obtain:

$$\begin{pmatrix} u(\vec{R}_A) \\ v(\vec{R}_B) \end{pmatrix} = \frac{1}{\sqrt{2}} \begin{pmatrix} e^{-i\frac{\theta(\vec{q})}{2}} \\ e^{i\frac{\theta(\vec{q})}{2}} \end{pmatrix} e^{iq_x x} e^{iq_z z} \tag{4.45}$$

while for electrons in the valence band (negative energies):

$$\begin{pmatrix} u(\vec{R}_A) \\ v(\vec{R}_B) \end{pmatrix} = \frac{1}{\sqrt{2}} \begin{pmatrix} e^{-i\frac{\theta(\vec{q})}{2}} \\ -e^{i\frac{\theta(\vec{q})}{2}} \end{pmatrix} e^{iq_x x} e^{iq_z z} \tag{4.46}$$

with $\theta(\vec{q})$ defined as:

[2]Sometimes, in the literature, one finds that negative energies correspond to holes, but this is not true[91].

$$tg(\theta(\vec{q})) = \frac{q_z}{q_x} \tag{4.47}$$

It is noticeable the similarities of these eigenfunctions with the Dirac spinor, but I emphasize that it does not have the same meaning as the Dirac spinor, but the contribution of each sublattice A and B in the total wave function in Equation (4.4), because of this similitude, it is called pseudospin. It is also very relevant, that Equation (4.39) is the conditional pseudo-Dirac equation, since the potential term V includes the g and h potential terms (see Equation (3.11)). Therefore, as it was expected, it is just required to add to extra potential terms (one real and the other complex) to the original Dirac equation.

4.3 Graphene electron trajectories

To obtain the current density, I must find out firstly which is the continuity equation and then obtain the current. One must follow the same procedure as it is done with the Schrödinger Hamiltonian but now using the Dirac Hamiltonian (Equation (4.48)).

$$i\hbar\frac{\partial\psi(\vec{r},t)}{\partial t} = -i\hbar v_f(\vec{\sigma}\cdot\vec{\nabla})\psi(\vec{r},t) \tag{4.48}$$

Now, I multiply the Hamiltonian by the conjugated wave function:

$$\psi(\vec{r},t)^\dagger i\hbar\frac{\partial\psi(\vec{r},t)}{\partial t} = -i\psi(\vec{r},t)^\dagger\hbar v_f(\vec{\sigma}\cdot\vec{\nabla})\psi(\vec{r},t) \tag{4.49}$$

and I conjugate and transpose this last equation (Equation (4.49)):

$$\psi(\vec{r},t)\frac{\partial\psi(\vec{r},t)^\dagger}{\partial t} = -\psi(\vec{r},t)v_f(\vec{\sigma}\cdot\vec{\nabla})\psi(\vec{r},t)^\dagger \tag{4.50}$$

This last relationship is possible because the Pauli matrices are hermitian. If I now subtract Equation (4.49) - Equation (4.50) I get:

$$\psi(\vec{r},t)^\dagger\frac{\partial\psi(\vec{r},t)}{\partial t} - \psi(\vec{r},t)\frac{\partial\psi(\vec{r},t)^\dagger}{\partial t} = -\left[\psi(\vec{r},t)^\dagger v_f(\vec{\sigma}\cdot\vec{\nabla})\psi(\vec{r},t) - \psi(\vec{r},t)v_f(\vec{\sigma}\cdot\vec{\nabla})\psi(\vec{r},t)^\dagger\right] \tag{4.51}$$

which leads directly to the continuity equation:

$$\frac{\partial|\psi(\vec{r},t)|^2}{\partial t} + \vec{\nabla}\cdot\left(v_f\psi(\vec{r},t)^\dagger\vec{\sigma}\psi(\vec{r},t)\right) = 0 \tag{4.52}$$

where I can easily identify the density current as:

$$\vec{J}(\vec{r},t) = v_f\psi(\vec{r},t)^\dagger\vec{\sigma}\psi(\vec{r},t) \tag{4.53}$$

From here, I can also identify the Bohmian velocities, because (similarly as it was done in Chapter 3) $\vec{J}(r,\vec{t}) = \rho\vec{v} = |\psi(\vec{r},t)|^2\vec{v}$:

$$\vec{v}(\vec{r},t) = \frac{J(\vec{r},t)}{|\psi(\vec{r},t)|^2} = \frac{v_f\psi(\vec{r},t)^\dagger\vec{\sigma}\psi(\vec{r},t)}{|\psi(\vec{r},t)|^2} \tag{4.54}$$

In the case of dealing with the eigenfunctions shown in Equation (4.45) and Equation (4.46), the Bohmian velocities are:

$$v_x(\vec{r},t) = \frac{J_x(\vec{r},t)}{|\psi(\vec{r},t)|^2} = \frac{v_f\psi(\vec{r},t)^\dagger\sigma_x\psi(\vec{r},t)}{|\psi(\vec{r},t)|^2} = v_f cos(\theta(\vec{q})) \tag{4.55}$$

$$v_z(\vec{r},t) = \frac{J_z(\vec{r},t)}{|\psi(\vec{r},t)|^2} = \frac{v_f\psi(\vec{r},t)^\dagger\sigma_z\psi(\vec{r},t)}{|\psi(\vec{r},t)|^2} = v_f sin(\theta(\vec{q})) \tag{4.56}$$

Since Equation (4.55) and Equation (4.56) are independent of s, it it is noticeable that independently if electrons are in the conduction or valence band, electron move in the same direction. It is important to emphasize that this wave function corresponds to the (plane waves) Hamiltonian eigenstates. Thus, the following Bohmian velocity are only valid for such wave functions. In the case of any other wave function, Equation (4.54) should be used to obtain the velocities.

4.4 Analytic evolution of a Gaussian wave packet in graphene

In this section, I will present an approximated solution for the evolution of a free particle (when its potential energy is zero everywhere) described by a Gaussian wave packet in graphene. With the Schrödinger equation, this problem is completely analytic, and we can obtain a simple equation which describes the motion of a free particle[71]. The initial Gaussian wave packet is:

$$\Psi_G(x,0) = \left(\frac{2}{\pi a^2}\right)^{1/4} e^{ik_0x}e^{-\frac{x^2}{a^2}} \tag{4.57}$$

being $\frac{a}{2}$ the initial dispersion and the central momentum of the wave packet k_0.

$$\Psi_G(x,t) = \left(\frac{2a^2}{\pi}\right)^{1/4} \frac{e^{i\phi}e^{ik_0x}}{\left(a^4 + \frac{4\hbar^2t^2}{m^2}\right)^{1/4}} e^{-\frac{\left(x-\frac{\hbar k_0 t}{m}\right)^2}{a^2+\frac{2i\hbar t}{m}}} \tag{4.58}$$

where m is the electron effective mass, $\phi = -\theta - \frac{\hbar k_0^2 t}{2m}$ with $tan(2\theta) = \frac{2\hbar t}{ma^2}$. Then, the spreading of the wave packet is:

$$a(t) = \frac{a}{2}\sqrt{1 + \frac{4\hbar^2t^2}{m^2a^4}} \tag{4.59}$$

When dealing with the bispinor Dirac equation, the analytic solution of a Gaussian wave packet has no longer an analytic solution. The main problem occurs because the Dirac energy dispersion is no longer separable, contrary to the parabolic dispersion obtained with the Schrödinger equation. However, when making one approximation (which I will discuss at the end of this section), one can reach an equation for its motion. Here, I will just show the results, in order to see the complete derivation, see Appendix B. The initial bispinor Gaussian wave packet is the following:

$$\Psi_G(x,z,0) = \begin{pmatrix}\psi_1\\ \psi_2\end{pmatrix} = \begin{pmatrix}s_1\\ s_2\end{pmatrix} \frac{1}{\sqrt{\sigma_x\sigma_z\pi}} e^{-\frac{(x-x_0)^2}{2\sigma_x^2}} e^{-\frac{(z-z_0)^2}{2\sigma_z^2}} e^{ik_0x}e^{ik_0z} \tag{4.60}$$

where the central position of the wave packet is (x_0, z_0) and its initial momentum is $\vec{k_0} = (k_{0_x}, k_{0_z})$. Hereafter, I will assume the same initial dispersion for the x and z directions, i.e., $\sigma_x = \sigma_z = a$ and $\begin{pmatrix}s_1\\ s_2\end{pmatrix} = \begin{pmatrix}1\\ e^{i\theta_{k_0}}\end{pmatrix}$ where $\theta_{k_0} = arctg(k_{z_0}/k_{x_0})$. This last assumption is to guaranteed that most of the eigenstates composing the Gaussian wave packet belongs to the same (either positive or negative) band. Then, one can reach the following analytic equation for the wave packet:

$$\Psi_G(x,z,t) = C_4 exp(-\frac{\sigma_z^2(t)}{2}k_{z_0}^2) exp(-i(z - z_0 - v_f\frac{k_{z_0}}{|k_0|}t)) \sqrt{\frac{2\pi}{\sigma_z^2(t) + v_f^2\frac{k_{x_0}^2k_{z_0}^2k_z^2}{4\sigma_x^2(t)|k_0|^6}t^2}}$$
$$exp\left(\frac{\left(\frac{-(x-x_0-v_f\frac{k_{x_0}}{|k_0|}t - v_f\frac{k_{x_0}k_{z_0}^2}{2|k_0|^3}t)v_fk_{x_0}k_{z_0}t}{2|k_0|^3\sigma_x^2(t)} - i(z - z_0 - v_f\frac{k_{z_0}}{|k_0|}t) - k_{z_0}\frac{\sigma_z^2(t)}{2}\right)^2}{2\left(v_f^2\frac{k_{x_0}^2k_{z_0}^2k_z^2}{4\sigma_x^2(t)|k_0|^6}t^2 + \sigma_z^2(t)\right)}\right) \tag{4.61}$$

where C_4 is a constant whose exact shape can be seen in Appendix B. Although establishing the dispersion as a function of time for the wave packet is not directly seen in Equation (4.61), what I can see from Equation (B.17), Equation (B.18) and Equation (4.61) is that in the case where $k_{x_0} = 0$ ($k_{z_0} = 0$), the dispersion $\sigma_x(t) = a$ ($\sigma_z(t) = a$) and therefore there is no dispersion in the x (z) direction, only in the z (x) direction. This fact is also understood from Equation (4.55) and Equation (4.56), the velocity depends on the angle $\theta(\vec{q})$, which in the case of propagation in the x (z) direction $\theta(\vec{q}) = 0$ ($\theta(\vec{q}) = \frac{\pi}{2}$) and then $v_z = 0$ ($v_x = 0$). This is completely different from the Schrödinger case, where its dispersion, given by Equation (4.59) is independent of the initial values of the initial momentum, i.e., the wave packet will always spread.

In order to obtain Equation (4.61), the only approximation I made was to assume $\theta_k \approx \theta_{k_0}$. In Figure 4.3, where two different wave packets are plotted in the momentum space, we can clearly see which are the implications of such approximation. Let me consider two different situations. The first one (Figure 4.3 a)) wave packets, labelled 1 and 2, with (in the momentum space) different momentum dispersion, where $\sigma_{k_1} = \frac{1}{a_1} > \sigma_{k_2} = \frac{1}{a_2}$ and the same energy $|k_1| = |k_2|$. In that case, if we approximate in both wave packets θ_k by θ_{k_0}, clearly there is more difference in the wave packet 2 between the maximum value of θ_k and θ_{k_0} ($\Delta\theta_{k_1} < \Delta\theta_{k_2}$) and the approximation will be less accurate for that wave packet. In the other scenario (Figure 4.3 b)), where both wave packets (labelled by 1 and 3) have the same momentum dispersion ($\sigma_{k_1} = \frac{1}{a_1} = \sigma_{k_3} = \frac{1}{a_3}$) but different energy ($|k_1| > |k_3|$), because of similar argument we see that $\Delta\theta_{k_1} < \Delta\theta_{k_3}$ and the approximation is less accurate for wave packet 3. As a summary, the approximation works better for extended wave packets in real space (large dispersion are translated into small momentum dispersions) and for higher energies than lower.

In Figure 4.4, we see the evolution of the same wave packet at two different times. In Figure 4.4a), we see the analytic evolution, while in Figure 4.4b) it is plotted the numerical evolution. The dispersion of the Gaussian wave packet is $a = 40\,nm$. Its energy is $E = 0.08eV$ and its initial momentum in the z direction is $k_{z_0} = 0$, and then we expect according to Equation (B.17) we do not expect dispersion in the x direction. Even if the energy is quite low (and then being close to the scenario plotted in Figure 4.3 b)), the evolution of both wave packets is extremely similar. As differences, we can barely appreciate that the numerical wave packet velocity is a bit lower than the numerical one. Also, the dispersion in the numerical one in the z direction is a bit different and it tends to curve the wave packet, while the numerical one goes straight.

The conclusion here is that the analytic expression is very accurate, even in scenarios where where in principle we are not very close to satisfy the $\theta_k \approx \theta_{k_0}$ approximation

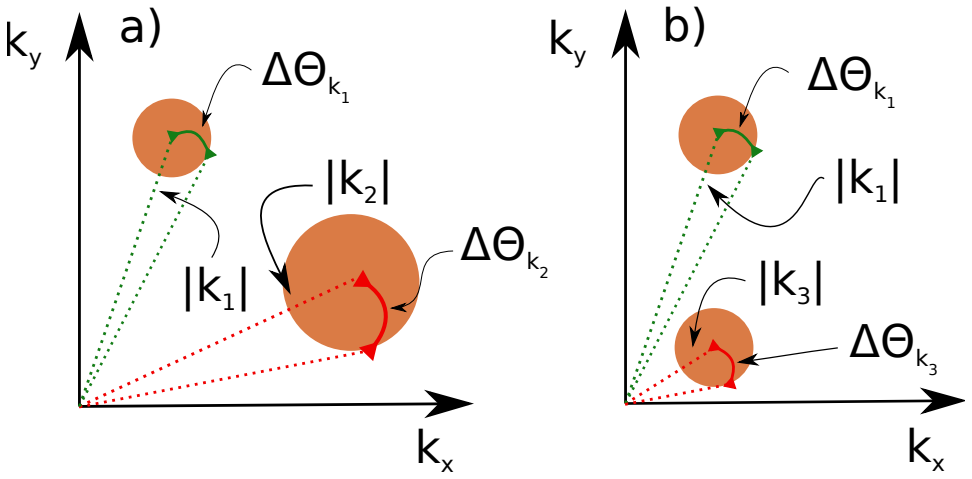

FIGURE 4.3: a) Two different wave packets (named 1 and 2) in momentum space with the same energy, but with different initial momentum dispersion. b) Two different wave packets (named 1 and 3) in momentum space with different energy, but with the same initial momentum dispersion.

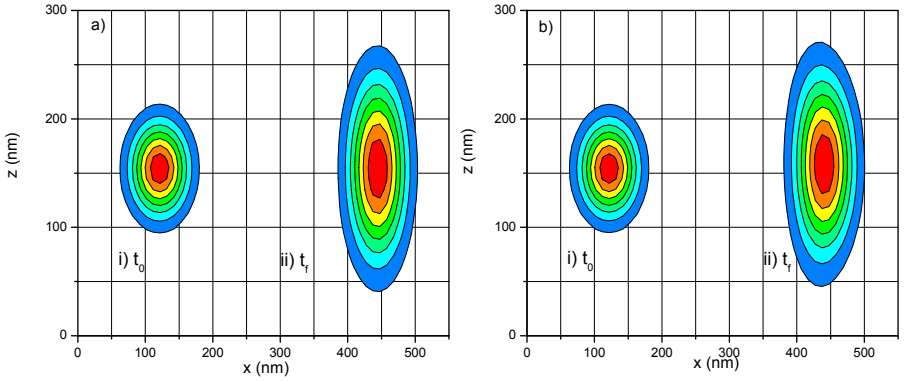

FIGURE 4.4: Evolution of a electron wave packer a) analytically and b) numerically at two different times ($t_0 = 0\,ps$, $t_f = 0.3\,ps$). The electron energy is $E = 0.08eV$ and dispersion $a = 40\,nm$.

(as in Figure 4.4). In other more favourables numerical examples that I made, both (analytical and numerical) evolutions match even better.

4.5 Graphene in the BITLLES simulator

In order to introduce linear band structures (such as grahene) in the BITLLES simulator, it could be done through the tight-binding model (TB), Equation (4.27), or through the Dirac equation, Equation (4.39). There advantages and inconveniences of introducing the Dirac equation and not directly the tight-binding performed in Equation (4.27). Next, I will present a comparison between both methods.

- While the TB represents all the physics of graphene, the Dirac equation is just an approximation for wave vectors close to the Dirac (K and K') points. One should just consider energies below (approximately) 0.7 eV (see Figure 4.2).
- The notation in the TB is more intuitive, there are no bispinors and thus less misunderstandings. The wave function is a scalar, as in other materials (without considering real spin). In the Dirac model, pseudospin appears and the (pseudo) bispinor wave function can be confused with a bispinor wave function (considering spin).
- Equation (4.27) is less easy to handle, the hopping parameters $t(\vec{R}, \vec{R}'$ differs if they correspond to a A or a B atom, and therefore expression are more complex than with the Dirac equation.
- The TB needs a grid separation around the separation between two carbon atoms, $a_C = 1.42$ Å. Since graphene is a 2D material, this fact implies a huge computational burden. On the other hand, there are methods to solve the Dirac equation (which will be commented below), where one could even introduce a spatial grid of $dx = dz \approx 1\, nm$ and $dt \approx 10^{-16}\, s$.

Considering these points, the TB model has many advantages, but the time-evolution of a wave packet in this dense mesh would take too long. Just because the TB is computationally too expensive, it was chosen to implement the Dirac equation in the BITLLES simulator.

There are several methods to include the time dependent Dirac equation through [92–96]. However, they badly suffer from the Fermion doubling problem[93, 97]. This problem consists in the appearance of additional Dirac cones in the Brillouin zone due to the space discretization.

The method introduced in the BITLLES is the leapfrog scheme on a staggered grid. All details can be found in Refs.[98, 99]. This method still suffers from the fermion doubling problem, but there is just one extra Dirac cone, located at the edges of the Brillouin zone. For that reason, the wave vectors associated to that erroneous cone are never used in practice. Therefore, the method allows a perfect implementation in the BITLLES to solve the time-dependent Dirac equation. In addition, absorbing boundary conditions were implemented using complex potential terms[100].

Next, I will show two different numerical examples performed with the Bitlles which exemplifies both, its ability to tackle the many-body problem as well as the complexity

and counter-intuitive behaviour of graphene, well represented by the Klein Tunnelling effect.

4.5.1 Klein Tunnelling effect

Here I show an example of an electron, that suffers the relativistic effect called Klein Tunnelling[101] to show the successful implementation of the method in the simulator. To see more details about this effect, see Appendix C. In the Figure 4.5 it can be seen how an initial electron impinges perpendicularly on a potential barrier, and (contrarily as it is expected in a normal material following the Schrödinger equation) the wave function is completely transmitted. In Figure 4.5, different Bohmian trajectories are also plotted.

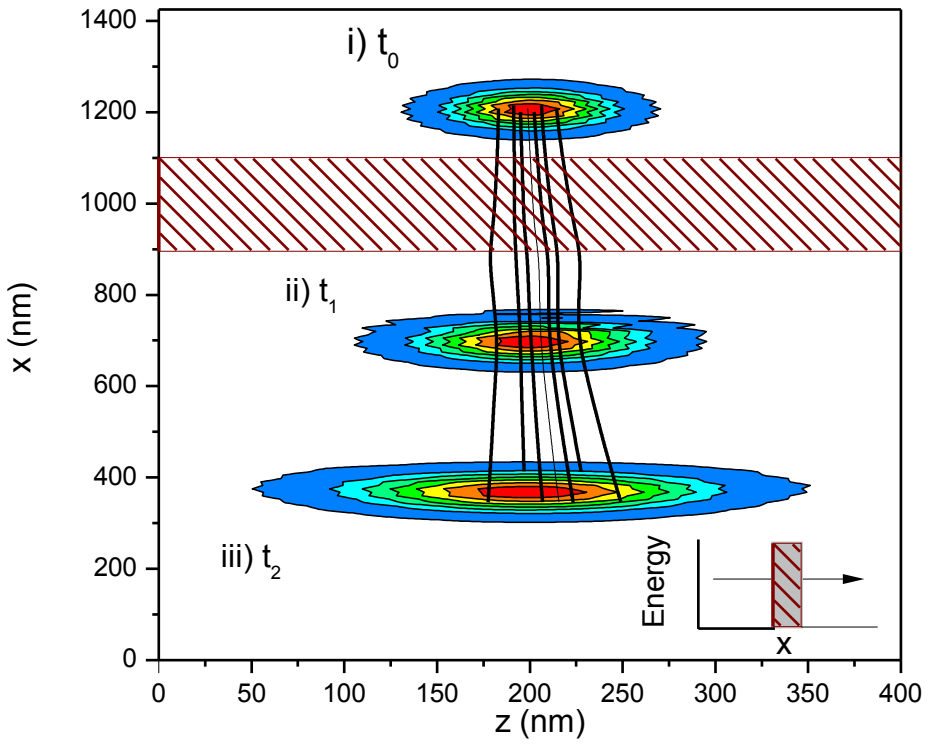

FIGURE 4.5: Square modulus of the wave function at three different times, $t_0 = 0\,ps$, $t_1 = 0.4\,ps$ and $t_3 = 0.7\,ps$. An initial electron (whose energy is 0.2 eV) impinges on a potential barrier (whose height is 0.4 eV and width 200 nm). It can be seen how the electron wave packet suffers the Klein Tunnelling effect and the wave packet is fully transmitted. In the inset, it is sketched the energy potential profile, with an arrow it is indicated the kinetic energy of the electron.

In fact, this effect is called Klein Tunneling effect, but it is not really what it is understood by tunneling (where the wave function occupies forbidden states), but just a wave interference (since the wave function does not occupy any forbidden state, the energy dispersion is a continuum).

4.5.2 Coulomb interaction

Here I present a numerical many-body numerical example which can be made with the BITLLES simulator, thanks to the conditional wave function. Usually, when one thinks about two electrons which move towards each other in free space, one expect them to be repulsed because of the Coulomb interaction. In fact, when one analyses this many-body Coulomb problem with the Schroödinger equation beyond mean field [72, 102] the last assertion is true.

However, things are different in graphene. Let me present the following example, two different electrons moves toward each other with the same dispersion ($a = 40$ nm) and different energy $E_1 = -0.1$ eV and $E_2 = 0.1$ eV. I choose different energies just because I will not include explicitly the exchange interaction. The inclusion of the exchange interaction would not modify the discussion presented here.

The two pseudo Dirac equations for both electrons in the small entanglement approximation [72] are the following:

$$i\hbar\frac{\partial\psi(\vec{x_1},t)}{\partial t} = \left[-i\hbar v_f\vec{\sigma}\cdot\vec{\bigtriangledown}_1 + V_C(\vec{x_1},\vec{X}_2(t),t)\right]\psi(\vec{x_1},t) \tag{4.62}$$

$$i\hbar\frac{\partial\psi(\vec{x_2},t)}{\partial t} = \left[-i\hbar v_f\vec{\sigma}\cdot\vec{\bigtriangledown}_2 + V_C(\vec{X}_1(t),\vec{x_2},t)\right]\psi(\vec{x_2},t) \tag{4.63}$$

where V_C is the Coulomb interaction term. Importantly, as already mentioned along the text, the use of the conditional wave function, allows to split the N many body problem in N different single-particle equations (in this case, there is no advantage, since $N = 2$, but in general it is a very relevant advantage. Each conditional electron wave function has its own (different) Coulomb term V_C, which depends on the position of the other particle, and therefore it goes beyond the mean field approximation, which can be a good approximation, specially when there are many electrons in the system, but not in this two-particle system.

When solving numerically this problem, surprisingly, one reaches the conclusion that even with the Coulomb interaction, the electrons are not repulsed. The electron is not affected with the Coulomb potential because of the Klein Tunnelling effect (which was explained previously in Section 4.5.1). Both electrons do not modify substantially their path, since they tunnel through the Coulomb potential. This result can be appreciated in Figure 4.6, where two electrons are injected with opposite momentum (in the x direction) from the drain and source, with energies $E_1 = 0.06eV$ (injection from the conduction band) and $E = -0.2eV$ (injection from the valence band) respectively. The simulation is performed in the XZ plane, but the results are presented as a projection in the transport (x) direction.

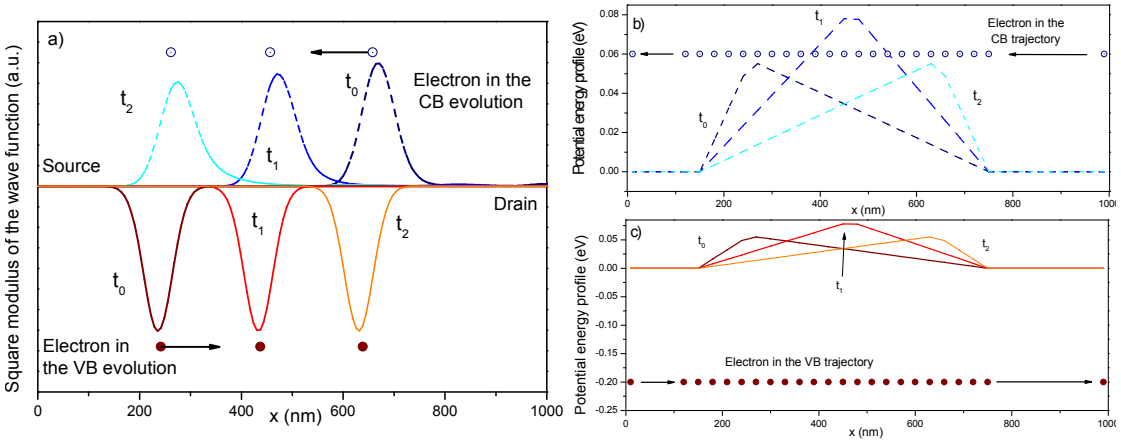

FIGURE 4.6: a) Wave packet evolution (projected in the x transport direction) at three different times ($t_0 = 0$ ps, $t_1 = 0.2$ ps, and $t_2 = 0.4$ ps). The one injected from the conduction band is plotted with dashed lines. The one injected from the valence band is plotted looking down with solid lines. The Bohmian electron positions are also plotted with a circle sign. b) Potential energy profile (projected in the x transport direction) seen by the drain wave packet. It is also plotted the electron trajectory at its energy level. We can see how it tunnels through the Coulomb potential, because of the Klein Tunnelling effect. c) Same as b), but for the source wave packet. In this case, the electron was initially in the valence band and is not affected by the Coulomb potential.

In Figure 4.6a) the projection in the x axis of the modulus square of the wave function is plotted for both wave packets for three different times ($t_0 = 0$ ps, $t_1 = 0.2$ ps, and $t_2 = 0.4$ ps). In order to do more understandable the evolution of both wave packets, I plotted looking down with solid lines the wave packet injected from the valence band (with negative energy). In addition, the electron Bohmian position is also plotted with a circle sign. We can appreciate how at the initial time t_0, both are spatially separated and how at time t_1 both wave packets are at the same position. Finally, the one injected from the source reaches the drain and vice versa, without being repelled. In Figure 4.6b) and c), the energy potential profile is plotted, as well as the Bohmian trajectory for both electrons at their corresponding energies. It can be seen in Figure 4.6b) how the electron injected from the conduction band tunnels through the Coulomb potential due to the

Klein Tunneling effect. This is opposite to what it would have happened in a typical material, where the electron would not have been able to tunnel the Coulomb potential and would have been reflected.

This is a clear example where we see how the BITLLES simulator is able to treat a many-body in a reasonable and computationally efficient way, being able of going beyond the mean field approximation.

Chapter 5

Quantum Dissipation

In this Chapter, a Bohmian approach to study dissipation is presented. Firstly, in Section 5.1 I discuss what dissipation is, in which kind of systems it can be found, what a completely positive method is and why these methods are desired. In Section 5.2, phase space (quasi) distributions will be presented and it will be showed which problems could arise when negative probabilities appear, giving the Boltzmann collision operator as an example. After this, in Section 5.3 the Bohmian approach will be presented, providing numerical results performed with the BITLLES simulator.

5.1 Dissipation and Completely Positive methods

5.1.1 What is Dissipation?

As stated in Chapter 3, in the Bohmian theory all existing particles in the universe are entangled and it exists just one wave function, the one which describes the whole universe and relates those particles (holistic theory). However, since this is scenario is clearly intractable, one can usually assume that some systems are completely isolated from their surroundings (or environment), i.e., there is no interaction or interchange of particles or energy, this is what is called a *closed system*. Assuming that I have a closed quantum system, the wave function dynamics of that system are given by either the Schrödinger equation (for parabolic band structures) or the Dirac equation (for linear band structures). Its evolution is unitary, linear and reversible. So far, dissipation still did not appear, since energy as well as particles are conserved quantities in a closed system.

However, systems have so many degrees of freedom (remember the exponential growth of the configuration space in quantum mechanics, leading to the many body problem seen in Chapter 2) that it is technically impossible to deal with more than just a few parameters. Therefore, from all the particles composing the system under consideration, some of them (the ones that have especial interest for us) must be chosen. Then, what is commonly done is to split the whole system in (at least) two parts: the subsystem of interest and the environment. The subsystem and the environment are entangled, that is they interact with each other and the evolution of the subsystem depends strongly on the environment. This is what is called an *open system* [103]. I am interested in the dynamics of that subsystem, that are not longer (in general) treated by a unitary, linear and time reversible quantum equation of motion.

In electron transport, we always deal with open systems. The active region of a device is connected to two leads, which are connected in turns to the reservoirs and usually there is also at least one gate. Electrons are continuously injected and traversing the active region of the device. Treating the dynamics of such a (open) quantum system implies taking into account many complex processes. From all the parameters and degrees of freedom, what it is usually considered as subsystem are the electrons going through the active region of the electron device, which carry current. The other elements will be considered as *environment*. This environment will impose many conditions on our subsystems. For instance, the amount of electrons that are injected in the active region, as it will be seen in Chapter 6. It will also determine the potential shape to be considered or the boundary conditions that should be applied. This constant energy exchange between our subsystem and the environment will cause *dissipation*.

Dissipation is a very understandable process, where particles loose or gain energy because of scattering with other electrons, phonons or other types of interactions. As stated previously, if it were possible to consider all particles, dissipation would be obtained in a natural way. In the same way, including the computations of atoms (with their vibrations) would allow us to see how electrons loose or gain energy. However, since this is not possible, these events are complex to introduce in the dynamical equations of motion in a successful way, i.e., describing correctly the experimental dynamics of a system. Starting from the unitary quantum equations of motion is not straightforward at all, and many attempts in different directions has been done. One important and desired requirement is that the evolution of the subsystem will never lead to unphysical situations, such as obtaining negative presence probabilities. This point, which seems to be naive and obvious, is not as common as it may seem. In Section 5.2, I present why phase spaces are interesting, why they should be defined in a quantum theory

which holds its existence, how the well known Boltzmann collision operator applied to quantum transport introduces dissipation and how unphysical results may be obtained. The appearance of such unphysical results in only one simple system is enough to warn that such implementation of the collision operator can lead to unphysical results in more complex or realistic simulations.

5.1.2 Completely positive dynamical maps

As stated before, the dynamics of a subsystem are always conditioned to the environment state which in principle is unknown. To facilitate the understanding of the problem, let me introduce how closed quantum systems are treated.

Assuming that we have a closed quantum system, the wave function dynamics of that system are given by either the Schrödinger equation or the Dirac equation. Its evolution is unitary, linear and reversible. From an initial state at time t_0 defined as $|\Psi(0)\rangle$, we can obtain its time-evolved state as $|\Psi(t)\rangle = \hat{U}(t)|\Psi(0)\rangle$, where $\hat{U}(t) =$ is the unitary evolution operator. From the initial state, we can define the density matrix as $\rho(0) = |\Psi(0)\rangle\langle\Psi(0)|$. The density matrix at time t_0 has unit trace and is a semidefinite-positive operator (meaning that the eigenvalues are equal or greater than zero). It can be easily proven that the dynamics are described by the dynamical map β_{t,t_0}, which transforms the density matrix from t to t_0. Then, the density matrix at time t is obtained through the transformation $\rho(t) = |\Psi(t)\rangle\langle\Psi(t)| = \beta_{t,t_0}\rho(0) = \hat{U}(t)\rho(0)\hat{U}^{\dagger}(t)$. Since the trace of $\rho(t)$ is also one, and it is also a semidefinite-operator, this transformation is called completely positive.

As I mentioned before, open quantum systems are the most general and usual scenario in electron devices. In this kind of systems (called also as composited), we can divide the whole system in a subsystem S and its environment E. We are interested in the dynamics of the subsystem, which is interacting with the environment. In that cases we can define the density matrix of the whole system as tensor product $\rho_s(0) = |\Psi_S(0)\rangle\langle\Psi_S(0)| \otimes |\Psi_E(0)\rangle\langle\Psi_E(0)| = \rho_s(0) \otimes \rho_E(0)$. The information that we can obtain from the subsystem is the reduced density matrix $\rho_r(0)$, which is obtained by tracing out the degrees of freedom from the environment, $\rho_r(0) = Tr_E(\rho(0))$ where Tr is the trace of the density matrix.

A proper equation of motion of the reduced density matrix must lead to a dynamical map that satisfies complete positivity [104–108], which guarantees that such a reduced density matrix is always a positive operator. If I now want to obtain information from

the dynamics of the subsystem (we cannot longer use the previous transformation β_{t,t_0} since it involves information from the environment that we cannot access), we need a dynamical map, which allow us to go from the state $\rho_r(0)$ to the state $\rho_r(0)$, here I call it Ω_{t,t_0}. We want this dynamical transformation to map the initial $\rho_r(0)$ into $\rho_r(t)$ at each time, maintaining the property of still being semidefinite-positive, otherwise negative eigenvalues could be obtained, leading to unphysical results.

There are several methods in the literature which describes the shape of this transformation in order to be completely positive. Three very popular ones are the following, the Kraus representation[109], the process matrix[110] and the Lindbland superoperator[111]. It can be shown that these methods can be converted ones into the others[112]. In Section 5.3 I will introduce another completely positive approach within the Bohmian formalism. One of the advantages of that method is that, contrarily to other methods, it can be easily applied in practical scenarios. In our case, we will use it to include dissipation in electron devices.

Before that, in next Section 5.2, I will further discuss which are the consequences of not having a completely positive method to account for the dynamics of subsystems, putting as an example the well known Boltzmann Collision operator[1]S. It is out of doubt that this Collision operator has been extremely useful to face many scenarios [114–118], but one must be careful when using methods that are not completely positive, because even if in simple cases they work and one does not obtain unreal results, problems can arise in more complex and real scenarios.

5.2 Quantum Phase space distributions and the Boltzmann Collision operator

Phase spaces are desirable maps when one tries to include dissipation. For example in electronics, the interaction of atoms (which are vibrating around their equilibrium position) with electrons leads to the appearance of a quasi-particle (called phonons) which simplifies this interaction. Phonons are massless quasiparticles carrying momentum. When they collide with an electron, phonons give or take momentum from the electron. From that perspective, functions which depend on momentum and space are interesting. The importance of choosing a good quantum theory where it is possible to

[1]Other techniques, such as the seminal Caldeira Leggett master equation [113] also violates the completely positive condition.

correctly introduce a phase space is usually ignored, but as it will be shown, it plays an important role and carries surprising consequences.

5.2.1 Phase space in Classical mechanics

In classical mechanics, a particle has well-defined position $x(t)$ and momentum $p(t)$ (for simplicity I consider a one dimensional single particle system). Then, when considering a large number N of trajectories (for example, by repeating the same experiment with different initial conditions), it is possible to define a classical phase space distribution $F_c(x, p, t)$ by counting the number of trajectories at each point $\{x, p\}$ of the phase space:

$$F_c(x, p, t) = \frac{1}{N} \sum_{i=1}^{N} \delta(x - x_i(t))\delta(p - p_i(t)) \tag{5.1}$$

where $x_i(t)$ and $p_i(t)$ are the actual position and momentum of the i-th experiment at time t with $i = 1, ..., N$. The evolution of this classical phase space distribution can be found by directly solving the Newton laws of the N trajectories or by solving the Boltzmann equation.

At this point, I want to clarify that the discussion will be focused on one-particle systems. The function $F_c(x, p, t)$ is constructed by repeating the experiment $N \to \infty$ times (or by dealing simultaneously with N independent particles). All conclusions elaborated hereafter about one-particle phase space probability functions (called as distribution functions) can be straightforwardly generalized for many-particle systems, but with a large increment of notation complexity that would later become irrelevant for the conclusions[2]. For the same reason, only one spatial degree of freedom and one momentum degree of freedom for each particle will be considered.

5.2.2 Phase space in Quantum mechanics

The proper definition of the *phase space* is not so obvious in quantum mechanics, at least in those quantum theories that does not allow for a proper definition of position and momentum simultaneously.

Let me start by discussing why there is no phase space in the Copenhagen (*orthodox*) quantum theory. According to Dirac, the observables are represented by operators in

[2]Strictly speaking, the phase space of a system of 2 interacting particles is not $\{x, p\}$ but $\{x_1, x_2, p_1, p_2\}$.

Hilbert space [52]. The commutator of these operators specifies which quantities can be known simultaneously and which not [52] . In the case of position $\hat{x}$ and momentum $\hat{p}$, I have:

$$[\hat{x},\hat{p}]|\psi\rangle = \hat{x}\hat{p}|\psi\rangle - \hat{p}\hat{x}|\psi\rangle = i\hbar|\psi\rangle \tag{5.2}$$

Therefore the orthodox theory does not support the simultaneous knowledge of local positions and momenta. Strictly speaking, there is no phase space in the orthodox theory of quantum mechanics. Even worst, there are no properties of an electron when there is not measurement. Nevertheless, several (quasi) probability distributions (in Appendix D it is discussed which conditions are required for being a probability distribution) have been constructed under the orthodox theory. Here, the Wigner and the Husimi quasi probability distributions are presented (since they do not accomplish the condition given in Equation (D.1), they are not truly phase space probability distributions). Both defines a phase space with a well-defined value for the position and the momentum of particles, through the use of the Wigner-Weyl transform under the orthodox theory. Finally, the (not quasi) Bohmian probability distribution is presented.

5.2.2.1 Wigner Distribution

One quite common way of describing a quantum mechanical system in phase space is by the so-called Wigner distribution (F_W). For a given state $|\psi\rangle$, one can construct the density matrix operator $\hat{\rho} = |\psi\rangle\langle\psi|$ and express it in the position representation $\langle x|\hat{\rho}|x'\rangle$=$\langle x|\psi\rangle\langle\psi|x'\rangle$ or in the momentum representation $\langle p|\hat{\rho}|p'\rangle$=$\langle p|\psi\rangle\langle\psi|p'\rangle$. Therefore, somehow, the Wigner distribution can be interpreted as an intermediate representation between this two and it is given by a Wigner-Weyl transform of the density matrix:

$$F_W(x,p) = \frac{1}{h}\int \psi(x+\frac{y}{2})\psi^*(x-\frac{y}{2})e^{i\frac{py}{\hbar}}dy \tag{5.3}$$

where $\psi(x) = \langle x|\psi\rangle$. It is noticeable that the (mathematical) variable p in the Wigner (quasi) phase space $\{x,p\}$ appears due to a Fourier transform of a type of autocorrelation function of the wave function. In the case of mixed states, the density matrix can be written as $\hat{\rho} = \sum_j c_j|\psi_j\rangle\langle\psi_j|$ where c_j specifies the fraction of the ensemble in the pure state $|\psi_j\rangle$. For the sake of simplicity we avoid the explicit time dependence of the wave

function and c_j. Therefore, the Wigner distribution function for a mixed state is the following:

$$F_W(x,p) = \frac{1}{h}\sum_j c_j \int \psi_j(x+\frac{y}{2})\psi_j^*(x-\frac{y}{2})e^{ipy/\hbar}dy \tag{5.4}$$

Being the extension to mixed states straightforwardly achieved without any modification in the discussion [119], for simplicity, only pure states are considered in the next discussion.

The Wigner distribution is just a quasi-probability distribution because it does not satisfy, in general, the condition given in Equation (D.1). In Appendix D.3 we can see why this distribution can be negative at some values. In addition, in Section 5.2.3.2 we report a numerical example where the probability in the phase space is clearly negative.

We can calculate also the ensemble average of N experiments $Q_W(x)$ and $J_W(x)$ directly using Equation (D.3) and Equation (4.53). The results obtained (the derivation can be seen at Appendix D) are:

$$Q_W(x) = |\psi(x)|^2 \tag{5.5}$$

$$J_W(x) = |\psi(x)|^2 \frac{\partial S(x)}{\partial x} \tag{5.6}$$

being $S(x)$ the angle of the polar representation of the wave function $\psi(x,t) = R(x)exp(iS(x)/\hbar)$ (for a detailed explanation see Appendix D.2). The results (5.5) and (5.6) are the ones that one will get by directly using $|\psi\rangle$. At this point, because of (5.5) and (5.6), not because of the Wigner function itself, we see that $F_W(x,p)$ is a good candidate to study quantum transport. However, we will see later that it is "dangerous" to take seriously the Wigner (quasi) phase space when further developing the basic steps described here. For example, when including transitions between the phase space points $\{x,p\}$ and $\{x,p'\}$ due to the (Fermi Golden rule) scattering.

5.2.2.2 Husimi distribution

The Husimi distribution (F_H) is another possible phase space distribution built from the Copenhagen school. In this case, it does satisfy the condition (D.1) by construction. For this purpose, we use a set of minimum non-orthogonal uncertainty states localized in phase space ($|q,p\rangle$) [119]. Using them, the Husimi distribution is the following:

$$F_H(x,p) = \frac{1}{2\pi\hbar}\langle x,p|\hat{\rho}|q,p\rangle \tag{5.7}$$

Since $\hat{\rho} = |\psi\rangle\langle\psi|$, the following equation where it is reflected the positiveness of the Husimi distribution is obtained:

$$F_H(x,p) = \frac{1}{2\pi\hbar}\langle x,p|\psi\rangle\langle\psi|x,p\rangle = \frac{1}{2\pi\hbar}|\langle x,p|\psi\rangle|^2 \tag{5.8}$$

However, it is not also a true probability distribution because it does not fulfill the marginal property (D.3). It can be also seen that the Husimi distribution is just a Gaussian smoothed version of the Wigner distribution [119]:

$$F_H(x,p) = \frac{1}{\pi\hbar}\int F_W(x',p')e^{\frac{-(x-x')^2}{2s^2}}e^{\frac{-(p-p')^2 2s^2}{\hbar^2}}dx'dp' \tag{5.9}$$

Next, the ensemble average charge and current densities $Q_H(x)$ and $J_H(x)$ will be computed, similarly as done for the Wigner function (in order to see the complete derivation see Appendix D.2):

$$Q_H(x) = \frac{1}{\sqrt{2\pi s^2}}\int |\psi(x')|^2 e^{-\frac{(x-x')^2}{2s^2}}dx' \tag{5.10}$$

$$J_H(x) = \frac{1}{\sqrt{(2\pi s^2)}}\int R^2(x')\frac{\partial S(x')}{\partial x'}e^{-\frac{(x-x')^2}{2s^2}}dx' \tag{5.11}$$

These results are the ones obtained for the Wigner function, but smoothed by a Gaussian function. From Equation (5.9) we can understand why the Husimi distribution does not

accomplish Equation (D.3). The broadening of the probabilities changes the momentum and position distributions. For these reasons it is considered also a quasi-probability distribution. The difficulties in properly providing the current and charge densities are a dramatic drawback for the correct simulation of quantum electronic devices with the Husimi distribution.

5.2.2.3 Bohmian distribution

As it was already derived in Section 5.1.2, the local Bohmian velocity is:

$$v(x,t) = \frac{\hbar}{m}\mathrm{Im}\frac{\nabla\psi}{\psi} = \frac{\hbar}{m}\frac{\partial S(x_1)}{\partial x_1} \tag{5.12}$$

Let me remember that, as it was seen in Chapter 3, particles mean point-like particles. With Equation (5.12), particles can be described by trajectories which have a definite position and momentum. Then, we can again compute the quantum Bohmian phase space distribution[3] similarly to the classical case:

$$F_B(x,p,t) = \lim_{N\to\infty}\frac{1}{N}\sum_{i=1}^{N}\delta(x - x_i(t))\delta(p - p_i(t)) \tag{5.13}$$

where N is the number of different trajectories of an ensemble of experiments, each experiment has a different initial position[4]. In Equation (5.13), $x_i(t)$ is a position of the trajectory at time t, while $p_i(t) = mv(x_i(t),t)$ is the momentum of the particle related to the velocity in Equation (5.12) with the electron mass m. Let us emphasize that, by construction, the phase space distribution constructed with Bohmian mechanics is always non-negative. The number of Bohmian trajectories with momentum p_i at the position x_i must be positive (or zero if there are no particles).

From the Bohmian distribution, the ensemble average charge and current densities are:

$$Q_B(x) = |\psi(x)|^2 \tag{5.14}$$

[3]We notice that the variables x and p in the Bohmian phase space $\{x,p\}$ are directly defined in the theory itself. They are part of the ontology of Bohmian mechanics. For this reason, the Bohmian phase space is a *natural* space, without mathematical tricks.

[4]Let me emphasize that the different $x_i(t)$ and $p_i(t)$ are not associated to different particles (as I have said, for simplicity, here I only deal with single-particle one-degree-of-freedom problems), but to different realizations of the same experiment. The probability obtained from the wave function $\psi(x,t)$ has exactly the same (ensemble) meaning.

$$J_B(x) = |\psi(x)|^2 \frac{\partial S(x)}{\partial x} \tag{5.15}$$

As it can be seen, these results are exactly the same as the ones obtained from the Wigner distribution (and different from the ones obtained from the Hussimi distribution). Therefore, the Bohmian distribution is an excellent tool to study quantum electron transport. Apart from obtaining the same ensemble results as in the Wigner case, it does no provide negative values that as it will be seen below that may lead to unphysical results.

5.2.2.4 Comparing Numerical Results for the different distributions

Here, I provide numerical examples for the three mentioned quantum phase space distributions and the related charge density and current density. For simplicity, I consider a simple one-dimensional Gaussian wave packet impinging in a symmetric double barrier. At the initial time t_0, the wave function of a Gaussian wave packet at the left of the barrier is :

$$\psi(x, t_0) = (\frac{1}{2\pi a_0^2})^{\frac{1}{4}} e^{ik_0(x-x_0)} exp\left(-\frac{(x-x_0)^2}{4a_0^2}\right) \tag{5.16}$$

where $a_0 = 7.5\, nm$ is the initial spatial variance of the wave packet, $x_0 = 100\, nm$ is the initial central position and $k_0 = 0.69\, nm^{-1}$ is the central wave vector. In addition, for the Husimi evolution, the same dispersion: $s = 7.5\, nm$ was used.

The time evolution of the initial wave packet is computed by numerically solving the Schrödinger equation. Then, the three quantum phase space distributions at three different times are computed. These times correspond to the initial time $t_0 = 0\, ps$, the time $t_1 = 0.09\, ps$ when the wave packet is interacting with the barrier and the time $t_2 = 0.3\, ps$ when the interaction is nearly finished and the initial wave packet is clearly split into a transmitted and a reflected components. The information corresponding to these three times are plotted in Figs. 5.1, 5.2 and 5.3, respectively.

Firstly, I compare the evolutions of the Wigner, Husimi and Bohmian distributions in Figs. 5.1-5.3. It is clearly seen that the Bohmian and Husimi distributions have non-negative values everywhere at any time, satisfying clearly the first probability axiom (D.1). At the initial time, the Wigner distribution is also non-negative, however, in

later times at t_1 and t_2, negative values appears in some regions of the phase space. I will further discuss such unphysical feature and their consequences later. [5]

Next, I compare the charge and current densities calculated, using Equation (D.3) and Equation (4.53), for the three quantum distributions. Let me emphasize again that, as discussed in Section 5.2.3.3, the values obtained from the Wigner and Bohmian distributions are always exactly equal. However, the values of Equation (5.10) and Equation (5.11) for the Husimi distribution does not provide the correct charge and current densities obtained from the wave function. It is clearly seen that the module squared of the wave packet (blue lines) in Figure 5.1b, Figure 5.2b and Figure 5.3b are equivalent to the charge density of the Wigner and Bohmian distributions, but not to the Husimi one.

After confirming, from the numerical simulations, the main features that are expected from the distributions (i.e. the negative values of the Wigner distribution, the mistaken results for the charge and current densities for the Husimi distribution and the success in both aspects of the Bohmian distribution) I discuss an important undesired characteristic of the Wigner distribution. After the interaction with the double barrier, say at the time t_2, the initial wave packets $\psi(x,t)$ splits into a reflected $\psi_R(x,t)$ part and a transmitted $\psi_T(x,t)$ part.

[5] I also want to emphasize that the Bohmian distribution has only one value of the velocity at each position (this is just a consequence that the wave function can take only a single-value at each position.). In fact, a realistic example in quantum transport must deal with open systems. Then, the pure state has to be substituted by a mixed state (a sum of conditional wave functions in the Bohmian language) and the Bohmian distribution will provide a distribution of velocities (each conditional wave function will have its own velocity) at each position in a very natural way. We just avoid the consideration of mixed states to simplify the present discussion.

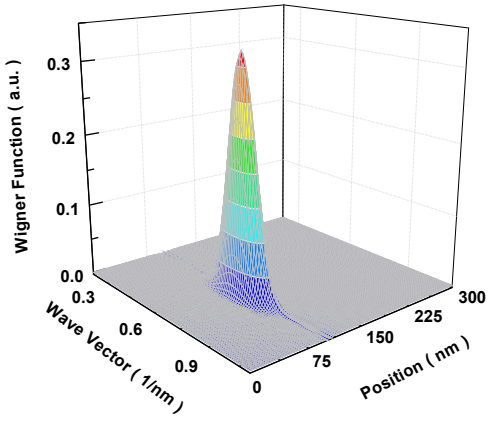

(A) Wigner distribution at t_0.

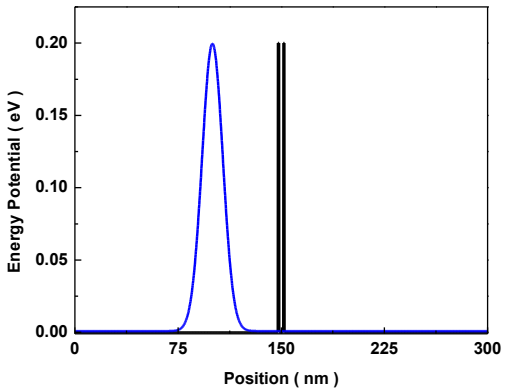

(B) Wave packet impinging on a tunneling barrier at t_0.

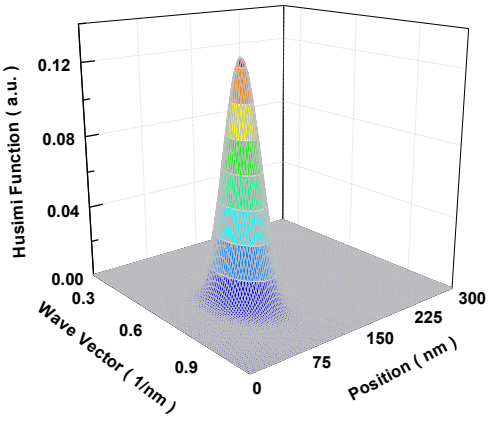

(C) Husimi distribution at t_0.

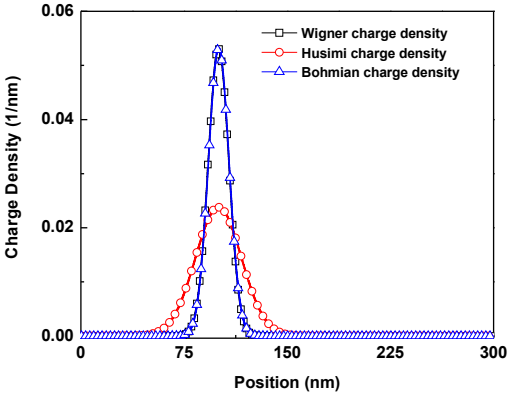

(D) Charge density for the three quantum phase space distributions at t_0.

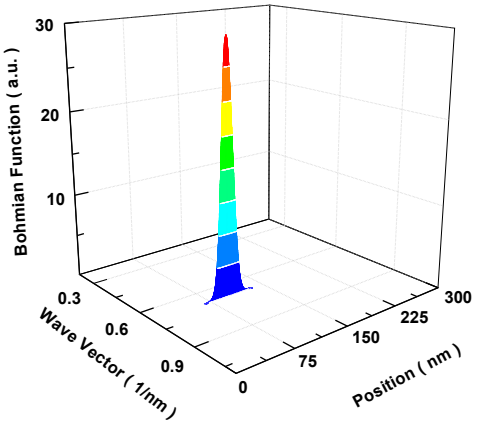

(E) Bohmian distribution at t_0.

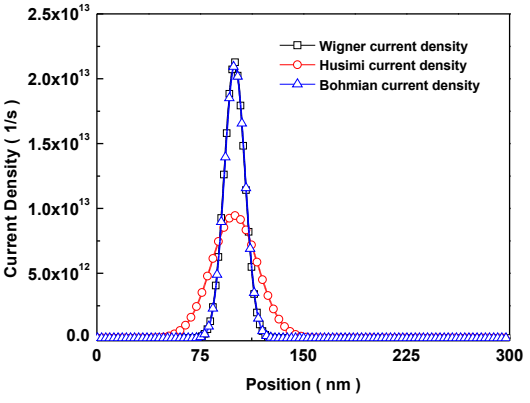

(F) Current density for the three quantum phase space distributions at t_0.

FIGURE 5.1: Simulation of the (a) Wigner distribution, (c) Husimi distribution and (e) Bohmian distribution at the initial time t_0. (b) simulation of the wave packet impinging on a double barrier, the simulation parameters are: $E = 0.09\,eV$, $m^* = 0.2m_0$, where m_0 is the free-electron mass, the barrier height is $0.2\,eV$, the barrier width is $0.8\,nm$ and the well depth is $3.2\,nm$ (d) and (f) are the charge and current densities for the three phase space distributions, respectively.

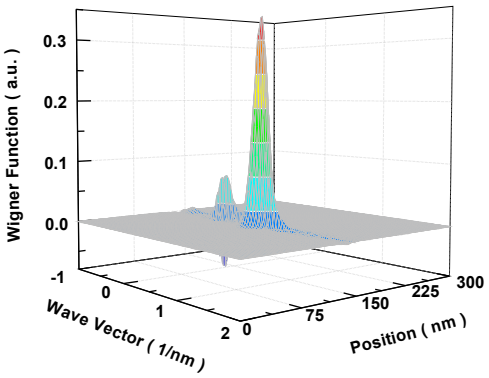

(A) Wigner distribution at t_1.

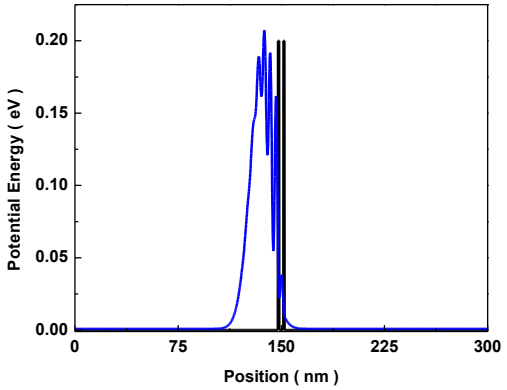

(B) Wave packet impinging on a tunneling barrier at t_1.

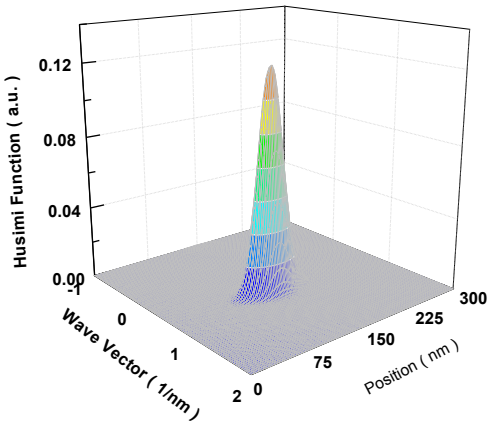

(C) Husimi distribution at t_1.

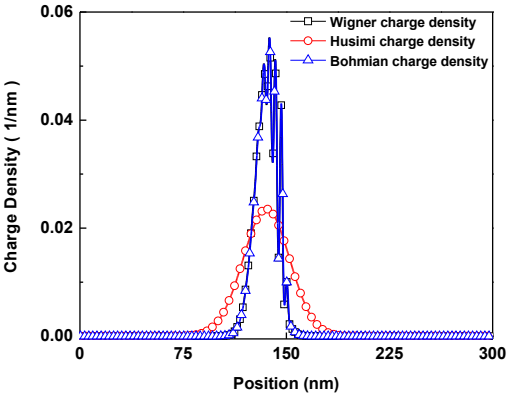

(D) Charge density for the three quantum phase space distributions at t_1.

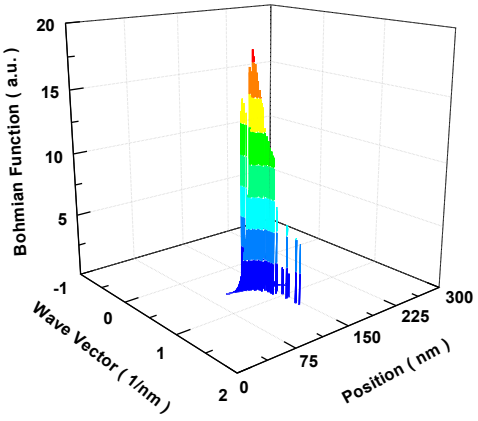

(E) Bohmian distribution at t_1.

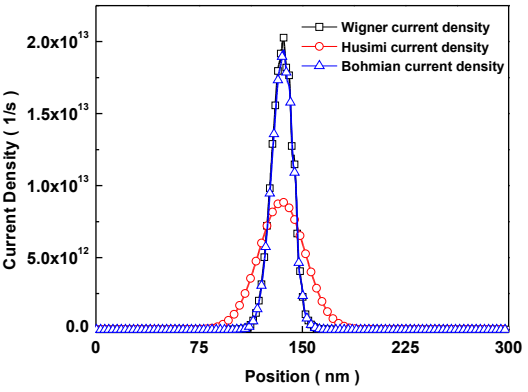

(F) Current density for the three quantum phase space distributions at t_1.

FIGURE 5.2: Simulation of the (a) Wigner distribution, (c) Husimi distribution and (e) Bohmian distribution at the time t_1. (b) simulation of the wave packet impinging on a tunneling barrier with the same parameters as in Figure 5.1. (d) and (f) are the charge density and current density for the three phase space distributions, respectively.

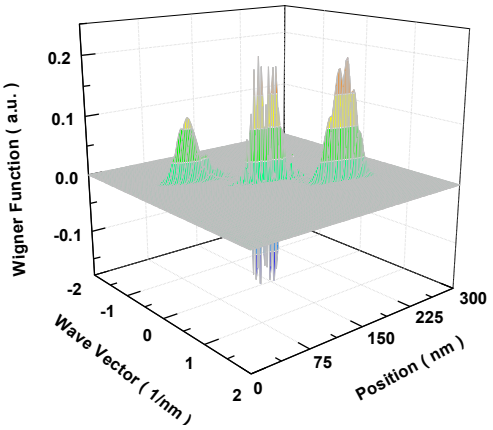

(A) Wigner distribution at t_2.

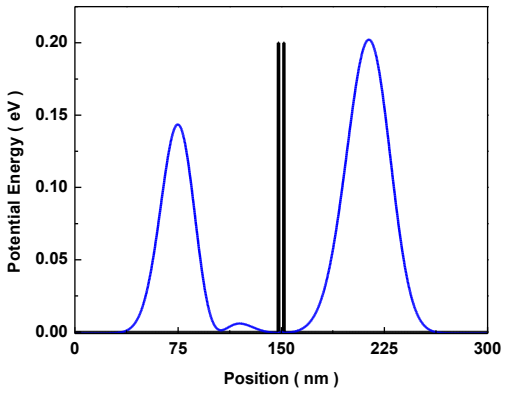

(B) Wave packet impinging on a tunneling barrier at t_2.

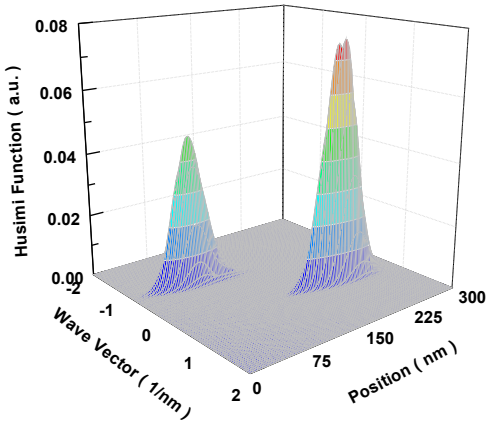

(C) Husimi distribution at t_2.

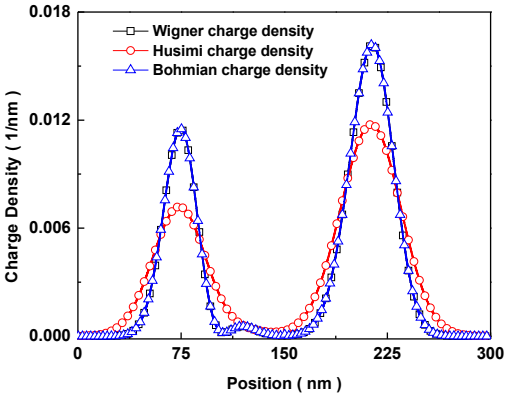

(D) Charge density for the three quantum phase space distributions at t_2.

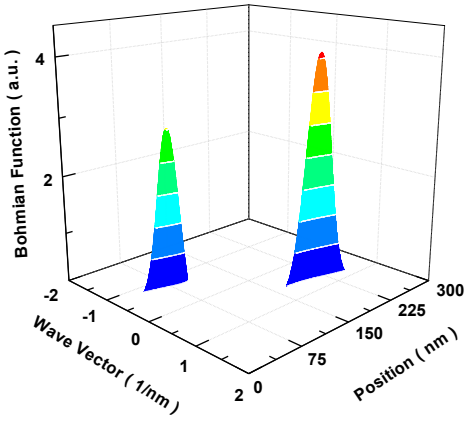

(E) Bohmian distribution at t_2.

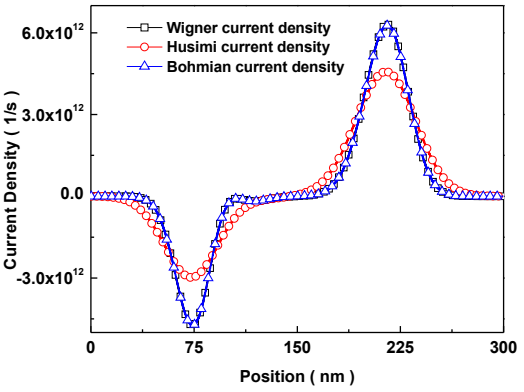

(F) Current density for the three quantum phase space distributions at t_2.

FIGURE 5.3: Simulation of the (a) Wigner distribution, (c) Husimi distribution and (e) Bohmian distribution at the time t_2. (b) simulation of the wave packet impinging on a tunneling barrier with the same parameters as in Figure 5.1. (d) and (f) are the charge density and current density for the three phase space distributions, respectively.

As it is seen in Figure 5.3b, the reflected part and transmitted parts of the wave function are located at both sides of the barrier (not inside). Identically, in the Wigner distribution in Figure 5.3a it is easily recognized the spatial locations of $F_W(x,p)$ from the reflected $\psi_R(x,t)$ and transmitted $\psi_T(x,t)$ parts. However, in addition, there are large non-zero values (negative and positive, because when integrating this region of the phase space the result must be zero) of $F_W(x,p)$ in the middle of the barrier, $x = 150\ nm$, at places where no probability presence of the electron is supposed to be according to Figure 5.3b. The reason of such spurious result is clear from the mathematical Wigner-Weyl transform. At time t_2, the spatially separated reflected $\psi_R(x,t)$ and transmitted $\psi_T(x,t)$ of the wave function $\psi(x,t)$ have to be spatially displaced to compute $F_W(x,p)$. In particular, for the value of $y = 2d$, in Equation (5.4) I have the following terms: $\psi_R(x+d,t)$, $\psi_T(x+d,t)$, $\psi_R^*(x-d,t)$ and $\psi_T^*(x-d,t)$. Finally, according to Equation (5.4), the $F_W(x,p)$ at time t_2 at position $x_C = 150\ nm$ for any value of the momentum p is:

$$F_W(x_C,p) \propto \frac{1}{h}\psi_R(x_C+d)\psi_T^*(x_C-d)e^{i\frac{2pd}{\hbar}} \tag{5.17}$$

since d is the distance between barrier and the reflected part, which I consider equal to the distance between the transmitted part and the barrier, the product $\psi_R(x_C + d)\psi_T^*(x_C - d)$ in Equation (5.17) is different from zero at the barrier region x_C.

Despite this unphysical feature described in Equation (5.17) (I know from the wave function evolution that in that region there is no probability presence), I emphasize that by integrating the positive and negative values of $F_W(x,p)$ around x_C we will reproduce correctly the charge density at this point.

In Figure 5.3d, there is no charge density at position $x_C = 150\,nm$. However, if one tries to gives a physical meaning to $F_W(x,p)$ at these points in Figure 5.3a (as a *true* physical probability distribution of the electron at the phase space) and deduce other physical consequences, one must be very careful and one should notice that it may be a source of unphysical results.

For example, introducing an *ad-hoc* scattering term (due to impurities, for example) in the quantum equation of motion of the Wigner function (such as the Boltzmann Collision operator as it will be seen in next Section 5.2.3), the negative values may lead to unphysical results. If such *ad-hoc* term is introduced as a transition from an old phase space point $\{x_C, p\}$ towards a new point $\{x_C, p'\}$ through the Fermi golden rule probability $S_{p,p'}$, we are moving probability presence of electrons from positions (for example $x_C = 150\,nm$) where, in fact, there are no electrons. The mistake in the

transition of probability from regions without electrons occurs because the scattering mechanism is introduced by hand as an extra *ad-hoc* term in the quantum equation of movement.

Obviously, this spurious effect will not be present if the scattering mechanism (with the impurity) is introduced directly in the Hamiltonian inside the unitary quantum equation of motion (as done in Section 5.3). The mentioned undesired features will never occur within the Bohmian distribution (even when using the conditional wave function), because as it is seen in Figure 5.3e, only non-zero (positive) probabilities are seen at locations where the electrons may be reflected or transmitted, but not in other regions.

5.2.3 The Boltzmann Collision operator

AS It was previously discussed, that the negative values of the Wigner function may lead to unphysical results when including an *ad-hoc* scattering term such as the Boltzmann collision operator. Here I show that, in general, adding *ad-hoc* terms may lead to unphysical results, even in more general scenarios, where there are not negative values in the Wigner function.

5.2.3.1 Wigner Function dynamics

The time evolution of the Wigner distribution function can be directly derived from the Liouville equation. Therefore, the transport equation for the Wigner distribution function in Equation (5.4) can be written as a sum of a term given by the operator $\hat{L}_W\left[F_W(x,k,t)\right]$ plus a generic collision term $\hat{C}_W\left[F_W(x,k,t)\right]$ as:

$$\frac{\partial F_W(x,k,t)}{\partial t} = \hat{L}_W\left[F_W(x,k,t)\right] + \hat{C}_W\left[F_W(x,k,t)\right] \tag{5.18}$$

The term $\hat{L}_W\left[F_W(x,k,t)\right]$ can be written as:

$$\begin{aligned}\hat{L}_W\left[F_W(x,k,t)\right] = &-\frac{\hbar k}{m^*}\frac{\partial F_W(x,k,t)}{\partial x} - \frac{2}{\pi\hbar}\int_{-\infty}^{\infty}\mathrm{d}k'\int_0^{\infty}\mathrm{d}x' e^{[-i(k-k')2x']} \\ &\times[V(x+x') - V(x-x')]F_W(x,k,t)\end{aligned} \tag{5.19}$$

under the effective mass approximation. The other collision term $\hat{C}_W\left[F_W(x,k,t)\right]$ has many different practical implementations (based on different approximations).

5.2.3.2 The origin of problem: the Boltzmann collision operator

The classical Boltzmann collision operator

The Boltzmann collision operator was initially proposed for classical systems [120]. For such systems, it has a very easy and understandable theory. The Boltzmann collision operator is just a rule for counting the number of electrons in and out of a volume of the phase space ΔV due to a collision. The total number of electrons at time $t + \Delta t$ in ΔV is equal to the previous number of electrons that were there at t, before the collision, plus the number of electrons that arrive at ΔV from outside due to collision, minus the number of electrons that leave ΔV due during the collision.

Imagine a classical electron at x_0 with a velocity v_0 that interacts with another particle (for example, a phonon). Because of the interaction, the electron losses kinetic energy and its final velocity is v_f. For simplicity, I assume that the initial position remains unchanged. Such collision process can be easily modelled in terms of the Boltzmann collision operator. The initial classical distribution function in phase space before the collision (apart from constant factors), at time t_0, is:

$$F_c(x, k, t_0) \quad = \quad \delta(x - x_0)\delta(k - k_0) \tag{5.20}$$

being k_0 the wave vector associated to v_0. The Boltzmann collision operator generates the effect of the collision by subtracting an electron with momentum k_0 and adding a new electron with momentum k_f. The final classical distribution function in phase space after the collision, at time $t = t_0 + \Delta t$, is:

$$\begin{aligned} & F_c(x, k, t_0 + \Delta t) = \delta(x - x_0)\delta(k - k_0) - \delta(x - x_0)\delta(k - k_0) + \delta(x - x_0)\delta(k - k_f) \\ = \quad & \delta(x - x_0)\delta(k - k_f) \end{aligned} \tag{5.21}$$

The final result is obviously $F_c(x, k, t_0 + \Delta t) = \delta(x - x_0)\delta(k - k_f)$. Up to here, the discussion seems very trivial. However, let me emphasize that it has been relevant that the negative part of the distribution function generated by the Boltzmann collision operator $-\delta(x - x_0)\delta(k - k_0)$ is exactly compensated by the original positive one $\delta(x - x_0)\delta(k - k_0)$. In this sense, the use of the Boltzmann collision operator in classical systems will never be problematic.

The quantum Boltzmann collision operator

However, the application of the quantum version of the Boltzmann collision operator can be problematic because we have to add/subtract wave functions, not point particles. As we will see below, the problem appears when we do not know the states that built the density matrix of the open system.

If I consider an electron device as an open system with M electrons which are distributed in N different states. Say, there are M_1 electrons described by state $|\psi_1\rangle$ where I define $p_1 = M_1/M$. There are M_2 electrons with probability $p_2 = M_2/M$ described by the state $|\psi_2\rangle$ and so on. A mixed state through the density matrix that describes the system can be constructed as:

$$\hat{\rho}(t_0) = \sum_{i=1}^{N} p_i(t_0)|\psi_i(t_0)\rangle\langle\psi_i(t_0)| \tag{5.22}$$

with the conditions $\sum_{i=1}^{N} p_i(t_0) = 1$ and $\sum_{i=1}^{N} M_i = M$. Because of the interaction of one electron with a phonon, the Boltzmann collision operator will add a new final state of the electron $|\psi_F\rangle$ and will subtract another state associated to the electron $|\psi_O\rangle$. Then, the new density matrix after the scattering, at time $t_S = t_0 + \Delta t$, is:

$$\hat{\rho}(t_S) = \hat{\rho}(t_0) - \frac{1}{M}|\psi_O\rangle\langle\psi_O| + \frac{1}{M}|\psi_F\rangle\langle\psi_F| \tag{5.23}$$

In next Section 5.2.3.3, I will show explicitly with the Wigner formalism how the effect of collisions modelled by the Boltzmann collision operator can effectively be written as Equation (5.23). The problem with the Boltzmann collision operator is that if I subtract an state $|\psi_O\rangle = |\psi_2'\rangle$ that is not present in the density matrix before the collision, $\hat{\rho}(t_0)$, then I cannot simplify the density matrix to remove the negative sign that appears in the second term of the right hand side of Equation (5.23). Then, by a simple computation, the new expression of the charge density from Equation (5.23) is:

$$Q(x,t) = \sum_{i=1}^{N} p_i|\psi_i(x,t)|^2 - \frac{1}{M}|\psi_2'(x,t)|^2 + \frac{1}{M}|\psi_F(x,t)|^2 \tag{5.24}$$

The charge density is a sum of positive and negative terms. The dramatic problem with Equation (5.24) is that, when the time-evolution of the negative term $\psi_2'(x,t)$ is not perfectly balanced by the positive term $\psi_2(x,t)$ (or by other states that build $\hat{\rho}(t)$) at every

time and position, the possibility of getting negative values $Q(x,t)$ in Equation (5.24) is opened. Negative pseudoprobabilities can be accepted, but not negative charges.

The solution of the unphysical result originated by a negative charge density is, in principle, quite simple. If I subtract a state $|\psi_O\rangle$ which is present in the density matrix $\hat{\rho}(t_0)$, for example, $|\psi_O\rangle = |\psi_2\rangle$, then, I can write the density matrix in Equation (5.23) at any time t after the scattering time t_S as:

$$\hat{\rho}(t) = \sum_{i=1;i\neq 2}^{N} p_i(t)|\psi_i(t)\rangle\langle\psi_i(t)| + \frac{M_2-1}{M}|\psi_2(t)\rangle\langle\psi_2(t)| + \frac{1}{M}|\psi_F(t)\rangle\langle\psi_F(t)| \quad (5.25)$$

The relevant point now is that, by construction, the term $(M_2-1)/M$ will be positive at any time t. Obviously, in the selection of the scattering process it has to be ensured that $M_2 \geq 1$, because if not, I am subtracting a non existent state. Therefore, independently of the time-evolution of all the states, the charge density computed from Equation (D.3) (or Equation (5.25)) is just a sum of positive terms:

$$Q(x,t) = \sum_{i=1;i\neq 2}^{N} p_i|\psi_i(x,t)|^2 + \frac{M_2-1}{M}|\psi_2(x,t)|^2 + \frac{1}{M}|\psi_F(x,t)|^2 \quad (5.26)$$

Let me mention, however, that this procedure requires a knowledge of the pure states that build the density matrix (or the Wigner distribution function) of our open system. This information is usually not available in most quantum transport simulations. An exception being the BITLLES simulator, where each electron inside the device has its own conditional wave function, see Chapter 3.

5.2.3.3 Numerical example of the problem

Here I will show with numerical results the potential drawbacks of the combination of the Wigner distribution function and the Boltzmann collision operator discussed in the previous section. In some scenarios, such combination can lead to negative values of the charge density. Later, in Section 5.2.3.4, I will introduce a novel way of facing the scattering problem (taking care of adding and subtracting states present in the density matrix of an open system) where the previous unphysical feature disappears by construction. This new way of introducing the scattering will lead to the Bohmian Scattering approach explained in Section 5.3.

Boltzmann collision operator for Hamiltonian eigenstates

The Boltzmann collision operator in the Wigner formalism is given in the literature by[121]:

$$\hat{C}\left[F_W(x,k,t)\right] = \frac{1}{2\pi}\int_{-\infty}^{\infty}\{W_{kk'}F_W(x,k',t) - W_{k'k}F_W(x,k,t)\}\mathrm{d}k' \tag{5.27}$$

where $W_{kk'}$ is the rate of scattering from the (*unperturbed* Hamiltonian) eigenstate with eigenvector k' to the (*unperturbed* Hamiltonian) eigenstate with eigenvector k. The transition probabilities $W_{kk'}$ are obtained from the Fermi Golden rule according to [122] are:

$$W_{\vec{k}\vec{k'}} = \frac{2\pi}{\hbar}|M_{\vec{k}\vec{k'}}|^2\delta(E_{\vec{k}} - E_{\vec{k'}} \mp \hbar\omega) \tag{5.28}$$

where $M_{\vec{k}\vec{k'}}$ are the matrix elements for the transitions from state $\vec{k'}$ to $\vec{k}$, and ω is the frequency of the phonon for inelastic scattering. The bold symbols represents vectors in the 3D space. For technical reasons, since only one dimension is considered here, the 3D scattering rates must be "projected " onto the one-dimensional model to find $W_{kk'}$ defined in Equation (5.27):

$$W_{kk'} = \frac{\lambda_T^2}{(2\pi)^3}\int_{-\infty}^{\infty}\mathrm{d}^2k'_{\perp}\int_{-\infty}^{\infty}\mathrm{d}^2k_{\perp}W_{\vec{k}\vec{k'}}exp(-\frac{\lambda_T^2k_{\perp}^2}{2}) \tag{5.29}$$

where k and k' are now the one dimensional initial and final states respectively[6]. A very relevant point in this discussion is that the Fermi Golden rule Equation (5.28) forces to use Hamiltonian eigenstates (of the Hilbert space without the interacting potential).

Next I will show a simple example of the application of Equation (5.18) for a simple initial state and scattering rates $W_{kk'}$, that, surprisingly, gives unphysical results in the form of negative charge density in Equation (5.5).

[6]Here I assume that the distribution of electrons is Maxwellian with respect to the transverse wave vector $k_{\perp}$ of the initial state, and λ_T is the spatial dimension factor given by:

$$\lambda_T = \frac{\hbar^2}{KTm^*} \tag{5.30}$$

where K is the Boltzmann constant and T is the absolute temperature.

Electron in a double barrier with a collision event

Here I am not focused on the simulation of realistic nanodevices, but only in showing with a very simple example an unexpected result when combining the Boltzmann collision operator and the Fermi Golden rule. The violation of the requirement $Q(x,t) \geq 0$ in only one simple system is enough to warn that such implementation of the collision operator can lead to unphysical results in more complex or realistic simulations.

Now I consider here an electron impinging in a double barrier. Above, it was discussed how negative values of the Wigner function could lead to problematic results when including scattering terms that were able to move this negative values in the phase space due to a scattering term.

In this case, I will consider a more general case. I will consider that the interaction will occur before the interaction with the double barrier occurred. This is seen in the inset of Figure 5.4. For simplicity, I consider a 1D Hilbert space with the following uniform grid $x_j = j\Delta x$, for $j = 1, 2, \ldots M$ with $\Delta x = 0.2$ nm the spatial step and $M = 3000$ the number of grid points. The simulation box is large enough (it extends from 0 till 600 nm) to avoid any spurious interaction of the electron wave packet with the spatial boundaries. In the simulation, the temporal step is $\Delta t = 3$ fs.

At the initial time t_0 I consider an arbitrary initial pure state $\langle x|\psi\rangle$ whose support fits perfectly inside the simulation box. Since I am interested in describing such system with the Wigner distribution function, the density matrix of this initial pure state is given by $\hat{\rho} = |\psi\rangle\langle\psi|$, and the Wigner distribution function just needs the Wigner-Weyl transform given by Equation (5.3). The time-evolution of the Wigner distribution function can be computed directly by solving the Schrödinger equation (plus a Wigner-Weyl transform) or by solving the Wigner transport equation Equation (5.18) without the collision operator. Then, at time t_S, a scattering process takes place according to the Boltzmann collision operator.

It is usually assumed in the literature that the scattering process is sufficiently instantaneous[7] so it can be assumed that the evolution of the Wigner distribution function from the t_S till $t_S + \Delta t$ is:

$$\frac{F_W(x,k,t_S+\Delta t) - F_W(x,k,t_S)}{\Delta t} = \frac{1}{2\pi}\int \{W_{kk'}F_W(x,k',t_S) - W_{k'k}F_W(x,k,t_S)\}\mathrm{d}k' \tag{5.31}$$

[7] As indicated in [123], such assumption is not always valid. In any case, the consideration of a larger time will not significantly change the drawbacks of the Boltzmann collision operator mentioned here.

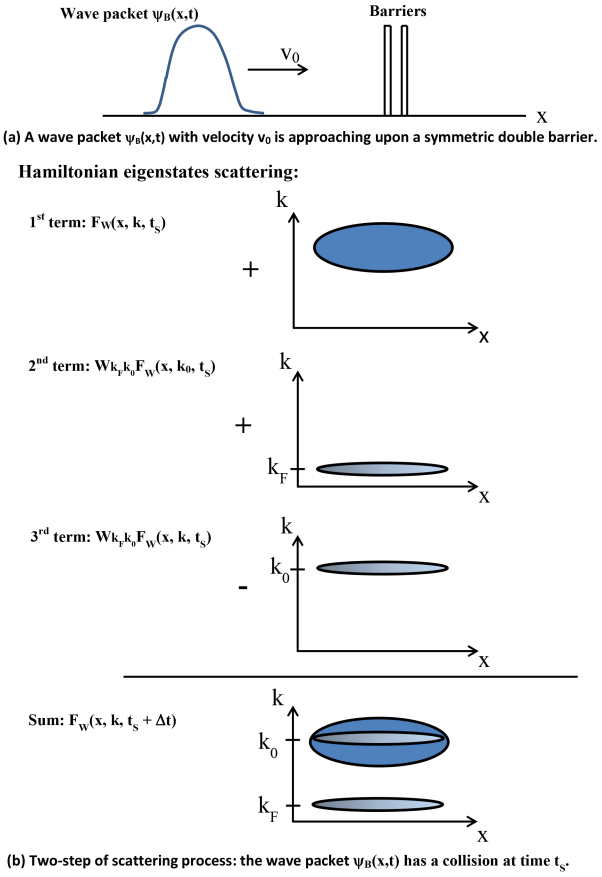

FIGURE 5.4: Schematic representation of the two-step Hamiltonian eigenstates scattering process. (a) Simulation of a wave packet impinging on double barriers, the collision is performed at time t_S before the wave packet touches the barriers. (b) A simple physical picture of the two-step Hamiltonian eigenstates scattering process.

A further elaboration of Equation (5.31) requires the specification of the scattering rates $W_{kk'}$ and $W_{k'k}$. In this case, for simplicity, I will account just for one collision process of one electron with one phonon. In particular, I will consider that, because of the collision, the initial wave vector of the electron k_0 changes to a final value k_F. By using the Fermi golden rule in Equation (5.29), such electron-phonon interaction can be associated to the terms:

$$W_{kk'} = \alpha\delta(k' - k_0) \lim_{\sigma\to 0} e^{-\frac{(k-k_F)^2}{\sigma^2}} \tag{5.32a}$$

$$W_{k'k} = \alpha\delta(k' - k_F) \lim_{\sigma\to 0} e^{-\frac{(k-k_0)^2}{\sigma^2}} \tag{5.32b}$$

where the parameter α takes into account all (irrelevant for this simple example) details of the specific computation of the Fermi Golden rule. The parameter $\sigma \to 0$ means that rates $W_{kk'}$ and $W_{k'k}$ are localized closely to momentum $k = k_F$ and $k = k_0$, respectively.

For numerical reasons, I avoid writing explicitly delta functions in the right hand side of Equation (5.32a) and Equation (5.32b). In simple words, $W_{kk'}$ is the transition rate associated to an electron initially in $k' = k_0$ that appears finally at $k = k_F$ (see 2^{nd} term in Figure 5.4), and $W_{k'k}$ is associated to an electron initially in $k = k_0$ that finally disappears from k_0 (see 3^{rd} term in Figure 5.4). The summary of this scattering process described in Equation (5.31) (or in the sum in Figure 5.4) is just that an electron with initial momentum $\hbar k_0$ gets a final momentum to $\hbar k_F$ because of the interaction with a phonon.

Substituting the scattering rates written in Equation (5.32a) and Equation (5.32b) into Equation (5.31) and rearranging it, it is obtained:

$$F_W(x,k,t_S+\Delta t) = F_W(x,k,t_S) + \frac{\alpha\Delta t}{2\pi}F_W(x,k_0,t_S)e^{-\frac{(k-k_F)^2}{\sigma^2}} - \frac{\alpha\Delta t}{2\pi}F_W(x,k,t_S)e^{-\frac{(k-k_0)^2}{\sigma^2}} \tag{5.33}$$

Since there is a one-to-one correspondence between the Wigner distribution function and the density matrix [124, 125], one can obtain the density matrix by the inverse Wigner-Weyl transform of the Wigner distribution function as:

$$\hat{\rho}(x,x',t) = \int_{-\infty}^{\infty} F_W(\frac{x+x'}{2},k,t)e^{ik(x-x')}\mathrm{d}k \tag{5.34}$$

As a consequence, I can rewrite Equation (5.33) as:

$$\begin{aligned}\hat{\rho}(x,x',t_S+\Delta t) &= \hat{\rho}(x,x',t_S) + \frac{\alpha\Delta t}{2\pi}F_W(\frac{x+x'}{2},k_0,t_S)e^{ik_F(x-x')} \\ - \quad &\frac{\alpha\Delta t}{2\pi}F_W(\frac{x+x'}{2},k_0,t_S)e^{ik_0(x-x')}\end{aligned} \tag{5.35}$$

which can be rewritten in the form of positive and negative addends discussed in Equation (5.23) as:

$$\hat{\rho}(t_S+\Delta t) = \hat{\rho}(t_S) + \hat{\rho}_P(t) - \hat{\rho}_N(t) = |\psi\rangle\langle\psi| + |\psi_P\rangle\langle\psi_P| - |\psi_N\rangle\langle\psi_N| \tag{5.36}$$

where the first term in the right-hand side, $\hat{\rho}$, describes the density matrix before the collision, the second and third terms are the terms generated (by the Boltzmann Collision

operator) due to the collisions. It is important to underline that I am selecting α small enough to ensure that the charge density of the density matrix $\hat{\rho}(x, x', t_S + \Delta t)$ in Equation (5.35) is strictly non-negative everywhere just after the scattering. As commented previously, it would be a nonsense to subtract more probability presence than what there is in one specific location at t_S. Even with this important requirement, the problem may appear later when the time evolution of $\hat{\rho}(x, x', t_S)$ and $-\frac{\alpha \Delta t}{2\pi} F_W(\frac{x+x'}{2}, k_0, t_S) e^{ik_0(x-x')}$ (or $-|\psi_N\rangle\langle\psi_N|$) becomes different.

I compute the charge probability distribution from Equation (D.3) at four different times corresponding to the initial time $t_0 = 0$ ps, just after the scattering time $t_S = 0.006$ ps, at $t_2 = 0.315$ ps when the wave packets ψ and ψ_N are interacting with the barriers, and at time $t_3 = 0.66$ ps when the interaction is nearly finished and the initial wave packets ψ and ψ_N are clearly split into transmitted and reflected components. The information corresponding to these four times is plotted in Figure 5.5.

In order to enlarge the typical interference effects, at the initial time t_0 I consider the following initial state $\langle x|\psi\rangle = C\langle x|\psi_1 + \psi_2 + \psi_3\rangle$ with C a normalization constant. Each wave function $\psi_j(x, t_0)$ at the initial time t_0 is a Gaussian wave packet $\psi_j(x, t_0) = (\frac{2}{\pi a_0^2})^{\frac{1}{4}} e^{ik_0(x-x_{0j})} exp\left(-\frac{(x-x_{0j})^2}{a_0^2}\right)$ but with different initial central positions x_{0j}. In particular, the left wave packet ψ_1 has $x_{01} = 250$ nm, the middle wave packet ψ_2 has $x_{02} = 280$ nm and the right wave packet is ψ_3 has $x_{03} = 310$ nm. The initial spatial variance of the three wave packets is $a_0 = 15$ nm, their central wave vector $k_0 = 0.69$ nm^{-1} and the effective mass $m^* = 0.2\, m$ with m being the free electron mass. The center of the barriers is at $x = 350$ nm. Both barriers have a 0.8 nm width, the energy height is 0.2 eV, and they are separated by 4 nm.

After the scattering process, the evolution of the whole density matrix in Equation (5.36) requires the specification of the new term ψ_P with new momentum $\hbar k_F$ (associated to the density matrix is $\hat{\rho}_P$ in Equation (5.36)) and the new terms ψ_N with the old momentum $\hbar k_0$ (associated to the density matrix $\hat{\rho}_N$ in Equation (5.36)). The two additional wave packets ψ_N and ψ_P are Gaussian wave packets with the same very large dispersion $a_{0S} = 2a_0\left(\sqrt{1 + \frac{4\hbar^2 t_S^2}{m_*^2 a_0^4}}\right)$ (to mimic a plane wave) and the same central position $x_{0S} = x_0 + \frac{\hbar k_0}{m_*} t_S$. The wave vectors for ψ_N and ψ_P are k_0 and $-k_0$ (here I assume $k_F = -k_0$), respectively.

The results of the charge (or probability presence) densities in the right hand side of Figure 5.5 are just Equation (D.3), that is the integral of the Wigner distribution function in the left-hand side of the figure over all momenta (for a fixed position). The negative values of the Wigner distribution function in the figures is not at all problematic as far as the marginal integral in Equation (D.3) satisfies $Q(x, t) \geq 0$. Before and just after the

collision, there is not unphysical evolution of the charge. Just after the collision, the new state $|\psi_P\rangle$ gives only positive charge density and the negative contribution of the new state $|\psi_N\rangle$ is, obviously, smaller than the positive one provides by $|\psi\rangle$ at each location. Figure 5.5(e) and (f) show the same information at the new time $t_2 = 0.315$ ps when the wave packets $\langle x|\psi\rangle$ and $\langle x|\psi_N\rangle$ have evolved with time and interacting with the barriers. At position $x = 300$ nm, negative charge (presence probability) appears. This result is totally unphysical in the same sense that a wave function with a negative modulus will be unphysical, i.e. inconsistent with the probabilistic (Born's law) interpretation of quantum mechanics. After the interaction is completed, at time $t_2 = 0.66$ ps, the spurious phenomenon becomes even worse. In this particular simple example, there are more positions (for example $x = 492$ nm) with negative value probabilities.

I have also performed simulations (not shown here) where the scattering process is strictly performed according to Equation (5.35) using $-\frac{\alpha\Delta t}{2\pi}F_W(\frac{x+x'}{2}, k_0, t_S)e^{ik_0(x-x')}$ instead of $|\psi_N\rangle\langle\psi_N|$. The results are quite similar to the ones shown Figure 5.5, but because of the own positive/negative oscillation of the $F_W(\frac{x+x'}{2}, k_0, t)$, the charge probability results are even worse than the ones plotted here. The amplitude where the negative probability occurs is larger and such negative value appears in more positions, which is affected by the factor $\frac{\alpha\Delta t}{2\pi}F_W(x, k_0, t_S)$ presenting the scattering strength. It is important to point out that the unphysical spurious behaviours become even worst with longer time evolution (related to the device active region). The scattering strength are relevant factors when the decoherence in nanodevices are investigated. See the works of Dollfus and co-workers [121, 126, 127]. In conclusion, the presence of negative charge is not because of the exact shape of the ρ_N and ρ_P, either pure states or mixed states, but because the time-evolution of the states ρ_N is different from ρ because, at some times t, their positive and negative contribution cannot be compensated (even if they were compensated at t_0).

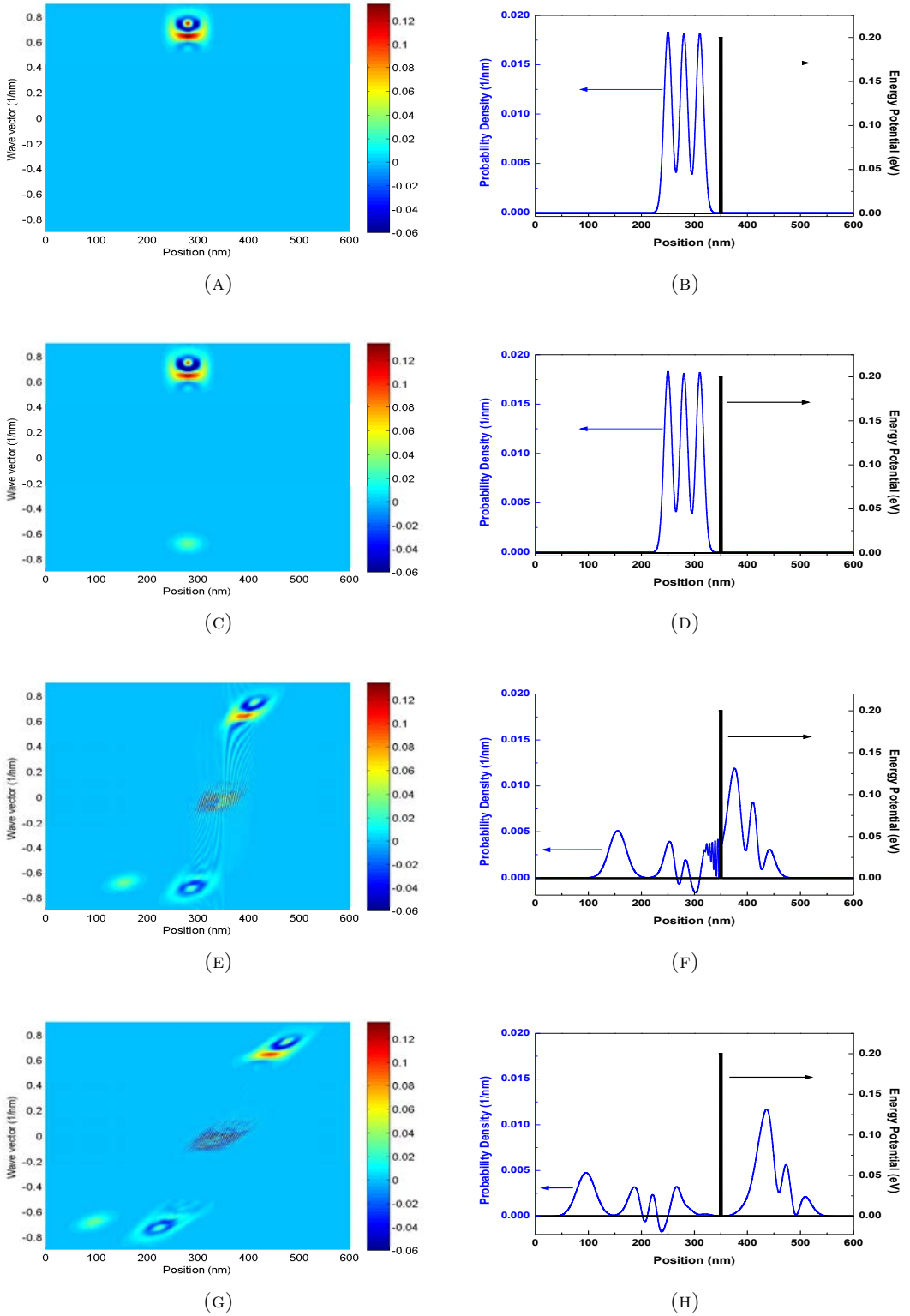

FIGURE 5.5: (Color online) Evolution of Gaussian wave packets coupled with the Hamiltonian eigenstates scattering approach moving towards barriers. (a), (c), (e), (g) are the Wigner distribution function and (b), (d), (f), (h) are the corresponding probability (charge) density at four different times: initial time $t_1 = 0$ ps, scattering time $t_S = 0.006$ ps before touching the barriers, time $t_2 = 0.315$ ps when wave packets are interacting with the barriers and time $t_3 = 0.66$ ps when the interaction is completely done. The simulation parameters are: $E = 0.09$ eV, $m^* = 0.2\ m_0$, where m_0 is the free electron mass, the barrier height is 0.2 eV, the barrier width is 0.8 nm and the well depth is 4 nm.

5.2.3.4 Numerical example of the solution

As indicated in Section 5.2.3.2 the solution to avoid these unphysical results of Figure 5.5, while still using the simple ideas of the Boltzmann collision operator, is having an exact knowledge of the states involved in the description of the density matrix. By construction, this way of working will not provide any negative charge density.

Boltzmann collision operator for general states

Let me assume that I have a perfect knowledge of all the states, $|\psi_i\rangle$ with $i = 1, ..., N$, that are needed to build the density matrix of the open system. Firstly, I define $F_W^i(x, k, t)$ as the Wigner-Weyl transform with respect to the element of the density matrices $p_i|\psi_i\rangle\langle\psi_i|$ in Equation (5.22). Then, because of the linearity of the Wigner distribution function with respect to the density matrix, before the collision, the whole Wigner distribution function can be written as follows:

$$F_W(x, k, t) = \sum_{i=1}^{N} F_W^i(x, k, t) \tag{5.37}$$

Inspired in the classical application of the Boltzmann collision operator, a collision operator in Equation (5.27) that provides transitions between different states can be defined as:

$$\hat{C}\left[F_W(x, k, t)\right] = \frac{1}{2\pi} \sum_{i=1}^{N^*} \sum_{j=1}^{N^*} \{Z_{ij} F_W^j(x, k, t) - Z_{ji} F_W^i(x, k, t)\} \tag{5.38}$$

where the terms Z_{ij} provides the scattering rate (for the *general* states used in each case) from the $j-$ state $|\psi_j\rangle$ to the $i-$ state $|\psi_i\rangle$. The sums in Equation (5.38) are carried out over the N^* possible existent terms (which are in principle infinite, but I can limit to a reasonable number of possible states in a practical application). We do not use $W_{kk'}$ in Equation (5.38) because, in principle, they are computed only for Hamiltonian eigenstates, while I define Z_{ji} using our general states $|\psi_i\rangle$[8].

[8] As a reasonable approximation, if the general wave packet has (a more or less) well defined momentum (for example, the mean momentum of the wave packet) the terms $W_{kk'}$ can be numerically used instead of Z_{ji} in Equation (5.38)

Example: Electron in a double barrier with a collision event

I discuss here the same numerical example presented in Section 5.2.3.3, but here with the new general collision operator in Equation (5.38). I use the same initial density matrix $\hat{\rho}(t_0) = |\psi\rangle\langle\psi|$ in Equation (5.22). I consider that there are two electrons with such state, $M_1 = M = 2$. Then, when the scattering take place, one of the two electrons with initial state $|\psi\rangle$ changes its state, while the other remains unaffected. The new density matrix in Equation (5.23) is $\hat{\rho}(t_S) = \hat{\rho} - (1/2)|\psi\rangle\langle\psi| + (1/2)|\psi_F\rangle\langle\psi_F|$. The new density matrix after scattering can be greatly simplified to $\hat{\rho}(t_S) = (1/2)|\psi\rangle\langle\psi| + (1/2)|\psi_F\rangle\langle\psi_F|$ because $|\psi_N\rangle \equiv \frac{1}{\sqrt{2}}|\psi\rangle$. This collision process is explained in Figure 5.6.

In this numerical example, the same initial wave packet $|\psi\rangle$ discussed in Figure 5.5 is used. At the initial time $t_0 = 0$ ps, the information of the Wigner function and the charge probability distribution plotted in Figure 5.7 is identical to that in Figure 5.5. Then, at time $t_S = 0.006$ ps, the new collision operator in Equation (5.38) acts on the Wigner distribution function. The final state is equal to half the initial state plus half the initial state but with a opposite momentum. After the scattering, the system state is $\hat{\rho} = |\psi\rangle\langle\psi| + |\psi_P\rangle\langle\psi_P| - |\psi_N\rangle\langle\psi_N| = \frac{1}{2}|\psi\rangle\langle\psi| + \frac{1}{2}|\psi_F\rangle\langle\psi_F|$. As a consequence, the negative values disappear. Therefore, the unphysical results are removed. These conclusions are perfectly corroborated and numerically visualized in Figure 5.7.

The argument against the Boltzmann collision operator is that it adds or subtracts states (through the use of the terms $W_{kk'}$) to the old density matrix built by other different states. On the other hand, this new application of the Boltzmann collision operator with general states always adds or subtracts wave functions of electrons which are present in the density matrix before collision. In simple words, if it is desired a collision model without the possibility of negative charges, it must be ensured that the wave function of the electron that we are removing when applying the Boltzmann collision operator is effectively present in the density matrix or the Wigner distribution function.

I remark also that this new algorithm for collision explained here is relevant for the time-dependent modelling of quantum transport. In addition, since it requires a perfect knowledge of the states that built the density matrix, its practical implementation fits perfectly with the BITLLES simulator developed with the conditional wave functions [72, 75, 128, 129] explained in Chapter 3. Then, the mentioned algorithm for dissipative quantum transport can be straightforwardly implemented for quantum transport by directly including the interaction between electrons and phonons in the kinetic part of the Hamiltonian that describes the wave function of each electron.

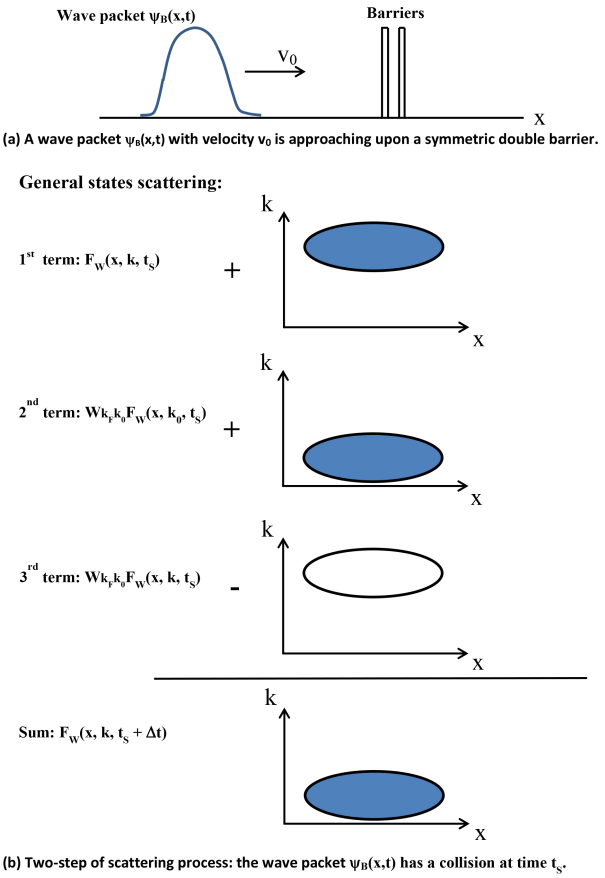

FIGURE 5.6: Schematic representation of the two-step general states scattering process. (a) Simulation of a wave packet impinging on double barriers, the collision is performed at time t_S before the wave packet touches the barriers. (b) A simple physical picture of the two-step general states scattering process.

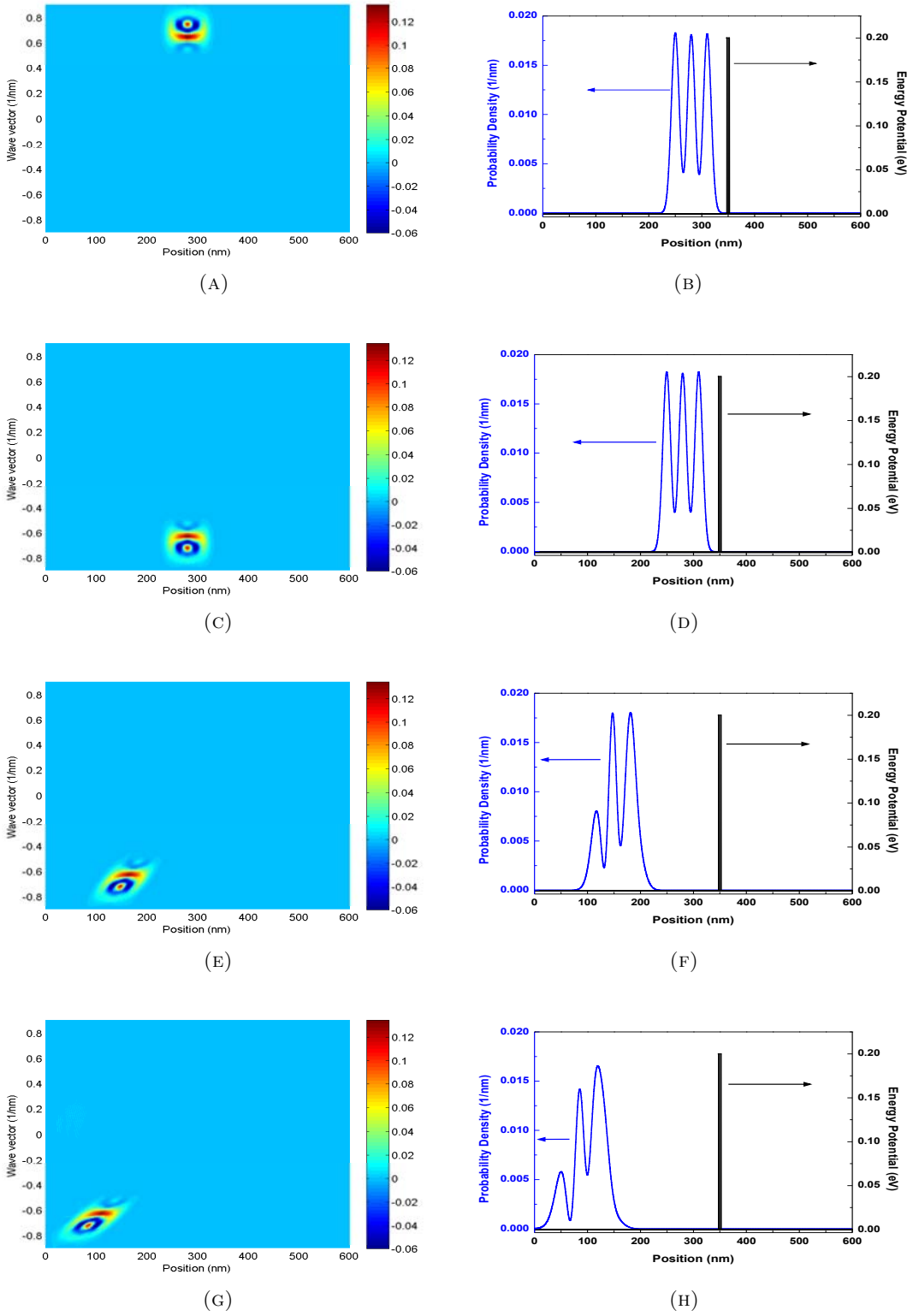

FIGURE 5.7: (Color online) Evolution of Gaussian wave packets coupled with general states scattering approach moving towards barriers. (a), (c), (e), (g) are Wigner distribution and (b), (d), (f), (h) are corresponding probability density of state at for different times, which is identical to the time in Figure 5.5: $t_1 = 0$ ps, $t_S = 0.006$ ps, $t_2 = 0.315$ ps and $t_3 = 0.66$ ps. The simulation parameters are: $E = 0.09$ eV, $m^* = 0.2\ m_0$, where m_0 is the free electron mass, the barrier height is 0.2 eV, the barrier width is 0.8 nm and the well depth is 4 nm.

5.3 Bohmian Scattering Approach

Until now, I have shown some problematic features when using non completely positive approaches and how the appearance of these problems can be avoided. In this section, a completely positive approach based on the conditional wave function (see Chapter 3) is presented.

But before that, let me also briefly introduce two kinds of open systems, Markovians (which ultimately is an approximation) and non-Markovian ones.

5.3.1 Markovian and non-Markovian systems

Markovian systems are the ones where the correlation time between the subsystem and the bath is considered to be infinitesimally small. In order to obtain the evolution at $t' + dt$, only information about time t' is needed. In other words, it is a memoryless system. On the other hand, non-Markovians systems are systems whose correlation time is enough large enough, and then the evolution at time $t' + dt$ depends on times $t < t'$.

For Markovian evolutions, the Lindblad master equation [130–132] preserves complete positivity, but its connection to realistic practical scenarios and its extension beyond Markovian dynamics are still challenging [86, 133, 134].

Alternatively, inspired by the spontaneous collapse theories [54, 135], Diósi, Gisin, and Strunz developed the stochastic Schrödinger equations (SSEs) to *unravel* the reduced density matrix in non-Markovian systems [136–139]. Continuous measurement theory allows the definition of a wave function of the open system conditioned on one *monitored* value associated with the environment[140–145]. This approach preserves positivity because the reduced density matrix is built from a sum of projectors associated with the states solution of a Schrödinger-like equation[86, 103, 143, 144]. In practical applications, the non-hermitian Hamiltonians can provoke states of the SSE to lose their norm and therefore their statistical relevance[103].

In this framework, a discussion about the physical interpretation of the pure-state solution of the SSE is relevant. It is well recognized that the continuous measurement of an open system with Markovian dynamics can be described by a SSE[103]. Therefore, the pure-state solution of SSE can be interpreted as the state of the Markovian system while the environment is under (continuous) observation. However, such a physical interpretation cannot be given to the solutions of the SSE for non-Markovian systems[140–145].

In such non-Markovian systems, a continuous measurement requires a non-trivial interaction of the system with the environment so that the physical description of the continuously measured open system needs to be done through the reduced density matrix [103](not through the pure-state given by the non-Markovian SSE, which becomes just a numerical tool). The physical interpretation that one can assign to the solution of the non-Markovian SSE (conditioned to some environment value) is the following: the state of the open system at a given time if a measurement is performed in the environment at that time, yielding the mentioned value for the environment. Linking SSE states of the open system (or values of the environment) at different times is just a fiction.

However, within Bohmian mechanics, the conditional wave function is always a well-defined physical state for Markovian and non-Markovian open systems, with continuous or non-continuous measurements. The general expression of the equations of motion of such a conditional wave function with or without dissipation was already discussed in Section 3.5. I anticipate two important features of the Bohmian approach. First, since our approach deals directly with wave functions, it provides a completely positive map for either Markovian or non-Markovian dynamics with an unproblematic physical interpretation of the wave function of the open system at different times. Secondly, contrary to other completely positive methods, the numerical inclusion of different dissipative phenomena in the equation of motion of the conditional wave function can be done straightforwardly with a microscopic and realistic implementation. These properties make the approach very relevant for many different research fields.

5.3.2 The approach

Consider an isolated, i.e. closed, quantum system described by a full many-body state $|\Psi\rangle$ solution of the unitary, reversible, and linear Schrödinger equation. The total Hilbert space of N particles can be decomposed as $\hat{H} = \hat{H}_a \otimes \hat{H}_b$, with $\vec{r} = \{\vec{r}_a, \vec{r}_b\}$ being $\vec{r}_a$ the position of the a-particle and $\vec{r}_b = \{\vec{r}_1, .., \vec{r}_{a-1}, \vec{r}_{a+1}, .., \vec{r}_N\}$ the position of all other particles.

5.3.2.1 Complete positivity

The expectation value $\langle O_a \rangle \equiv \langle \Psi | \hat{O}_a \otimes 1_b | \Psi \rangle$ associated with an operator $\hat{O}_a$ acting on the a-particle, with 1_b being the identity operator for $\hat{H}_b$, can be computed as:

$$\langle O_a \rangle = \int d\vec{r}_a O_a \rho(\vec{r}_a, \vec{r'}_a, t)|_{\vec{r'}_a = \vec{r}_a} \tag{5.39}$$

where $\rho(\vec{r}_a, \vec{r'}_a, t)$ is the reduced density matrix:

$$\rho(\vec{r}_a, \vec{r'}_a, t) \quad = \quad \int d\vec{r}_b \Psi^*(\vec{r'}_a, \vec{r}_b, t)\Psi(\vec{r}_a, \vec{r}_b, t) \tag{5.40}$$

where $\Psi(\vec{r}_a, \vec{r}_b, t) \equiv \langle \vec{r}_a, \vec{r}_b | \Psi \rangle$ is the total wave function and O_a is the position representation of $\hat{O}_a$.

The same system can be described with the Bohmian theory [66, 67, 75] as follows. For each experiment, labeled by j, a Bohmian quantum state is defined by the same wave function $\Psi(\vec{r}_a, \vec{r}_b, t)$ plus a set of well-defined trajectories in physical space, $\{\vec{r}^j_1[t], ..., \vec{r}^j_N[t]\}$. The velocity of each trajectory is (see Chapter 3):

$$\vec{v}^j_a[t] = \frac{d\vec{r}^j_a[t]}{dt} = \frac{\vec{J}_a(\vec{r}^j_a[t], \vec{r}^j_b[t], t)}{|\Psi(\vec{r}^j_a[t], \vec{r}^j_b[t], t)|^2} \tag{5.41}$$

where $\vec{J}_a = \hbar \, \mathrm{Im}(\Psi^* \nabla_a \Psi)/m_a$ is the (ensemble value of the) current density with m_a the mass of the a-th particle. The set of N positions $\{\vec{r}^j_1[t], ..., \vec{r}^j_N[t]\}$ in different $j = 1, ..., W$ experiments is distributed (in quantum equilibrium [85]) as:

$$|\Psi(\vec{r}_a, \vec{r}_b, t)|^2 = \frac{1}{W} \sum_{j=1}^{W} \delta(\vec{r}_a - \vec{r}^j_a[t]) \delta(\vec{r}_b - \vec{r}^j_b[t]) \tag{5.42}$$

The identity in Equation (5.42) requires $W \to \infty$. Numerically, it is just required a large enough W.

The key element of our approach is the conditional wave functions associated with the a-th particle in the open system during the j-th experiment. It was already explained in Section 3.3 and it was defined as $\psi^j_a(\vec{r}_a, t) \equiv \Psi(\vec{r}_a, \vec{r}^j_b[t], t)$. I emphasize that $\psi^j_a(\vec{r}_a, t)$ provides an unproblematic (Bohmian) definition of the wave function of an open system, as seen in Section 3.3. A different conditional wave function for each simulated particle of the open system and for each simulated experiment is computed.

Next, the reduced density matrix, Equation (5.40), can be constructed using the fundamental elements of the Bohmian theory to show that our approach based on conditional wave functions is completely positive. I define the (tilde) conditional wave function of the a-th particle in the j-th experiment as:

$$\tilde{\psi}^j_a(\vec{r}_a, t) \equiv \frac{\Psi(\vec{r}_a, \vec{r}^j_b[t], t)}{\Psi(\vec{r}^j_a[t], \vec{r}^j_b[t], t)} \tag{5.43}$$

Notice that the denominator $\Psi(\vec{r}_a^j[t], \vec{r}_b^j[t], t)$ is just a pure time dependent term (without spatial dependence) that has no net effect on the definition of the velocity in Equation (5.41). The Bohmian velocity of the a-particle computed from $\tilde{\psi}_a^j(\vec{r}_a, t)$ is exactly the same value as the one it is got from $\psi_a^j(\vec{r}_a, t)$. Putting Equation (5.42) into $\langle O_a \rangle \equiv \langle \Psi | \hat{O}_a \otimes 1_b | \Psi \rangle$, integrating all degrees of freedom and using the definition of the (tilde) conditional wave function in Equation (5.43), it is obtained:

$$\langle O_a \rangle = \sum_{j=1}^{W} \left[p_j \tilde{\psi}_a^{j*}(\vec{r}_a, t) O_a \tilde{\psi}_a^j(\vec{r}_a, t) \right]_{\vec{r}_a = \vec{r}_a^j[t]} \tag{5.44}$$

where $p_j = 1/W$. Equation (5.44) allows to compute $\langle O_a \rangle$ from Equation (5.39) as:

$$\langle O_a \rangle = \int d\vec{r}_a \left[O_a \sum_{j=1}^{W} p_j \tilde{\psi}_a^{j*}(\vec{r'}_a, t) \tilde{\psi}_a^j(\vec{r}_a, t) \right]_{\vec{r'}_a = \vec{r}_a = \vec{r}_a^j[t]} \tag{5.45}$$

which directly allows the definition of the following density matrix [146]:

$$\rho(\vec{r}_a, \vec{r'}_a, t) = \sum_{j=1}^{W} p_j \tilde{\psi}_a^{j*}(\vec{r'}_a, t) \tilde{\psi}_a^j(\vec{r}_a, t) \tag{5.46}$$

The generalization to conditional wave functions with an arbitrary number of particles is straightforward. The time-evolution of Equation (5.46) ensures, trivially, that the dynamical map associated with the Bohmian approach is completely positive. In the position representation, the density operator $\hat{\rho} = \sum_{j=1}^{W} p_j |\tilde{\psi}_a^{j*}(t)\rangle\langle\tilde{\psi}_a^j(t)|$ gives $\langle \vec{r}_o | \hat{\rho} | \vec{r}_o \rangle = \sum_{j=1}^{W} p_j |\langle \vec{r}_o | \tilde{\psi}_a^j(t) \rangle|^2 \geq 0$ at any time[9] and at any position $\vec{r}_o$. The last step to conclude the CP demonstration is quite simple. If the density matrix in Equation (5.46) is positive, then the diagonal elements of $\langle \vec{r}_o | \hat{\rho} | \vec{r}_o \rangle$ evaluated only at $\vec{r}_o = \vec{r}_a^j[t]$ and defined as $\langle \vec{r}_o | \hat{\rho} | \vec{r}_o \rangle_B \equiv \sum_{j=1}^{W} p_j |\langle \vec{r}_o | \tilde{\psi}_a^j(t) \rangle|^2 \delta(\vec{r}_o - \vec{r}_a^j[t]) \geq 0$ are, by construction, also positive.

In fact, the term $\langle \vec{r}_o | \hat{\rho} | \vec{r}_o \rangle_B$ has a very simple interpretation. For the j experiment, the tilde conditional wave function in Equation (5.43) evaluated at $\vec{r}_o = \vec{r}_a^j[t]$ is $\langle \vec{r}_a^j[t] | \tilde{\psi}_a^j(t) \rangle = \tilde{\psi}_a^j(\vec{r}_a^j[t], t) \equiv \Psi(\vec{r}_a^j[t], \vec{r}_b^j[t], t) / \Psi(\vec{r}_a^j[t], \vec{r}_b^j[t], t) = 1$. Then, since $p_j = 1/W$, I get $\langle \vec{r}_o | \hat{\rho} | \vec{r}_o \rangle_B \equiv \sum_{j=1}^{W_B} 1/W = W_B/W$ where W_B is just the number of experiments where the position

[9] The fact that we deal with a CP definition, more than just a positive operator can be trivially demonstrated here, coming from the fact that the same $\psi_a^j(t)$ will be obtained if we enlarge the environment with additional degrees of freedom.

of the trajectory $\vec{r}_a^{\,j}[t]$ coincides with $\vec{r}_o$. In conclusion, as far as dealing with conditional wave functions and Bohmian trajectories in the dynamical description of the quantum systems with dissipation, the completely positivity of the approach is always satisfied (the number W_B of trajectories with position $\vec{r}_o = \vec{r}_a^{\,j}[t]$ can be zero, but it cannot be negative).

5.3.2.2 Comparison with other techniques

Several techniques use Bohmian trajectories as a mathematical/computational tool to solve some *reduced* equations of motion [147–150]. Here, on the contrary, Equation (5.42) guarantees empirical equivalence between Bohmian and standard quantum (non-relativistic) results in the whole closed system. This implies not only the correct description of any smaller portion of the closed system, i.e. our open systems, but also empirical equivalence in the measured values [68, 85]. It is important to emphasize that Gambetta and Wiseman [143, 144] pointed out that the only physical continuous-in-time interpretation of the wave functions solution of non-Markovian SSEs, i.e. with back-action from the environment to the system, has to be based on the Bohmian theory. In other words, in spite of its mathematical interest as a computational tool, the *improper* sum of wave functions of an open system in Equation (5.46) has a problematic ontological meaning within standard quantum mechanics, as indicated by D'Espagnat [151][10]. On the contrary, the Bohmian theory allows a *proper* definition of a wave function of an open system with or without continuous measurements, for both Markovian and non-Markovian dynamics. We can always interpret (part of) $\vec{r}_b^{\,j}[t]$ as the pointer of a measuring apparatus. Therefore, the Bohmian conditional wave function $\psi_a^j(\vec{r}_a, t)$ can be thought as the wave function of SSE conditioned to a continuous observation defined by the (part of) $\vec{r}_b^{\,j}[t]$ as the pointer.

To the best of my knowledge, this is the first method that develops a practical SSE algorithm using conditional wave functions solutions of Equation (3.11). In the Bohmian framework, the ensemble values can be directly computed from the trajectories and not from the conditional wave function. Therefore, the technical problems of SSE due to norm degradation are avoided in the approach. It is a remarkable fact that the velocity of $\vec{r}_a^{\,j}[t]$ computed from $\psi_a^j(\vec{r}_a, t)$ gives the exact same value as using $\Psi(\vec{r}_a, \vec{r}_b^{\,j}[t], t)$. Thus, the velocity, as seen in Equation (5.41), is totally independent of the norm of the conditional

[10] If we ignore what state is actually present in a closed system (all we know is that several states $|\psi_1\rangle, |\psi_2\rangle, ...$ are possible with several probabilities $p_1, p_2, ...$), the statistical operator $\rho = \sum_w p_w |\psi_w\rangle\langle\psi_w|$ is unproblematically defined as a *proper* mixture of states. However, the states $|\psi_1\rangle, |\psi_2\rangle, ...$ for an open (sub)system have no ontological meaning within standard quantum theory[151]. Then, the reduced density matrix is an *improper* mixture of states because the states themselves are ontologically undefined in the standard theory. Our ignorance plays a secondary role in an open system.

wave functionBohm. This explains why Equation (3.11) deals with a non-normalized wave function.

Since the approach deals with a *realistic* definition (i.e. with a clear ontological meaning, see Section 3.3) of the wave function of an open system, $\psi_a^j(\vec{r}_a, t)$, a relevant advantage is that it allows a *realistic* description of the stochastic sources of dissipation (beyond the typical environmental noise sources introduced in SEE[103]), while maintaining complete positivity. Below, as an example, I provide the stochastic conditioned potential of Equation (3.11), which tackles the electron-lattice energy dissipation in tunnelling devices.

5.3.3 Application to electron-lattice interaction

To analyse the electron-lattice interaction, here, the exact expression for Equation (3.11) is developed for electrons interacting with the lattice. For that purpose, I consider N_e electrons with positions $\vec{r} = \{\vec{r}_1, ..., \vec{r}_{N_e}\}$ and N_h ions located at $\vec{R} = \{\vec{R}_1, ..., \vec{R}_{N_h}\}$. Although not explicitly indicated, N_h includes also all additional particles required to deal with a closed system with the many body wave function $\Psi(\vec{r}_a, \vec{r}_b, t) \equiv \langle \vec{r}_a, \vec{r}_b | \Psi \rangle$ mentioned in Section 5.3.2.1. To simplify the notation, hereafter, I define $\vec{r} = \{\vec{r}_a, \vec{z}_a\}$ with $\vec{z}_a = \{\vec{r}_1, .., \vec{r}_{a-1}, \vec{r}_{a+1}, .., \vec{r}_{N_e}\}$. These new variables are related to previous ones through $\vec{r}_a = \vec{r}_a$ and $\vec{r}_b = \{\vec{z}_a, \vec{R}\}$, with $\vec{r} = \{\vec{r}_a, \vec{r}_b\}$.

I compute the evolution of the full wave function $\Psi(\vec{r}, \vec{R}, t) = \Psi(\vec{r}, t)$ under the effect of the full Hamiltonian $\hat{H}$ in Equation (3.11). The position representation of the Hamiltonian $\hat{H}$ gives:

$$H(\vec{r}, \vec{R}) = K_e(\vec{r}) + K_h(\vec{R}) + V_{ee}(\vec{r}) + V_{hh}(\vec{R}) + H_{ep}(\vec{r}, \vec{R}) \tag{5.47}$$

with $K_e(\vec{r})$ the electron kinetic energies, $K_h(\vec{R})$ the nucleus kinetic energies, $V_{ee}(\vec{r})$ the electron-electron interactions, $V_{hh}(\vec{R})$ the nucleus-nucleus interactions, and $H_{ep}(\vec{r}, \vec{R})$ the total electron-lattice interaction. The last term can be split into $H_{ep} = H_{ep,\vec{R}_0} + H_{ep,\vec{u}}$. The first term, $H_{ep,\vec{R}_0}$, corresponds to the interaction of the electrons with the fixed (equilibrium) positions of the ions $\vec{R}_0$. The second one, $H_{ep,\vec{u}}$, includes the interaction of the electrons with the displacement of the ions, $\vec{u} = \vec{R} - \vec{R}_0 = \{\vec{u}_1, ..., \vec{u}_{N_h}\}$, and it is the only term that prevents the exact separation of the many-particle wave function. Thus, I can rewrite Equation (5.47) as:

$$H(\vec{r}, \vec{R}) = H_c(\vec{r}, \vec{R}) + H_{ep,\vec{u}}(\vec{r}, \vec{R}) \tag{5.48}$$

with $H_c(\vec{r},\vec{R}) = K_e(\vec{r}) + K_h(\vec{R}) + V_{ee}(\vec{r}) + V_{hh}(\vec{R}) + H_{ep,\vec{R}_0}(\vec{r},\vec{R}_0)$. Finally, the computation of H_a just requires the explicit evaluation of the terms:

$$\langle \vec{r}_a, \vec{z}_a, \vec{R}|\hat{H}_{ep,\vec{u}}|\Psi(t)\rangle|_{\vec{z}_a^j[t],\vec{R}^j[t]} \tag{5.49}$$

and

$$\langle \vec{r}_a, \vec{z}_a, \vec{R}|\hat{H}_c|\Psi(t)\rangle|_{\vec{z}_a^j[t],\vec{R}^j[t]} \tag{5.50}$$

The relevant interaction of the (conditional) wave packet with the moving lattice, present in $\hat{H}_{ep,\vec{u}}$, will be evaluated in Section 5.3.3.1 in the second-quantization formalism. The less relevant interaction of the (conditional) wave packet with the fixed (equilibrium) lattice due to H_c present in Equation (5.50) is discussed in Appendix E.2.

5.3.3.1 Electron-phonon stochastic potential

Assuming a small displacement of the ions $\vec{u}_h = \vec{R}_h - \vec{R}_{h,0}$ from their equilibrium positions $\vec{R}_{h,0}$, the electron-lattice Hamiltonian for small displacements of ions in the position representation can be written as $H_{ep,\vec{u}}(\vec{r},\vec{R}) = \sum_{e,h} \vec{u}_h \partial U(\vec{r}_e - \vec{R}_h)/\partial \vec{R}_h|_{\vec{R}_{h,0}}$. The (second-quantization) electron-lattice Hamiltonian is then:

$$\hat{H}_{ep,\vec{u}} = \sum_{e,p} g_{\vec{k}_e}^{\vec{q}_p} \hat{c}^\dagger_{\vec{k}_e+\vec{q}_p} \hat{c}_{\vec{k}_e} (\hat{b}_{\vec{q}_p} + \hat{b}^\dagger_{-\vec{q}_p}) \tag{5.51}$$

with $\hat{b}_{\vec{q}_p}$ and $\hat{b}^\dagger_{\vec{q}_p}$ being the annihilation and creation operators of the atomic vibrational eigenstate $|\vec{q}_p\rangle$. Similarly, $\hat{c}_{\vec{k}_e}$ and $\hat{c}^\dagger_{\vec{k}_e}$ are the corresponding operators of the (Bloch) eigenstate $\langle \vec{r}_e|\hat{c}^\dagger_{\vec{k}_e}|0\rangle = \langle \vec{r}_e|\vec{k}_e\rangle = \phi_{\vec{k}_e}(\vec{r}_e)$. The coupling constant $g_{\vec{k}_e}^{\vec{q}_p}$ specifies the transition between the eigenstates. The first-quantization explanation of the electron-lattice interaction and the definition of $g_{\vec{k}_e}^{\vec{q}_p}$ are given in Appendix E.1. The initial many-body (electron and lattice) quantum state is:

$$\Psi(\vec{r},\vec{R},t_0) = \sum_{\vec{k},\vec{q}} a(\vec{k},\vec{q},t_0)\Phi_{\vec{k}}(\vec{r})\Phi_{\vec{q}}(\vec{R}) \tag{5.52}$$

with $a(\vec{k},\vec{q},t_0)$ accounting for an arbitrary superposition, $\Phi_{\vec{k}}(\vec{r}) \equiv \langle \vec{r}|\hat{c}^\dagger_{\vec{k}_1}...\hat{c}^\dagger_{\vec{k}_{N_e}}|0\rangle$ the Slater determinant with $\vec{k} = \{\vec{k}_1,...,\vec{k}_{N_e}\}$, and $\Phi_{\vec{q}}(\vec{R})$ the atomic part with $\vec{q} = \{\vec{q}_1,\vec{q}_2,...\}$

representing a phonon base. The Slater determinant of electrons can be expanded in minors giving:

$$\Psi(\vec{r}_a,\vec{z}_a,\vec{R},t)=\sum_{\vec{k},\vec{q}}a(\vec{k},\vec{q},t)\Phi_{\vec{q}}(\vec{R})\sum_{\vec{k}_w}\phi_{\vec{k}_w}(\vec{r}_a)s_{a,w}\langle\vec{z}_a|\hat{c}^\dagger_{\vec{k}_1}..c^\dagger_{\vec{k}_{w-1}}c^\dagger_{\vec{k}_{w+1}}..\hat{c}^\dagger_{\vec{k}_N}|0\rangle \quad (5.53)$$

with $s_{a,w}$ the sign of the (a,w) cofactor. Then, the term in Equation (5.51) acting on Equation (5.53) is (for more details see Appendix E.1):

$$\begin{aligned}\langle\vec{r}_a,\vec{r}_b|\hat{H}_{ep,\vec{u}}|\Psi(t)\rangle &= \sum_{e,p}g^{\vec{q}_p}_{\vec{k}_e}\langle\vec{r}_a,\vec{r}_b|\hat{c}^\dagger_{\vec{k}_e+\vec{q}_p}\hat{c}_{\vec{k}_e}(\hat{b}_{\vec{q}_p}+\hat{b}^\dagger_{-\vec{q}_p})|\Psi(t)\rangle \quad (5.54)\\ = \sum_{e,p}g^{\vec{q}_p}_{\vec{k}_e}\sum_{\vec{k},\vec{q}}a(\vec{k},\vec{q},t)\Phi'_{\vec{q}}(\vec{R})\sum_{\vec{k}_w}\phi_{\vec{k}_w+\vec{q}_p}(\vec{r}_a)s_{a,w}&\langle\vec{z}_a|\hat{c}^\dagger_{\vec{k}_1}..c^\dagger_{\vec{k}_{w-1}}c^\dagger_{\vec{k}_{w+1}}..\hat{c}^\dagger_{\vec{k}_N}|0\rangle\end{aligned}$$

I use $\Phi'_{\vec{q}}(\vec{R})$ to account for the effect of the electron-lattice interaction in the atomic part.

When conditioning Equation (5.53) and Equation (5.54) to $\{\vec{z}^j_a[t],\vec{R}^j[t]\}$, the variable $\vec{q}^j_p$ is also fixed to some particular values in this j-th experiment. The exact (deterministic) description of the electron-lattice interaction would require perfect knowledge of all ions dynamics through $\vec{R}^j[t]$. However, since ions are considered here as the *environment* of electrons (they are not explicitly simulated), their effect stochastically is introduced in the equation of motion of electrons in Equation (3.11), ensuring that the probabilities of different phonon modes satisfy some well-known precomputed probabilities[152]. It is assumedd that only one (or none) phonon mode $\vec{q}^j_p$ becomes relevant at each time. Then, the (envelope) conditional wave function before a collision $t<t_c$ is:

$$\psi^j_a(\vec{r}_a,t)=\sum_{\vec{k}_w}f(\vec{k}_w,t)\phi_{\vec{k}_w}(\vec{r}_a) \quad (5.55)$$

Assuming that $g^{\vec{q}^j_p}_{\vec{k}_a}\approx g^{\vec{q}^j_p}_{\vec{k}_{0a}}$ with $\vec{k}_{0a}$ the central wave vector of the a wave packet, the final (envelope) conditional wave function in Equation (5.54) after the collision $t>t_{c2}$ is $\psi^j_a(\vec{r}_a,t)\equiv\langle\vec{r}_a,\vec{r}^j_b[t]|\hat{H}_{ep,\vec{u}}|\Psi(t)\rangle$ which can be written as (see Appendix E.1):

$$\psi_a^j(\vec{r}_a,t) = g_{\vec{k}_{0a}}^{\vec{q}_p^j} \sum_{\vec{k}_w} f(\vec{k}_w,t)\phi_{\vec{k}_w+\vec{q}_p^j}(\vec{r}_a) \tag{5.56}$$

where the $\vec{r}_a$-dependence in Equation (5.55) and Equation (5.56) is given by $\phi_{\vec{k}_a}(\vec{r}_a)$ and $\phi_{\vec{k}_w+\vec{q}_p}(\vec{r}_a)$ respectively, and $f(\vec{k}_w,t)$ includes all other terms evaluated at $\{\vec{z}_a^j[t],\vec{R}^j[t]\}$.

These results have a simple and intuitive explanation. During the collision, the (Bloch state) quasi-momentum eigenstates that build the wave packet change from $|\vec{k}_a\rangle$ to $|\vec{k}_a+\vec{q}_p^j\rangle$, while its weight $f(\vec{k}_w,t)$ remains constant.

I remark that these collisions introduce not only stochastic dynamics in the evolution of the conditional wave function, but also time-irreversibility in the whole simulation, since, in general, $g_{\vec{k}_{0a}}^{\vec{q}_p} < g_{\vec{k}_{0a}+\vec{q}_p}^{-\vec{q}_p}$, where positive (negative) $\vec{q}_p$ means phonon absorption (emission).

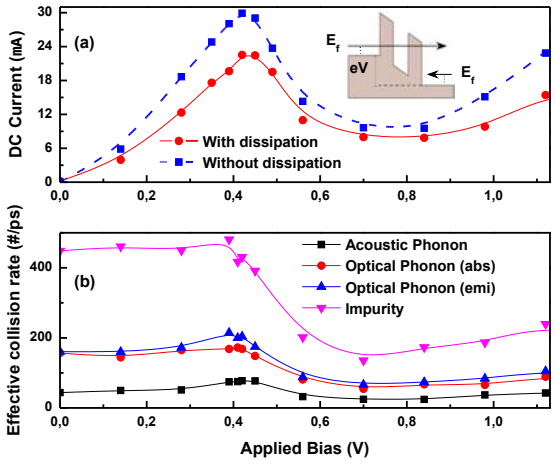

FIGURE 5.8: (a) Current-voltage characteristic for a RTD with (solid red curve) and without (blue dashed curve) dissipation due to acoustic and optical phonons and impurities. The barrier height and width are 0.5 eV and 1.6 nm and the well width is 2.4 nm. A n-type doping with a Fermi level of $E_f = 0.15\,eV$ above the conduction band is considered. (b) Effective collision rate as a function of bias. The optical phonons lead to an inelastic change of the electron energy of $\pm 0.036\,eV$.

5.3.3.2 Dissipative transport in parabolic-band structures

Now, I apply the approach for the simulation of a typical GaAs/AlGaAs Resonant Tunneling Device (RTD) when elastic (acoustic phonons and impurities) and inelastic (optical phonons) collisions are considered. In particular it can be shown that the required evolution of the conditional wave function ψ_a interacting with a phonon $\vec{q}_p = \{q_{px}, q_{py}, q_{pz}\}$ in a material with parabolic band structure can be obtained from Equation (3.11):

$$i\hbar\frac{\partial\psi_a}{\partial t} = \left[\frac{1}{2m^*}\left(\vec{p}_a + \vec{\lambda}_a\Theta_{t_c}\right)^2 + V_a\right]\psi_a \tag{5.57}$$

where $\vec{p}_a = -i\hbar\vec{\nabla}_a$, $m^* = 0.067m_e$ is the electron effective mass (m_e is the free electron mass), $\vec{\lambda}_a = \hbar\vec{q}_p$ and $\Theta_{t_c} \equiv \Theta(t-t_c)$ is the Heaviside step function. In Appendix E.3 it is proved that Equation (5.57) exactly reproduces the transition of ψ_a from Equation (5.55) to Equation (5.56). Each electron $a = \{1, 2, .., N_e\}$ has its own Equation (5.57) to compute ψ_a and $\vec{r}_a[t]$ by time-integrating its velocity in Equation (5.41). The term V_a provides the Coulomb correlation among all simulated electrons including the appropriate boundaries. The injection model locates the initial conditional wave function outside the simulation box and defines it from typical Gaussian wave packets with a dispersion $\sigma = 40$ nm. The properties of the injected electrons are selected according to some well-defined assumptions. For example, the energies of the injected electrons from one contact (assumed in thermodynamical equilibrium) into the open system fulfill a Fermi-Dirac distribution. This randomness in the injection of electrons introduces a source of stochasticity in the description of the properties of the open system.

The current is computed as the net number of trajectories $\vec{r}_a[t]$ transmitted from one side to the other, divided by the total simulation time (5 ps). Identically the DC current is also computed as the time average of the total (conduction plus displacement) current. Both types of DC computations provide the same value at each bias point, showing the accuracy of the simulation. Technically, the experiment is not repeated, but the numerical simulation takes so long that electrons are entering and leaving the active region many times, providing repeated scenarios. The number and type of collisions are obtained from the Fermi Golden Rule for GaAs materials[152]. The collision in Equation (3.11) does not introduce any artificial decoherence. The expected reduction of the transmission[153, 154] seen in Figure 5.8(a) is because of the randomization of the momentum due to acoustic phonons and to the energy dissipation due to the emission of optical phonons.In Figure 5.8(b) it is seen that the number of collisions at resonance is three times larger that out of resonance, showing that the ballisticity of tunnelling devices also depends on the electron transit time that varies from one voltage to another, due to different back-actions of our non-Markovian (phonon) environment [133, 134].

5.3.3.3 Dissipative transport in linear-band structures

Next, the Bohmian trajectories and the conditional wave function evolution of one electron during a collision with a phonon in graphene are presented, with a richer band structure than GaAs. By the use of the conditional bispinor wave function, Equation (4.39)

the inclusion of the collision in a 2D bispinor $\psi_a \equiv (\psi_{a,1}, \psi_{a,2})^T$ gives:

$$i\hbar\frac{\partial\psi_a}{\partial t} = v_f\begin{pmatrix} V_a/v_f & p_a^- + \lambda_a^-\Theta_{t_c} \\ (p_a^+ + \lambda_a^+\Theta_{t_c})\chi_{t_c} & V_a\chi_{t_c}/v_f \end{pmatrix}\psi_a \tag{5.58}$$

where v_f=10^6 m/s is the Fermi velocity. I define $p_a^\pm = -i\hbar\partial_{x_a} \pm \hbar\partial_{y_a}$ and $\lambda_a^\pm = \lambda_{ax} \pm i\lambda_{ay}$ as the change in momentum $\vec{\lambda}_a = \hbar\vec{q}_p$ due to the interaction with a phonon with wave vector $\vec{q}_p = \{q_{px}, q_{py}\}$. When the interaction occurs, the term $\chi_{t_c} = e^{i(m\pi+\beta_{\vec{k}_{fa}}-\beta_{\vec{k}_{0a}})\Lambda_{t_c}}$ makes sure that the final state is either in the conduction band (positive energy branch) or in the valence band (negative energy states). If the electron changes from the conduction to the valence band (or vice versa), I use $m = 1$ and if there is no change of band $m = 0$, with $e^{i\beta_{\vec{k}_{0a}}} = (k_{0ax} + ik_{0ay})/|\vec{k}_{0a}|$, where $\vec{k}_{0a}$ ($\vec{k}_{fa}$) is the central initial (final) wave vector and $e^{i\beta_{\vec{k}_{fa}}}$ having the same definition. χ_{t_c} is only relevant at t_c, i.e. $\Lambda_{t_c} \equiv \Lambda_{t_c}(t) = 0$ except $\Lambda_{t_c}(t = t_c) = 1$. In Appendix E.4 it is proved that Equation (5.58) produces the transition of the 2D bispinor ψ_a from Equation (5.55) to Equation (5.56).

Wave function evolution with a scattering event

In Figure 5.9 and Figure 5.10 I present numerical results for the electron-phonon collisions in graphene, whose dynamics near the Dirac points are given by Equation (5.58). The initial state in both examples is a Gaussian wave packet with dispersion $\sigma = 40\,nm$ and wave vector $|\vec{k}_{0a}| = 2.27 \cdot 10^8\ m^{-1}$, whose initial pseudospin lies in the conduction band.

In both figures (Figure 5.9 and Figure 5.10), it can be seen how the inital electron is deviated from its initial trajectory, because the collision event with a phonon.

Graphene current-voltage curves with dissipation

Here I present different current-voltage curves for a graphene transistor (GFET) for both ballistic and dissipative quantum transport. The GFET simulated channel length is $L_x = 40$ nm, its width $L_y = 250$ nm and the Fermi energy is 0.15 eV above the Dirac point. It has a bottom and top gates, whose voltages are set equal to zero, $V_{bg} = V_{tg} = 0$ V. Electrons are injected described by conditional Gaussian wave packets, following Fermi statistics at room temperature as indicated in Figure 5.11 (the injection model will be further discussed in Chapter 6).

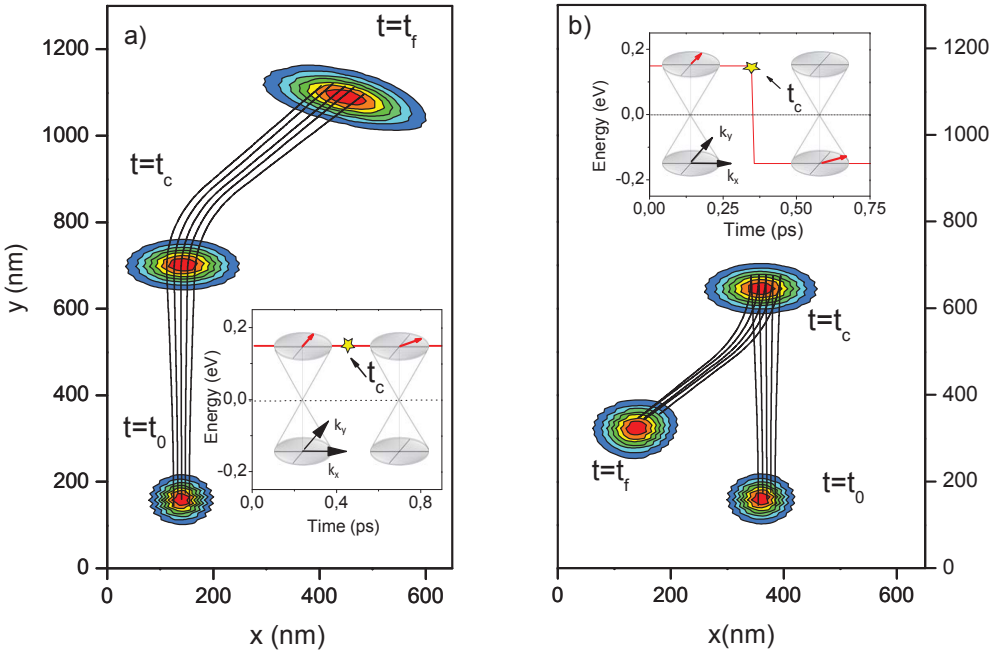

FIGURE 5.9: a) Time evolution of the modulus squared of the conditional bispinor for an electron initially at t_0 in the conduction band, with wave vector $(k_{0ax}, k_{0ay}) = (0, |\vec{k}_{0a}|)$, suffering an elastic collision at t_c with a phonon that provides a final wave vector $(k_{fax}, k_{fay}) = (|\vec{k}_{0a}|/\sqrt{2}, |\vec{k}_{0a}|/\sqrt{2})$. The associated Bohmian trajectories are also shown. Inset: Electron energy conservation for the elastic collision. b) Same change of wave vector as in a) but with an inelastic collision that produces a final electron in the valence band (where velocity and momentum are opposite).

In Figure 5.12 (a), four different current-voltage characteristics are plotted. The dashed lines correspond to ballistic transport, whereas the solid ones takes into account energy dissipation. The insets of Figure 5.12(a) are related to the one plotted in Figure 5.11 indicating the relevant presence of electrons with energy above the Dirac point, conduction band, and below, valence band. In particular we consider acoustic and optical phonons with emission and absorption from, both, zone edge and zone center with energy interchange of ± 0.160 and ± 0.196 eV, respectively. The scattering rates are obtained from [155]. Since typical graphene mean free path values are low, the dark blue (without dissipation) and orange (with dissipation) lines are very similar. For that reason, I added the red line where the scattering rates are enhanced. We see in Figure 5.12 (b) and (c) the effective collision rate as a function of the applied bias for the orange and red lines respectively. In the treatment of scattering in graphene structures one has to remind that graphene is gapless. Thus, in principle, there is no minimal value of energy required for an electron to suffer phonon emission. However, in practice, the Pauli principle avoids collision where the final energy of the electron is lower than the Fermi energy[11]. For that reason, we observe in Figure 5.12 (b) that phonon emission is

[11]The Fermi energy is not well defined inside the device because it is a system outside of thermodynamical equilibrium when an external bias is applied. However, a reasonable estimation of a quasi-Fermi energy inside the device can be easily approximated to take into account such many-body (exchange

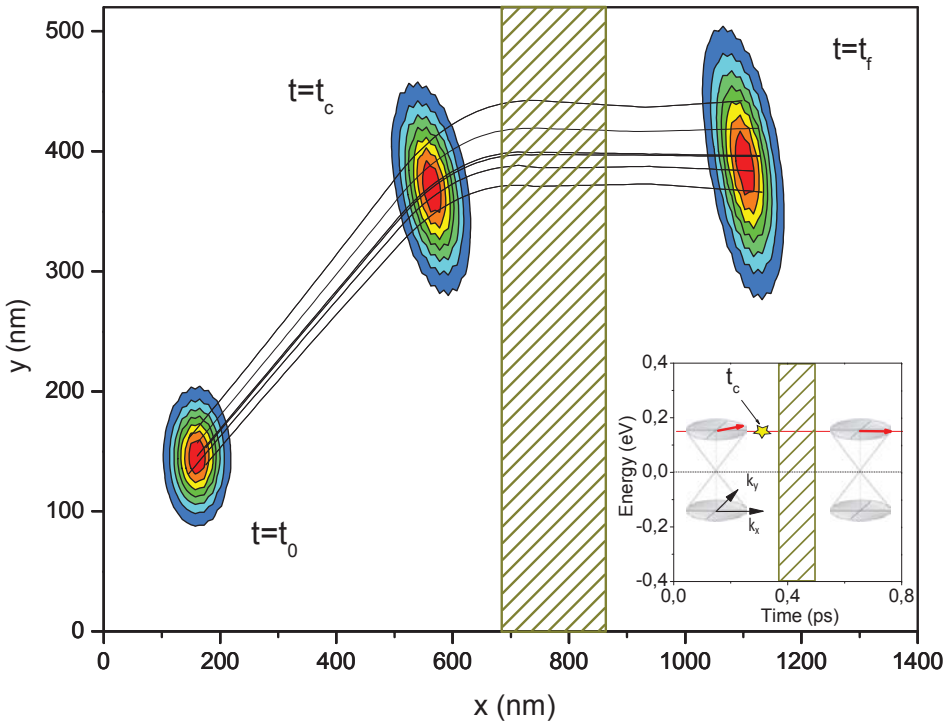

FIGURE 5.10: Time evolution of the modulus squared of the conditional bispinor for an electron which impinges on a 0.4 eV barrier with a width of 200 nm. The initial $t = t_0$ direction is $\beta_0 = \pi/6$ so Klein tunneling should be minimal. At $t = t_c$, an elastic collision deviates the electron in a perpendicular direction to the barrier maximizing the Klein tunneling.

only relevant for applied bias (V_{ds}) higher than the optical phonon energy for zone edge and zone center (± 0.160 and ± 0.196 eV respectively). In such situations, an electron injected with an energy roughly equal to the Fermi energy will acquire enough kinetic energy during its ballistic transport along the device to thermalize. If this condition is fulfilled, emission is higher than absorption, obtaining current values smaller than in the ballistic scenario. I also remind that forward scattering is prohibited and backscattering is preferred for zone edge phonons and just the opposite for acoustic phonon scattering, while the zone center phonons are isotropic [155].

To successfully explain the shape of the current-voltage characteristic of Figure 5.12 (a), it is necessary to i) understand how electrons are injected in graphene and which ones participate in the current and ii) the density of states of graphene. Since the injection model will be further discussed in Chapter 6, let me make just a brief summary. Contrary to standard semiconductors with energy gap, apart from electrons in the conduction band, electrons belonging to the valence band also contribute to the current.

interaction) effect in a manageable way. I defined such quasi-Fermi energy so that the difference between the electrostatic potential and the Fermi energy level in the reservoir is constant along the device.

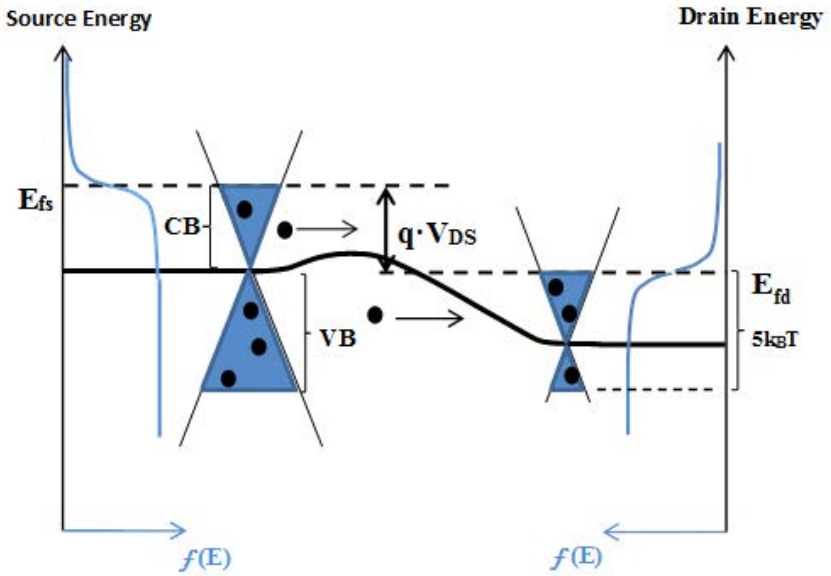

FIGURE 5.11: Schematic representation of an energy profile in the transport direction of devices in BITLLES simulator. The applied drain-source bias, V_{DS}, provides a different source, E_{fs}, and drain, E_{fd}, Fermi levels, the Fermi-Dirac distribution function at each contact are indicated. Relevant electrons for computing the quantum current are the ones belonging to the blue shaded energy region.

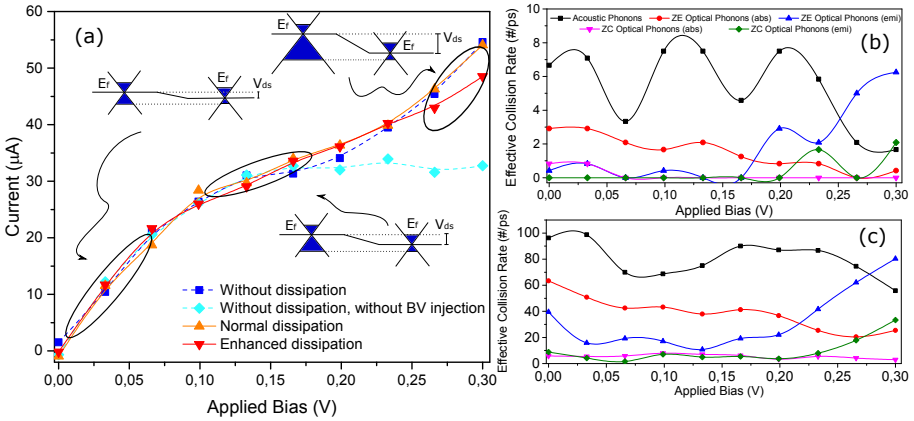

FIGURE 5.12: (a) Current-voltage characteristic for the GFET described in the text for ballistic transport (dashed lines) and transport with dissipation (solid ones). The dark blue (square) line corresponds to normal graphene injection (electrons injected from the conduction and the valence band), while in the light blue (diamond) line only electrons from the conduction band are injected. The orange (up triangle) line takes into account dissipation due to acoustic and optical phonons. The red (down triangle) line corresponds to enhanced dissipation. The insets sketch different energy profiles for applied bias. Similarly to Figure 5.11, only electrons in the blue energy (above and below the Dirac point) are relevant. (b) Effective collision rate as a function of the applied bias for the orange (up triangle) line in (a) for acoustic and optical phonons. (c) Same as (b) but for the red (down triangle) line in (a), where dissipation is enhanced.

As sketched in Figure 5.11, relevant electrons for transport are the ones whose energy is in between the Fermi energies of the drain and source, i.e. electrons from the blue area

in Figure 5.11 (strictly speaking, Fermi statistics are taken into account since we are at room temperature). This means that, contrary to normal FETs, there is no saturation current, since the more the voltage is applied between source and drain, the more number of electrons are transmitted from the source to the drain (from valence band in the source to conduction band in the drain). In Figure 5.12 we can appreciate a saturation region when the applied voltage is close to the Fermi energy level. To understand this behaviour it is important to be aware that the density of states is proportional to the energy, i.e. $D_{gr}(E) \propto E$. Then, if due to the dynamics of the system, electrons in an energy level E_1 try to move to a lower energy level E_2 not all electrons will be able to arrive, since in this scenario $D_{gr}(E_2) < D_{gr}(E_1)$. Thus, some of the electrons will be rejected. This is sketched in the different insets of Figure 5.12 (a). In these insets, similarly to Figure 5.11, the blue area depicts the relevant electrons contributing to the current and explains the saturation when the voltage is close to the Fermi energy level.

The dark blue current-voltage characteristic behaviour can be easily understood with the above considerations. When increasing the drain voltage, more electron flows from the source to the drain and current increases. However, when the voltage corresponds to the Fermi energy, the density of states vanishes in the drain and no more electrons can reach the drain, thus current saturates. However, if the drain voltage keeps on increasing, density of states again is non zero, and more electrons from the source in the valence band can reach the drain in the conduction band. In the case of the light blue curve, when no electrons are injected from the valence band, current saturates because after the voltage reaches the Fermi energy value, the same amount of electrons from the conduction band are injected independently of the applied voltage. This is similar to typical FETs with semiconductors with energy gap where typically only electrons from the conduction band (or only electrons from the valence band) are considered. Since graphene mean free path is of the order of a micron and our device is much smaller, when scattering is considered (orange line), the current-voltage line is very similar to the ballistic one. On the contrary, if I increase the scattering rates (red line), dissipation occurs and then current decreases compared to the ballistic case.

5.4 Conclusions

In this chapter I have presented which are the problems when dealing with no completely positive methods. I have presented an approach to analyze quantum dissipation based on Bohmian conditional wave functions that preserves complete positivity. It allows a realistic consideration of dissipative sources. Formally, the approach follows

the SSE technique[136] for non-Markovian scenarios [86, 140–144], but allowing a physical interpretation of the output results under a continuous measurement. Other open system techniques are rarely applied to the simulations of electron devices (with exceptions such as the Wigner-Boltzmann approach, which has unphysical problems as mentioned in Section 5.2.3, or other density matrix approaches that have difficulties in being adapted to spatially well-defined models respecting the different spatial regions (with well-defined boundaries) typical in electron devices[156, 157]). Typically, dissipation in quantum electron transport is simulated through a partition of the full Hilbert space into smaller spaces where sets of eigenstates are perfectly determined. Interactions (dissipation) between different spaces are introduced through coupling constants [31, 158, 159]. The solution of such models implicitly involves an improper mixture of states [151] that, in spite of its computational interest, has no ontological definition within standard quantum mechanics. The Bohmian conditional wave functions provide a *unproblematic* way to define the wave function of an open system [143, 144], and it allows a realistic simulation of quantum dissipation in electron devices with linear and parabolic band structures.

With the accurate inclusion of quantum dissipation in the evolution of conditional wave functions, the *general* and *accurate* quantum-trajectory approach presented here is an excellent candidate to substitute the old Monte Carlo solution of the Boltzmann equation for semi-classical systems [152] in the new nanoelectronics/atomtronics quantum scenarios.

Chapter 6

Time Dependent electrical current and its fluctuations in high frequency device applications

In this chapter, I present results for the current and its fluctuations (noise) in different quantum systems. I start in Section 6.1 by introducing how the measurement problem appears when trying to model current and noise. There, I also explain how the total (particle plus displacement) current can be computed from the Ramo-Shockley-Pellegrini theorem and I introduce what is noise of the electrical current. After that, I discuss some relevant features regarding noise which are included in the BITLLES simulator, such as the importance of the injection model in Section 6.2 or a source of noise that appears when considering time dependent wave packet models in Section 6.3. Finally, in Section 6.4, an intrinsic limitation for the miniaturization of electron devices due to the discrete nature of particles is presented.

6.1 Introduction to electrical current and noise

Classical and quantum measurement are different from a technological and ontological point of view. The first difference between a classical and a quantum measurement is that the latter provokes an unavoidable perturbation of the quantum system while being measured. Even using the best technological means, it is impossible to develop a measuring apparatus that ensures no perturbation for all quantum systems. Second, when

I repeat a measurement in a quantum system, by preparing other quantum systems exactly in the same way as the initial one, the measured values varies in a random way. Again, such randomness cannot be avoided by technologically improving the measuring apparatus. When modeling a quantum system, therefore I have two options, to ignore the measurement perturbation of the system (something normal in classical modeling, but that has to be considered in quantum systems as an approximation) or to take it into account (something that is non trivial at all).

In quantum mechanics, the reality of the properties of a quantum object is not obvious. Different quantum theories give different definitions of what is real. Orthodox quantum mechanics do not say anything about the reality of the system properties when they are not being measured. What is the position of a particle from a orthodox point of view? Regarding this fact, Einstein said: "I like to think the moon is there even if I am not looking at it.". Particles behave as a wave, until the position is measured and then we know its location. From this point of view, the unmeasured system properties have no reality, and just when measuring it collapses to one of its possible eigenstates, with an eigenvalue that specifies the reality of the measured property. On the other hand, Bohmian mechanics accepts that, even if it is not being measured, systems have they own (hidden) reality of the position at any time, such positions provide the particle trajectories. The system particles have definite positions even when not being measured. However, because of the act of measuring we disturb the unmeasured system and then we can just extract information about the reality of our perturbed system, not from the original (unmeasured) one.

So, in order to model correctly our system and its corresponding measured observables, in Bohmian mechanics one has to model (somehow) the system plus the measuring apparatus, and therefore the perturbation that it introduces in our system under study. Because of the many-body problem (see Section 3.2), this issue is technically difficult to solve, and then the conditional wave function is used to tackle the problem as it was showed in Section 3.3. On the other hand, in the orthodox theory only the quantum system is simulated and the measuring apparatus is substituted by a proper hermitian operator. Such operators are mathematical entities relating eigenvalues and eigenstates. The eigenvalues are all real (each one corresponding to a possible experiment outcome) and whose eigenvectors are orthogonal (since different observable outcomes are exclusive). The orthodox theory does not provide us which operator has to be used, apart from the fact that it should provide us the same results (eigenvalues) as the experiments provide us. When measuring some properties, such as energy, spin or momentum, the explicit form of these operators is well known. However, when trying to measure more

complex properties the explicit mathematical expression of this operator is not known, this is the case of the displacement current, which will be interesting for me later. Furthermore, more problems arise, because depending of the type of measurement performed, strong or weak [160–165], different outcomes are expected. Therefore, many unknowns appear when looking for the correct operator.

Nevertheless, to our interests, Bohmian mechanics offers an attractive alternative, precisely because this theory contains definite positions for the particles of the system, even when not being measured. All properties, included total (displacement plus particle) current can be obtained from the bohmian positions and trajectories. In fact, I anticipate that a very desirable and manageable language in terms of velocities will appear later in Section 6.1.1. These velocities correspond to the electron velocities and reflect totally the quantum behavior of our system, since they are obtained from the Schrödinger or the Dirac equation (see Chapter 3 for more details). In fact, as a first approximation, we can neglect the effect of the apparatus, and just compute the system without simulating the measuring apparatus. This is obviously a first approximation, but extremely useful since it decreases enormously the computational burden.

Let me consider a particular scenario. I consider a device as the one showed in Figure 6.1, where I want to compute the current. As I will show in next Section 6.1.1, in order to obtain the current in my device I need to compute the total current through the Ramo-Shockley-Pellegrini theorem in the contacts. These contacts have an enormous amount of electrons ($\approx 10^{23}$ electrons) and in principle all of them should be simulated in order to introduce correctly the measuring perturbation, something impossible from a computational point of view. However, it was shown in [165, 166] this kind of measurement is a weak measurement. The contacts just adds noise in frequency (because of the time that electrons need to be screened by each other) and has nothing to do with the (quantum) measurement problem. The relevant thing is that with the use of the conditional wave function, the particle is computed either transmitted or reflected without the need of the contacts. This fact cannot be performed by the orthodox theory (without collapse). For that reason, some excellent models that work correctly for DC computations, such as the Landauer formalism, cannot provide answer for some properties, such as transients, high frequency properties or partition noise (see Section 3.4 for more details) and then more complex and non intuitive tools have to be added, such as the annihilation and creator operators introduced by Büttiker (to mimic the collapse law). However, in the Bohmian framework, the electron is either transmitted or reflected and then (among other properties) noise, AC and transients can be straightforwardly computed.

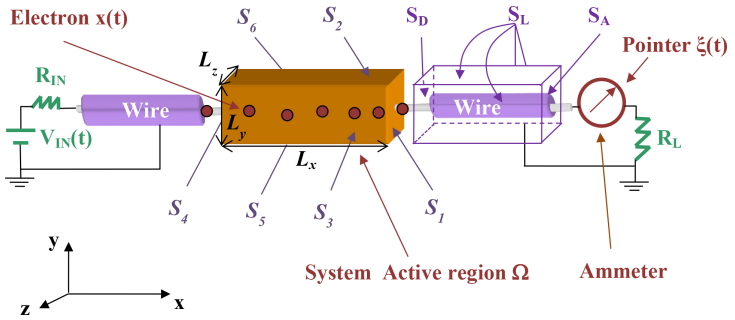

FIGURE 6.1: Common configuration for an electronic experimental set up. I am interested in measuring the current in S_1, but current can only be measured experimentally in S_A.

The conclusion here is that, in this particular scenario, when modeling electron devices through Bohmian trajectories, the simulation of the contacts (considered as part of the measuring apparatus) does only introduce fluctuations in the values of the measured current. If we are not interested in such very high frequency fluctuating noise (on the order of the screening time of the contacts, higher than THz frequencies) one can eliminate the specific simulation of the contacts, which implies an enormous computational simplification, without modifying substantially the results of the current that will be obtained. I emphasize that the effective collapse in the Bohmian model (discussed in Section 3.2) is introduced naturally as part of the dynamics of the wave and particle system and it is independent of the contacts. This approximation, on the contrary, cannot be done within the orthodox theory because the collapse law has to be explicitly modeled (taking active and crucial decisions about when the wave function collapse occurs, with which frequency or about how much perturbation we should introduce), in the simulated wave function of the systems. Thus, the bohmian approach, apart from other reasons, becomes an excellent option to compute quantum transport current and its fluctuations in nanoelectronic devices.

6.1.1 The importance of computing the displacement current in high frequency electronics

6.1.1.1 Equivalence between computed and measured currents

In Figure 6.1 it is shown the common configuration for an electronic experimental set up. The Ω volume is the active region, which is connected to the ammeter through a wire. I want to know the current in surface S_2, which is far from the ammeter. The wire touches the active region (S_2 is the same surface as S_D), and I can just measure the current obtained in surface S_A. So, what is the relationship between both surfaces?

Let me start from the current conservation law:

$$\vec{\nabla} \cdot \vec{j}_c(\vec{r},t) + \frac{\partial \rho(\vec{r},t)}{\partial t} = 0 \tag{6.1}$$

The first term on the left hand side of Equation (6.1) is the particle current density, ρ is the free electric charge density in the wire volume Λ enclosed by a larger surface $S = \{S_D, S_A, S_L\}$ and it can be related to the electric field by using the Gauss's law, which is:

$$\vec{\nabla}\Big(\epsilon(\vec{r})\vec{E}(\vec{r},t)\Big) = \rho(\vec{r},t) \tag{6.2}$$

With the use of Equation (6.2), Equation (6.1) can be rewritten as:

$$\begin{aligned} \vec{\nabla} \cdot \vec{j}_c(\vec{r},t) + \frac{\partial}{\partial t}\vec{\nabla}\Big(\epsilon(\vec{r})\vec{E}(\vec{r},t)\Big) &= \vec{\nabla} \cdot \vec{j}_c(\vec{r},t) + \vec{\nabla}\epsilon(\vec{r})\frac{\partial \vec{E}(\vec{r},t)}{\partial t} \\ = \quad \vec{\nabla} \cdot \Big(\vec{j}_c(\vec{r},t) + \epsilon(\vec{r})\frac{\partial \vec{E}(\vec{r},t)}{\partial t}\Big) &= 0 \end{aligned} \tag{6.3}$$

From Equation (6.3)), the total current density $\vec{J}_T(\vec{r},t)$ (a combination of the particle current density $\vec{J}_c(\vec{r},t)$ and the displacement current density $\vec{J}_d(\vec{r},t)$) can be defined as:

$$\vec{J}_T(\vec{r},t) = \vec{J}_c(\vec{r},t) + \vec{J}_d(\vec{r},t) = \vec{j}_c(\vec{r},t) + \epsilon(\vec{r})\frac{\partial \vec{E}(\vec{r},t)}{\partial t} \tag{6.4}$$

Using the divergence theorem, Equation (6.3) can be rewritten as:

$$\int_\Lambda \vec{\nabla} \cdot \vec{J}_T(\vec{r},t)\mathrm{d}v = \int_{S_D+S_L+S_A} \vec{J}_T(\vec{r},t) \cdot \mathrm{d}\vec{s} = 0 \tag{6.5}$$

For a cable, it can be assumed that $\int_{S_L} \vec{J}_T(\vec{r},t)d\vec{s} = 0$. Therefore, from Equation (6.5) it is obtained that:

$$\int_{S_D} \vec{J}_T(\vec{r},t)d\vec{s} = -\int_{S_A} \vec{J}_T(\vec{r},t)d\vec{s} \tag{6.6}$$

Thus, the relationship between currents in both surfaces (S_A and S_D) is not through the particle current, but through the total (current plus displacement) current.

However, in DC transport the time-average of the displacement current $I_d(t)$ is zero, and one just needs the computation of the particle current $I_p(t)$. But, as it will show in Section 6.1.1.2, when working in AC the displacement current is also needed.

6.1.1.2 Particle Current Versus Displacement Current

When modeling current, the displacement current is usually ignored. This fact occurs for many reasons. First, at very low frequencies, the displacement current becomes negligible in front of the particle current. This is the common working region of electronics. But, at frequencies high enough, the displacement current becomes the only relevant current. This is the common working scenario for electromagnetic applications. Next, I will make a simple estimation to the frequency where both currents are relevant. A direct expression of the typical drift (particle) current $I_p(t)$ on surface S is:

$$I_p(t) = \int_S \vec{J}_c(\vec{r},t)\cdot \mathrm{d}\vec{s} \approx nq\vec{v}A_S \tag{6.7}$$

where n is the number of electrons crossed the surface S per unit volume, q is the electron charge with sign, $\vec{v}$ is the drift velocity, A_S is the cross-sectional area of surface S. The particle current is related to the injection rate of electrons from the contact and it is substantially not modified when the input signal frequency f of the device is increased. Assuming that $n \approx 10^{20}$ m^{-3}, $q \approx 1.6\times10^{-19}$ C, $\vec{v} = 10^5$ m/s and $A_S = 10^{-12}$ m^2, a common estimation of the particle current is $I_p(t) \approx 10^{-6}$ A, independent of the frequency. The direct expression of the displacement current $I_d(t)$ on surface S is:

$$I_d(t) = \int_S \epsilon(\vec{r})\frac{\mathrm{d}\vec{E}(\vec{r},t)}{\mathrm{d}t}\cdot \mathrm{d}\vec{s} \tag{6.8}$$

where $\epsilon(\vec{r})$ is the electric permittivity, $\vec{E}(\vec{r},t)$ is the electric field. Imaging that the electric permittivity is $\epsilon(\vec{r}) \approx 10^{-12}$ F/m, the electric field is $\vec{E}(\vec{r},t) \approx E_0\cos(\omega t)$ being $E_0 \approx 10^6$ V/m a constant and $\omega = 2\pi f$ the angular frequency, then Equation (6.8) is rewritten as:

$$I_d(t) \approx A_S\cdot\epsilon(\vec{r})\frac{\mathrm{d}\vec{E}(\vec{r},t)}{\mathrm{d}t} \approx 2\pi A_S\epsilon(\vec{r})E_0 f \approx 10^{-18}f \tag{6.9}$$

which is linearly dependent on frequency f. In Figure 6.2 the comparison between particle and displacement current as a function of frequency is plotted.

The frequency where both currents becomes equal is around $f = 1$ THz. Therefore, for high frequency applications, the computation of the displacement current is completely required.

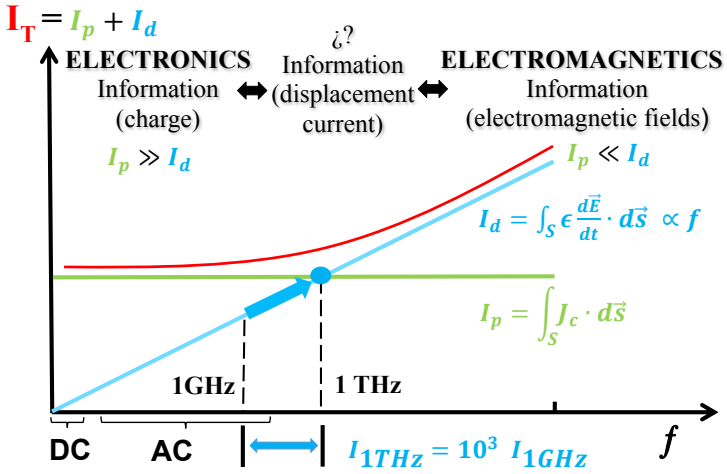

FIGURE 6.2: Frequency dependence of the particle and displacement current.

6.1.2 The Ramo-Shockley-Pellegrini Theorem

S. Ramo and W. Shockley were the first scientists who noticed the importance of the displacement current. In 1938, Ramo wrote [167]: *"In designing devices in which the electron transit time is relatively long, it is necessary to discard the low-frequency concept that the instantaneous current computed on a particular surface is proportional to the number of electrons crossed this surface per second (i.e., the particle current, which is also named as the conduction current), and a proper concept of current must also consider the instantaneous change of electrostatic flux lines which end on the surface (i.e., the displacement current)"*. At the same time, Shockley also wrote [168]: *"In the scenario that the electron transit time is of comparable duration with the periods of alternating circuits, it is consequently of interest to know the instantaneous value of the current induced by the moving charge over its entire time of transit"*.

Their work relating microscopic electron dynamics with macroscopic displacement currents is known now as the Ramo-Shockley theorem.

Here, I will not explain the Ramo-Shockley theorem, but the Ramo-Shockley-Pellegrini theorem [169]). The latter is an extension of the former. Pellegrini included scenarios where the dielectric properties of the electronic system are time and spatial dependent. This fact is very relevant, now it can be used with whatever boundary condition and conducting medium. In addition, and very importantly for the Bohmian formalism, this theorem allows to (in Pellegrini's words) *"connect in a straightforward way the corpuscular nature and motion of the single carriers to the output currents and voltages, give general and efficacious tools to study transport and noise phenomena of electrical systems and to solve open problems"*.

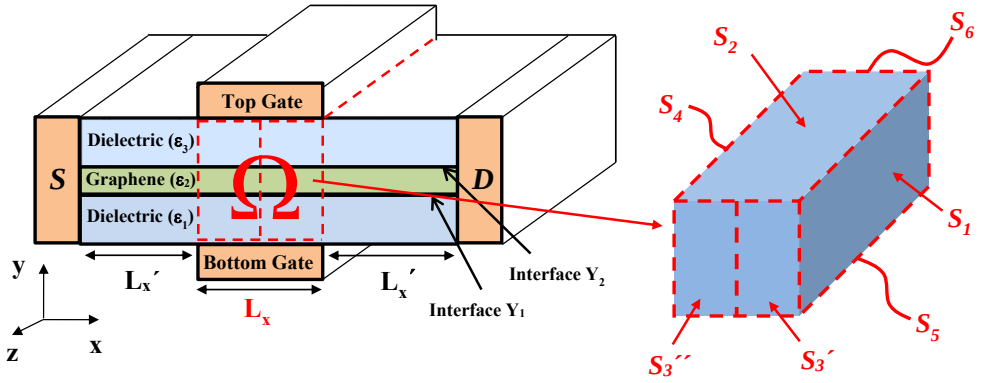

FIGURE 6.3: Schematic representation of a electronic device in BITLLES simulator. The channel (in this case graphene) is sandwiched between two dielectrics. The active region of the dual-gate 2D Fet is $\Omega = L \times (H' + H + H') \times W$, being L the gate length.

Consider the active region (volume $\Omega = L_x \times L_y \times L_z$ in Figure 6.3) as the device active region. The volume Ω is constrained by six closed surface S_j, where j runs from one to six. The total time-dependent current on a surface S_j is defined by the Ramo-Shockley-Pellegrini theorem as

$$I_j(t) = \Gamma_j^q(t) + \Gamma_j^e(t) \tag{6.10}$$

where $\Gamma_j^q(t)$ is [169]:

$$\Gamma_j^q(t) = -\int_\Omega \vec{F}_j(\vec{r}) \cdot \vec{J}_c(\vec{r},t)\, \mathrm{d}\nu = -\sum_{m=1}^{N} sign(\vec{v}_m)\; q\; \vec{F}_j(\vec{r}_m) \cdot \vec{v}_m(\vec{r}_m) \tag{6.11}$$

and $\Gamma_j^e(t)$ is:

$$\Gamma_j^e(t) = \int_{S_j} \epsilon(\vec{r})\, \frac{\mathrm{d}V(\vec{r},t)}{\mathrm{d}t}\, \vec{F}_j(\vec{r}) \cdot \mathrm{d}\vec{s} \tag{6.12}$$

where $\vec{J}_c(\vec{r},t)$ is the particle current density at the position $\vec{r}$ at time t, $\vec{v}_m(\vec{r}_m)$ is the m-electron velocity, $\vec{r}_m$ is the m-electron position, q is the electron charge without sign, N is the total number of electrons in the simulation box, $V(\vec{r},t)$ is the scalar potential at position $\vec{r}$ and time t. The function $sign(\vec{v}_m)$ is equal to 1 when one electron leaves the volume Ω through the surface S_j, while $sign(\vec{v}_m) = -1$ when the electron enters. The vector function $\vec{F}_j(\vec{r})$ is defined through:

$$\vec{F}_j(\vec{r}) = -\nabla\phi_j(\vec{r}) \tag{6.13}$$

where $\phi_j(\vec{r})$ is the solution of the Laplace equation $-\nabla(\epsilon(\vec{r})\vec{F}_j(\vec{r})) = 0$, with the following boundary conditions, $\phi_j(\vec{r}) = 1$ when $\vec{r} \in S_j$ and $\phi_j(\vec{r}) = 0$ when $\vec{r} \notin S_j$.

Let me emphasize that the terms $\Gamma_j^q(t)$ and $\Gamma_j^e(t)$ cannot be interpreted as particle current and displacement current. The term $\Gamma_j^q(t)$ includes itself the particle current and part of the displacement current altogether.

Ramo-Shockley-Pellegrini Theorem in a two terminal device

Equation (6.11) and Equation (6.12) have to be solved usually numerically. However, there is a special geometry case that can be obtained analytically. Consider a two terminal device (the one depicted in Figure 6.3, but without the top and bottom gates) between two metallic contacts, where $L_x << L_y, L_z$. Transport is assumed fully ballistic. Then, it is straightforward [167, 168] to obtain that $\vec{F}_j(\vec{r}) = \frac{1}{L_x}$ and then:

$$I(t) = \frac{q}{L_x} \sum_{k=1}^{N_e} v_x^k(t) \tag{6.14}$$

where N_e is the number of electron inside the active region and $v_x^k(t)$ the $k-th$ electron instantaneous velocity in the transport direction (x).

6.1.3 Noise and its fundamental explanation

6.1.3.1 What is noise?

Historically, the definition of noise was related to the sound: A noise is an unwanted, unpleasant and confusing type of sound.[1] However, such definition is ambiguous. What does it mean unwanted, unpleasant or confusing? An attempt to provide a more academic definition comes from music: Noise is a non-harmonious or discordant group of sounds. Again, however, the definition is not free from ambiguities because one man's noise is another man's music [170].

A more scientific definition closer to the electrical devices field comes from communications: A noise is an electric disturbance that interferes with or prevents reception of a signal or of information. For example, the buzz in a telephone call. Thus, once I have a precise definition of what is a signal, the meaning of what is noise becomes perfectly clear: It is the difference between the measured value and the signal.

[1] In fact, the word noise is etymologically derived from the Latin word *nausea*, meaning seasickness.

6.1.3.2 Quantum noise in electrical devices from an experimental point of view

As discussed above, the answer to what is noise in electrical devices depends on the definition of the electrical signal. For most DC applications, the signal is just a time average value of the current. For frequency applications, the signal is equivalently defined as a time average value, but using a shorter time interval (related to the inverse of the operating frequency). In other applications, mainly digital applications, the signal is related to a time average value of the voltage in a capacitor. Hereafter, I will assume that the electrical signal is the DC value of the current, referenced by the symbol $\langle I \rangle$. All fundamental and practical issues discussed here for the DC signal (and its noise) can be straightforwardly extended to those other types of electrical signals.

What is measured in a laboratory for the DC signal is the time average value of the instantaneous current $I(t)$ in a unique device during a large period of time T:

$$\langle I \rangle = \lim_{T \to \infty} \frac{1}{T} \int_0^T I(t) dt \tag{6.15}$$

Once the signal $\langle I \rangle$ is defined as the DC value, in principle, the noise can be quantified by time averaging the difference between the measured value of the current $I(t)$ and the signal in a unique device:

$$\triangle I^2 = \lim_{T \to \infty} \frac{1}{T} \int_0^T (I(t) - \langle I \rangle)^2 dt \tag{6.16}$$

The square of the difference avoids positive and negative cancellations. At this point, it is very important to realize that $I(t)$ presents very rapid fluctuations that cannot be captured by standard laboratory apparatuses. Any experimental set up that measures the current fluctuations behaves as a low-pass filter (i.e., the current fluctuations at frequencies higher than the apparatus cut-off frequency are not measured). Therefore, the experimentally accessible information about the current fluctuations is not given by Equation (6.16), but by the power spectral density of the fluctuations $S(w)$ (and its related magnitudes). From the Wiener-Khinchine relation, the power spectral density can be defined as the Fourier transform of the time average definition of this autocorrelation function $\triangle R(\tau)$:

$$\triangle R(\tau) = \lim_{T \to \infty} \frac{1}{T} \int_0^T \triangle I(t_1) \triangle I(t_1 + \tau) dt_1 \tag{6.17}$$

where $\triangle I(t) = I(t) - \langle I \rangle$. A straightforward development shows that Equation (6.17) can be rewritten as $\triangle R(\tau) = R(\tau) - \langle I \rangle^2$ with:

$$R(\tau) = \lim_{T \to \infty} \frac{1}{T} \int_0^T I(t_1) I(t_1 + \tau) dt_1 \tag{6.18}$$

Then, the Fourier transform of Equation (6.17) gives the noise power spectral density $S(w)$:

$$S(w) = \int_{-\infty}^{\infty} \triangle R(\tau) e^{-jw\tau} d\tau \tag{6.19}$$

It is quite trivial to realize that the definition of the spectral density $S(w)$ in Equation (6.19) and Equation (6.17) is consistent with the definition of the total noise[2] in Equation (6.16):

$$\triangle I^2 = \int_{-\infty}^{\infty} S(w) dw \tag{6.20}$$

where I have used the definition of a delta function $\delta(\tau) = \int_{-\infty}^{\infty} e^{-jw\tau} dw$. It is very relevant to realize that the measurement of $S(w)$ through the function $R(\tau)$ defined in Equation (6.18) requires the knowledge of the measured value of the current during all t. Thus, predictions about the evolution of the electronic device have to be made while being (continuously) measured. In a classical scenario, such discussion about measurement is generally ignored. On the contrary, for quantum systems, it has very relevant implications because the evolution of a system with or without measurement can be dramatically different.

If the electronic device satisfies the ergodic theorem [171, 172], a continuous measurement of the system can be avoided. Let us see in what sense ergodicity can simplify noise computations. In general, the *mathematical* concept of a random process is used to deal with noise. A random process requires a sample space. In this case, I can define an

[2]Technically, $S(w)$ defined in Equation (6.19) is non-negative and symmetric with respect to w. Then, since only positive frequencies w are measured in a laboratory, the measured density includes the $S(w)$ and $S(-w)$, and the integral of the noise spectrum measured in a laboratory runs from 0 till ∞.

ensemble of *identical* electrical devices[3], each one labelled by the sample space variable γ. Then, the (instantaneous) current is labelled by the random process $I^{\gamma}(t)$. For a fixed time, t_1, the quantity $I^{\gamma}(t_1)$ is a random variable. For a fixed device γ_1, the function $I^{\gamma_1}(t)$ is a well-defined non-random function of time. Finally, $I^{\gamma_1}(t_1)$ is just a real number. Often the sample space variable γ is omitted in the notation. The DC value of the current in Equation (6.15) can be alternatively defined for an ergodic system as:

$$\langle I \rangle = \sum_i I_i(t_1) P(I_i(t_1)) \tag{6.21}$$

where $P(I_i(t_1))$ is the probability of getting I_i at time t_1. These probabilities are defined as the ratio of the number of devices providing I_i divided by the total number of devices. It is important to realize that the experimental evaluation of Equation (6.21) requires only one measurement of the current at t_1 in a large number of *identical* γ-devices. Then, the theoretical predictions of Equation (6.21) do only need to determine the free (without measuring apparatus) evolution of the electronic device from the initial time t_0 till t_1. Obviously, I can compute the total noise represented in Equation (6.16) from a unique measurement in ergodic systems:

$$\triangle I^2 = \sum_i (I_i(t_1) - \langle I \rangle)^2 P(I_i(t_1)) \tag{6.22}$$

However, the noise measured in a laboratory is not given by $\triangle I^2$, but by $S(w)$ in Equation (6.19). I repeat the reason explained in Equation (6.16). The amount of noise generated by an instantaneous current evolving for example from $I(t_1) = 5$ mA to $I(t_2) = 10$ mA during a time interval of $t_2 - t_1 = \tau = 1$ fs, is not captured from state-of-the-art laboratory apparatuses (which already have difficulties to capture noise at frequencies higher than a few of Terahertzs). From an experimental point of view, in fact, it is easy to get $S(w \to 0)$, but impossible to get $S(w \to \infty)$. I can compute the noise power spectral density $S(w)$ from the ensemble average version of the autocorrelation defined in Equation (6.18) as:

$$R(t_1, t_2) = \sum_i \sum_j I_j(t_2) I_i(t_1) P\big(I_j(t_2), I_i(t_1)\big) \tag{6.23}$$

[3]At this point, the reader will wonder that, in typical laboratory experiments, only one electronic device is available (not an ensemble of them). Then, as a practical definition of ensemble, I can define the instantaneous current measured in different time-intervals: $I^{\gamma_1}(t)$ for the instantaneous current measured during the first time interval, $I^{\gamma_2}(t)$ for the second interval, and so on.

In general, it can be assumed that the instantaneous current in an electronic device behaves as a wide-sense stationary random process. Then, $\langle I \rangle$ in Equation (6.21) is constant and time-independent. Identically, the autocorrelation function in Equation (6.23) depends only on the time difference $\triangle R(t_1, t_1 + \tau) = \triangle R(\tau)$ with $t_2 = t_1 + \tau$. Finally, I use Equation (6.19) with $\triangle R(\tau)$ computed from Equation (6.23), to get the noise power spectral density $S(w)$.

It is important to emphasize (for a posterior discussion) that the probability $P\big(I_j(t_2), I_i(t_1)\big)$ implies a two-measurement process for each electronic device. The system evolves freely (without interaction with the measurement apparatus) from t_0 till t_1 when the current is measured, giving the value I_i. Then, the system evolves freely again until time t_2, when the system is measured again giving I_j. In summary, even if the ergodicity argument is invoked, the noise computation through the autocorrelation function requires, at least, two measurements at different times in a single device (and the average over all γ-devices). I anticipate that the computations with Bohmian mechanics will not assume ergodicity (which is not an obvious property for open systems out of equilibrium [171]), but the prior expressions requiring a continuous measurement of the current.

Let me emphasize that the previous discussion is valid for either classical or quantum devices. The adjective *quantum* emphasizes that the signal and the noise are computed or measured in an electrical device governed by quantum laws [41, 78, 81, 173]. If the electronic device is not ergodic, Equation (6.18) requires a continuous measurement of the current $I(t)$. On the contrary, for an ergodic electron device, Equation (6.21) requires one unique measurement, while Equation (6.23) requires a two-times measurement when dealing with the power spectral density $S(w)$.

Up to here, the definition of quantum noise seems very trivial. Then, why does the concept of quantum noise have a halo of mystery around it?

6.1.3.3 Quantum noise in electrical devices from a computational point of view

The previous definition on what is quantum noise does not answer the question on how it is computed. If I want to predict the values $I(t)$ used in Equation (6.16) and Equation (6.18) or the probabilities $P(I)$ and $P\big(I_j(t_2), I_i(t_1)\big)$ for Equation (6.21) and Equation (6.23), a quantum theory is required.

At this point, I want to clarify why quantum noise is specially sensible to fundamental quantum mechanical issues. Any electrical device (or any experiment) is connected to a measuring apparatus. In our case, an ammeter to get the electrical current. Quantum

noise is sensible to the (ammeter) measuring process. As stated in Equation (6.23), in order to obtain the noise, the quantum system has to be measured, at least, twice. This two-time measurement faces directly with one of the most complex issues in quantum mechanics explained in Section 3.4, the measurement problem[4]. One more time, the avalaible computational tools depends on the the election of the quantum theory.

6.2 Time-dependent BITLLES Model Injection

In this section I explain the BITLLES (see Chapter 3 for details about the BITLLES simulator) model injection for linear band (like graphene) or parabolic band (like black phosphorus) 2D materials, and why it is so important to obtain correct values of current and its fluctuations. From a computational point of view, the open system is defined as the simulation box that includes, at least, the device active region. The environment determines the boundary conditions at the borders of the simulation box through thermodynamical arguments [174, 175]. Most electron device simulation approaches are based on combining mechanical and thermodynamic arguments. An important part of the boundary conditions at the contacts are the so-called electron injection models.

In general, there are strong practical arguments in favor of using time-independent approaches for device simulation since they have less computational burden. In such time-independent models, the electron injection model basically reduces to a discussion on the density of states and the occupation function at the borders. However, time-independent approaches have difficulties to properly describe properties related to the dynamics of electrons (such as transient and AC performances [174, 176]) or to the stochastic and discrete nature of electrons (such as shot and thermal noise [41, 82]).

The time-dependent electron injection model explained here can be applied to semi-classical or quantum simulators. For semi-classical modeling [13, 177], electrons are described as point-particles, while for quantum modeling, the wave nature of electrons is accounted by time-dependent wave packets.

6.2.1 Local conditions of the injection model

In this section, I will discuss those spatial local (depending on the properties of only one contact, not both) effects that are relevant in the discussion of the electron injection model.

[4] I also mention that the fundamental understanding/computing of the measurement process can be largely relaxed when dealing with DC predictions. They can be computed from an ensemble of devices with only one measurement in each device, so the evolution of the quantum system after the measurement can be ignored.

There is no unique local argument to define a time-dependent electron injection model. For example, when the boundary conditions are defined far from the device active region (for large simulation boxes), it is reasonable to assume that the electron injection model has to satisfy charge neutrality. This local condition in the physical (real) space determines how many electrons need to be injected at each time step of the whole simulation. However, in positions closer to the device active region (for small simulation boxes) charge neutrality is not fully justified. Then, it is assumed that electrons entering into the simulation box are in thermodynamic equilibrium (with an energy distribution determined by a Fermi-Dirac function) with the rest of electrons in the contact [178]. The thermodynamic equilibrium in this second model is basically imposed on electrons entering into the simulation box, not on those leaving it. This second model is the one explained here for 2D materials.

6.2.1.1 Density of electrons in the phase-space

We consider a 2D material. The position of electrons in such material are defined with the 2D vector $\{x, z\}$ (as indicated later, for quantum description of the electron, the mentioned position can be assigned to the central position of the wave packet describing the electron). Electron transport (from source to drain) takes place in the x direction. Then, I define a phase-space cell, labeled by the position $\{x_0, z_0\}$ and wave vector $\{k_{x0}, k_{z0}\}$ with a volume $\Delta x\Delta z\Delta k_x\Delta k_z$, as the degrees of freedom $\{x_0, z_0, k_x, k_z\}$ satisfying $x_0 < x < x_0+\Delta x$, $z_0 < z < z_0+\Delta z$, $k_{x0} < k_x < k_{x0}+\Delta k_x$ and $k_{z0} < k_z < k_{z0}+\Delta k_z$. As a consequence of the Pauli exclusion principle [178], the maximum number of available electrons n_{2D} in this phase-space cell in the contact borders is:

$$n_{2D} = g_s g_v \frac{\Delta x\Delta z\Delta k_x\Delta k_z}{(2\pi)^2} \tag{6.24}$$

where the g_s and g_v are the spin and valley degeneracies, respectively. See Appendix F to specify the physical meaning of Δx, Δz, Δk_x, Δk_z in terms of the wave packet nature of (fermions) electrons with exchange interaction. Equation (6.24) specifies that, in average, each electron requires at least a partial volume 2π for each *position* $\times$ *wave vector* product of the phase space. Each electron requires a volume $(2\pi)^2$ of the whole available phase space in a 2D material. Certainly, I can imagine a many-particle wave function with more than n_{2D} electrons inside the phase space cell. However, because of the Pauli principle, such many-particle wave functions are not common.

6.2.1.2 Minimum temporal separation t_0 between electrons

At any particular time t, all electrons with wave vector $k_x \in [k_{x0}, k_{x0} + \Delta k_x]$ inside the phase cell will attempt to enter into the simulation box during the time-interval Δt. I define $\Delta t = \Delta x / v_x$ as the time needed for the electrons with velocity component in the transport direction v_x to move a distance Δx. Δt is always positive, because electrons entering from the right contact with negative velocity move though a distance $-\Delta x$. Notice that I have assumed that the phase space cell is so narrow in the wave vector directions that all electrons have roughly the same velocity v_x. Therefore, the minimum temporal separation, t_0 between injected electrons from that cell, defined as the time step between the injection of two consecutive electrons into the system from the phase space cell, can be computed as the time-interval Δt divided by the number of available carriers n_{2D} in the phase-space cell:

$$t_0 = \frac{\Delta t}{n_{2D}} = \frac{(2\pi)^2}{g_s g_v} \frac{1}{|v_x| \Delta z \Delta k_x \Delta k_z} \tag{6.25}$$

As I have mentioned above, the injection model described here is valid for either classical or quantum systems. For a quantum systems, electrons are described by wave packets. Such wave packets in the contacts can be expected to be defined by wave functions, like Gaussian wave packets or Gaussian bispinors, where a meaningful definition of its mean (central) position and wave vector is given.

For materials with a parabolic band structure, the velocity in the transport direction is $v_x^p = \frac{1}{\hbar} \frac{\partial E^p}{\partial k_x} = \frac{\hbar k_x}{m^*}$, m^* being the electron effective mass. Substituting v_x^p into Equation (6.25) I obtain:

$$t_0^p = \frac{(2\pi)^2}{g_s g_v} \frac{m^*}{\hbar k_x \Delta z \Delta k_x \Delta k_z} \tag{6.26}$$

From Equation (6.26), it is clear that the t_0 is only affected by the wave vector k_x, and for instance an electron with higher k_x needs less injection time t_0 to enter in the system.

For materials with a linear band structure, the velocity of electrons in the transport direction is $v_x^l = s v_f k_x / |\vec{k}|$, being s the band index and v_f the Fermi velocity. It is important to emphasize that the x component electron velocity v_x^l is explicitly dependent on both wave vector components k_x and k_z, which is different from the v_x^p whose velocity is only determined by k_x. Then the minimum temporal separation is written as:

$$t_0^l = \frac{(2\pi)^2}{g_s g_v} \frac{|\vec{k}|}{s v_f k_x \Delta z \Delta k_x \Delta k_z} \tag{6.27}$$

According to Equation (6.27), the temporal separation between two electrons with smaller k_z will be shorter than that with a larger k_z. As a consequence, almost all electrons in graphene are injected with a low k_z (with $k_x \approx |\vec{k}|$) and with a velocity close to the maximum value, i.e. $v_x \approx v_f$.

6.2.1.3 Thermodynamic equilibrium

I assume that electrons inside the contacts are in thermodynamic equilibrium. For electrons (fermions), the Fermi-Dirac distribution $f(E)$ provides the probability that a quantum state with energy E is occupied:

$$f(E) = \frac{1}{exp[(E - E_f)/(k_B T)] + 1} \tag{6.28}$$

where E_f is the quasi Fermi level (chemical potential) at the contact, k_B is the Boltzmann constant and T is the temperature. The electron energy E is related to its wave vector by the appropriate linear or parabolic energy dispersion. I emphasize that the assumption of thermodynamic equilibrium is an approximation because the battery drives the electron device outside of thermodynamic equilibrium (this approximation explains why I define a quasi-Fermi level, not an exact Fermi level). I remark that there is no need to anticipate the energy distribution or electrons leaving the simulation box (the equations of motion of electrons implemented inside the simulation box will determine when and how electrons leave the open system).

6.2.1.4 Probability of injecting N electrons during the time interval τ

At temperature $T = 0$, the mean number of electrons in the phase-space cell $q\langle N\rangle$ is equal to $\langle N\rangle \equiv n_{2D}$ given by Equation (6.24), which means that electrons are injected regularly at each time interval t_0. At higher temperature $T > 0$, the mean number of electrons in the cell $\langle N\rangle$ is lower than n_{2D}. In fact, because of Equation (6.28), I get $\langle N\rangle \equiv n_{2D} \cdot f(E)$. The statistical charge assigned to this cell is therefore equal to $\langle Q_{2D}\rangle \equiv -q \cdot n_{2D} \cdot f(E)$. Here q is the elementary charge without sign. The physical meaning of $\langle N\rangle \equiv n_{2D} \cdot f(E)$ is that the number of electrons N in the cell (all with charge $-q$) varies with time. I cannot know the exact number N of electrons at each particular time, but statistical arguments allow us to determine the probabilities of states with different N. Such randomness in N implies a randomness in the number of electrons injected from each cell. This temperature-dependent randomness is the origin of the thermal noise [178, 179].

It is known that the injection processes follow the Binomial distribution with a probability $Prob(E)$ [178]. For example, for the local conditions discussed here I can assume that the probability of successfully injecting electrons with energy E is given by the Fermi-Dirac statistics discussed in Equation (6.28), i.e., $Prob(E) \equiv f(E)$. The probability $P^i(N,\tau)$ that N electrons are effectively injected into a particular cell i adjacent to the contact during a time-interval τ is defined as:

$$P^i(N,\tau) = \frac{M_\tau!}{N!(M_\tau - N)!} Prob(E)^N (1 - Prob(E))^{M_\tau - N} \tag{6.29}$$

where M_τ is the number of attempts of injecting carriers in a time-interval τ, defined as a number rounds the quotient τ/t_0 to the nearest integer number towards zero, i.e. $M_\tau = floor(\tau/t_0)$. The number of injected electrons is $N = 1, 2, \ldots, M_\tau$.

6.2.2 Non-local conditions of the injection model

I now discuss some non-trivial non-local effects that have to be considered in the practical development of an electron injection model for 2D materials.

6.2.2.1 Transport, non-transport electrons and holes in parabolic bands

In order to simplify the computations, not all electrons present in an open system are explicitly simulated. Only transport electrons, defined as those electrons whose movements are relevant for the computation of the current, are explicitly simulated. The contribution of the non-transport electrons to the current is negligible and their charge is included as part of a fixed charge. What determines if an electron is a transport electron or not? In principle, one erroneously argues that the quasi-Fermi level provides a local rule to determine if an electron is a transport electron or not. Those electrons with energies close to the quasi-Fermi level are transport electrons, while those electrons with energies well below are irrelevant for transport. This local rule is not always valid for all materials and scenarios.

When modeling traditional semiconductor devices usually the applied bias in the edges of the active region is less than the energy band gap. See Figure 6.4(a) and (b). Then, one can assume that transport electrons belong to just one band along the whole device, either the valence or the conduction band. Then, one can consider, for example, that all electrons in the CB are transport electrons. Electrons in the VB do not participate in the transport because there are not available states. See blue regions for transport electrons in CB and orange region in the VB of Figure 6.4(a) and (b). The important

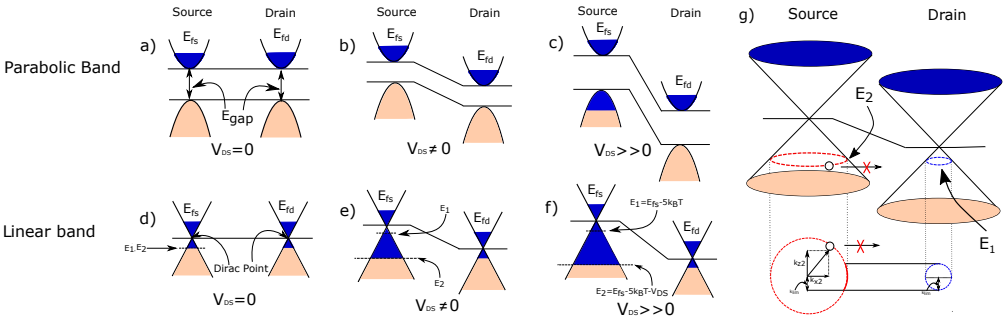

FIGURE 6.4: The energy profile for a device with parabolic CB and VB separated by a energy bandgap E_{gap} and with a gapless material with linear CB and VB. In the insets (a) and (b), the selection of transport and non-transport electrons is independent of the bias (same number of electrons are simulated that contribute to transport). The inset (c) corresponds to the energy profile corresponding to a Zener diode where additional transport electrons in the VB have to be considered. In the insets (d), (e) and (f) for a gapless structure, the number of transport electrons is bias dependent. The electrons in the energy range from $E_1 = E_{fs} - 5k_BT$ to $E_2 = E_{fs} - 5k_BT - V_{DS}$ are the additional transport electrons that have to be added at each bias point. Blue electrons and orange electrons are transport and non-transport ones, respectively. (g) Representation of an electron traveling from the source to the drain. Only electrons in the red solid line can reach the drain contact due to the conservation of k_z.

point is that the number of transport electrons is bias independent, meaning that the number of transport electrons remains the same in Figure 6.4(a) and (b). I anticipate that the division between transport and non-transport electrons in scenarios such as Figure 6.4(c), which could correspond to a Zener diode[180] where a very large bias (greater than the energy gap) is applied, cannot be treated in the same way as the previous scenarios. Instead, this case which occurs rarely in devices with parabolic bands and large energy gap, should be treated as I treat gapless materials below.

The distinction between transport and non-transport electrons does also apply when the quasi-Fermi level is close to electrons in the VB. Then, there is no transport of electrons in the CB because there is no electrons there. I can consider as transport electrons, for example, those electrons in the valence band whose energy is no lower than $\alpha k_B T$ (generally, it is sufficient to define $\alpha = 5$) below the quasi-Fermi level at the contact. The rest of electrons in the VB with energies lower than $E_f - 5k_BT$ are non-transport electrons. In order to simplify the computational burden of transport electrons in the VB, traditionally, one simulates the absence of electrons in the VB, defined as holes, instead of the transport electrons themselves. The total current I can be computed by summing the current I_i of each transport electron in the VB, $I = \sum_{i=1}^{n} I_i$, where n is the number of transport electrons in the VB (with positive and negative velocities). However, if n is quite close to maximum number of allowed electrons in that region n_{max}, then, by knowing that a VB full of electrons (equal number of electrons with positive and negative energies) does not have net transport. i.e. $I_{max} = \sum_{i=1}^{n_{max}} I_i = 0$, I get:

$$I = \sum_{i=1}^{n} I_i - \sum_{i=1}^{n_{max}} I_i = \sum_{j=1}^{n_{max}-n} (-I_j) \tag{6.30}$$

Thus, instead of simulating $i = 1, .., n$ transport electrons I can simulate $j = 1, ..., n'$ transport holes with $n' \equiv n_{max} - n$, assuming that the current of the holes $(-I_j)$ is the opposite of the electron current I_i. This can be achieved by considering that holes have positive charge $+q$.

Let me define the fixed charge (belonging to dopants or non-transport electrons below $E = E_f - 5k_B\Delta T$) is Q_{fix} in the VB. Then, the computation of the charge in the VB of parabolic materials can be also done using electrons or holes. I also define $Q_{max} = \sum_{i=1}^{n_{max}}(-q_i)$ as the charge belonging to transport electrons when the energy region above $E = E_f - 5k_B\Delta T$ is full of electrons. Therefore the charge due to the n electrons in that energy region when considering the transport of holes, is:

$$Q = \quad Q_{fix} + \sum_{i=1}^{n}(-q_i) = Q_{fix} + Q_{max} + \sum_{j=1}^{n'} q_j \tag{6.31}$$

I have to consider the holes as carriers with positive charge $+q$ and consider a fixed charge Q_{max}, in addition to Q_{fix}, when dealing with device electrostatics through the n' holes. The use of holes can be useful in scenarios like the ones in Figure 6.4(a) and (b), when it is true that $n' << n$ along the whole simulation box.

The problem with the simulation of holes (instead of transport electrons) in the VB appears when electrons move from the VB to the CB in a band-to-band-tunneling process. Then, there are regions of the simulation box with more holes than other regions, see Figure 6.4(c). Within the language of holes, such electron transit from VB to CB can be modeled as an electron-hole generation process inside the device [181]. During the transition of the electron from the VB to the CB, I can assume that an electron is effectively created in the CB, while a hole is also effectively created (an electron disappears) in the VB. Such transition probability depends on the number of electrons (number of holes) in a particular region of the phase space inside the device, which in turn depends on the occupation probability. What is the occupation probability $f(E)$ inside the device? A fundamental simulation wants a mechanical description of the electrons inside the device, not a statistical one. Therefore, no *a priori* assumption about the occupation function inside the device is accessible in such simulations. Obviously, I can assume some thermodynamic quasi-equilibrium occupation function in these regions

of the phase space inside the device. This strategy implies an important reduction of the computational burden, at the price of reducing the fundamental character of the simulation [181, 182].

6.2.2.2 Transport, non-transport electrons and holes in linear bands

The utility of the holes and the uniformity of Q_{fix} has to be revisited when dealing with linear band materials (as well as in parabolic band structure materials when the applied bias is greater than the energy bandgap as discussed in Figure 6.4(c)) because the transition from VB to CB is unavoidable.

In Figure 6.4(d)-(f), I see those electrons depicted in blue (dark gray) whose energy is well below the local quasi-Fermi level in the source E_{fs}, but that effectively contribute to current because such electrons in the VB in the source contact with negative kinetic energy are able to travel through the device, cross the Dirac point via Klein tunneling and arrive at the CB with positive kinetic energy in the drain contact. I define the zero of total energy at the Dirac point. The same scenario for parabolic bands is depicted in Figure 6.4(c). The argument saying that the VB is full of electrons in the source giving zero current ($I_{max} = \sum_{i=1}^{n_{max}} I_i = 0$) is false here. Such argument is a local argument that does not take into account the non-local relation between the source and the drain contacts. How many transport electrons contribute to the current in Figure 6.4(d)-(f)? I have seen that electrons with energies above $E = E_{fd} - 5k_B\Delta T$ in the drain are relevant for the transport. In addition, electrons with energies below $E = E_{fs} - 5k_B\Delta T$ in the source are also relevant for transport. In order to minimize the number of transport electrons in the simulating box, it is very convenient to use a different criteria for the selection of the transport electrons in the source than in the drain contacts. In the source contact, the transport electrons are all electrons within the energies in the range $[E_{fd} - 5k_B\Delta T, E_{fs} + 5k_B\Delta T]$ defined in Figure 6.4(d)-(f), while the energy range $[E_{fd} - 5k_B\Delta T, E_{fd} + 5k_B\Delta T]$ is used for the drain. Since I can consider that $E_{fs} = E_{fd} + V_{DS}$ with V_{DS} the applied voltage, the number of transport electrons selected with the overall criteria is bias-dependent and position-dependent. Other criteria are also possible in the selection of the transport electrons [5]. The criteria specified here to select the transport electrons as explained in Figure 6.4(d)-(f) is the one that minimizes the overall number of transport electrons.

The simulation of holes (instead of electrons) in the VB of graphene is also possible. However, there are two important difficulties. First, as discussed at the end of Section 6.2.2.1, the electron-hole generation to describe the band-to-band Klein tunneling

[5] We notice that considering more or less transport electrons in the simulation is not a physical problem, but a computational problem because it increases the computational effort

would requires some type of estimation for the thermodynamic quasi-equilibrium distribution of holes inside the simulation box [181]. Second, such probability would require an ad-hoc definition of Klein tunneling transmission coefficient. However, Klein tunneling is a pure quantum interference phenomena depending on several items (energy, direction of propagation, potential profile, etc.) implying important difficulties when attempting to develop ad-hoc analytic expressions of the Klein tunneling transmission probability [6]. None of the above two important difficulties (definition of the occupation function inside the simulation box and the definition of an ad-hoc Klein tunneling transmission probability) are present when only transport electrons, not holes, are considered in the VB and simulated through the Dirac equation as I will shown in Section 6.2.4.2.

From Figure 6.4(e), I can rewrite the charge assigned to electrons in the CB and VB of the drain contacts for a gapless material as follows:

$$Q_{drain} = Q_{fix} + \sum_{i=1}^{n_{drain}} (-q_i) \tag{6.32}$$

The charge distribution in the source is not exactly the same as in Equation (6.32) because, as discussed above, the number of transport electrons in the source n_{source} is different from n_{drain}. Therefore, I get:

$$Q_{source} = Q_{fix} + \sum_{i=1}^{n_{source}} (-q_i) - Q_{add}(x_{source}) \tag{6.33}$$

where $Q_{add}(x_{source})$ is just the additional charge assigned to the additional number of transport electrons $n_{source} - n_{drain}$ simulated in the source. In fact, as I will discuss at the end of Section 6.2.2.3, in each point of the device, and each bias point, I have to consider a different value of $Q_{add}(x)$. In particular, I notice that Equation (6.32) can be written as Equation (6.33) with the condition $Q_{add}(x_{drain}) = 0$. Finally, I notice again that the consideration of this position dependent charge can be avoided by just using the same number of transport electrons in the drain and in the source, but this would imply an increment of the computational effort to transport electrons that, in fact, do not provide any contribution to the current. In conclusion, minimizing the number of transport electrons implies a positions and bias dependent definition of $Q_{add}(x)$.

[6] For a full quantum time-dependent electron transport simulator, such electron-hole generation would require a definition of the electron and hole wave packets in the middle of the simulation box. I can assume a Gaussian type for the wave packet at the borders of the simulation box, however, the type of wave packet generated in the middle of the simulation box, while doing Klein tunneling, is hardly anticipated by ad-hoc models.

6.2.2.3 Pauli principle between the source and drain contacts and conservation laws

There is another strategy to further minimize the number of transport electrons in the simulation box, by taking into account the Pauli exclusion principle between source and drain contacts. This strategy is based on the following two assumptions. First, I consider that electrons move quasi-ballistically inside the simulation box, so that the I can reasonably predict which is the energy of an electron at the drain, initially injected from the source, and vice-versa. The second assumption is that the occupation functions at the drain and source do not only provide the energy distributions of electrons entering into the simulation box, but also provide a reasonable prediction of the energy distribution of electrons leaving it. Under these two assumptions, the injection of electrons from one side that will not be able to arrive to the other side in a later time because other electrons are occupying that region of the phase-space (positions and wave vectors) can be avoided. Let me notice that this new strategy can be removed if the many body Pauli exclusion principle could be included somehow into the equation of motion of electrons inside the simulation box (see Section 3.3 or [72, 183]).

Let me assume an electron moving *ballistically* inside the graphene channel with total energy E satisfying the energy conservation law. If an electron with energy E is effectively injected from the source contact, the probability that it will arrive to the drain (in thermal equilibrium) with the same energy E is given by the probability that such region of the phase space is empty of electrons, which is $f_{sd}(E) = (1 - f(E))$ with $f(E)$ given by Equation (6.28) and $E_f \equiv E_{fd}$ indicating the quasi-Fermi level at the drain contact.

A similar argument can be invoked for momentum conservation. When considering transport electrons incident on a potential barrier that is translationally invariant in the z direction (perpendicular to the transport direction), i.e., $V(x, z) = V(x)$, in addition to the conservation of electron energy E, the conservation of the momentum projection k_z can also be taken into account. Let me give an example on how the conservation of momentum projection k_z affects our injection model in graphene. I consider one electron with energy E injected successfully from the source contact into the system and that the electron is transmitted (without being scattered) through a potential barrier and finally arriving at the drain contact. According to the linear dispersion relation in graphene, the maximum absolute value of momentum projection k_z that the electron can obtain is $k_{lim} = |(E + qV_{DS})/(\hbar v_f)|$, see the definition of k_{lim} in Figure 6.4(g).

In the source, all those electrons whose $|k_z| > k_{lim}$ will not be able to reach the drain, i.e. only electrons whose k_z belongs to the solid red arc circumference could reach the

drain. Therefore, at the source contact, the probability P_{k_z} that an injected electron will satisfy the conservation of momentum is given by:

$$P_{k_z} = \left(1 - \Theta\Big(|k_z| - k_{lim}\Big)\right) \tag{6.34}$$

where $\Theta(|k_z| - k_{lim})$ is a Heaviside step function.

Up to now, I have mentioned three (one local and two non local) conditions to determine the probability that an electron is effectively injected from the source. At the source contact, the probability $f_{sum}(E)$ that the electron is effectively injected from the source as a transport electron is:

$$\begin{aligned} f_{sum}(E) = f_s(E) f_{sd}(E) P_{k_z} = \frac{1}{exp[(E - E_{fs})/(k_B T)] + 1} \\ \times \left(1 - \frac{1}{exp[(E - E_{fd})/(k_B T)] + 1}\right) \times \left(1 - \Theta\Big(|k_z| - |k|_{lim}\Big)\right) \end{aligned} \tag{6.35}$$

The Fermi-Dirac distribution in Equation (6.28) is a general law used in most nanoscale simulators. The other two additional laws are optional requirements of the injection model that allow a reasonable reduction of the simulated number of transport electrons without affecting the current computations, which could be eliminated if a many body treatment of the equation of motion of electrons is present in the simulation box. However, in traditional single-particle treatment of the equation of motion, such requirements tend to capture the role of the Pauli exclusion principle in the dynamics of the electrons inside the simulation box.

The Figure 6.5 illustrates how the additional two laws (non-local conditions) affect the energy distribution in the new injection model in the case of injected electrons have ballistic transport in graphene transistors. In Figure 6.5(a), all the electrons in VB are attempted to be injected into the system. However, in Figure 6.5(b), when the non-local conditions are included, the energy distribution in VB is different from that in Figure 6.5(a). In Figure 6.5(b), less electrons from VB attempt to be injected into the system with an important reduction of the number of injected electrons, which in case of being injected would not contribute to transport properties. The occupation probability for the electrons in VB with $k_z > 0.5$ nm^{-1} equals to 0, which is a result of the k_z conservation. The probability for the electrons in VB with energy $E > 0.2$ eV (for $|\vec{k}| > 0.5$ nm^{-1}) approximates to 0, which is a result of the correlation between the source and drain contacts.

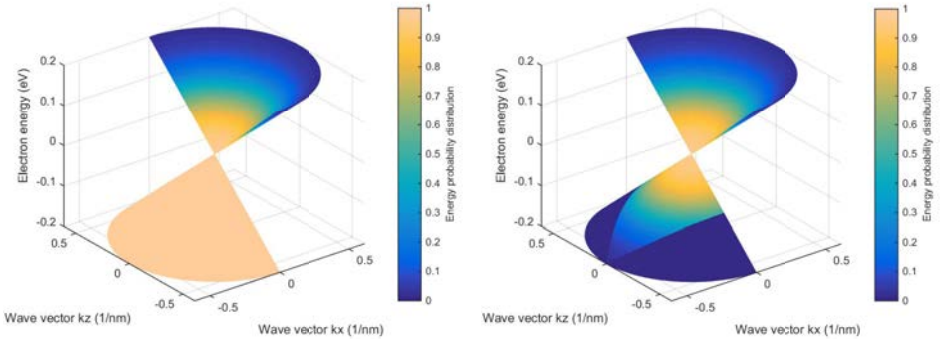

(A) (B)

FIGURE 6.5: The energy distribution of the electrons with positive (in CB) and negative energies injected from the source contact plotted in (a) which computed from equation (6.28) and in (b) which computed from Equation (6.35). The absolute temperature $T = 300$ K, Fermi-level at the source contact $E_{fs} = 0.1$ eV, an voltage drop $V_{DS} = 0.3$ V applied to the device and the Fermi velocity $v_f = 5 \times 10^5$ m/s.

Finally, let me exemplify how I introduce the additional charge in Equation (6.32) and Equation (6.33) in a graphene device. Our purpose here is to compute the charge of electrons that will be injected in a non equilibrium scenario, but not injected in the equilibrium scenario (Figure 6.4(c)). The density of states in 2D linear graphene is:

$$D_{gr}(E) = \frac{g_s g_v |E|}{2\pi\hbar^2 v_f^2} \tag{6.36}$$

where the spin degeneracy $g_s = 2$ and the valley degeneracy $g_v = 2$. Regarding Figure 6.4(f), in principle the amount of charge Q_{add} would be computed from the integral of $D_{gr}(E)$ from E_2 to E_1. However, this is not fully true. Firstly, only electrons going in the transport direction are simulated, so I just need half of this charge. In addition, as presented above I also have to account for the conservation of momentum k_z for all energy levels from E_2 until E_1. For that reason, for example not all electrons from the energy level E_2 will be able to arrive to the drain, and just a fraction of them will be injected. This fraction is easily understood from Figure 6.4(g). Only electrons belonging to the circumference arc will be injected and will be able to reach the drain. The semi-circumference length is $L = \pi E_2$ and the length of the mentioned circumference arc is $L_a = 2|E_2| arcsin\,(E_1/E_2)$. Therefore, the ratio to be injected is $L_a/L = 2arcsin\,(E_1/E_2)\,/\pi$. This calculus must be performed along the device. Then, the amount of charge to be added (Q_{add}) in each point of the device is the following:

$$Q_{add}(x) = q \int_{E_{fs}-5k_BT-V_{DS}}^{E_{fs}-5k_BT-V(x)} \frac{g_s g_v |E|}{2\pi\hbar^2 v_f^2} F_{corr}\, dE \tag{6.37}$$

where F_{corr} is the correction factor and is equal to $F_{corr} = L_a/2L$.

6.2.3 Practical implementation of the electron injection model in the BITLLES simulator

In this part, I describe the procedure for implementing the electron injection model described above in the time-dependent BITLLES simulator:

Step 1. Define a grid for the whole phase-space associated to the injecting contact

We select the phase-space of the contacts. The spatial limits selected by the boundaries of the contact surfaces. The limits of the reciprocal space $\{k_x, k_z\}$ are selected indirectly by the occupation function $f_{sum}(E)$ in Eq.(12) in the main text. That is, the maximum value of the wave vector components, $k_{x,max}$ and $k_{z,max}$, must be selected large enough to be sure that $f_{sum}(E(k_{x,max})) = f_{sum}(E(k_{z,max})) \approx 0$. The minimum value of the wave vector components is assumed to be $k_{x,min} = -k_{x,max}$ and $k_{z,min} = -k_{z,max}$.

In principle, the values Δx, Δz, Δk_x and Δk_z has to be selected according to the development done in appendix A. See Equation (F.7) and Equation (F.8). However, if I are interested only in studying dynamics of electrons at frequencies much lower than $1/t_o$ (with t_o defined in Eq. (2) in the text as the minimum temporal separation between consecutive injected electrons), then I can use larger values of Δx, Δz, Δk_x and Δk_z to speed up the computational burden of the injection algorithm. Then, the spatial step Δz can be chosen as large as the contact surface (i.e. $\Delta z = L_z$, L_z being the lateral width). The spatial step Δx is arbitrary and has no effect on the injection rate. The wave-vector cell $\{\Delta k_x, \Delta k_z\}$ has to ensure that all electrons have similar velocities in the x direction. The selection of Δk_x needs to be small in either parabolic or linear band structures. For parabolic bands, since the v_x velocity is independent of k_z, to speed the computation, I can select $\Delta k_z = 2 \cdot k_{z,max}$. However, for the material with linear band, due to the fact that v_x is explicitly dependent on both wave vector components k_x and k_z, the interval Δk_z should also be selected small enough to roughly maintain the constant velocity v_x for all electrons inside the cell. This grid has to be repeated for all the contacts (source and drain) and all the energy bands (conduction band and valence band) involved in the device simulation.

Step 2. Consider the charge of the non-simulated electrons for each bias point

According to discussion in the main text, the charge inside the simulation box has two different origins. First, the charge assigned to the explicitly simulated particles, i.e. the

transport electrons (injected) in the simulation box. Second, the charge assigned to non-simulated particles, i.e. the charge assigned to the doping and to the non-transport electrons. From each bias condition, the charge assigned to non-transport electrons varies. Therefore, at each bias point, I have to compute the charge $Q_{add}(x)$ defined in Eq.(14) in the text as part of the *fixed* charge in the simulation box when computing device electrostatics.

Step 3. Select the minimum temporal separation t_0 for each phase-space cell

At each time step Δt of the simulation, the algorithm for the injection of electrons has to be considered. For all the cells of the phase space (for all the contacts and all the energy bands involved in the device simulation) defined in **Step 1**, a computation of the minimal injection time t_0 in Eq.(3) and Eq.(4) in the main text is required. When the time of the simulation is equal to a multiple of t_0, an attempt to inject an electron from this particular phase-space cell into the simulation box happens.

Step 4. Decide if the electron is effectively injected or not

For each electron trying to be injected according to **Step 3**, a random number r uniformly distributed between zero and one is generated. The electron is considered to be successfully injected only if $r < f_{sum}(E)$, being E the kinetic energy the electron taken. This stochastic procedure reproduces the binomial probability described in Eq.(6) with the probability $Prob(E) \equiv f_{sum}(E)$ given by Eq.(12) in the main text. Since $f_{sum}(E)$ depends on the temperature, the **Step 4** not only provide the correct average value of the number of injected electrons in a particular energy, but also the physical fluctuations responsible for the thermal noise of the contacts.

Step 5. Select the other properties of the effective injected electron

Once the electron is effectively injected, some additional effort to define its physical properties is required. The information about the momentum, velocity and x position for the electron are specified from the selection of the injection cell in **Step 1** and **Step 4**. Since I consider confinement in the y direction of the 2D materials, the y position is fixed. On the contrary, the z position of the electron is selected with a uniform random distribution along the lateral width of the spatial cell Δz. If I deal with quantum particles, the previous properties of position and momentum refers to the central values

of the position and momentum of the wave packet (conditional wave function) that is associated to the electron[7].

Step 6. Repeat the complete injection procedure during all the simulation

The **Step 3** is repeated at each step Δt of the simulation time. In addition, **Step 4** and **Step 5** are repeated for all attempts to inject an electron.

6.2.4 Numerical results

In Section 6.2.4.1, I provide a discussion on how the local conditions studied in Section 6.2.1 provide some important differences in the injection from linear or parabolic 2D materials. Then, in Section 6.2.4.2, I will discuss the results of the local and non-local conditions on the electron injection model when applied to graphene transistors.

6.2.4.1 Local conditions on the electron injection from parabolic or linear 2D materials

The effect of the material energy spectrum on the number of attempts of injecting electrons into the system is plotted in Figure 6.6. As it can be seen in Figure 6.6(b), only electrons with large k_x are injected into the system. However, in the case of materials with linear dispersion relations, as shown in Figure 6.6(a), the majority of injected electrons have smaller k_z. As a consequence, most injected electrons move in the transport direction at the saturation velocity $v_x \approx v_f$ (with $|k_x| \approx |\vec{k}|$).

This difference in the type of injection can imply relevant differences between the electrical properties of electrons devices fabricated with 2D materials with linear or parabolic bands. As a simple estimation, I assume ballistic transport in the electronic device and compute the (instantaneous) total current I from each electron inside the simulation box. The current I is computed by using the (Ramo-Shockley-Pellegrini) expression $I = qv_x/L_x$ being L_x the source-drain distance. As plotted in Figure 6.7(a), almost all electrons injected from a contact with linear band structure have the same velocity and carry the same instantaneous current I. On the contrary, in Figure 6.7(b), electrons injected from a parabolic band structure material has large dispersion in both the velocity and instantaneous current I. The current dispersion (noise) of both types of band structures are dramatically different, which can have relevant effects in the intrinsic behavior of AC and noise performances.

[7] If the Bohmian approach for the quantum transport is taken into account, as done in the BITLLES, the initial position of the Bohmian particle has to be defined according to quantum equilibrium [75].

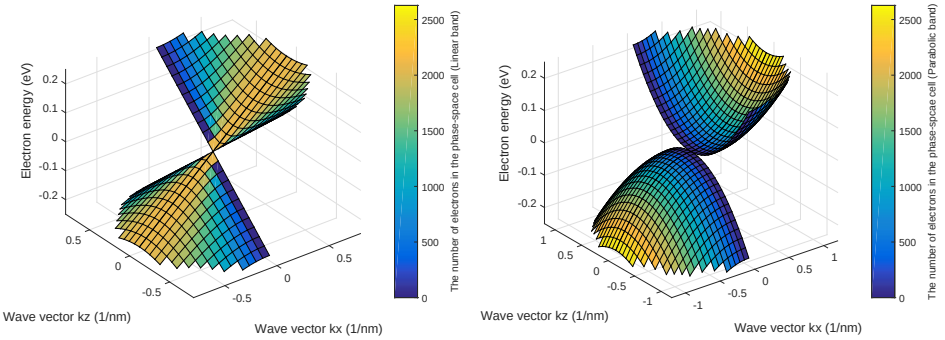

(A) Linear band structure (B) Parabolic band structure

FIGURE 6.6: Number of attempts of injecting electrons computed from Equation (6.27) plotted in (a) and from Equation (6.26) in (b) for a cell $\Delta x \Delta z \Delta k_x \Delta k_z$ during a simulation time $\Delta t = 0.1$ ns at zero temperature. The parameter $m^* = 0.2m_0$ being m_0 the free electron mass, $g_s = 2$, $g_v = 2$, Fermi velocity $v_f = 5 \times 10^5$m/s, the dimensions of the phase-space cell are selected as $\Delta x = \Delta z = 1 \times 10^{-7}$ m, $\Delta k_x = \Delta k_z = 3 \times 10^7 \text{m}^{-1}$.

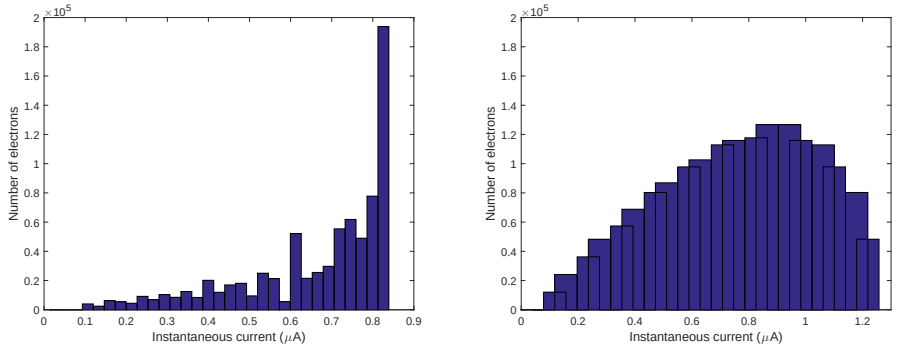

(A) The linear band structure (B) The parabolic band structure

FIGURE 6.7: Number of electrons as a function of instantaneous current I for materials with (a) a linear and (b) a parabolic band structure during $\tau = 0.1$ ns at zero temperature. The simulation conditions are the same as in Figure 6.6 and with Fermi level $E_f = 0.32$ eV.

6.2.4.2 Simulation of graphene transistors

I present numerical results for two different graphene transistors (GFET) performed with the BITLLES simulator following the injection model presented here including the additional charge.

Current-voltage characteristic

The first GFET simulated has the following parameters: channel length is $L_x = 40nm$, width $L_z = 250nm$ and Fermi energy is 0.15 eV above the Dirac point. It has bottom and top gates, whose voltages are set equal to zero, $V_{bg} = V_{tg} = 0$ V. In Figure 6.8,

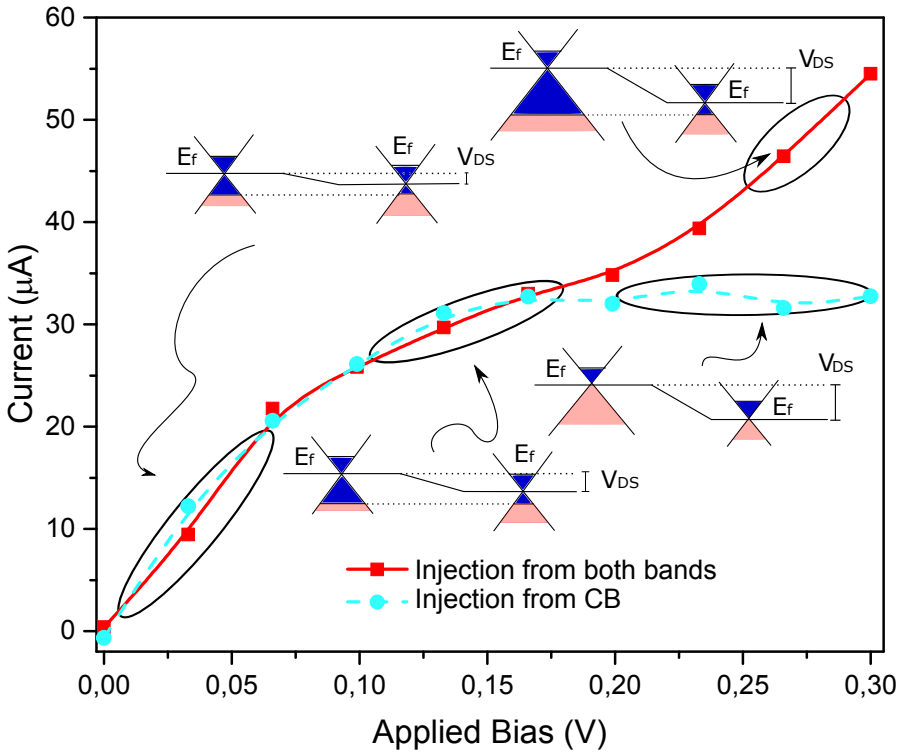

FIGURE 6.8: Current-voltage characteristic for the GFET. The red solid (square) line corresponds to normal graphene injection (electrons injected from both the CB and VB) current-voltage characteristic, while in the blue dashed (circle) line only electrons from the CB are injected. The insets sketch different energy profiles for applied bias.

I see two different current-voltage characteristics of a ballistic GFET. The insets are related to the one plotted in Figure 6.4 indicating the relevant presence of electrons with energy above the Dirac point (CB), and below (VB). The solid curve corresponds to the scenario where electrons are injected from both CB and VB. Contrary to normal FETs, there is no saturation current, since the more the voltage is applied between source and drain, the more number of electrons are transmitted from the source to the drain (from valence band in the source to conduction band in the drain). On the other hand, in the dashed curve, I allow only injection from the CB. Then, current saturates because after the voltage reaches the Fermi energy value, the same amount of electrons from the conduction band are injected independently of the applied voltage. This is similar to typical FETs with semiconductors have energy gap large enough that typically only electrons from the conduction band (or only electrons from the valence band) are considered.

Transient

In this other example, I present (see Figure 6.9) the instantaneous current after a transient perturbation in the gates. This scenario is required to study high-frequency effects

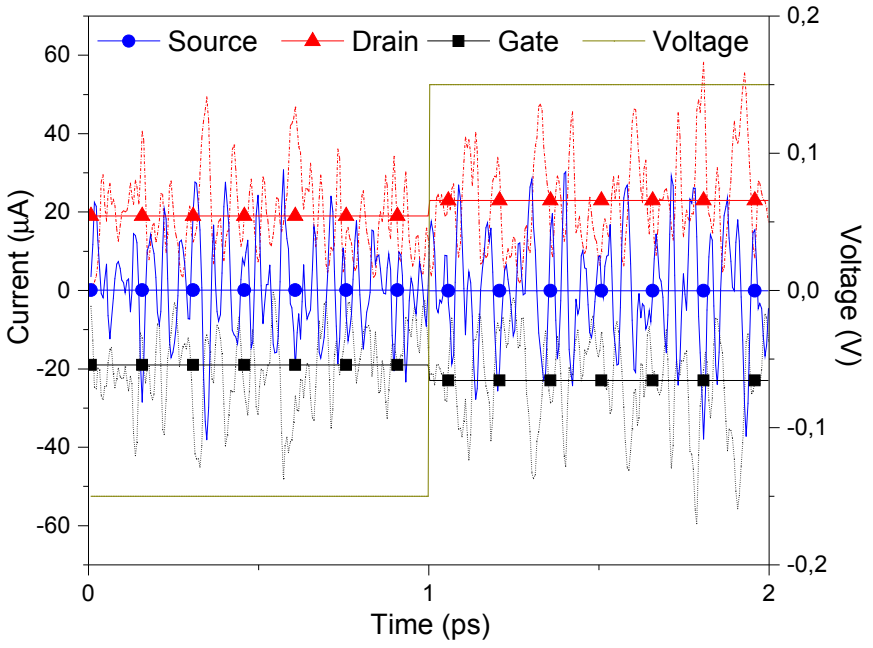

FIGURE 6.9: The transient current in a GFET. Initially both (top and bottom) gates voltage values are set to $V_{bg} = V_{tg} = -0.15$, at time $t = 1$ ps this values is changed to $V_{bg} = V_{tg} = 0.15$.

[184]. I used another GFET with the same parameters, except for the channel length, which is $L_x = 400nm$. In Figure 6.9, I see with solid thick lines the mean current in the drain, source and gate as function of time, and with thinner lines their instantaneous current. After time $t = 1$ ps, the current in the drain increases, opposite to the source, that decreases after the gate voltage perturbation. I notice that the total (particle plus displacement) current has computed for each contact. At each time step, the sum of the three currents is zero satisfying current conservation law. I see in Figure 6.9 the transient dynamics related to the electron dwell time (with Klein tunneling) and the noise induced by the randomness in the electron injection process.

6.3 Time dependence wave packet consequences: two particles at the same place

As explained in the previous section, the BITLLES simulator injects wave packets through the contacts and evolve each of them according to its own pseudodynamical equation. Different electrons have a conditional wave function, this fact makes that in some scenarios, two different electrons can be located at the same place, because their conditional wave function are orthogonal. This effect which appears naturally in the

BITLLES simulator, is a source of noise which can be just reproduced with time dependent discrete injection simulators, as it will be seen in this section.

Most time-independent models developed for quantum transport are based on the reasonable assumption that the energy width of the wave packet is small enough so that the transmission coefficient is essentially constant on the wave packet energy range. However, when this is no longer true, time dependent models are desired to analyze this scenarios [185]. Here, I analyze a type of Hong-Ou-Mandel (HOM) experiment [186, 187] with tunneling and exchange. Two identical electrons are injected simultaneously from two different inputs and after scattering on an electron beam splitter they are measured at two different outputs. The correlation between the detection of the two outputs is measured depending on the injection delay. From these correlation values one can directly obtain quantum noise, i.e., the fluctuations in the number of detected electrons. In particular, I focus on a situation quite close to the experiment mentioned above, but where the scattering region is a double barrier potential with an oscillatory quantum well in a 1D system, see Figure 6.10. In particular, I focus on the case where there is no delay in the injection among both electrons. Then, in principle it is expected that quantum noise is suppressed due to Pauli principle, which states that two electrons cannot be at the same place with the same state [188]. As a consequence, it is expected that each electron will be located at a different output with no (zero frequency) fluctuations. However, our numerical results and the experiment in this type of HOM system show that, even if quantum noise is reduced it is not completely suppressed, indicating the non-zero probability of detecting simultaneously two electrons at the same side. At the end of this section, an experiment is also presented which could test these non expected non zero probabilities.

6.3.1 Two-particle probabilities

I consider two particles injected from two different sources, impinging upon a tunneling barrier as indicated in Figure 6.10. In order to simplify the discussion, I consider electrons with identical spin orientations. Each one is individually defined in a 1D physical space. The two-particle quantum system can be defined by the (orbital) wave function $\Phi \equiv \Phi(x_1, x_2, t)$ in the 2D configuration space. Such wave function is the solution of the many-particle (non-relativistic) Schrödinger equation:

$$i\hbar\frac{\partial\Phi}{\partial t} = \left[-\frac{\hbar^2}{2m}\frac{\partial^2}{\partial x_1^2} - \frac{\hbar^2}{2m}\frac{\partial^2}{\partial x_2^2} + V(x_1, x_2)\right]\Phi \tag{6.38}$$

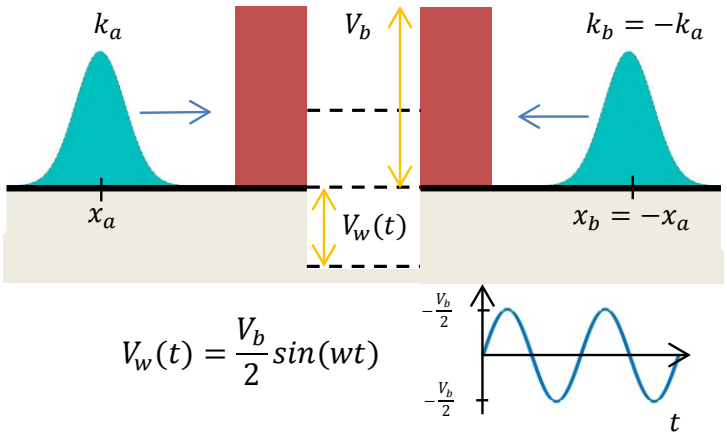

FIGURE 6.10: Double barrier with a time-dependent oscillatory quantum well $V_w(t)$, whose shape is depicted in the inset figure. Two wave packets ($\phi_a(x)$ and $\phi_b(x)$) are located at each side of the barrier at the same distance ($x_b = -x_a$) describing each one an electron with the same energy but with opposite momentum ($k_b = -k_a$). With this experiment, the reliability of the predictions explained in the text can be proven.

where m is the electron mass and $V(x_1, x_2)$ takes into account the two-particle Coulomb interaction between the electrons and also the one-particle interaction between one electron and a tunneling barrier. The exchange interaction is introduced in the shape of the initial wave function $\Phi(x_1, x_2, t_0)$. The anti-symmetrical/symmetrical (orbital) many-particle wave function for Fermions/Bosons is:

$$\Phi(x_1, x_2, t_0) = \frac{\phi_a(x_1, t_0)\phi_b(x_2, t_0) \mp \phi_a(x_2, t_0)\phi_b(x_1, t_0)}{\sqrt{2}} \tag{6.39}$$

The above expression can be interpreted as the determinant/permanent of a 2×2 matrix constructed from the one-particle wave function $\phi_a(x, t_0)$ and $\phi_b(x, t_0)$ [71]. Hereafter, upper/lower signs correspond to (non-relativistic) massive Fermions/Bosons. Although I mainly deal with electrons (fermions), I will also compute probabilities for (massive) Bosons. The initial one-particle wave functions $\phi_a(x, t_0)$ and $\phi_b(x, t_0)$ in expression Equation (6.39) are completely general. The only relevant condition for $\phi_a(x, t_0)$ is that its modulus square is normalized to unity and it is totally located at the left of the barrier at time $t = t_0$. Identical conditions for $\phi_b(x, t_0)$ which is localized at the right. Additionally, according to the type of HOM experiment discussed here, both wave packets have opposite (central) momentum so that they impinge upon the barrier after a while, as depicted in Figure 6.10. By construction, the time evolution of $\Phi(x_1, x_2, t)$ using Equation (6.38) preserves the initial norm and the initial (anti)symmetry of the wave function.

Let me argue why it is reasonable to expect non-zero probability for finding both electrons at the same side of the barrier. The reason is quite simple and intuitive. Pauli principle forbids two fermions being at the same position with the same state [188]. However, a pertinent question appears: *When is reasonable the assumption that the reflected and transmitted states are exactly identical?* Certainly, both transmitted and reflected states are identical when only one state is available in the spatial region where they coincide. This restriction on the available states is evident when the initial state has a unique (well-defined) energy E_k i.e., a mono-energetic state. Then, because of the elastic nature of the interaction with the barrier (i.e., energy conservation), only one state at the right of the barrier and one at the left with the same energy E_k (and the pertinent momentum going outside from the barrier) are available at the final time. Nevertheless, as stated previously, I require a superposition of mono-energetic eigenstates (i.e., a wave packet) to describe an initial state with a spatially localized support outside of the barrier region. Then, in principle, there is the possibility of different time-evolution for the transmitted and reflected components. In such time-dependent scenarios, one can expect probabilities different from zero as mentioned before and indicated in Figure 6.14 and Figure 6.15. Notice the different shapes of the reflected and transmitted wave packet in Figure 6.12.

I consider a particular time t_1 large enough so that the interaction with the barrier is almost finished, i.e., the probability presence inside the barrier region is negligible. Then, using Born's rule [71] [8] in the $2D$ configuration space, $\{x_1, x_2\}$, the probability of detecting one electron at each side of the barrier (on regions S_{LR} or S_{RL} of the configuration space depicted in Figure 6.11) at this $t = t_1$ is:

$$\mathcal{P}_{\mathcal{LR}} = \int_{\mathcal{S}_{\mathcal{LR}}} |\Phi|^2 dx_1 dx_2 + \int_{\mathcal{S}_{\mathcal{RL}}} |\Phi|^2 dx_1 dx_2 = 2 \int_{\mathcal{S}_{\mathcal{LR}}} |\Phi|^2 dx_1 dx_2 \tag{6.40}$$

Due to the exchange symmetry, the wave function on $\mathcal{S}_{\mathcal{LR}}$ is identical to that on $\mathcal{S}_{\mathcal{RL}}$, as seen in Figure 6.11. The two integral in the left hand side of Equation (6.40) are exactly equal, so the total contribution of finding one electron at each side of the barrier is twice one of the integrals. Equivalently, the probability of detecting the two electrons at the left of the barrier (on the region $\mathcal{S}_{\mathcal{LL}}$ of the configuration space) is:

[8] The detection of the two electrons is a measurement of the wave function that implies a non-unitary evolution (not accessible from the unitary Schrödinger evolution). As usual, it is assumed that particle detectors provide a collapse of wave function only in those positions $\{x_1, x_2\}$ of the configuration space where the measurement is present. Notice that only reflected or transmitted components are plotted for each wave packet in Figure 6.10.

$$\mathcal{P}_{\mathcal{LL}} = \int_{\mathcal{S}_{\mathcal{LL}}} |\Phi|^2 dx_1 dx_2 \tag{6.41}$$

Finally, the probability of two electrons at the right of the barrier (on the region $\mathcal{S}_{\mathcal{RR}}$) is:

$$\mathcal{P}_{\mathcal{RR}} = \int_{\mathcal{S}_{\mathcal{RR}}} |\Phi|^2 dx_1 dx_2 \tag{6.42}$$

I define $\mathcal{P}_{\mathcal{LR}}$, $\mathcal{P}_{\mathcal{LL}}$ and $\mathcal{P}_{\mathcal{RR}}$ as two-particle probabilities. In Figure 6.11(a) I plot the probability presence of the initial two-particle state in the 2D configuration space. According to Equation (6.39), the wave packet $\phi_a(x_1, t_0)\phi_b(x_2, t_0)$ has its support on $\mathcal{S}_{\mathcal{LR}}$, while the wave packet $\phi_a(x_2, t_0)\phi_b(x_1, t_0)$ on $\mathcal{S}_{\mathcal{RL}}$. There is no initial probability presence in the other regions. The first relevant issue seen on the regions $\mathcal{S}_{\mathcal{LL}}$ and $\mathcal{S}_{\mathcal{RR}}$ of Figure 6.11(b) is that $\mathcal{P}_{\mathcal{LL}} \neq 0$ and $\mathcal{P}_{\mathcal{RR}} \neq 0$. I explain the reason of these non-zero probabilities in next section. In general, there is no reason to expect that the probability of detecting two electrons at the left of the barrier is equal to the probability of detecting them at the right, $\mathcal{P}_{\mathcal{RR}} \neq \mathcal{P}_{\mathcal{LL}}$ as seen in Figure 6.11(b).

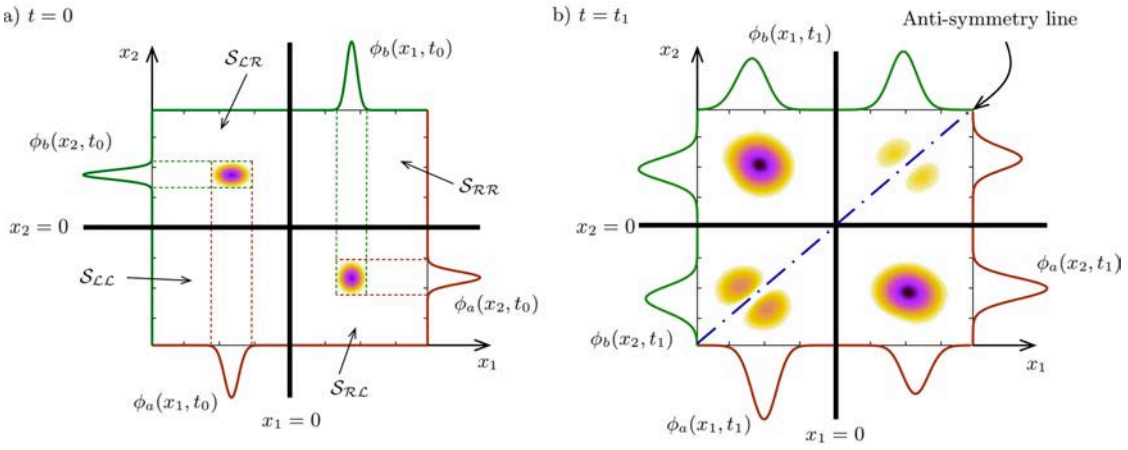

FIGURE 6.11: a) Modulus square of the wave function $\Phi(x_1, x_2, t_0)$ at the initial time t_0 in the configuration space $\{x_1, x_2\}$. With black solid line is represented the scattering barrier. Along the axes the single particle wave packet $\phi_a(x, t_0)$ (red solid line) and $\phi_b(x, t_0)$ (green solid line) are reported for both variables (x_1 and x_2). The dotted line visualizes how the anti-symmetrical wave function is constructed. The different region of configuration space $\mathcal{S}_{\mathcal{LL}}, \mathcal{S}_{\mathcal{LR}}, \mathcal{S}_{\mathcal{RL}}$ and $\mathcal{S}_{\mathcal{RR}}$ are explicitly indicated. b) Modulus square of the wave function $\Phi(x_1, x_2, t_1)$ at the final time t_1 (such that the interaction with the barrier is already accomplished). Along the axes $\phi_a(x, t_1)$ (red solid line) and $\phi_b(x, t_1)$ (green solid line) for both variables $\{x_1, x_2\}$ are reported . With dashed dotted blue line the anti-symmetry line for Fermions is indicated. As asserted in the text the probabilities $\mathcal{P}_{\mathcal{RR}} \neq \mathcal{P}_{\mathcal{LL}} \neq 0$.

To certify the unavoidable fundamental (not spurious) origin of the non-zero probabilities for $\mathcal{P}_{\mathcal{LL}}$ and $\mathcal{P}_{\mathcal{RR}}$, hereafter, I consider exactly the same idealized conditions used in

[41, 79, 82] when they discuss the two-particle probabilities. I take the two wave packets $\phi_a(x,t_0)$ and $\phi_b(x,t_0)$ as identical as possible. In particular, I impose the following three conditions:

- Condition (i): A separable potential $V(x_1,x_2)$ in Equation (6.38) without Coulomb interaction:
$$V(x_1,x_2) = V_B(x_1) + V_B(x_2) \tag{6.43}$$
where $V_B(x)$ is the symmetrical potential energy of a tunneling barrier, i.e., $V_B(x) = V_B(-x)$, with $x = 0$ at the center of the barrier region. See Figure 6.12(a).
- Condition (ii): All parameters of the initial wave packet a and b are identical, except for the initial central momentum which accomplishes $k_b = -k_a$ and central positions $x_b = -x_a$. See Figure 6.12(a).
- Condition (iii): Electrons are injected exactly at the same time.

Because of these conditions, as discussed in Appendix G, the two initial wave packets are defined with (almost) identical parameters. In particular, I have $g_a(k) = g_b(-k)$ where $g_a(k) = \langle\phi_a(x,t_0)|\,\psi_k(x)\rangle$ is the complex value that weights the superposition of the scattering states to build the wave packet $\phi_a(x,t_0)$. See Equation (G.4) in Appendix G. Identical definition for $g_b(k)$.

Under these conditions, I can anticipate the evolution of $\Phi(x_1,x_2,t)$ and also the origin of the non-zero probabilities for arbitrary wave packets. I consider the initial (anti-symmetrical) wave function of two electrons $\Phi(x_1,x_2,0)$ defined by Equation (6.39). Since the time-evolution of Schrödinger equation satisfies the superposition principle, I can discuss the time-evolution of $\phi_a(x_1,t_0)\phi_b(x_2,t_0)$ and $\phi_a(x_2,t_0)\phi_b(x_1,t_0)$ independently. Then, since I are dealing with a separable Hamiltonian, the evolution of $\phi_a(x,t)$ and $\phi_b(x,t)$ can be computed from two simpler single particle Schrödinger equations. At a time $t = t_1$, after the interaction with the barrier, each wave packet splits into two (non-overlapping) components:

$$\phi_a(x,t_1) = \phi_a^r(x,t_1) + \phi_a^t(x,t_1) \tag{6.44}$$
$$\phi_b(x,t_1) = \phi_b^r(x,t_1) + \phi_b^t(x,t_1) \tag{6.45}$$

where the upperindices r and t refer to the reflected and transmitted component of each wave packet (ϕ_a and ϕ_b), respectively. Then, the two particle wave function in the region of the configuration space $\mathcal{S}_{\mathcal{LL}}$ at $t = t_1$ is:

$$\Phi(x_1,x_2,t_1)\big|_{\mathcal{S}_{\mathcal{LL}}} = \frac{\phi_a^r(x_1,t_1)\phi_b^t(x_2,t_1) - \phi_a^r(x_2,t_1)\phi_b^t(x_1,t_1)}{\sqrt{2}} \tag{6.46}$$

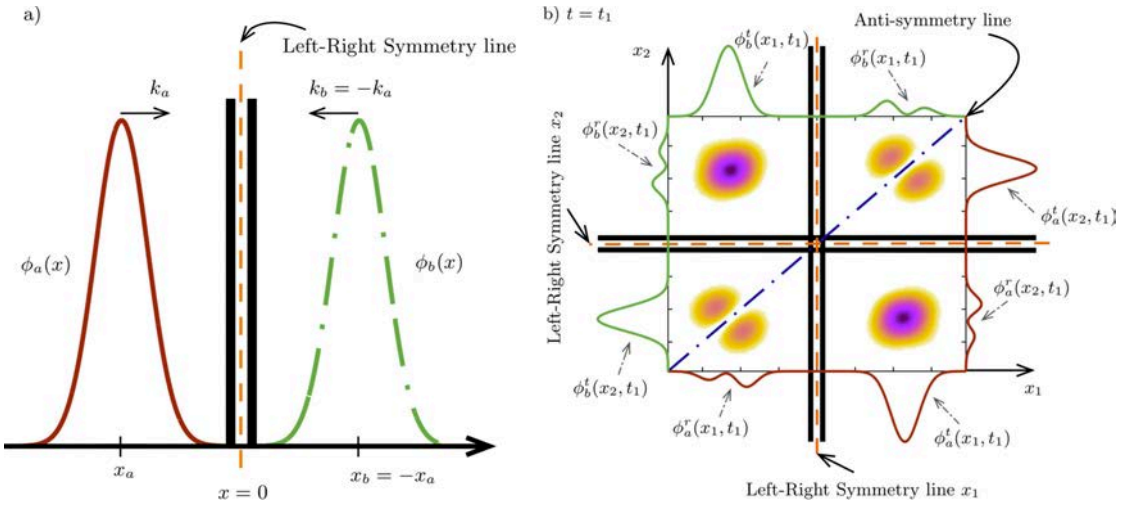

FIGURE 6.12: a) Schematic representation of the initial wave packets in the physical space under the conditions (i), (ii) and (iii). With black solid line the double barrier structure is depicted. With orange dashed line the Left-Right symmetry of the problem is depicted. With red solid line wave packet $\phi_a(x)$ centered in x_a and with momentum k_a is depicted. With green dashed dotted line the wave packet $\phi_b(x)$ centered in $x_b = -x_a$ and momentum $k_b = -k_a$ is reported . b) Modulus square of the wave function $\Phi(x_1, x_2, t_1)$ at the final time t_1 at the configuration points $\{x_1, x_2\}$. With dashed dotted blue line the anti-symmetry line for Fermions is indicated and with orange dashed lines the Left-Right symmetry for each degree of freedom (x_1 and x_2) is reported. Along the axes, the modulus square of the ϕ_a (red line) and ϕ_b (green line) wave functions are plotted for each degree of freedom (x_1 and x_2). The upperindices r or t indicate reflected or transmitted components, respectively.

Let me notice that the region $\mathcal{S}_{\mathcal{LL}}$ was initially empty of probability, as seen in Figure 6.11(a). The initial wave packet $\phi_a(x_1, t_0)$ on $\mathcal{S}_{\mathcal{LR}}$ (which is identical to the one plotted in Figure 6.11(a)) evolves into the part $\phi_a^r(x_1, t_1)$ on $\mathcal{S}_{\mathcal{LL}}$ in Figure 6.12(b). Equivalently, the initial wave packet $\phi_b(x_2, t_0)$ in Figure 6.11(a) evolves into the part $\phi_b^t(x_2, t_1)$ on $\mathcal{S}_{\mathcal{LL}}$ in Figure 6.12(b). Identical explanations for the presence of $\phi_b^t(x_1, t_1)$ and $\phi_a^r(x_2, t_1)$ on $\mathcal{S}_{\mathcal{LL}}$. Clearly, since $\mathcal{P}_{\mathcal{LL}}$ in Equation (6.41) is computed from an integral of non-negative real numbers, the requirement for obtaining the result $\mathcal{P}_{\mathcal{LL}} = 0$ in Equation (6.46) is that $\phi_a^r(x_1, t_1)\phi_b^t(x_2, t_1) = \phi_a^r(x_2, t_1)\phi_b^t(x_1, t_1)$ at all positions $\{x_1, x_2\} \in \mathcal{S}_{\mathcal{LL}}$ [9]. This last condition can only be obtained when $\phi_b^t(x, t_1) = \phi_a^r(x, t_1)$ and $\phi_a^t(x, t_1) = \phi_b^r(x, t_1)$. On the contrary, if the transmitted and reflected wave packet components differ, i.e., if the time-evolution giving the transmitted component $\phi_a^t(x, t_1)$ is different from $\phi_b^r(x, t_1)$, then I get $\Phi(x_1, x_2, t_1) \neq 0$, which implies $\mathcal{P}_{\mathcal{LL}} \neq 0$. Analogous consideration can be done for the configuration space region $\mathcal{S}_{\mathcal{RR}}$.

After discussing the origin of the non-zero probabilities, I present a technical question that I will test numerically later. The conditions (i), (ii) and (iii) impose an additional symmetry on the problem. Apart from the intrinsic anti-symmetry of the wave function

[9] By construction, only in the configuration space points $\{x_1, x_2\} \in \mathcal{S}_{\mathcal{LL}}$ such that $x_1 = x_2$, the wave function is always strictly zero (see anti-symmetry line in the Figure 6.12 b).

implicit in Equation (6.39), there is an additional Left-Right symmetry. This means that, being $x = 0$ the center of the barrier region as depicted in Figure 6.12(a), the wave function under the separable Hamiltonian of Equation (6.43) has to satisfy $\Phi(x_1, x_2, t) = -\Phi(-x_1, -x_2, t)$ at all times. This additional symmetry implies that the probability of detecting two electrons on the left is exactly equal to detect them on the right, i.e., $\mathcal{P}_{\mathcal{LL}} = \mathcal{P}_{\mathcal{RR}}$ as depicted in Figure 6.12(b). However, let us notice that, in general, when conditions (i), (ii) and (iii) are not satisfied, I have $\mathcal{P}_{\mathcal{LL}} \neq \mathcal{P}_{\mathcal{RR}}$ as depicted in the preceding Figure 6.11(b).

The exact values of $\mathcal{P}_{\mathcal{LR}}$, $\mathcal{P}_{\mathcal{LL}}$ and $\mathcal{P}_{\mathcal{RR}}$ depend on the effective overlapping between $\phi_a^t(x, t_1)$ and $\phi_b^r(x, t_1)$. In Appendix G I develop analytic calculations of the range of values that the probabilities seen in Equation (6.40)-Equation (6.42) can take when conditions (i), (ii) and (iii) are assumed. When reflected and transmitted wave packets are identical, then Equation (6.40)-Equation (6.42) can be rewritten as:

$$\mathcal{P}^M_{\mathcal{LL}} = \mathcal{P}^M_{\mathcal{RR}} = RT \mp RT\mathcal{P}^M_{\mathcal{LR}} = (R \pm T)^2 \tag{6.47}$$

which corresponds to the well-known result $\mathcal{P}^M_{\mathcal{LL}} = \mathcal{P}^S_{\mathcal{LL}} = 0$, $\mathcal{P}^M_{\mathcal{RR}} = \mathcal{P}^S_{\mathcal{RR}} = 0$ and $\mathcal{P}^M_{\mathcal{LR}} = \mathcal{P}^S_{\mathcal{LR}} = 1$. For bosons, I obtain $\mathcal{P}^M_{\mathcal{LL}} = \mathcal{P}^M_{\mathcal{RR}} = 2RT$ and $\mathcal{P}^M_{\mathcal{LR}} = (R - T)^2$. Let us notice that the sum of the three probabilities is equal to one (for Fermions or Bosons) because I deal with a unitary evolution. I use the upperindex M denoting that the overlapping between the transmitted and reflected components is maximum. In summary, I have tested that our general definitions of the two-particle probabilities in Equation (6.40)-Equation (6.42) exactly reproduce, as a particular example, the results found in the literature for scattering states in [79, 82, 170, 173].

For other scenarios, for example a double barriers with wave packets with resonant energies, I show in Appendix G that the transmitted and reflected components become orthogonal. Then, the probabilities seen in Equation (6.40) - Equation (6.42) in this type of experiments at resonances can be written as:

$$\mathcal{P}^m_{\mathcal{LL}} = \mathcal{P}^m_{\mathcal{RR}} = RT \tag{6.48}$$

$$\mathcal{P}^m_{\mathcal{LR}} = R^2 + T^2 \tag{6.49}$$

where the upperindex m here indicates that the overlapping between transmitted and reflected components is zero (minimum). Again, the sum of the probabilities is one because of the unitary evolution. These last probabilities $\mathcal{P}^m_{\mathcal{LL}}, \mathcal{P}^m_{\mathcal{RR}}$ and $\mathcal{P}^m_{\mathcal{LR}}$ show no

difference between Fermions or Bosons. In fact, these results are identical to the probability of distinguishable particles. In conclusion, even with both electrons at the same position at the same time, the Pauli principle has no effect in these HOM scenarios because the wave nature of electrons is described by different (orthogonal) wave functions. I emphasize that, in general, the two-particle probabilities in equations (6.40)-(6.42) can take any value between the limits imposed by Equation (6.47)-Equation (6.47) and Equation (6.48)-Equation (6.49). I emphasize that all the previous results are valid for any shape of quasi-particle wave packets.

6.3.2 Quantum noise with the new probabilities

In this section, after having developed the new two-particle scattering probabilities $\mathcal{P}_{\mathcal{RR}}$, $\mathcal{P}_{\mathcal{LL}}$ and $\mathcal{P}_{\mathcal{LR}}$, I compute the quantum noise formula with the new possibilities (Figure 6.11 c) and d)) described above. Noise will be computed under the following approximations:

- I assume that the noise contribution comes from one- and two-particle processes. In detail, I consider (i) one electron injected from the left and none from the right, (ii) one from the right and none from the left and (iii) one from left and one from right. These restrictions are reasonable for standard devices working at room temperature.
- I treat classically the interaction between electrons and the quasi-electrostatic potential barrier. In other words, I neglect the photon nature of the electromagnetic field because the frequencies and the electric field I deal with are such that the number of available photons is large enough [189].
- In order to simplify the final noise expression, I consider a symmetric system, therefore I will assume that $T_a = T_b$, $R_a = R_b$ and $\mathcal{P}_{\mathcal{RR}} = \mathcal{P}_{\mathcal{LL}}$. The generalization to non-symmetrical scenarios can be done straightforwardly.
- I assume that the measurement of the current is done at zero or low frequencies, where displacement currents can be neglected because their contributions are zero after time averaging.

Under this approximations, noise can be computed from the knowledge of the number N of transmitted particles through the barrier during the time t_d as:

$$\langle S \rangle = lim_{t_d \to \infty} 2q^2 \frac{\langle N^2 \rangle_{t_d} - \langle N \rangle_{t_d}^2}{t_d} \tag{6.50}$$

We define $\langle N\rangle_{t_d} = \sum_{N=-\infty}^{N=\infty} P(N)N$ and $\langle N^2\rangle_{t_d} = \sum_{N=-\infty}^{N=\infty} P(N)N^2$, where $P(N)$ is the probability of N particles being transmitted from the left to the right reservoir. The probabilities $P(N)$ are computed from the direct solution of the two-particle Schrödinger equation including exchange interaction and summarized in Figure 6.13.

a / **b**		Injection: Transmitted	Injection: Reflected	No injection
Injection	Transmitted	$\frac{\mathcal{P}_{\mathcal{LR}}}{2} f_a f_b$	$\mathcal{P}_{\mathcal{LL}} f_a f_b$	$T(1-f_a)f_b$
		0	-1	-1
	Reflected	$\mathcal{P}_{\mathcal{RR}} f_a f_b$	$\frac{\mathcal{P}_{\mathcal{LR}}}{2} f_a f_b$	$R(1-f_a)f_b$
		1	0	0
No injection		$Tf_a(1-f_b)$	$Rf_a(1-f_b)$	$(1-f_a)(1-f_b)$
		1	0	0

FIGURE 6.13: Probability (upper) that N (lower) electrons are transmitted from the left to right reservoir during the time interval t_d. f_i is the Fermi distribution ($i = a, b$) and T_i and R_i the i-wave packet single particle transmission and reflection coefficients.

Now, one can determine the noise $\langle S\rangle$, which due to the new $P(N)$, is related to $\mathcal{P}_{\mathcal{LL}}$ and $\mathcal{P}_{\mathcal{RR}}$:

$$\langle S\rangle = \frac{4q^2}{h}(T[f_a(1-f_a)+f_b(1-f_b)] + T(1-T)(f_a-f_b)^2 + 2\mathcal{P}_{\mathcal{LL}} f_a f_b) \tag{6.51}$$

Equation (6.51) contains the usual Landauer-Büttiker formalism noise expression in the case where $\mathcal{P}_{\mathcal{RR}} = \mathcal{P}_{\mathcal{LL}} = 0$. However, I have showed that generally, $\mathcal{P}_{\mathcal{LL}} \neq 0$ and quantum noise is increased. In the limit of the distinguishable particles behavior, the classical noise results (understood as a noise due to tunneling of electrons without considering exchange interaction among them) are recovered $\mathcal{P}_{\mathcal{LL}} = RT$ and electrons behave like classical particles. In general, the results predicted by Equation (6.51) lie among the Landauer-Büttiker formalism and the classical results.

Regarding Equation (6.51), one may wonder if the fluctuation-dissipation theorem [190, 191] is not fulfilled, but I emphasize that this expression is obtained under the assumption that I work at high temperatures, with only one- and two-particle scattering processes. At lower temperatures more electrons should be taking into account.

6.3.3 Numerical results for a two-particle scenario with a separable and symmetrical double barrier potential

I consider the double barrier plotted in Figure 6.12(a) and also in the inset of Figure 6.14. The potential profile is built by two barriers of 0.4 eV of height and 0.8 nm of width between a quantum well of 5.6 nm. This potential profile has Left-Right symmetry. The $x = 0$ is situated at the center of the quantum well. The (effective) mass of the electrons (m) is 0.067 times the free electron mass. The first resonant energy of such structure is $E_R = 0.069\ eV$. At the initial time t_0, the initial state is defined for numerical convenience by two Gaussian wave packets (other choices are possible), $\phi_a(x, t_0)$ and $\phi_b(x, t_0)$ [71] whose spatial support is located at the left and right of the barrier, respectively. Let us notice that such Gaussian wave packets have point-localized or fully-extended mono-energetic states as two limiting cases. Both wave packets have the same central energy $E_a = E_b$, but opposite central wave vectors $k_b = -k_a$ and central positions $x_a = -x_b$. In Figure 6.14 the time evolution of Equation (6.40))-Equation (6.42) are depicted. First, I see that for a wave packet whose energy is far from the resonant energy E_R, I obtain $\mathcal{P}^S_{\mathcal{LR}} \equiv \mathcal{P}^M_{\mathcal{LR}} = 1$, $\mathcal{P}^S_{\mathcal{LL}} \equiv \mathcal{P}^M_{\mathcal{LL}} = 0$ and $\mathcal{P}^S_{\mathcal{RR}} \equiv \mathcal{P}^M_{\mathcal{RR}} = 0$, at $t_1 = 0.7\ ps$. However, for the resonant energy $E_a = E_b = E_R$ I get the results $\mathcal{P}_{\mathcal{LR}} \equiv \mathcal{P}^m_{\mathcal{LR}} = 1 - 2RT$, $\mathcal{P}_{\mathcal{LL}} \equiv \mathcal{P}^m_{\mathcal{LL}} = RT$ and $\mathcal{P}_{\mathcal{RR}} \equiv \mathcal{P}^m_{\mathcal{RR}} = RT$ that correspond to the values of indistinguishable particles predicted by Equation (6.48)-Equation (6.49). To test these last expressions numerically, I notice that this potential profile and wave packets give $T = 0.806$ and $R = 0.194$, where R and T are the single particle reflection and transmission coefficients. As explained (see Appendix G), the latter set of probabilities correspond to a scenario in which the transmitted and reflected components are orthogonal. In other words, the transmitted wave packet is basically built by a superposition of resonant scattering states, while the reflected one by mainly non-resonant scattering states.

As mentioned in the beginning of the section, dealing with the time-dependent Schrödinger equation implies that the results depend also on the initial wave packet shape. In Figure 6.15, I study the dependence of the two-particle probabilities of Figure 6.14 on the *size* of the initial wave packet. I define the size of the initial wave packet as the double of the full width at half maximum (FWHM) of the probability presence of the Gaussian wave packet at $t = t_0$. Such size can be related with the spatial dispersion σ_x of the initial wave packet from $2 \times FWHM = 4\sqrt{\ln(2)}\sigma_x$. In the limit of $\sigma_x \to \infty$, a wave packet approaches to a scattering state.

The maximum wave packet dimensions considered in Figure 6.15 are much larger than typical reservoir sizes in quantum transport with semiconductors [192] and I still clearly see $\mathcal{P}_{\mathcal{LL}} = \mathcal{P}_{\mathcal{RR}} \neq 0$. In addition, if I consider barriers much higher than 0.4 eV,

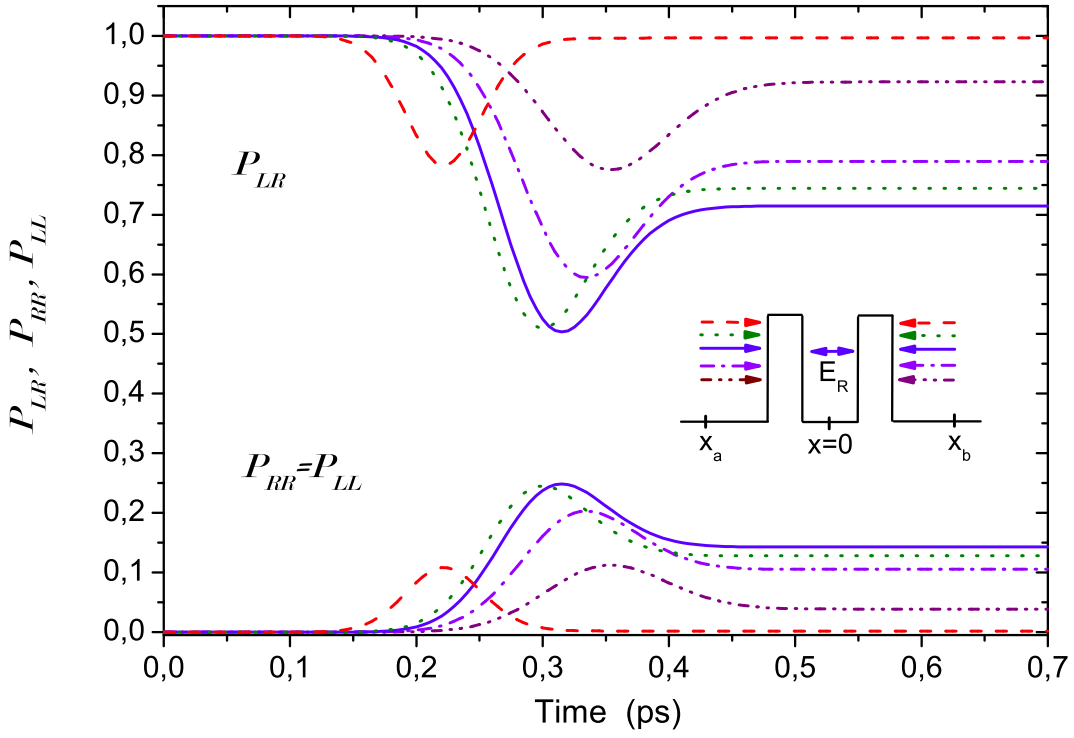

FIGURE 6.14: Time evolution of $\mathcal{P}_{\mathcal{LR}}$ (upper lines) and $\mathcal{P}_{\mathcal{LL}} = \mathcal{P}_{\mathcal{RR}}$ (lower lines) from $\Phi(x_1, x_2, t)$ built by two initial wave packets located at $x_a = -175$ nm and $x_b = 175$ nm with opposite momenta and equal spatial dispersion $\sigma_a = \sigma_b = 35\ nm$. The energies are $E_a = E_b = 0.12\ eV$ (red dashed line), $E_a = E_b = 0.075\ eV$ (green dot line), $E_a = E_b = E_R = 0.069\ eV$ (blue solid line), $E_a = E_b = 0.06\ eV$ (dash dot violet line) and $E_a = E_b = 0.05\ eV$ (dash dot dot purple). The inset shows the potential profile.

the resonance becomes much sharper and wave packets with $\sigma_x \approx 1\ \mu m$ still show $\mathcal{P}_{\mathcal{LL}} = \mathcal{P}_{\mathcal{RR}} \neq 0$.

6.3.4 Numerical results for an oscillatory proposed experiment

There is a HOM experiment [186] where two identical electrons are injected simultaneously from two inputs and measured in two outputs. In the experiment, it is found out that the possibility of measuring both electrons at the same side is not zero, as usually expected. Apart from [193, 194] that explain this result because of the interaction among different Landau levels in the inner channels, other explanations appeal for decoherence [195], spurious results [196] and time delay in the injection [197].

With the approach explained previously in Section 6.3.1 and Section 6.3.2, alternatively, a fundamental (non-spurious) reason for the experimental results can be given. Due to the time and energy dependence evolution of the electron wave packet, after the interaction with the barrier, the reflected and transmitted components of the wave packets do

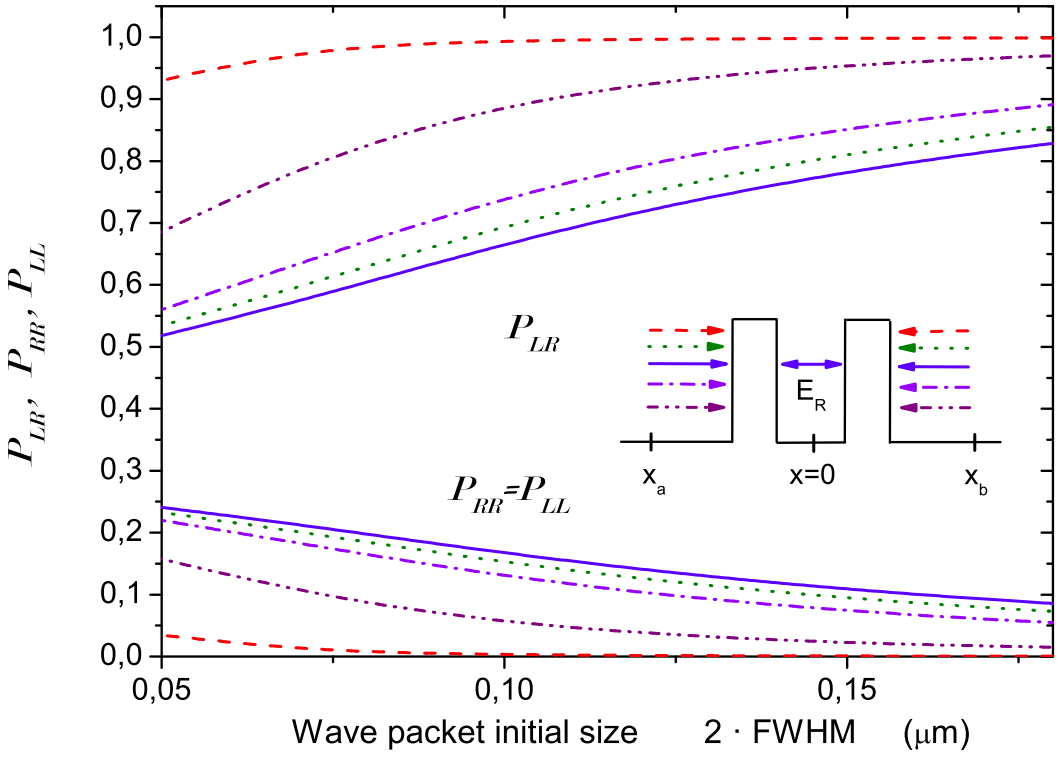

FIGURE 6.15: The probabilities of $\mathcal{P}_{\mathcal{LR}}$ (upper lines) and $\mathcal{P}_{\mathcal{LL}} = \mathcal{P}_{\mathcal{RR}}$ (lower lines) from $\Phi(x_1, x_2, t_1)$ at time $t_1 = 0.7$ ps with the same initial wave packets and energies of Figure 6.14 but with variable spatial dispersion $\sigma_x = \sigma_a = \sigma_b$. The inset shows the potential profile.

not overlap completely. Thus, there is no reason to expect that they cannot be detected at the same place because their states are different and then the exclusion Pauli principle does not apply.

In this section, an experiment with oscillating potentials which would be able to test the reliability of the explanation for the unexpected noise results is presented. I analyze the case where two electrons are injected simultaneously with the same energy from both sides of a double barrier at the same distance from the barrier. This double barrier system has a time-dependent well (see Figure 6.10), which oscillates periodically according to expression $V_w = \frac{V_b}{2} sin(wt)$. In order to increase the visualization of these new probabilities, I will consider the injection of electrons whose energies are close to the (first) resonant energy of the double barrier. For these energies, the transmission coefficient has a sharp energy-dependence so that the reflected and transmitted wave packets become almost orthogonal, $|I^{r,t}_{a,b}|^2 \approx 0$. This resonant scenario is selected to maximize the condition that the transmission coefficient is not constant in the wave packet energy range $[E - \Delta E/2, E + \Delta E/2]$. Then, the new probabilities become more relevant.

It can be reasonably expected that, by changing the potential level of the well inside the barrier, the resonant energy of the double barrier will change accordingly, while the electron approaches the barrier region. This will cause that for some electrons that in the time-independent case were not resonant, and therefore their probability of finding both at same place was low, will be resonant, increasing enormously the probabilities of finding both of them at the same side of the barrier.

In our proposed experiment two electrons are *artificially* injected, one from each side of the barrier simultaneously. Artificially means that the standard injection from the mesoscopic contacts at thermal equilibrium is not pertinent in this experiment. Then, in Equation (6.51), the temperature is not relevant and $f_a = f_b = 1$. No thermal noise has to be considered in this type of experiments with *artificial* injection. Under these considerations, the only term which survives in Equation (6.51) is the last one, which contains the new probability $\mathcal{P}_{\mathcal{LL}}$ of finding both particles at the same side. Therefore, in this particular scenario, the computation of $\mathcal{P}_{\mathcal{LL}}$ provides directly, apart from a constant factor, the quantum noise in Equation (6.51)

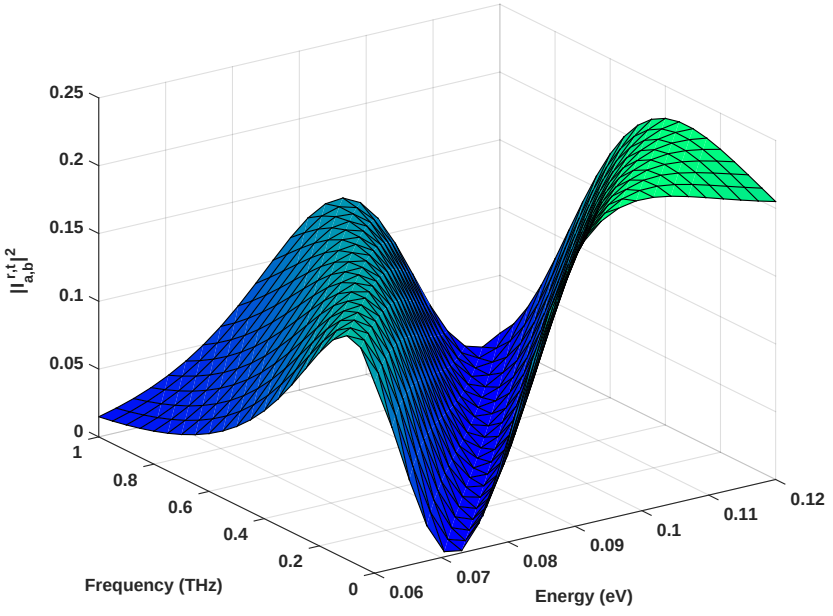

FIGURE 6.16: The overlapping term $|I^{r,t}_{a,b}|^2$ is plotted as a function of the frequency of the oscillation well and also as a function of the central energy of the injected electrons. I see that for certain values, the overlapping is almost zero, corresponding to the resonant energies.

I performed simulations for the experiment, as a function of the energy of the injected electrons and also of the frequency of the oscillation of the bottom potential of the quantum well. I chose as initial state for the electron wave functions $\phi_a(x, t_0)$ and $\phi_b(x, t_0)$ a Gaussian function $\phi_i = [2/(\sigma^2\pi)]^{1/4} e^{ik_0(x-x_0)} e^{-(x-x_0)^2/\sigma^2}$, whose initial position is

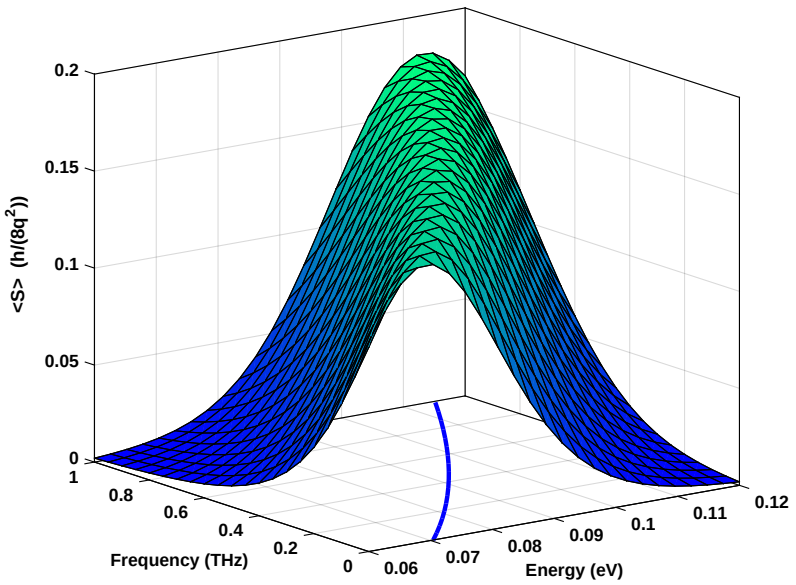

FIGURE 6.17: Noise is plotted as a function of the frequency of the oscillation well and also as a function of the central energy of the injected electrons. I appreciate how there is are a line where maximum values are achieved. In the blue solid line, I see the maximum values expected for the noise from Equation (6.56), the data fit accurately.

$x_0 = 175\,nm$ far from the center of the barrier, dispersion $\sigma = 50\,nm$ and initial central momentum is $k_0 = \sqrt{2m^*E}/\hbar$. The barrier is $0.4\,eV$ high, its thickness is $1.0\,nm$ and the quantum well length is $5.2\,nm$. I emphasize that any other localized wave function can be chosen without modifying qualitatively the results discussed here, as far as the transmission coefficient is not constant on the energy range of the wave packet $[E - \Delta E/2, E + \Delta E/2]$.

This result is seen in Figure 6.16 and Figure 6.17, where I plot the overlapping term $I^{r,t}_{a,b}$ and noise $\langle S \rangle$ respectively, as a function of the energy of the electrons and also of the oscillatory frequency of the well. The results corresponding to the static case (no oscillatory well) are seen at frequency equal to zero. In this static situation, the resonant energy is $E_r = 0.073\,eV$, and I appreciate in Figure 6.16 that at this energy value, the overlapping is minimum, and in Figure 6.17 that noise achieves its maximum value.

In Figure 6.16 (Figure 6.17), I observe that when I switch on the oscillation, the minimum (maximum in Figure 6.17) value for the overlapping $I^{r,t}_{a,b}$ (noise $\langle S \rangle$ in Figure 6.17) moves. Therefore, as I expected, resonant energies could be found for other energies even if in the static case they were not. Moreover, the position of the maximum values of $\langle S \rangle$ in Figure 6.17 for different frequencies and energies can be easily understood. In our scenario, the applied potential energy at the well is:

$$V_w(t) = \frac{V_b}{2} sin(\omega t) = \frac{V_b}{2} sin(\omega t_b + \omega(t - t_b)) \tag{6.52}$$

where I have defined t_b as the time that the electron takes to arrive at the double barrier. I consider that the electron transit time τ_t, i.e., the time spent by the electron in the double barrier, is much shorter than the inverse of the frequencies I are dealing with. Taking that $\omega(t - t_b) \ll 1$ for $t_b < t < t_b + \tau_t$ I can provide a Taylor approximation to expand Equation (6.52) as:

$$\begin{aligned} V_w(t) = \frac{V_b}{2}[sin(\omega t_b)cos(\omega(t - t_b)) + cos(\omega t_b)sin(\omega(t - t_b))] \approx \\ \frac{V_b}{2}\left[sin(\omega t_b)\left(1 - \frac{\omega^2(t - t_b)^2}{2}\right) + cos(\omega t_b)\omega(t - t_b)\right] \approx \frac{V_b}{2} sin(\omega t_b) \end{aligned} \tag{6.53}$$

Therefore, the electron perceives a "static" potential when it is inside the barrier and no harmonics should be taken into account [198]. Finally, a valid approximation to compute the resonant energy is:

$$E_r = E_{r0} + \frac{V_b}{2} sin(w t_b) \tag{6.54}$$

where E_{r0} is the resonant energy when there is no oscillation in the well and t_b the time that the electron takes to arrive to the barrier. This time t_b is the ratio between the distance (x_0) from the place where the injection takes place until the barrier, and the velocity of the electron (v_e):

$$t_b = \frac{x_0}{v_e} = \frac{x_0 m^*}{\sqrt{(2m^* E_r)}} \tag{6.55}$$

From Equation (6.54) and Equation (6.55) one realizes that the frequency for the maximum probabilities as a function of the resonant energy is:

$$w(E_r) = \frac{\sqrt{(2m^* E_r)}}{x_0 m^*} arcsin\left(\frac{2(E_r - E_{r0})}{V_b}\right) \tag{6.56}$$

which is in perfect agreement with the results observed in Figure 6.17. There, I see that the peak values for noise at each energy, move accordingly to Equation (6.56), which is plotted in the *frequency-energy* plane with a blue solid line.

Therefore, the simulations performed with sinusoidal potentials provide a clear behavior: when I move to higher frequencies, quantum noise will be increased as I move to higher energies and will achieve a maximum at the new resonant energy. The experiment can be modified and include other behaviors when changing the potential according to another expression. For instance, $V_w = -\frac{V_b}{2} sin(wt)$, in this case the resonant energy will decrease as frequency increases (mathematically, the negative sign in front of the sinusoidal signal can also be introduced as a negative frequency in Figure 6.17). Here, I propose that this very particular behavior of the maximum of the quantum noise $\langle S \rangle_{max}$ in the *frequency-energy* plane can be use as a test of our novel physical explanation of non-zero correlations in this type of HOM experiments with exchange and tunneling. The experimental confirmation of such predictions will, in fact, give support for the need of using time-dependent states when modeling quantum noise in such experiments even for static (DC) conditions.

6.4 Charge discreteness as ultimate limit for THz operation electronic devices

The main interests for decreasing electron devices towards nanoscale dimensions are providing large scale transistor integration, lower power dissipation and high speed commutation. The drawbacks and solutions of such scaling strategy for the usual GHz frequency performance of ultra-small devices are well established (high-K dielectrics avoid spurious gate tunneling, multi-gate structures avoid short-channel effects, etc.). Therefore, typical structures like Fin-FETs, Gate-All-Around FETs, Silicon nanowires or graphene (or other 2D materials) nanoribbons are the typical ultra-small devices expected to play an important role in next-future electronics. All previous structures have very small active regions. Not only channel lengths below 10 nm or lower are being considered for such state-of-the-art devices, but also lengths as small as 2 nm for the lateral dimensions. Such ultra-small devices are said to allow logic application working at THz frequencies.

In this section, I show that, due to the discrete nature of electrons, the noise in small electron devices at high frequencies make the fast logic operation unpractical. I anticipate that when the number of electrons in the active device region is very small, then,

the intrinsic uncertainties in the dynamics of electrons imply important variations in the number of electrons inside the active region and in its dynamical behavior. Such uncertainties are directly translated in the instantaneous current as fluctuations of THz noise over the mean value, understood as the signal. This high frequency noise disappears if the information about the current is obtained by averaging the instantaneous current over times much larger than the typical electron transit time (as the problem of discrete dopants would easily disappear if an ensemble over different devices were allowed). This fact also explains why the dramatic conclusions explained here are relevant at frequencies comparable to the inverse of the transit time. Therefore, there is an intrinsic limit in the nanoscale scaling of electron devices imposed by the discreteness of the charge and its noise.

As stated in Section 6.1.1, the study of high-frequency scenarios in the quantum domain is one field which needs to deal with multi-time measurements. In the same way, that there was a first simulation revolution when changing from semiclassical tools to quantum tools (and then mixing band structure and electron transport) when quantum effects could not be longer neglected in (small) electron devices, nowadays a second revolution from static quantum tools to dynamic quantum tools needs to be made in order to account properly for high frequency effects. In this second revolution, not only the quantum evolution (given by the many-body Schrödinger law) is needed, but also the non-unitary collapse law will be required. In that sense, the Bohmian theory provides a natural language and tools to lead this second revolution (for a longer discussion, see Section 6.1.1).

6.4.1 Current, noise and signal to noise ratio for different frequency operation regimes

Any electron device is expected to work at some clock frequency. I define the (clock) frequency of operation of the electron device as $1/T$, where T is the time interval (named as clock time) that correctly the device spends in connecting correctly the input and output signals. Therefore, I do not need to deal with the instantaneous current $I_j(t)$ defined in Equation (6.10), but I can assume a time-averaged value of the instantaneous current in the surface S_j (see Figure 6.1) during the time interval $[t-T, t]$, defined as:

$$I_{T,j} = \frac{\int_{t-T}^{t} I_j(t')dt'}{T} \tag{6.57}$$

The standard deviation $\sigma_{T,j}$ of the averaged current quantifies the noise of such a device, in Equation (6.20)[10],

$$\sigma_{T,j} = \sqrt{\triangle I^2} = var(I_{T,j}) \tag{6.58}$$

Let me notice that the noise is suppressed when $T \to \infty$ in Equation (6.57). Thus, Equation (6.57) can be considered as a low pass filter process. The signal to noise ratio is a very important parameter when characterizing a device, since it tell us how strong is the signal compared to the noise, and how much noise we can accept in our system. We can now write the signal-to-noise ratio, for each particular value of T, as:

$$SNR_{T,j} = \frac{\langle I_j^{DC} \rangle}{\sigma_{T,j}} \tag{6.59}$$

where $\langle I_j^{DC} \rangle$ is the DC value of the current (which is independent of T), i.e., $I_j^{DC} \equiv I_{T,j}$ when $T \to \infty$.

To study analytically how the discreteness of charge affects the noise in an electronic device, I will consider a two terminal device, with a volume $\Omega = L \cdot W \cdot H$, where $L >> W, H$. In that case (for a device having two metallic contacts of infinite lateral size separated by a distance L), the Ramo-Shockley-Pellegrini theorem provides and alternative expression for Equation (6.57) (see Section 6.1.2):

$$I_T(t) = \frac{\frac{q}{L} \sum_{k=1}^{N_e} \Delta x^k(t)}{T} \tag{6.60}$$

where $\Delta x^k(t)$ is the distance completed by the electron during the time interval $t - T \leq t' \leq t$ inside the spatial limits of the device $0 \leq r_k^x(t') \leq L$. We get $0 \leq \Delta x^k(t) \leq L$.

For simplicity I will consider a uniform velocity $v_k^x(t) \approx v_e$ (in fact, this approximation is obviously valid for linear bands structure materials such as graphene). Then, Equation (6.60) can be rewritten as:

$$I_T(t) = \frac{q}{TL} N_e \Delta x \tag{6.61}$$

[10] Remember the discussion in Section 6.1.3 about the experimental problems to measure infinite frequencies, i.e., $T \to 0$.

where N_e is the number of electrons inside the volume Ω. Two different frequency operations regimes can be distinguished here, when T is much shorter than the typical electron transit times (scenario "a") and when it is much larger (scenario "b").

6.4.2 The limit T much shorter than the transit time τ ($T << \tau$)

The first corresponds to the case where T is much shorter than the transit time τ of most of the electrons crossing the device, $T << \tau$. In that case, electrons are not able to cross the volume Ω during the time T. Since $\Delta x = v_e \cdot T$, Equation (6.61) can be rewritten as:

$$I_{T_a}(t) = \frac{q}{L} v_e N_{T_a}(t) \tag{6.62}$$

where $N_{T_a}(t)$ is the number of electrons inside the device during the time interval T. From Equation (6.58), the noise then is:

$$\sigma_{T_a}(t) = \frac{q v_e}{L} \sqrt{var(N_{T_a}(t))} \tag{6.63}$$

In order to understand better Equation (6.62) and Equation (6.63), let us take two different devices, the one we are interested in (with length L) and an arbitrary one (L_a). Since electrons have no time to cross the device, different length devices implies a difference in the number of particles inside the device. Because, under our ballistic assumption, there is no correlation between the electrons in the device, $var(N_{T_a}(t)) = \frac{L}{L_a} var(N_a(t))$. Then, the ratio between the noise of both devices is:

$$\frac{\sigma_{T_a}(t)}{\sigma_a(t)} = \frac{\frac{q v_e}{L}\sqrt{var(N_{T_a}(t))}}{\frac{q v_e}{L_a}\sqrt{var(N_a(t))}} = \sqrt{\frac{L_a}{L}} \tag{6.64}$$

From Equation (6.64) we can then obtain that the noise of our device is:

$$\sigma_{T_a}(t) = \sqrt{\frac{L_a}{L}}\sigma_a(t) = \frac{q v_e}{\sqrt{L_a}}\sqrt{var(N_a(t))}\frac{1}{L} = \frac{cte_a}{\sqrt{L}} \tag{6.65}$$

Equation (6.65) implies that when $T << \tau$, the noise is inversely proportional to the root square of the length in the transport direction. The device with smaller L provides more noise. The reason why an electron inside the active region (without reaching the contacts), still provides current and charge fluctuations on the contact is because the original Equation (6.61) includes the displacement current. Without the explicit

consideration of such displacement current, this limit cannot be established. We remind that the limit of noise at the transit time is also valid in classical or quantum regimes, without fixing any geometry factor of the device expect the length L.

6.4.3 The limit T much larger than the transit time τ ($T >> \tau$)

When the averaging time is much larger than the transit time, electrons completes the distance L during the time interval T, so $\Delta x = L$ in Equation (6.61) and then the current is:

$$I_{T_b}(t) = \frac{q}{T \cdot L} N_{T_b}(t) L = \frac{q}{T} N_{T_b}(t) \tag{6.66}$$

where now $N_{T_b}(t)$ is the number of electrons crossing the device during the time interval T. From Equation (6.66), the noise is:

$$\sigma_{T_b}(t) = \frac{q}{T} \sqrt{var(N_{T_b}(t))} \tag{6.67}$$

Now, we will do a similar procedure as in Section 6.4.2. But, let me remark that the situation now is different to the previous one. In this case, electrons cross the device during time T, and then the number of particles $N_{T_b}(t)$ is independent of the device length. So, let us take an arbitrary time T_0 . Then, we can establish that $var(N_{T_b}(t)) = \frac{T_b}{T_0} var(N_0(t))$. If we compute the ratio between the noise in this two different averaging times:

$$\frac{\sigma_{T_b}(t)}{\sigma_{T_0}(t)} = \frac{\frac{q}{T}\sqrt{var(N_{T_b}(t))}}{\frac{q}{T_0}\sqrt{var(N_{T_0}(t))}} = \sqrt{\frac{T_0}{T}} \tag{6.68}$$

And then, the noise of our device is:

$$\sigma_{T_b}(t) = \sqrt{\frac{T_0}{T}} \sigma_{T_0}(t) = \frac{q}{\sqrt{T_0}} \sqrt{var(N_{T_0}(t))} \frac{1}{T_a} = \frac{cte_b}{\sqrt{T}} \tag{6.69}$$

From Equation (6.69), we see that effectively, in this limit, noise is independent of the device length.

6.4.4 Numerical simulations

In this section I present different simulations, which certifies that, independently of the classical or quantum regime, the previous predictions presented in last section are completely valid.

6.4.4.1 Classical numerical simulations

Firstly, I present semiclassical Monte Carlo simulations. The mean velocity v_e inside the active region is defined through the Silicon band-dispersion. The variations in the number of particles come from the randomness of the injection of electrons into the active region (see Section 6.2 for more details): the thermal noise. In Figure 6.18, the value of σ_T computed from Monte Carlo simulations using Equation (6.58) are plotted. Numerical results were provided by Tomás González research group, from the University of Salamanca. Three different device lengths are studied. For simplicity, injection from one of the contacts is just considered without bias applied. The limits σ_{T_a} and σ_{T_b} are clearly reproduced in Figure 6.18. Notice the dependence on $1/\sqrt{T}$ for $T >> \tau$ and the dependence on $1/\sqrt{L}$ for $T << \tau$, as indicated in Equation (6.65) and Equation (6.69), respectively.

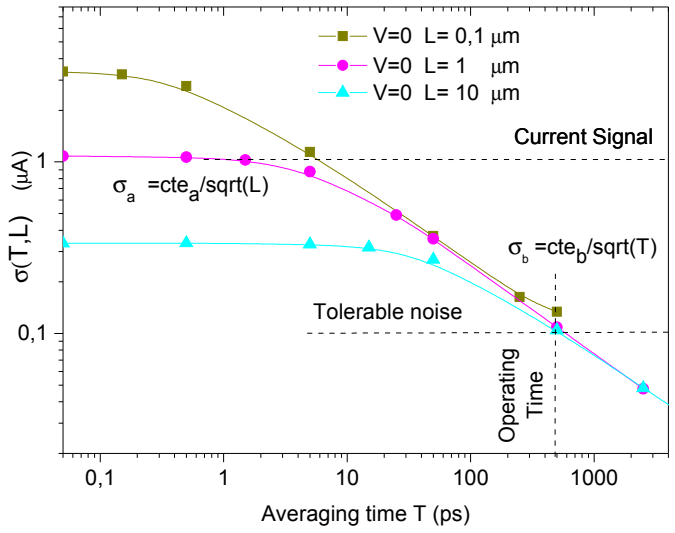

FIGURE 6.18: Noise as a function of the averaging time T for three different Silicon devices, when there is no bias applied. Simulation were performed with the semiclassical Monte Carlo approach. I accept as tolerable noise a signal to noise ratio equal to 11 [199].

Let me now imagine that I design a device with $L_x = 100$ nm for very high-frequency applications with an expected operating time of $T = \tau = 1$ ps (i.e., an operating

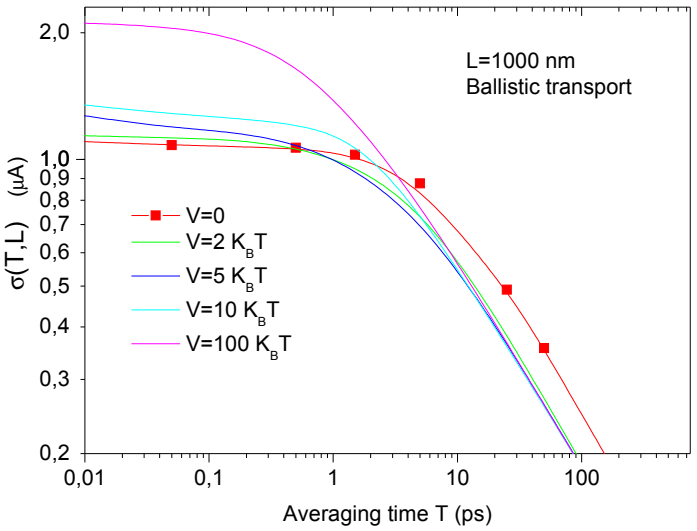

FIGURE 6.19: Noise as a function of the averaging time T for the same device as in Figure 6.18, when different bias are applied. Simulation were performed with the semiclassical Monte Carlo approach.

frequency of 1 THz). For example, the design has a signal current value of $\langle I \rangle_{DC} = 1$ μA (horizontal dashed line in Figure 6.18) and that our particular application requires a typical factor 10 for the signal-to-noise ratio (see tolerable noise in the horizontal dashed line in Figure 6.18). Thus, I conclude, that the expected length $L = 100$ nm and operating time $T = 1$ ps are incompatible with the required level of noise $\sigma_T = 0.1$ μA. Such noise level can only be obtained working at $T = 500$ ps (see vertical line in Figure 6.18) where the three different lengths provide the same noise level. In conclusion, at the end of the day, there is no reason to prefer the shorter device. The larger one is equally valid. Let me remind that increasing the value of the current signal is not a generally acceptable solution because low power consumption is also a mandatory requirement for ultra-small devices.

Equation (6.64) also give us the ratio between different noises when T is much shorter than the transit time, which can be compared with the numerical data presented in Figure 6.18. For instance, we see that according to Equation (6.64), the ratio between device with $L_1 = 0,1\ \mu m$ and $L_2 = 1\ \mu m$ should be $\sqrt{\frac{L_2}{L_1}} = 3.16$. According to the numerical results, the ratio is 3.05. Therefore, analytic and numerical results fit perfectly, showing the success of the results presented. The same calculus can be done with the other device ($L_3 = 10\ \mu m$), showing the same accuracy.

In Figure 6.19, I plot the same information as in Figure 6.18 for several applied bias. The consideration of far from equilibrium conditions does not change the previous overall

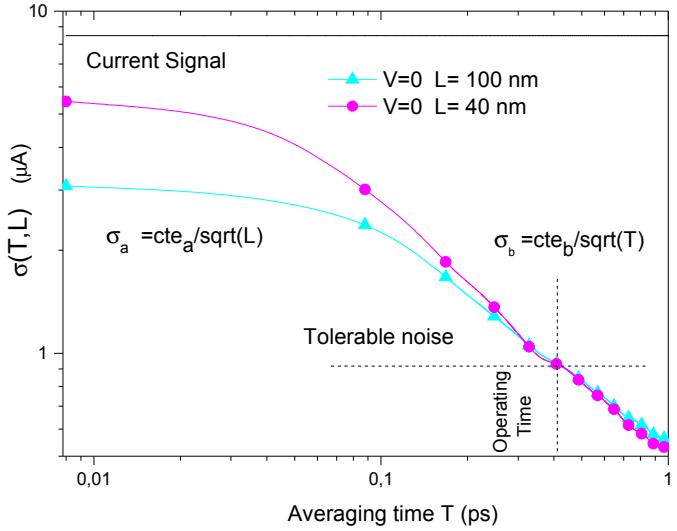

FIGURE 6.20: Noise as a function of the averaging time T for the same device, when different bias are applied. Simulations were performed with the fully quantum BITLLES simulator. I accept as tolerable noise a signal to noise ratio equal to 11 [199].

conclusion (the bias conditions only modifies the quantitative values). I notice in Figure 6.19 that, for small averaging times $T << \tau$, the value of σ_{T_a} grows when larger bias is considered because the (mean) velocity of electrons, v_e, present in Equation (6.65), increases with bias. For the same reason, for large averaging times $T >> \tau$, the value of σ_{T_b} decreases when large bias are considered because the faster electrons spent less time in the active region and $var(N_{T_b}(t))$ decreases, decreasing the its noise in Equation (6.69).

6.4.4.2 Quantum numerical simulations

Now, I will present similar numerical results as the ones showed previously, but using all the work performed during the thesis, i.e., I will simulate a graphene transistor (instead of a Silicon transistor) with the use of all the formalism developed in Chapter 4 and the model injection developed in Section 6.2. Thus, I will perform similar simulations as the ones presented in Figure 6.18 (injecting just from one side without applying any bias), but this time instead of using the semiclassical Monte Carlo approach, I will use the full quantum BITLLES simulator.

In Figure 6.20, differences appear regarding the values of the current and noise. This is because graphene is a linear band structure material, and therefore it has a constant velocity (independently of the electrons energy) whose value ($v_f = 10^6 m/s$) is high compared to the typical ones in Silicon. Since the particles velocity is proportional

to the current, as it can be seen from Equation (6.14), current values in graphene are higher than the usual ones in the typical semiconductor devices. In addition, we see that the averaging times T are much shorter, this fact occurs because the transit times τ are much shorter because the devices are smaller and the carriers velocity is higher. This fact makes that the operating time for these graphene transistors is much smaller, $T \approx 0.5$ ps, with a clock frequencies around $f \approx 2$ THz.

Apart from this difference, the shape of Figure 6.18 and Figure 6.20 are very similar. We see that in both of them, for averaging times smaller than the transit time, noise scales as $\sigma_{T_a} = \frac{cte_a}{\sqrt{L}}$. Whereas for averaging times larger than the transit time, $\sigma_{T_b} = \frac{cte_b}{\sqrt{T}}$. Therefore, even when accounting for quantum effects, it can be seen that Equation (6.65) and Equation (6.69) are completely valid. In addition, if we compute the ratio between the noise for different device lengths, when the T is much shorter than the transit time, we can see again the success of our predictions. According to Equation (6.64), the ratio of the noise of the devices is $\sqrt{\frac{L_2}{L_1}} = \sqrt{\frac{100}{40}} = 1.58$ and regarding the simulations, this ratio is 1.74, showing again an very good accuracy.

6.4.5 On/Off switching time

In this section, I went one step further and I focused on observing how the previous discussion affects the On/Off switching times in a graphene double gate transistor (source, drain, bottom and top gates), as the one depicted in Figure 6.3. I remark that this scenario is a realistic device simulation (injection is performed from both sides and there are two gates) and it goes beyond the analytic description of Section 6.4.2 and Section 6.4.3, but the physics does not change, and then I expect the same qualitative results.

For that purpose, I will analyze a transient, i.e., I will establish a constant bias between the drain and source and I will change the gate voltage bias. Then I will obtain the switching time by time averaging the instantaneous total (particle plus displacement) current (obtained with the most general expression of the Ramo-Shockley-Pellegrini theorem explained in Section 6.1.2) through Equation (6.57).

In order to establish the best value of the drain-source bias (V_{ds}) and the top and bottom gate values ($V_t = V_b \equiv V_g$) to perform the transient, I made different current-voltage characteristic curves for different gate values and I will look for the values that maximizes the differences between the current that I will consider as the ON state and the one that I consider the OFF state. According to Figure 6.3, the transistor volume Ω is $\Omega = 20 \times (5+1+5) \times 250\ nm^3$ and the total device length $L = L'_x + L_x + L'_x = 40$ nm.

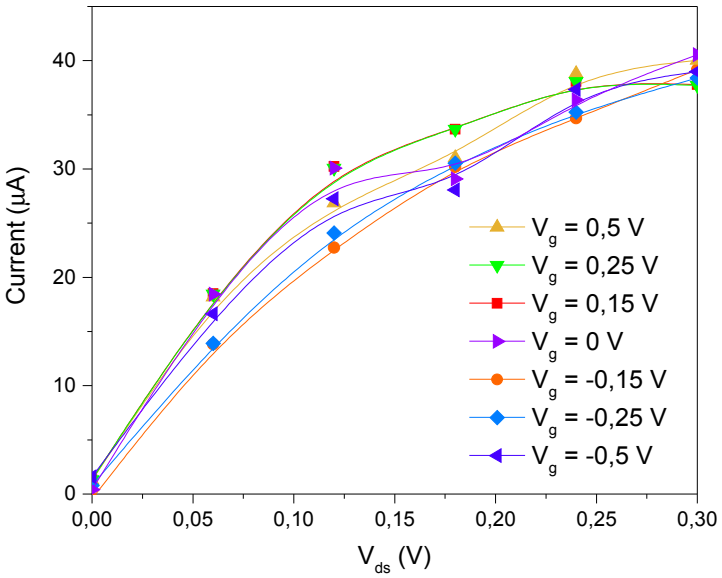

FIGURE 6.21: Current-voltage characteristics for the four terminal transistor whose active region volume is $Omega = 20 \times (5+1+5) \times 250\ nm^3$. The optimum values for maximizing the ON and OFF currents are $V_{DS} = 0.12$ and $V_g = \pm 0.15$.

Results are plotted in Figure 6.21[11]. There we see that the maximum difference between current is achieved for a value of $V_{DS} = 0.12$ V and $V_g = \pm 0.15$ V. Therefore, the ON state corresponds to $V_g = 0.15$ V, while the OFF state corresponds to $V_g = -0.15$ V.

Next, I will make a simulation where a transient is performed and I will analyze the switching times obtained. Initially, the gates value is $V_g = -0.15$ V. After four ps, the gate value is changed to $V_g = -0.15$, as shown in Figure 6.22. The main value of the current during both interval times is $\langle I_1^{DC} \rangle$ and $\langle I_2^{DC} \rangle$ respectively.

Here, numerical results for two different devices (labeled by A and B) are presented. The Ω volume of device A is $\Omega_A = 20 \times (5+1+5) \times 250\ nm^3$, its total channel length is $L_A = 40$ nm and its transit time is $\tau_A = \frac{L_A}{v_f} = 0.04$ ps. On the other hand, $\Omega_B = 50 \times (5+1+5) \times 250\ nm^3$, its total channel length is $L_B = 100$ nm and the transit time is $\tau_B = 0.1$ ps.

The instantaneous current for the two different devices is plotted in Figure 6.22. We can see there the instantaneous current as a function of time, as well as the gate voltage as a function of time. Current increases when switching the gate voltage. Clearly, without time averaging the current (with the use of Equation (6.57)), noise does not allow us to

[11] The Fermi energy is $E_f = 0.15$ eV. The shape of these curve characteristics was explained in Section 5.3.3.3.

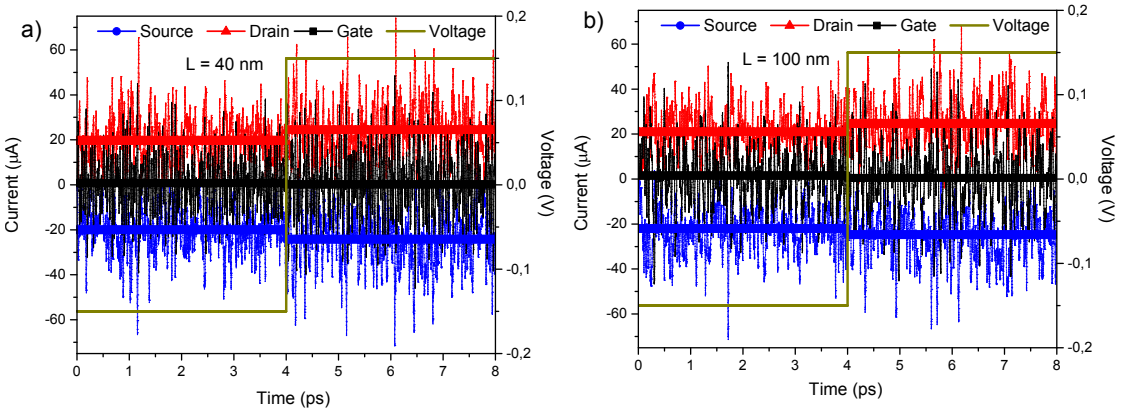

FIGURE 6.22: a) Instantaneous current and its mean value as a function of time for device A. b) Same information as in a), but for device B.

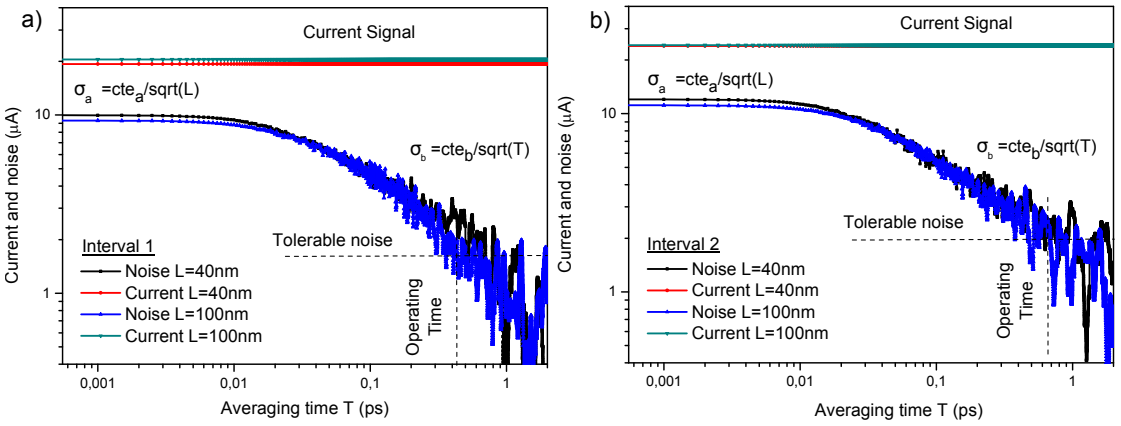

FIGURE 6.23: a) Current and noise as a function of the averaging time T for the first time interval for device A and device B. I accept as tolerable noise a signal to noise ratio equal to 11 [199]. b) Same information as in a), but for the time interval 2.

differentiate the ON and OFF states. The question now is from which T, we can affirm that we are able to distinguish both states.

I remark that the results presented will not be obtained from an average of different experiments, since when a device is working, there is no interest in mean values of different experiments, we are just interested on the time where the device "decides" that it is on the ON state and when it is in the OFF state.

With this information, we can obtain the time averaged current and its associated noise (in the same way as it was done in Section 6.4.4) for both time intervals (before and after switching the gate voltage). Results are plotted in Figure 6.23[12].

[12]Differently from Figure 6.20, results are noisier for large averaging times. This is because in Figure 6.20 I averaged the results through different simulations in order to see very clearly the noise values. In this case, since I am interested just in what occurs in one experiment, I did not make the averaging between different simulations and results are noisier.

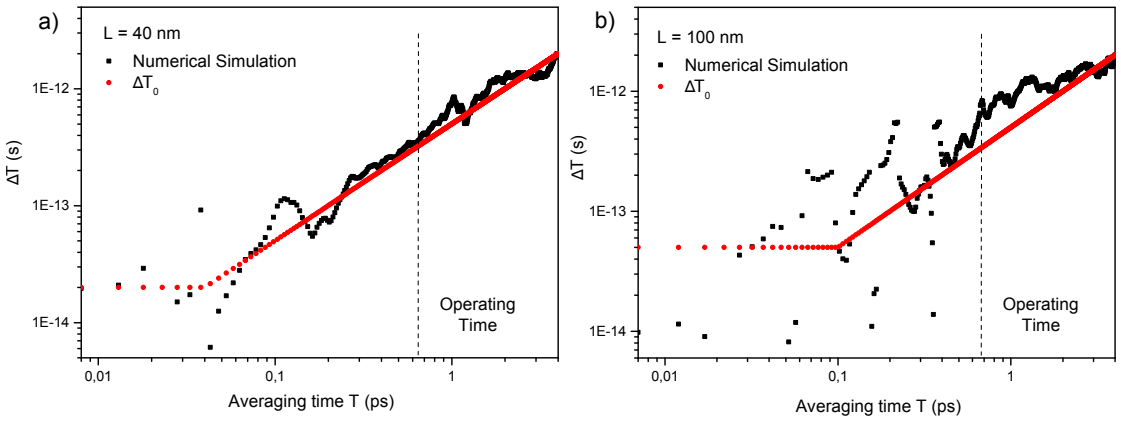

FIGURE 6.24: a) Δ_T as a function of the averaging time T for device A. In red circles, the case when the discrete nature of charge is not taken into account is plotted. In dark squares, it is plotted the data obtained from simulations. The operation time are the ones seen in Figure 6.23. b) Same information of a), but for the device B.

Regarding Figure 6.23, even if this scenario is very different from the one studied in Section 6.4.4 (there was no applied bias and there were no gates), we can still recognize the two different limits, when $T << \tau$ (see that in both intervals, noise due to device A is greater that the one of device B) and when $T >> \tau$ (noise becomes independent of device channel length). Therefore, as expected, all our predictions are still present in the system. This fact will make that incorrect switching times will be obtained for small averaging times. This is is seen in Figure 6.24. There, it can be clearly seen that just for large averaging times T, the numerical results approach to the case when the discrete nature of charge is not taken into account. So the one determining the frequency at which a device can work is not the transit time τ, but T.

The switching time from numerical results (circle red points in Figure 6.24) ΔT is defined as the time needed after applying the switch for going from the current value $\langle I_1^{DC} \rangle$ until $\langle I_1^{DC} \rangle + \frac{\langle I_2^{DC} \rangle}{2}$, i.e., to increase the current a quantity equal to $\frac{\langle I_2^{DC} \rangle - \langle I_1^{DC} \rangle}{2}$. On the other hand, without taking into account the noise induced by the discrete nature of charge (square black points in Figure 6.24), the switching time is either $\Delta T_0 = \frac{\tau}{2}$ when $T < \tau$ or $\Delta T_0 = \frac{T}{2}$ when $T > \tau$.

6.4.6 Intrinsic noise limit in the nanoscaling of electron devices

During decades, the relation between the clock frequency f and the channel length L has been determined by the transit time limit [200]. The clock frequency of a CPU is usually 1/3 of the cut-off frequency. Thus, neglecting parasitic effects, f is inversely proportional to the electron transit time τ:

$$f \leq \frac{1}{3\tau} = \frac{v}{3L} \tag{6.70}$$

Since 2005, as seen in Table 6.26, the clock frequency has stagnated around f=5 GHz independently of the channel length to keep acceptable values of the heat dissipated by the $10^9 - 10^{10}$ transistors present in a CPU (see orange line in Figure 6.25). This heat is a global CPU limit, not a limit on each individual transistor as in Equation (6.70).

Here, I discuss that apart from this transit time limit, there is another intrinsic limit for the clock frequency of transistors because of the discrete nature of electrons. It is clear that, from Equation (6.70), one can never work at higher frequencies than the one given by the inverse of the transit time. But let me analyze analytically what is the noise limit imposed by Equation (6.67).

I assume a binomial probability distribution injection, being p the probability of success. I consider N_τ electron that attempt to be injected during the time τ, then $\langle N_\tau \rangle = pN_\tau$ and $var(N_\tau) = \langle N_\tau \rangle (1-p)$. If I compute the number of electrons inside a 3D active region from the phase-space density, $N_\tau = gLL_yL_zk_f^3/\pi^3$, I get from Equation (6.67):

$$f \leq \frac{gLWHk_f^3}{\pi^3 SNR^2} \frac{p}{(1-p)} \tag{6.71}$$

where g is the (spin or valley) degeneracy [13].

In Figure 6.25, I plot the clock frequency f as a function of the typical size of the Si MOSFETs obtained from the data of CPUs in Table 6.26. The clock frequencies of all transistors follow the trend associated with the transit time limit, plotted with a solid blue curve from Equation (6.70) (with v obtained from [201]). On the other hand, the red dashed line corresponds to the noise limit given by Equation (6.71) and obtained with $E_f = 0.026$ eV, $p = 0.5$, $g = 2$, $W = H$ given by the feature size from Table 6.26 and $SNR \approx 11$ [199]. Additionally, nowadays there is also a limit concerned to power dissipation. One of the great advantages of CMOS technology is that it lacks of dissipation, except when it switches among the ON and OFF state. The dissipation is proportional to the number of switches, i.e., the higher frequency we want to work, the more dissipation will occur. For that reason, I also plotted with a orange horizontal

[13] For 2D material devices, a similar expression can be found, but introducing the phase-space density for a two dimensional material.

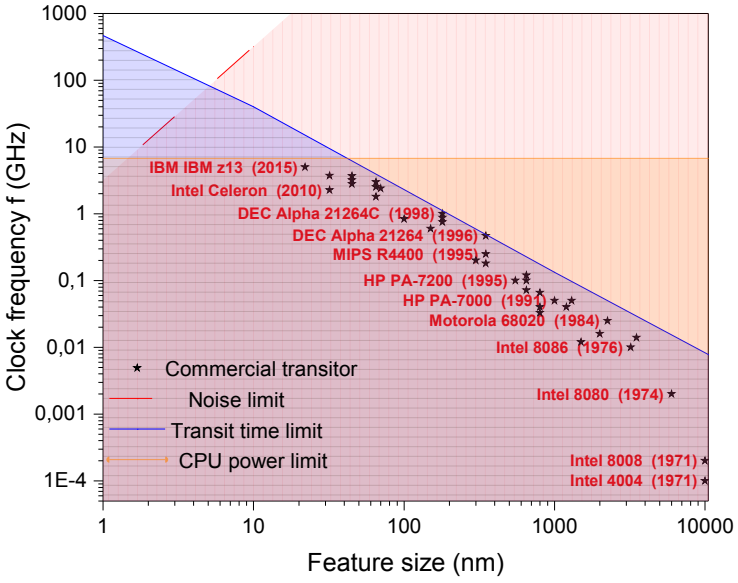

FIGURE 6.25: Clock frequency f from a set of commercial transistors available in last decades as a function of the typical size. Future nanoscale transistors have to work in the triangle given by the transit time (solid blue line) and the noise (dashed red line) limits, above the power (orange line) limit for improved cooling strategies.

solid line the actual power limit. I want to emphasize that this limit is not an intrinsic limit, and it may be overcome with new strategies and improvements.

Regarding Figure 6.25, the conclusion is that there are two intrinsic and different limits for the clock frequency at which a device can work. On the one hand, for low frequencies, the transit time limit (solid blue line) is the one that limits the clock frequency. At higher frequencies, due to the device miniaturization and because of the discreteness of the few electrons of the system, the noise limit (red dashed line) cannot longer be neglected and it competes with the transit time. At enough high frequencies it can even overcome the transit time limit, and then it will represent the true and unavoidable fundamental limitation to reach THz transistors.

Let me notice that typical quantum devices simulators are unable to capture the discussions done here. They work with the time-independent models that finally try to solve the many-body time dependent Schrödinger equation. However, the Schrödinger equation is just a valid law for part of the quantum systems, this which are not measured. For high frequency electronics (and not just static scenarios where the DC information is enough), the valid way to analyze quantum systems is to collapse it. It is in this sense

Year	Designer	Model	f (MHz)	L (nm)	F. size (nm)
1971	Intel	4004	0,1	10000	10000
1971	Intel	8008	0,2	10000	10000
1974	Intel	8080	2	6000	6000
1976	Intel	8086	10	3200	3200
1979	Motorola	68010	14	3500	3500
1982	Intel	80286	12	1500	1500
1984	Motorola	68020	25	2250	2250
1986	MIPS	R2000	16	2000	2000
1987	Motorla	68030	50	1300	1300
1988	MIPS	R3000	40	1200	1200
1991	AMD	80386	40	800	800
1991	Motorola	68040	33	800	800
1991	HP	PA-7000	50	1000	1000
1992	Intel	80486	66	800	800
1992	Intel	Pentium	66	800	800
1992	Ross	hyperSPARC	72	650	650
1993	Cyrix	486DX	100	650	650
1993	Cyrix	5x86	120	650	650
1994	MIPS	R4400	200	300	300
1995	MIPS	R10000	180	350	350
1995	MIPS	R4400	250	350	350
1995	HP	PA-7200	100	550	550
1996	DEC	Alpha 21264	466	350	350
1998	IBM	RS64 IV	750	100	180
1998	HP	PA-8700+	875	100	180
1998	DEC	Alpha 21264C	1000	100	180
2002	Fujitsu	SPARC64 GP	600	150	150
2005	Intel	Core 2 Duo	1800	35	65
2005	Intel	Core 2 Quad Extreme	3000	35	65
2007	AMD	Phenom II	3200	25	45
2007	AMD	Opteron	2800	25	45
2008	Fujitsu	SPARC64 VII	2520	30	65
2010	IBM	Power7	3700	25	45
2010	Intel	Celeron	2267	18	32
2010	Intel	Core i5	3730	18	32
2015	IBM	IBM z13	5000	25	22

FIGURE 6.26: Characteristics of some commercial transistors in last four decades. Data obtained from http://cpudb.stanford.edu

that we talk about a second revolution for the electronic simulations, and in this framework the BITLLES simulator is an excellent simulator to study such high-frequency scenarios.

Part III

PART THREE: CONCLUSIONS

o

Chapter 7

Conclusions

In this thesis, an improvement of the electron BITLLES simulator was performed and used to obtain quantum transport properties in different scenarios. This simulator models electron nanodevices with the use of Bohmian mechanics, a quantum theory which in its ontology -apart from the wave function- particles have always definite positions and describe trajectories.

In **Chapter 1** I introduced the electron device simulators state-of-the-art. Because of "Moore's law", electron devices have reached the nanoscale regime. Quantum effects appear and then, classical simulators are unable to reproduce these effects. For that reason, new full quantum simulators are needed. I presented the most popular and used ones.

In **Chapter 2** I explained which are the different quantum theories that tries to explain and construct a reality for all the quantum effects observed in experiments. Apart from the well known Copenhagen theory, the GRW theory, the many-worlds theory and the Bohmian theory are explained.

In **Chapter 3** Bohmian mechanics is deeply discussed. It is shown how it faces the measurement problem in a very elegant way, without the need of collapse. In addition, the conditional wave function (a unique tool of Bohmian mechanics which corresponds to the wave function of a subsystem) is explained. I also presented the BITLLES simulator and how it works.

In **Chapter 4** I introduced the importance of graphene (which has a linear band structure) in nowadays electron devices, making its inclusion in current electron device simulators mandatory. In this Chapter I showed how linear band structures can be modeled by the the bispinor Dirac equation, and I showed how implemented it in the BITLLES simulator, with its associated Bohmian trajectories. I also presented an analytic evolution of a bispinor Gaussian wave packet in graphene.

In **Chapter 5** I presented what are the problems of phase spaces in quantum theories where one cannot define simultaneously positions and momenta when including scattering. I made emphasis in the well known Boltzmann Collision operator and showed why it is not a completely positive method. In this Chapter, I showed a new completely positive method for Markovian and non-Markovian systems based on the Bohmian theory.

In **Chapter 6** I explained why the BITLLES simulator is so suitable for computing AC currents, transients and high-frequency scenarios. I presented the time dependent model injection, as well as a source noise which cannot be captured by time independent models. In addition, I showed a limitation for the miniaturization of electron devices due to the discrete nature of electrons.

Certainly, this thesis is unusual in the sense that it merges concepts belonging to foundations of quantum mechanics and practical issues about state-of-the-art nanoelectronic devices. The reader can wounder why such mixing of concepts. However, as showed during the thesis, Bohmian mechanics provides excellent tools to model high frequency electron nanodevices and its fluctuations, because in its ontology, apart from the wave function, particles have definite positions. Therefore, this theory deserves to be explored and exploited. The fact that Bohmian mechanics is not a well established theory as the orthodox one is not a scientific reason to reject it and not to use it in the electron device simulator framework, specially when it offers so many advantages.

One of the typical criticisms done to the Bohmian theory is that it is not useful for computations and then, it is worst than the orthodox one. In this thesis, I developed several computations where I showed that this is not true. At a minimum it can provide different approaches with different approximations. Even more,it can provide advantages over the orthodox one. Specifically, the (bohmian) BITLLES simulator was adapted to the necessities for modeling nowadays electron nanodevices, i.e., dissipation was included (through a new Bohmian scattering approach) as well as the possibility of modeling materials with linear band structures, such as graphene (by solving the time-dependent

bispinor Dirac equation). With these new two ingredients, the simulator becomes an excellent candidate to extend the successful (semiclassical) Monte Carlo approach into the quantum regime. Some examples that reflect the versatility of the simulator can be found in Chapter 5 and Chapter 6, but many other time dependent scenarios can be envisioned and will be performed in the near future.

I hope that this thesis can contribute to the quantum community to better appreciate the capabilities and opportunities that the Bohmian theory offers, and somehow, also to help the Bohmian theory to occupy the rightful position that it deserves.

Journal Publications Related to This Thesis

- D. Marian, E. Colomés, Z. Zhan and X. Oriols, *Quantum Noise from a Bohmian perspective: fundamental understanding and practical computation in electron devices*, Journal of Computational Electronics, **14**, 114 (2015).
- D. Marian, E. Colomés and X. Oriols, *Time-dependent exchange and tunneling: detection at the same place of two electrons emitted simultaneously from different sources*, Journal of Physics: Condensed Matter, **27**, 245302 (2015).
- E. Colomés, Z. Zhan and X. Oriols, *Comparing Wigner, Husimi and Bohmian distributions: Which one is a true probability distribution in phase space?*, Journal of Computational Electronics **14**, 894 (2015).
- E. Colomés, D. Marian and X. Oriols *Quantum noise with exchange and tunneling: Predictions for a two-particle scattering experiment with time-dependent oscillatory potentials*, Journal of Statistical Mechanics: Theory and experiment **2016** (5), 054009 (2016).
- Z. Zhan, E. Colomés, A. Benali, D. Marian and X. Oriols, *Time-dependent simulation of particle and displacement currents in THz graphene transistors*, Journal of Statistical Mechanics: Theory and experiment, **2016** (5), 054019 (2015).
- Z. Zhan, E. Colomés and X. Oriols, *Unphysical features in the application of the Boltzmann collision operator in quantum transport*, Journal of Computational Electronics **15** (4), 1206 (2016).
- D. Marian and E. Colomés, *Noise in Quantum Devices: A Unified Computational Approach for Different Scattering Mechanisms*, Fluctuation and Noise Letters **15**, 1640008 (2016).

- Z. Zhan, E. Colomés and X. Oriols, *Limitations of the Intrinsic Cutoff Frequency to Correctly Quantify the Speed of Nanoscale Transistors* IEEE Transactions on Electron Devices, **64** (6) 2617 (2017).

- E. Colomés, Z. Zhan, D. Marian and X. Oriols, *Quantum dissipation with conditional wave functions: Application to the realistic simulation of nanoscale electron devices*, Phys. Rev. B **96**, 075135 (2017).

- E. Colomés, G. Albareda, Z. Zhan, A. Alarcón, D. Pandey, F. Traversa and X. Oriols, Chapter 6 in *Applied Bohmian Mechanics from Nanoscale Systems to Cosmology*, Pan Stanford Publishing, Singapore, 2nd version (2018).

- Z. Zhan, E. Colomés, D. Pandey, S. Yuan and X. Oriols, *Electron injection model for linear and parabolic 2D materials: Full quantum time-dependent simulation of graphene devices*, submitted.

- E. Colomés, J. Mateos, T. González and X. Oriols, *Noise and charge discreteness as ultimate limit for the THz operation of ultra-small electronic devices*, in preparation.

Appendix A

Calculus for obtaining the Dirac equation

A.1 Taylor approximations for computing $f(\vec{K}^{(\prime)} + \vec{q})$

The aim is this section is to obtain the following equations (Equation (A.2)):

$$\begin{aligned} f(\vec{K}^{(\prime)} + \vec{q}) &= -\frac{3a}{2}(\alpha q_x + i q_z) \\ f^*(\vec{K}^{(\prime)} + \vec{q}) &= -\frac{3a}{2}(\alpha q_x - i q_z) \end{aligned} \tag{A.1}$$

We start from:

$$\begin{aligned} f(\vec{k}) = \left(1 + e^{-i\vec{k}\vec{a}_1} + e^{-i\vec{k}\vec{a}_2}\right) &= \left(1 + e^{-i(\vec{K}^{(\prime)} + \vec{q})\vec{a}_1} + e^{-i(\vec{K}^{(\prime)} + \vec{q})\vec{a}_2}\right) \\ f^*(\vec{k}) = \left(1 + e^{i\vec{k}\vec{a}_1} + e^{i\vec{k}\vec{a}_2}\right) &= \left(1 + e^{i(\vec{K}^{(\prime)} + \vec{q})\vec{a}_1} + e^{i(\vec{K}^{(\prime)} + \vec{q})\vec{a}_2}\right) \end{aligned} \tag{A.2}$$

Next, we consider the following relations according to Equation (4.1) and Equation (4.3):

$$\begin{aligned}
\vec{q}\vec{a}_1 &= -\frac{\sqrt{3}aq_x}{2} + \frac{3q_z a}{2} \\
\vec{q}\vec{a}_2 &= \frac{\sqrt{3}aq_x}{2} + \frac{3q_z a}{2} \\
\vec{K}\vec{a}_1 &= -\frac{2\pi}{3} \quad \vec{K}'\vec{a}_1 = \frac{2\pi}{3} \\
\vec{K}\vec{a}_2 &= \frac{2\pi}{3} \quad \vec{K}'\vec{a}_2 = -\frac{2\pi}{3}
\end{aligned} \tag{A.3}$$

Then, the exponential terms appearing in Equation (A.3) are (doing a Taylor expansion where $e^x \approx 1 + x$):

$$\begin{aligned}
e^{i\vec{q}\vec{a}_1} &\approx 1 - i\frac{\sqrt{3}aq_x}{2} + i\frac{3q_z a}{2} \\
e^{\vec{q}\vec{a}_2} &\approx 1 + i\frac{\sqrt{3}aq_x}{2} + i\frac{3q_z a}{2} \\
e^{\vec{K}^{(\prime)}\vec{a}_1} &= -\frac{1}{2} + i\alpha\frac{\sqrt{3}}{2} \\
e^{\vec{K}^{(\prime)}\vec{a}_2} &= -\frac{1}{2} - i\alpha\frac{\sqrt{3}}{2}
\end{aligned} \tag{A.4}$$

where $\alpha = 1$ close to the K point and $\alpha = -1$ close to the K' point. By introducing Equation (A.5) in Equation (A.3), it is directly obtained:

$$\begin{aligned}
f(\vec{K}^{(\prime)} + \vec{q}) &= -\frac{3a}{2}(\alpha q_x - iq_z) \\
f^*(\vec{K}^{(\prime)} + \vec{q}) &= -\frac{3a}{2}(\alpha q_x + iq_z)
\end{aligned} \tag{A.5}$$

A.2 Spatial Derivatives in Equation (4.37)

The aim of this sections is to achieve the results seen in Equation (4.37):

$$\begin{aligned}
\frac{\partial w(\vec{R}_j, t)}{\partial x} &= \delta_x w(\vec{R}_j, t) = i\sum_{\vec{q}} q_x e^{i\vec{q}\vec{R}_j} a_w(\vec{q}, t) \\
\frac{\partial w(\vec{R}_j, t)}{\partial z} &= \delta_z w(\vec{R}_j, t) = i\sum_{\vec{q}} q_z e^{i\vec{q}\vec{R}_j} a_w(\vec{q}, t)
\end{aligned} \tag{A.6}$$

where $(w,j)=(u',A)$ or $(w,j)=(v',B)$. In order to simplify the notation I will consider $w(\vec{R}_j,t)\equiv w$ and $\vec{R}_j\equiv\vec{R}$ and $m=x,z$. Then, Equation (A.7) can be rewritten as:

$$\delta_m w\equiv\frac{w(\vec{R}+\Delta m)-w(\vec{R})}{\Delta m}=i\sum_{\vec{q}}q_m e^{i\vec{q}\vec{R}}a_w(\vec{q},t) \tag{A.7}$$

I begin by introducing the Fourier series $w=\sum_{\vec{q}}e^{i\vec{q}\vec{R}}a_w(\vec{q},t)$ (same as in Equation (4.32) and Equation (4.33)) in Equation (A.7):

$$\delta_m w=\frac{\sum_{\vec{q}}e^{i\vec{q}(\vec{R}+\Delta m)}a_w(\vec{q},t)-\sum_{\vec{q}}e^{i\vec{q}\vec{R}}a_w(\vec{q},t)}{\Delta m}=\frac{\sum_{\vec{q}}(e^{iq_m\Delta m}-1)e^{i\vec{q}\vec{R}}a_w(\vec{q},t)}{\Delta m} \tag{A.8}$$

which, if I consider small values of q_m (something which is totally valid, since $\vec{q}$ are small values close to $\vec{K}^{(\prime)}$) becomes doing a Taylor expansion:

$$\delta_m w\approx\frac{\sum_{\vec{q}}(1+iq_m\Delta m-1)e^{i\vec{q}\vec{R}}a_w(\vec{q},t)}{\Delta m}=i\sum_{\vec{q}}q_m e^{i\vec{q}\vec{R}}a_w(\vec{q},t) \tag{A.9}$$

which is Equation (A.7).

Appendix B

Analytical evolution of a Gaussian wave packet

B.1 Initial bispinor Gaussian wave packet

The initial bispinor Gaussian wave packet that I consider is the following one:

$$\Psi_G(x,z,0) = \begin{pmatrix}\Psi_1\\ \Psi_2\end{pmatrix} = \begin{pmatrix}s_1\\ s_2\end{pmatrix} \frac{1}{\sqrt{\sigma_x\sigma_z\pi}} e^{-\frac{(x-x_0)^2}{2\sigma_x^2}} e^{-\frac{(z-z_0)^2}{2\sigma_z^2}} e^{ik_{0x}} e^{i\bar{k}_0 z} \tag{B.1}$$

where the central position of the wave packet is (x_0, z_0) and its initial momentum is $\bar{k}_0 = (k_{0x}, k_{0z})$. Hereafter, I will assume the same initial dispersions for the x and z directions, i.e. $\sigma_x = \sigma_z = a$ and $\begin{pmatrix}s_1\\ s_2\end{pmatrix} = \begin{pmatrix}1\\ se^{i\theta_{\bar{k}_0}}\end{pmatrix}$ where $\theta_{\bar{k}_0} = arctg(k_{z_0}/k_{x_0})$. This last assumption is to guaranteed that most of the eigenstates composing the Gaussian wave packet belongs to the same band ($s = 1$ for the positive one and $s = -1$ to the negative one. To simplify the notation I will choose an initial positive energy, i.e. $s = 1$. Then, the Equation (B.1) can be rewritten as:

$$\Psi_G(x,z,0) = \begin{pmatrix}\Psi_1\\ \Psi_2\end{pmatrix} = \begin{pmatrix}1\\ e^{i\theta_{\bar{k}_0}}\end{pmatrix} \frac{1}{\sqrt{a^2\pi}} e^{-\frac{(x-x_0)^2}{2a^2}} e^{-\frac{(z-z_0)^2}{2a^2}} e^{ik_{0x}} e^{ik_{0z}} \tag{B.2}$$

In order to obtain the evolution of the wave packet, I will project the initial Gaussian wave packet $\Psi_G(x,z,0)$ in the graphene eigenfunctions $\phi_k(x,z,t)$:

$$\begin{aligned}\Psi_G(x,z,t) &= \int_{-\infty}^{\infty}\left(\int_{-\infty}^{\infty}\phi_k^*(x,z,0)\Psi_G(x,z,0)dxdz\right)\phi_k(x,z,t)d\bar{k} \\ &= \int_{-\infty}^{\infty} g_{graph}(\bar{k})\phi_k(x,z,t)d\bar{k}\end{aligned} \tag{B.3}$$

The mentioned set of eigenfunctions $\phi_k(x,z,t)$ are:

$$\phi_k(x,z,t) = \frac{1}{\sqrt{2}}\begin{pmatrix}1\\ e^{i\theta_k}\end{pmatrix}e^{i\bar{k}\bar{r}}e^{-iE_kt/\hbar} \tag{B.4}$$

where $\theta_k = arctg(k_z/k_x)$. The main complication appears here, the linear energy dispersion E_k is no longer separable $\frac{E_k}{\hbar} = v_f\sqrt{k_x^2+k_z^2} = v_f|\bar{k}|$, as it occurs in the case of the parabolic energy dispersion. Then, the integral in Equation (B.4) is not analytical. For that reason, I will expand E_k with a second order Taylor expansion around the initial momentum $\bar{k}_0 = (k_{0x}, k_{0z})$.

B.2 Taylor approximation around $\bar{k}_0$

Hereafter, I write the terms need to make the Taylor expansion around $\bar{k}_0 = (k_{x_0}, k_{z_0})$ in $\frac{E_k}{\hbar} = v_f\sqrt{k_x^2+k_z^2} = v_f|k|$.

$$\frac{\partial E_k}{\hbar\partial k_x} = v_f\frac{k_x}{\sqrt{k_x^2+k_z^2}} \tag{B.5}$$

$$\frac{\partial^2 E_k}{\hbar\partial k_x^2} = v_f\frac{k_z^2}{\sqrt{k_x^2+k_z^2}^3} \tag{B.6}$$

$$\frac{\partial E_k}{\hbar\partial k_z} = v_f\frac{k_z}{\sqrt{k_x^2+k_z^2}} \tag{B.7}$$

$$\frac{\partial^2 E_k}{\hbar\partial k_z^2} = v_f\frac{k_x^2}{\sqrt{k_x^2+k_z^2}^3} \tag{B.8}$$

$$\frac{\partial^2 E_k}{\hbar\partial k_z\partial k_x} = -v_f\frac{k_xk_z}{\sqrt{k_x^2+k_z^2}^3} \tag{B.9}$$

Then, finally, the Taylor expansion of the energy dispersion around $\bar{k}_0$ is:

$$\begin{aligned}\frac{E_k}{\hbar} &= v_f\sqrt{k_x^2+k_z^2} \approx v_f\sqrt{k_{x_0}^2+k_{z_0}^2} + v_f\frac{k_{x_0}}{|\bar{k}_0|}(k_x-k_{x_0}) + v_f\frac{k_{z_0}}{|\bar{k}_0|}(k_z-k_{z_0}) \quad \text{(B.10)}\\ &+ v_f\frac{k_{z_0}^2}{2|\bar{k}_0|^3}(k_x-k_{x_0})^2 + v_f\frac{k_{x_0}^2}{2|\bar{k}_0|^3}(k_z-k_{z_0})^2 - v_f\frac{k_{x_0}k_{z_0}}{2|\bar{k}_0|^3}(k_x-k_{x_0})(k_z-k_{z_0})\end{aligned}$$

B.3 Time evolution

I begin by analysing the function a_{graph} in Equation (B.4)[1]:

$$\begin{aligned}g_{graph}(\bar{k}) &= \int_{-\infty}^{\infty}\phi_k^*(x,z,0)\Psi_G(x,z,0)dxdz \quad \text{(B.11)}\\ &= \int_{-\infty}^{\infty}\frac{1}{2}\begin{pmatrix}1 & e^{-i\theta_k}\end{pmatrix}e^{-i\bar{k}\bar{r}}\begin{pmatrix}1\\ e^{i\theta_{\bar{k}_0}}\end{pmatrix}\frac{1}{a\sqrt{\pi}}e^{-\frac{(x-x_0)^2}{2a^2}}e^{-\frac{(z-z_0)^2}{2a^2}}e^{i\bar{k}_0\bar{r}}dxdz\\ &= \frac{1}{2a\sqrt{\pi}}\left(1+e^{i(\theta_{\bar{k}_0}-\theta_k)}\right)\int_{-\infty}^{\infty}\int_{-\infty}^{\infty}e^{-ix(k_x-k_{x_0})}e^{-iz(k_z-k_{z_0})}e^{-\frac{(x-x_0)^2}{2a^2}}e^{-\frac{(z-z_0)^2}{2a^2}}dxdy\\ &= \frac{1}{2a\sqrt{\pi}}\left(1+e^{i(\theta_{\bar{k}_0}-\theta_k)}\right)g(\bar{k})\end{aligned}$$

where $g(\bar{k})$ is the usual Fourier Transform of a Gaussian wave packet (which I do not obtain here explicitly since it is a well known result, see [71] for a detailed derivation):

$$g(\bar{k}) = 2\pi a^2 e^{-ix_0(k_x-k_{x_0})}e^{-iz_0(k_z-k_{z_0})}e^{-\frac{(k_x-k_{x_0})^2}{2\sigma_k^2}}e^{-\frac{(k_z-k_{z_0})^2}{2\sigma_k^2}} \quad \text{(B.12)}$$

where $\sigma_k = 1/a$.

Finally, I obtain:

$$g_{graph}(\bar{k}) = a\sqrt{\pi}\left(1+e^{i(\theta_{\bar{k}_0}-\theta_k)}\right)e^{-ix_0(k_x-k_{x_0})}e^{-iz_0(k_z-k_{z_0})}e^{-\frac{(k_x-k_{x_0})^2}{2\sigma_k^2}}e^{-\frac{(k_z-k_{z_0})^2}{2\sigma_k^2}} \quad \text{(B.13)}$$

Then, by introducing Equation (B.13) and Equation (B.11) in Equation (B.4) I obtain:

[1] Along the computations, I will use several times the following integral: $\int_{-\infty}^{\infty}e^{-\alpha x^2}e^{-\beta x}dx = \frac{\sqrt{\pi}}{\alpha}e^{\frac{\beta^2}{4\alpha}}$ where $Re(\alpha) > 0$.

$$\Psi_G(x,z,t) = \int_{-\infty}^{\infty} a\sqrt{\pi}\left(1+e^{i(\theta_{\bar{k}_0}-\theta_k)}\right)e^{-ix_0(k_x-k_{x_0})}e^{-iz_0(k_y-k_{z_0})}e^{-\frac{(k_x-k_{x_0})^2}{2\sigma_k^2}} \tag{B.14}$$
$$e^{-\frac{(k_z-k_{z_0})^2}{2\sigma_k^2}}\frac{1}{\sqrt{2}}\begin{pmatrix}1\\ e^{i\theta_k}\end{pmatrix}e^{i\bar{k}\bar{r}}e^{-iE_kt/\hbar}d\bar{k}$$

$$= a\sqrt{\pi}\int_{-\infty}^{\infty}\int_{-\infty}^{\infty}\left(1+e^{i(\theta_{\bar{k}_0}-\theta_k)}\right)\begin{pmatrix}1\\ e^{i\theta_k}\end{pmatrix}e^{-ix_0(k_x-k_{x_0})}e^{-iz_0(k_z-k_{z_0})}e^{-\frac{(k_x-k_{x_0})^2}{2\sigma_k^2}}e^{-\frac{(k_z-k_{z_0})^2}{2\sigma_k^2}}$$
$$e^{ik_xx}e^{ik_zz}e^{-iv_f|\bar{k}_0|t}e^{-iv_f\frac{k_{x_0}}{|\bar{k}_0|}(k_x-k_{x_0})t}e^{-iv_f\frac{k_{z_0}}{|\bar{k}_0|}(k_z-k_{z_0})t}e^{-iv_f\frac{k_x^2}{2|\bar{k}_0|^3}(k_z-k_{z_0})^2t}e^{-iv_f\frac{k_z^2}{2|\bar{k}_0|^3}(k_x-k_{x_0})^2t}$$
$$e^{iv_f\frac{k_{x_0}k_{z_0}}{2|\bar{k}_0|^3}(k_x-k_{x_0})(k_z-k_{z_0})}dk_xdk_z$$

$$= a\sqrt{\pi}\int_{-\infty}^{\infty}\int_{-\infty}^{\infty}\begin{pmatrix}\left(1+e^{i(\theta_{\bar{k}_0}-\theta_k)}\right)\\ \left(e^{i\theta_k}+e^{i\theta_{\bar{k}_0}}\right)\end{pmatrix}e^{-ix_0(k_x-k_{x_0})}e^{-iz_0(k_z-k_{z_0})}e^{-\frac{(k_x-k_{x_0})^2}{2\sigma_k^2}}e^{-\frac{(k_z-k_{z_0})^2}{2\sigma_k^2}}$$
$$e^{ik_xx}e^{ik_zz}e^{-iv_f|\bar{k}_0|t}e^{-iv_f\frac{k_{x_0}}{|\bar{k}_0|}(k_x-k_{x_0})t}e^{-iv_f\frac{k_{z_0}}{|\bar{k}_0|}(k_z-k_{z_0})t}e^{-iv_f\frac{k_{x_0}^2}{2|\bar{k}_0|^3}(k_z-k_{z_0})^2t}e^{-iv_f\frac{k_{z_0}^2}{2|\bar{k}_0|^3}(k_x-k_{x_0})^2t}$$
$$e^{iv_f\frac{k_{x_0}k_{z_0}}{2|\bar{k}_0|^3}(k_x-k_{x_0})(k_z-k_{z_0})}dk_xdk_z$$

$$\approx C_1\int_{-\infty}^{\infty}\int_{-\infty}^{\infty}e^{-ix_0(k_x-k_{x_0})}e^{-iz_0(k_z-k_{z_0})}e^{-\frac{(k_x-k_{x_0})^2}{2\sigma_k^2}}e^{-\frac{(k_z-k_{z_0})^2}{2\sigma_k^2}}$$
$$e^{ik_xx}e^{ik_zz}e^{-iv_f|\bar{k}_0|t}e^{-iv_f\frac{k_{x_0}}{|\bar{k}_0|}(k_x-k_{x_0})t}e^{-iv_f\frac{k_{z_0}}{|\bar{k}_0|}(k_z-k_{z_0})t}e^{-iv_f\frac{k_{z_0}^2}{2|\bar{k}_0|^3}(k_x-k_{x_0})^2t}e^{-iv_f\frac{k_{x_0}^2}{2|\bar{k}_0|^3}(k_z-k_{z_0})^2t}$$
$$e^{iv_f\frac{k_{x_0}k_{z_0}}{2|\bar{k}_0|^3}(k_x-k_{x_0})(k_z-k_{z_0})t}dk_xdk_z$$

In order to obtain the last equality in Equation (B.15) I have done the approximation $\theta_k \approx \theta_{\bar{k}_0}$. The implications of this approximation is performed in the main text, Section 4.4. Then, C_1 appearing in Equation (B.15) is $C_1 = 2a\sqrt{\pi}\begin{pmatrix}1\\1\end{pmatrix}$. Then, I can rewrite Equation (B.15) as:

$$\Psi_G(x,z,t) = C_1e^{-iv_f|\bar{k}_0|t}\int_{-\infty}^{\infty}\int_{-\infty}^{\infty}e^{-i(k_x-k_{x_0})(x_0+v_f\frac{k_{x_0}}{|k_0|}t)}e^{ik_xx}e^{-i(k_z-k_{z_0})(z_0+v_f\frac{k_{z_0}}{|k_0|}t)}e^{ik_zz} \tag{B.15}$$
$$e^{-(k_x-k_{x_0})^2(\frac{1}{2\sigma_k^2}+iv_f\frac{k_{z_0}^2}{2|\bar{k}_0|^3}t)}e^{-(k_z-k_{z_0})^2(\frac{1}{2\sigma_k^2}+iv_f\frac{k_{x_0}^2}{2|\bar{k}_0|^3}t)}e^{iv_f\frac{k_{x_0}k_{z_0}}{2|\bar{k}_0|^3}(k_xk_z-k_{x_0}k_z-k_xk_{z_0}+k_{x_0}k_{z_0})t}dk_xdk_z$$

$$= C_2e^{ik_{x_0}x}e^{ik_{z_0}z}\int_{-\infty}^{\infty}\int_{-\infty}^{\infty}e^{i(k_x-k_{x_0})(x-x_0-v_f\frac{k_{x_0}}{|k_0|}t)}e^{i(k_z-k_{z_0})(z-z_0-v_f\frac{k_{z_0}}{|k_0|}t)}e^{-(k_x-k_{x_0})^2(\frac{1}{2\sigma_k^2}+iv_f\frac{k_{z_0}^2}{2|\bar{k}_0|^3}t)}$$
$$e^{-(k_z-k_{z_0})^2(\frac{1}{2\sigma_k^2}+iv_f\frac{k_{x_0}^2}{2|\bar{k}_0|^3}t)}e^{iv_f\frac{k_{x_0}k_{z_0}k_z}{2|\bar{k}_0|^3}(k_x-k_{x_0})t}e^{-iv_f\frac{k_{x_0}k_{z_0}^2}{2|\bar{k}_0|^3}(k_x-k_{x_0})t}dk_xdk_z$$

where $C_2 = C_1 e^{-iv_f|\bar{k}_0|t} e^{iv_f \frac{k_{x_0}^2 k_{z_0}^2}{2|\bar{k}_0|^3} t}$. Then, by rearranging some terms and integrating over k_x I obtain:

$$\Psi_G(x,z,t) = C_2 e^{ik_{x_0}x} e^{ik_{z_0}z} \int_{-\infty}^{\infty} \left(\int_{-\infty}^{\infty} e^{i(k_x-k_{x_0})(x-x_0-v_f\frac{k_{x_0}}{|\bar{k}_0|}t - v_f\frac{k_{x_0}k_{z_0}^2}{2|\bar{k}_0|^3}t + v_f\frac{k_{x_0}k_{z_0}k_z}{2|\bar{k}_0|^3}t)} \right. \tag{B.16}$$
$$\left. e^{-(k_x-k_{x_0})^2(\frac{1}{2\sigma_k^2} + iv_f\frac{k_{z_0}^2}{2|\bar{k}_0|^3}t)} \right) dk_x e^{i(k_z-k_{z_0})(z-z_0-v_f\frac{k_{z_0}}{|\bar{k}_0|}t)} e^{-(k_z-k_{z_0})^2(\frac{1}{2\sigma_k^2} + iv_f\frac{k_{x_0}^2}{2|\bar{k}_0|^3}t)} dk_z$$

$$= C_2 e^{ik_{x_0}x} e^{ik_{z_0}z} \int_{-\infty}^{\infty} \sqrt{\frac{2\pi}{\sigma_x^2(t)}} e^{\frac{\left(x-x_0-v_f\frac{k_{x_0}}{|\bar{k}_0|}t - v_f\frac{k_{x_0}k_{z_0}^2}{2|\bar{k}_0|^3}t + v_f\frac{k_{x_0}k_{z_0}k_z}{2|\bar{k}_0|^3}t\right)^2}{2\sigma_x^2(t)}}$$
$$e^{i(k_z-k_{z_0})(z-z_0-v_f\frac{k_{z_0}}{|\bar{k}_0|}t)} e^{-(k_z-k_{z_0})^2(\frac{1}{2\sigma_k^2} + iv_f\frac{k_{x_0}^2}{2|\bar{k}_0|^3}t)} dk_z$$

$$= C_3 e^{ik_{x_0}x} e^{ik_{z_0}z} e^{\frac{\left(x-x_0-v_f\frac{k_{x_0}}{|\bar{k}_0|}t - v_f\frac{k_{x_0}k_{z_0}^2}{2|\bar{k}_0|^3}t\right)^2}{2\sigma_x^2(t)}} \int_{-\infty}^{\infty} e^{v_f^2\frac{k_{x_0}^2k_{z_0}^2k_z^2}{8\sigma_x^2(t)|\bar{k}_0|^6}t^2} e^{\frac{\left(x-x_0-v_f\frac{k_{x_0}}{|\bar{k}_0|}t - v_f\frac{k_{x_0}k_{z_0}^2}{2|\bar{k}_0|^3}t\right)v_f\frac{k_{x_0}k_{z_0}k_z}{2|\bar{k}_0|^3}t}{\sigma_x^2(t)}}$$
$$e^{i(k_z-k_{z_0})(z-z_0-v_f\frac{k_{z_0}}{|\bar{k}_0|}t)} e^{-(k_z-k_{z_0})^2(\frac{1}{2\sigma_k^2} + iv_f\frac{k_{x_0}^2}{2|\bar{k}_0|^3}t)} dk_z$$

where $C_3 = C_2 * \sqrt{\frac{2\pi}{\sigma_x^2(t)}}$ and

$$a_x(t) = \sigma_x^2(t) = \frac{1}{\sigma_k^2} + iv_f\frac{k_{z_0}^2}{|\bar{k}_0|^3}t = a^2 + iv_f\frac{k_{z_0}^2}{|\bar{k}_0|^3}t \tag{B.17}$$

$$\sigma_z^2(t) = \frac{1}{\sigma_k^2} + iv_f\frac{k_{x_0}^2}{|\bar{k}_0|^3}t = a^2 + iv_f\frac{k_{x_0}^2}{|\bar{k}_0|^3}t \tag{B.18}$$

Then, I can rewrite Equation (B.17) as:

$$\Psi_G(x,z,t) = C_4 \int_{-\infty}^{\infty} e^{v_f^2 \frac{k_{x_0}^2 k_{z_0}^2 k_z^2}{8\sigma_x^2(t)|\bar{k}_0|^6} t^2} e^{\frac{\left(x - x_0 - v_f \frac{k_{x_0}}{|\bar{k}_0|} t - v_f \frac{k_{x_0} k_{z_0}^2}{2|\bar{k}_0|^3} t\right) v_f \frac{k_{x_0} k_{z_0} k_z}{2|\bar{k}_0|^3} t}{\sigma_x^2(t)}} \tag{B.19}$$
$$e^{i(k_z - k_{z_0})(z - z_0 - v_f \frac{k_{z_0}}{|\bar{k}_0|} t)} e^{-(k_z - k_{z_0})^2 (\frac{1}{2\sigma_k^2} + i v_f \frac{k_{x_0}^2}{2|\bar{k}_0|^3} t)} dk_z$$
$$= C_4 \int_{-\infty}^{\infty} e^{-\left(v_f^2 \frac{k_{x_0}^2 k_{z_0}^2 k_z^2}{8\sigma_x^2(t)|\bar{k}_0|^6} t^2 + \frac{\sigma_z^2(t)}{2}\right) k_z^2} e^{-\left(\frac{-(x - x_0 - v_f \frac{k_{x_0}}{|\bar{k}_0|} t - v_f \frac{k_{x_0} k_{z_0}^2}{2|\bar{k}_0|^3} t) v_f k_{x_0} k_{z_0} t}{2|\bar{k}_0|^3 \sigma_x^2(t)} - i(z - z_0 - v_f \frac{k_{z_0}}{|\bar{k}_0|} t) - k_{z_0} \frac{\sigma_z^2(t)}{2}\right) k_z}$$
$$e^{-\frac{\sigma_z^2(t)}{2} k_{z_0}^2} e^{-i(z - z_0 - v_f \frac{k_{z_0}}{|\bar{k}_0|} t)} dk_z$$

where $C_4 = C_3 \chi(x,y)$ and $\chi(x,y)$ is $\chi(x,y) = e^{ik_{x_0}x} e^{ik_{z_0}z} e^{\frac{\left(x - x_0 - v_f \frac{k_{x_0}}{|\bar{k}_0|} t - v_f \frac{k_{x_0} k_{z_0}^2}{2|\bar{k}_0|^3} t\right)^2}{2\sigma_x^2(t)}}$. Finally, integrating over k_z I obtain the analytic formula for a Gaussian bispinor wave packet in graphene:

$$\Psi_G(x,z,t) = C_4 e^{-\frac{\sigma_z^2(t)}{2} k_{z_0}^2} e^{-i(z - z_0 - v_f \frac{k_{z_0}}{|\bar{k}_0|} t)} \sqrt{\frac{2\pi}{\sigma_z^2(t) + v_f^2 \frac{k_{x_0}^2 k_{z_0}^2 k_z^2}{4\sigma_x^2(t)|\bar{k}_0|^6} t^2}} \tag{B.20}$$
$$e^{\frac{\left(\frac{-(x - x_0 - v_f \frac{k_{x_0}}{|\bar{k}_0|} t - v_f \frac{k_{x_0} k_{z_0}^2}{2|\bar{k}_0|^3} t) v_f k_{x_0} k_{z_0} t}{2|\bar{k}_0|^3 \sigma_x^2(t)} - i(z - z_0 - v_f \frac{k_{z_0}}{|\bar{k}_0|} t) - k_{z_0} \frac{\sigma_z^2(t)}{2}\right)^2}{2\left(v_f^2 \frac{k_{x_0}^2 k_{z_0}^2 k_z^2}{4\sigma_x^2(t)|k_0|^6} t^2 + \sigma_z^2(t)\right)}}$$

Although establishing the dispersion as a function of time for the wave packet is not directly seen in Equation (B.21), what I can see from Equation (B.17), Equation (B.18) and Equation (B.21) is that in the case where $k_{x_0} = 0$ ($k_{z_0} = 0$), the dispersion $\sigma_x(t) = a$ ($\sigma_z(t) = a$) and therefore there is no dispersion in the x (z) direction, only in the z (x) direction. This is completely different from the Schrödinger case, where the dispersion (see Equation (4.59)) is independent of the initial values of the initial momentum, i.e. the wave packet will always spread. In graphene, the wave packet will not spread in a certain direction if its initial momentum was zero.

Appendix C

Klein Tunneling effect

Here I consider the case where there is a potential barrier in graphene as shown in Figure C.1. We can assume that the scattering does not mix the momenta around K and K' points because the potential changes are smooth on the lattice scale [91]. Using the eigenfunctions obtained in Section 4.2.3.2 (fulfilling the Dirac Equation $H = -i\hbar\bar{\sigma}\cdot\bar{\bigtriangledown}\psi = E\psi$) we can establish the following relationships in order to calculate the wave function in any position of the space:

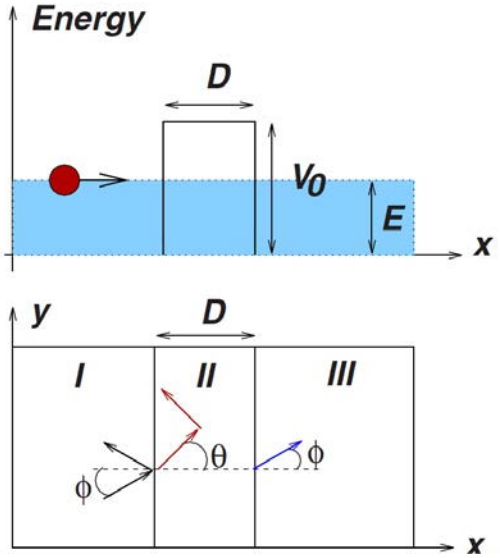

FIGURE C.1: Scheme of the potential barrier.

$$\psi_I = \frac{1}{\sqrt{2}}\begin{pmatrix}1\\ e^{i\phi(q)}\end{pmatrix}e^{i(q_x x+q_z z)} + \frac{r}{\sqrt{2}}\begin{pmatrix}1\\ e^{i(\pi-\phi(q))}\end{pmatrix}e^{i(-q_x x+q_z z)} \tag{C.1}$$

$$\psi_{II} = \frac{a}{\sqrt{2}}\begin{pmatrix}1\\ -e^{i\theta(q')}\end{pmatrix}e^{i(q'_x x+q_z z)} + \frac{b}{\sqrt{2}}\begin{pmatrix}1\\ -e^{i(\pi-\theta(q'))}\end{pmatrix}e^{i(-q'_x x+q_z z)} \tag{C.2}$$

$$\psi_{III} = \frac{t}{\sqrt{2}} \begin{pmatrix} 1 \\ e^{i\phi(q)} \end{pmatrix} e^{i(q_x x + q_z z)} \tag{C.3}$$

In these equations, I have assumed that the potential (V_0) is higher than the energy of the incident electron (E). Then,

$$q'_x = \sqrt{\frac{(E - V_0)^2}{\hbar^2 v_f^2} - q_z^2} \tag{C.4}$$

The minus that appears in ψ_{II} is because the incident electron is converted into a hole inside the barrier and the eigenfunction is different for holes (Equation (4.46)). The tangential component (q_z) is conserved due to boundary conditions.

We must notice, that it exists a critical angle (ϕ_c). For angles higher than ϕ_c, the plane wave will be completely reflected. The existence of this critical angle can be derived from Equation (C.4). If the potential V is close to E then the first term is almost zero and thus q'_x becomes purely imaginary and the resulting plane wave is evanescent. The value of the critical angle is obtained just equalling the right term of Eq.C.4 to zero. The result obtained is the following:

$$\phi_c = arcsin\left(\frac{|E - V_0|}{E}\right) \tag{C.5}$$

Our goal is to calculate the transmission coefficient (t) and using it, to find the transmission probability. I will show here the calculus just for normal incidence ($\phi = 0$). Firstly, we enforce continuity (in contrast with the Schrödinger equation, we only need to enforce continuity and not continuity in the derivative because in the Dirac equation appears only the first derivative) in both sides of the barrier:

$$\psi_I(x = 0, z) = \psi_{II}(x = 0, z) \tag{C.6}$$

$$\psi_{II}(x = D, z) = \psi_{III}(x = D, z) \tag{C.7}$$

we get:

$$\begin{pmatrix} 1 + r \\ 1 + r \end{pmatrix} = \begin{pmatrix} -a - b \\ -a + b \end{pmatrix} \tag{C.8}$$

$$\begin{pmatrix} -ae^{i(q'_x D)} - be^{i(-q'_x D)} \\ -ae^{i(q'_x D)} + be^{i(-q'_x D)} \end{pmatrix} = \begin{pmatrix} t \\ t \end{pmatrix} e^{i(q_x D)} \tag{C.9}$$

From here, we can straightforward obtain:

$$a = r = 0 \tag{C.10}$$

$$b = t = 1 \tag{C.11}$$

Therefore $T(\phi = 0) = tt^* = 1$, Klein Tunneling effect (no reflection at normal incidence, conservation of the pseudo-spin) appears as a consequence, and not as an imposition in order to obtain T=1. It is also noticeable that when there is full transmission, the incident state in zone I matches with the the b term in zone II, reversing its momentum. A more general expression for any angle can be obtained if one make the calculations more carefully[101]:

$$T(\phi) = \frac{cos^2(\theta)cos^2(\phi)}{(cos(Dq'_x)cos(\phi)cos(\theta))^2 + sin^2(Dq'_x)(1 + sin(\phi)sin(\theta))^2} \tag{C.12}$$

It is remarkable that there are other angles where transmission is also 1, but they depend on the potential (V_0), the energy of the carrier and the width of the potential (D).

In conclusion, the pseudospin (which indicates the sublattice we are dealing with) is always conserved. This fact is not an imposition, but a consequence of the full transmission.

Appendix D

Probability distributions

D.1 Definition of a probability distribution

Let me specify what it is understood by a well-defined probability distribution in the phase space, say $F_Q(x,p)$, for a quantum (or classical) system. One desires that this probability distribution fulfils the probabilities axioms[1]:

$$F_Q(x,p) \geq 0, \tag{D.1}$$

$$\int\int F_Q(x,p)dxdp = 1 \tag{D.2}$$

In addition, its marginal distribution should give the usual position or charge probability distributions[2]:

$$Q(x) = \int F_Q(x,p)dp \tag{D.3}$$

Equation (D.3) is an important quantity in quantum transport because it is related to the charge density, which is a very relevant magnitude in any self-consistent solution of the electron transport. Another important quantity built from this distribution is the current density, which can be expressed as:

[1] All the integration limits are from $-\infty$ to ∞ and thus I will not write them explicitly.

[2] For simplicity, I avoid the explicitly consideration of the charge q of an electron in Equation (D.3) and Equation (D.4). I notice also that the words charge or current densities can be misleading when a wave packet is partially transmitted or reflected, and the charge is in fact either fully transmitted or fully reflected, not both, when measured.

$$J(x) = \int pF_Q(x,p)dp. \tag{D.4}$$

D.2 Q(x) and J(x) derivations

In this appendix, I will develop the calculus in order to obtain the charge and current densities (Equation (D.3) and Equation (D.4)) for each of the three analyzed distributions.

D.2.1 Wigner distribution

The charge distribution is straightforwardly found out:

$$\begin{aligned} Q_W(x,p) &= \frac{1}{h}\int dp \int \psi(x+\frac{y}{2})\psi^*(x-\frac{y}{2})e^{i\frac{py}{\hbar}}dy = \\ &= \int \delta(y)\psi(x+\frac{y}{2})\psi^*(x-\frac{y}{2})e^{i\frac{py}{\hbar}}dy = |\psi(x)|^2 \end{aligned} \tag{D.5}$$

$$\bar{J}_W(x) = \int pF_W(x,p)dp = \frac{1}{h}\int p\int \psi(x+\frac{y}{2})\psi^*(x-\frac{y}{2})e^{i\frac{py}{\hbar}}dydp \tag{D.6}$$

Using the chain rule for a function $F(x,y)$ derivable and zero-valued at $y \to \pm\infty$, I can use the following relation:

$$\int dy e^{-ipy/\hbar}\frac{\partial}{\partial y}F(x,y) = \frac{i}{\hbar}p\int dy e^{-ipy/\hbar}F(x,y) \tag{D.7}$$

and using the polar form of the wave function ($\psi(x) = R(x)e^{iS(x)}$), then rewrite Equation (D.6) as:

$$\begin{aligned} \bar{J}_W(x) = \frac{-i}{2\pi}\int dp\int dy e^{-ipy/\hbar}\cdot\Big[R(x+\frac{y}{2})R(x-\frac{y}{2})\cdot e^{\frac{i}{\hbar}\left[S(x+\frac{y}{2})-S(x-\frac{y}{2})\right]}\frac{i}{\hbar}\Big(\frac{\partial S(x+\frac{y}{2})}{\partial y} - \frac{\partial S(x-\frac{y}{2})}{\partial y}\Big) + \\ + \quad e^{\frac{i}{\hbar}\left[S(x+\frac{y}{2})-S(x-\frac{y}{2})\right]}\frac{\partial}{\partial y}\Big(R(x+\frac{y}{2})R(x-\frac{y}{2})\Big)\Big] \end{aligned} \tag{D.8}$$

To proceed, let me focus on the following term:

$$\begin{aligned}
&\frac{\partial S(x+\frac{y}{2})}{\partial y}-\frac{\partial S(x-\frac{y}{2})}{\partial y}=\lim_{t\to 0}\left[\frac{S(x+\frac{y+t}{2})-S(x+\frac{y}{2})}{t}-\frac{S(x-\frac{y+t}{2})-S(x-\frac{y}{2})}{t}\right] \\
&= \frac{1}{2}\lim_{t\to 0}\left[\frac{S(x+\frac{t}{2}+\frac{y}{2})-S(x+\frac{y}{2})}{t/2}+\frac{S(x-\frac{y}{2})-S(x-\frac{t}{2}-\frac{y}{2})}{t/2}\right] \\
&= \frac{1}{2}\left[\frac{\partial S(x+\frac{y}{2})}{\partial x}+\frac{\partial S(x-\frac{y}{2})}{\partial x}\right]
\end{aligned} \tag{D.9}$$

which can be used to rewrite Equation (D.8) as:

$$\begin{aligned}
&J_W(x)=\int dy\delta(y)\Big[R(x+\frac{y}{2})R(x-\frac{y}{2})e^{\frac{i}{\hbar}\left[S(x+\frac{y}{2})-S(x-\frac{y}{2})\right]}\cdot\frac{1}{2}\Big(\frac{\partial S(x+\frac{y}{2})}{\partial x}+\frac{\partial S(x-\frac{y}{2})}{\partial x}\Big) \\
&- i\hbar e^{\frac{i}{\hbar}\left[S(x+\frac{y}{2})-S(x-\frac{y}{2})\right]}\cdot\frac{\partial}{\partial y}\Big(R(x+\frac{y}{2})R(x-\frac{y}{2})\Big)\Big]=R^2(x)\frac{\partial S(x)}{\partial x}
\end{aligned} \tag{D.10}$$

Equation (D.10) is the expression for the current density distribution for the Wigner function. In Equation (D.10) I have used the following property:

$$\int dp e^{-ipy/\hbar}=2\pi\hbar\delta(y) \tag{D.11}$$

and the fact that the second term within the integral in Equation (D.10) is zero:

$$\begin{aligned}
&\frac{\partial}{\partial y}\Big(R(x+\frac{y}{2})R(x-\frac{y}{2})\Big)\Big|_{y=0} \\
&= \frac{1}{2}\left[\frac{\partial R(x+\frac{y}{2})}{\partial x}R(x-\frac{y}{2})-R(x+\frac{y}{2})\frac{\partial R(x-\frac{y}{2})}{\partial x}\right]\Big|_{y=0}=0
\end{aligned} \tag{D.12}$$

D.2.2 Husimi distribution

The derivation of the Husimi charge and current density distributions is quite similar to the derivation realized for the Wigner distribution, with the only difference that now, the Wigner distributions are smoothed with a Gaussian function. In first place, I derive the charge distribution:

$$
\begin{aligned}
Q_H(x,p) &= \frac{1}{\pi\hbar}\iiint\frac{1}{h}\int\psi(x'-\frac{y}{2})\psi^*(x'+\frac{y}{2})e^{i\frac{p'y}{\hbar}}dy\, e^{-\frac{(x-x')^2}{2s^2}}e^{-\frac{(p-p')^2 2s^2}{\hbar^2}}dx'dp'dp \\
&= \frac{1}{\pi\hbar}\frac{1}{\sqrt{(2\pi s^2)}}\cdot\iiint\psi(x'-\frac{y}{2})\psi^*(x'+\frac{y}{2})e^{i\frac{p'y}{\hbar}}dy e^{-\frac{(x-x')^2}{2s^2}}dx'dp' \\
&= \frac{1}{\sqrt{(2\pi s^2)}}\iint\psi(x'-\frac{y}{2})\psi^*(x'+\frac{y}{2})\delta(y)dy e^{-\frac{(x-x')^2}{2s^2}}dx' \\
&= \frac{1}{\sqrt{(2\pi s^2)}}\int|\psi(x')|^2 e^{-\frac{(x-x')^2}{2s^2}}dx' \qquad \text{(D.13)}
\end{aligned}
$$

After that, I derive the current density distribution. For that purpose, Equation (D.7)), Equation (D.9), Equation (D.11) and Equation (D.13) will be also used.

$$
\begin{aligned}
J_H(x) &= \frac{1}{\pi\hbar}\int\int\int pF_H(x',p')e^{-\frac{(x-x')^2}{2s^2}}e^{-\frac{(p-p')^2}{2\sigma_p^2}}dx'dp'dp \\
&= \frac{1}{\pi\hbar}\int\int\int p\frac{1}{h}\int\psi(x'-\frac{y}{2})\psi^*(x'+\frac{y}{2})e^{i\frac{p'y}{\hbar}}dy e^{-\frac{(x-x')^2}{2s^2}}\cdot e^{-\frac{(p-p')^2 2s^2}{\hbar^2}}dx'dp'dp \\
&= \frac{1}{h}\frac{1}{\sqrt{(2\pi s^2)}}\int p'\psi(x'-\frac{y}{2})\cdot\psi^*(x'+\frac{y}{2})e^{i\frac{p'y}{\hbar}}dy e^{-\frac{(x-x')^2}{2s^2}}dx'dp' \\
&= \frac{1}{\sqrt{(2\pi s^2)}}\int R^2(x')\frac{\partial S(x')}{\partial x'}e^{-\frac{(x-x')^2}{2s^2}}dx' \qquad \text{(D.14)}
\end{aligned}
$$

Therefore, it can clearly be seen that these results are different from the Wigner results.

D.2.3 Bohmian distribution

The charge distribution is the following:

$$
\begin{aligned}
Q_B(x,t) &= \int\lim_{N\to\infty}\frac{1}{N}\sum_{i=1}^{N}\delta(x-x_i(t))\delta(p-p_i(t))dp = \\
&= \lim_{N\to\infty}\frac{1}{N}\sum_{i=1}^{N}\delta(x-x_i(t)) = |\psi(x,t)|^2 \qquad \text{(D.15)}
\end{aligned}
$$

The last equality in Equation (D.15) is due to the quantum equilibrium hypothesis, which states that the charge distribution at time t is equal to the modulus squared of the wave function. In a single-particle scenario it can be written as follows:

$$|\psi(x,0)|^2 = \lim_{M_\alpha \to \infty} \frac{1}{M_\alpha} \sum_{\alpha=1}^{M_\alpha} \delta(x - x_i(0)) \tag{D.16}$$

where as commented before, M_α is the number of different trajectories of the ensemble.

In order to calculate the current density, I need to express the wave function in the polar form (in the same way as done for the Wigner distribution) and I proceed in the following way:

$$\begin{aligned} J_B(x,t) &= \lim_{N\to\infty} \frac{1}{N} \sum_{i=1}^{N} p\delta(x - x_i(t))\delta(p - p_i(t))dp = \\ &= \lim_{N\to\infty} \frac{1}{N} \sum_{i=1}^{N} p_i \delta(x - x_i(t)) = R^2(x) \frac{\partial S(x)}{\partial x} \end{aligned} \tag{D.17}$$

Apart from using again the quantum equilibrium hypothesis, I have also used that the momentum in Bohmian mechanics in a single-particle case is:

$$p(x,t) = \mathrm{Im} \frac{\nabla \psi}{\psi} \equiv \frac{\partial S(x)}{\partial x} \tag{D.18}$$

D.3 Negative values of the Wigner distribution

If I manipulate the Wigner distribution (applying a change of variable), it is seen that it can be thought as a correlation function:

$$\begin{aligned} & F_W(x,p) = \frac{1}{h} \int dp \int \psi(x + \frac{y}{2}) \psi^*(x - \frac{y}{2}) e^{i\frac{py}{\hbar}} dy \\ = \;& 2 \int \psi(r) \psi^*(2x - r) e^{i\frac{py}{\hbar}} e^{i\frac{2p(r-2x)}{\hbar}} dr = 2 \int \psi(r) e^{i\frac{pr}{\hbar}} \left(\psi(2x - r) e^{-i\frac{2p(r-2x)}{\hbar}}\right)^* dr \\ = \;& 2 \int \phi(r) \phi^*(2x - r) dr \end{aligned} \tag{D.19}$$

The change of variable realized is the following: $x + \frac{y}{2} = r$. In addition, I have defined $\phi(r) = \psi(r) e^{i\frac{pr}{\hbar}}$.

With these considerations, I can prove that the Wigner function is real and can be negative:

$$\begin{aligned} &\int \big(\phi(r) + \phi(2x-r)\big) \cdot \big(\phi(r)^* + \phi^*(2x-r)\big) dr = \int |\phi(r) + \phi(2x-r)|^2 dr \\ = &\int \Big(|\phi(r)|^2 + |\phi(2x-r)|^2 + \phi(r)\phi^*(2x-r) + \phi(r)^*\phi(2x-r) \Big) dr \geq 0 \end{aligned} \tag{D.20}$$

By observing one of the last two terms in the right hand side (that we can rapidly identify with our Wigner function) and making a change of variable $r' = 2x - r$:

$$\begin{aligned} &\int \phi(r)^*\phi(2x-r) dr = -\int_{\infty}^{-\infty} \phi(r')^*\phi(2x-r') dr' \\ = &\int \phi(r')^*\phi(2x-r') dr' \end{aligned} \tag{D.21}$$

Therefore, both terms are exactly equal. Thus Equation (D.20) becomes:

$$\begin{aligned} &\int |\phi(r) + \phi(2x-r)|^2 dr = \int |\phi(r)|^2 dr + \\ + &\int |\phi(2x-r)|^2 dr + 2\int \phi(r)\phi^*(2x-r) dr \geq 0 \end{aligned} \tag{D.22}$$

Obviously, Equation (D.20) is positive because is the integral of a modulus squared quantity. The first two terms of the right side of Equation (D.20) are also positive for the same reason. Therefore, the value of the last term (Wigner function) must be real, but depending of the value of $\phi(r)$ and $\phi(2x-r)$ can be either positive or negative. In this way, it is proved that the Wigner function is a quasiprobability distribution, but not a true one.

Appendix E

Bohmian Scattering Approach calculus

E.1 Evaluation of the term $\langle \vec{r}_a, \vec{z}_a, \vec{R}|\hat{\mathcal{H}}_{ep,\vec{u}}|\Psi(t)\rangle|_{\vec{z}_a^j[t],\vec{R}^j[t]}$ in Equation (5.49):

I first evaluate the effect of the $\hat{\mathcal{H}}_{ep,\vec{u}}$ on the wave packet $\Psi(\vec{r}_a, \vec{z}_a, \vec{R}, t)$. For that purpose, I develop the explicit expression of $\hat{\mathcal{H}}_{ep,\vec{u}}$ and then I define an initial many-body wave packet $\Psi(\vec{r}_a, \vec{z}_a, \vec{R}, t)$.

E.1.1 Definition of the Electron-Phonon Hamiltonian:

The term H_{ep} in Equation (5.47) can be written as $H_{ep} = H_{ep,\vec{R}_0} + H_{ep,\vec{u}} = \sum_{e,h} V_{ep}(\vec{r}_e - \vec{R}_h)$. I decompose $V_{ep}(\vec{r}_e - \vec{R}_h)$ in a Taylor expansion around the equilibrium position of the h ions $\vec{R}_{h,0}$ as:

$$\begin{aligned} & \sum_{e,h} V_{ep}(\vec{r}_e - \vec{R}_h) \approx \sum_{e,h} V_{ep}(\vec{r}_e - \vec{R}_{h,0}) + (\vec{R}_h - \vec{R}_{h,0}) \cdot \nabla_h V_{ep}(\vec{r}_e - \vec{R}_h)|_{\vec{R}_h = \vec{R}_{h,0}} \\ = & \sum_{e,h} V_{ep}(\vec{r}_e - \vec{R}_{h,0}) + \vec{u}_h \cdot \nabla_h V_{ep}(\vec{r}_e - \vec{R}_h)|_{\vec{R}_h = \vec{R}_{h,0}} = H_{ep,\vec{R}_0} + H_{ep,\vec{u}} \end{aligned} \tag{E.1}$$

The term $V_{ep}(\vec{r}_e - \vec{R}_{h,0})$ will become later relevant for the electronic band structure, while $\vec{u}_h \cdot \nabla V_{ep}(\vec{r}_e - \vec{R}_h)|_{\vec{R}_h = \vec{R}_{h,0}}$ provides the interaction of the electron $\vec{r}_e$ with the ion $\vec{R}_h$ (neglecting second order Taylor terms in the atomic displacements expansion).

Instead of dealing with individual displacements $\vec{u}_h$, I consider the normal coordinate $\vec{Q}_{\vec{q}_p}$ defined from the Fourier transform:

$$\vec{u}_h = \sum_{\vec{q}_p} \vec{Q}_{\vec{q}_p} e^{i\vec{q}_p \vec{R}_{h,0}} \tag{E.2}$$

where $\vec{q}_p$ is a wave vector in the reciprocal space that labels each of the possible collective solutions of the movement of ions. Then, by performing the Fourier transform of the potential $V_{ep}(\vec{r}_e - \vec{R}_h)$:

$$V_{ep}(\vec{r}_e - \vec{R}_h) = \sum_{\vec{v}} e^{i\vec{v}(\vec{r}_e - \vec{R}_h)} U_{\vec{v}} \tag{E.3}$$

where $\vec{v}$ is another wave vector in the reciprocal space and $U_{\vec{v}}$ is the Fourier coefficients of the potential. I remark that $\sum_h V_{ep}(\vec{r}_e - \vec{R}_h)$ is a periodic potential, while $V_{ep}(\vec{r}_e - \vec{R}_h)$ alone is essentially a Coulomb potential with corrections due to screening. Then, the gradient of the potential in Equation (E.1) can be written as:

$$\nabla_h V_{ep}(\vec{r}_e - \vec{R}_h)|_{\vec{R}_h = \vec{R}_{h,0}} = \sum_{\vec{v}} (-i\vec{v}) e^{i\vec{v}(\vec{r}_e - \vec{R}_{h,0})} U_{\vec{v}} \tag{E.4}$$

Putting Equation (E.4) and Equation (E.2) altogether for all electrons and ions, finally I obtain:

$$\begin{aligned} H_{ep,\vec{u}} &= \sum_e H_{ep,\vec{u},\vec{r}_e} = \sum_e \sum_h \vec{u}_h \cdot \nabla_h V_{ep}(\vec{r}_e - \vec{R}_h)|_{\vec{R}_{h,0}} \\ &= \sum_e \sum_h \sum_{\vec{q}_p} e^{i\vec{q}_p \vec{R}_{h,0}} \vec{Q}_{\vec{q}_p} \sum_{\vec{v}} (-i\vec{v}) e^{i\vec{v}(\vec{r}_e - \vec{R}_{h,0})} U_{\vec{v}} \end{aligned} \tag{E.5}$$

Before discussing the interaction through the term $H_{ep,\vec{u}}$, let me define the initial electron-lattice wave packet.

E.1.2 Definition of the many body wave packet $\Psi(\vec{r},\vec{R},t)$:

The many body wave packet $\Psi(\vec{r},\vec{R},t)=\langle\vec{r}_a,\vec{z}_a,\vec{R}|\Psi(t)\rangle$ can be written as:

$$\Psi(\vec{r},\vec{R},t)=\sum_{\vec{k},\vec{q}} a(\vec{k},\vec{q},t)\Phi_{\vec{k}}(\vec{r})\Phi_{\vec{q}}(\vec{R}) \tag{E.6}$$

with $a(\vec{k},\vec{q},t)$ accounting for an arbitrary superposition of the many-body electron base $\Phi_{\vec{k}}(\vec{r})$ and many-body phonon base $\Phi_{\vec{q}}(\vec{R})$. The vector $\vec{k}=\{\vec{k}_1,\vec{k}_2,..,\vec{k}_{N_e}\}$ represents the many body index of the electronic (Bloch states) base and $\vec{q}=\{\vec{q}_1,\vec{q}_2,...\}$ the index of the ionic base. I define $\Phi_{\vec{k}}(\vec{r})\equiv\sum_{n=1}^{N_e!}\prod_{i=1}^{N_e}\phi_{\vec{k}_i}(\vec{r}_{p(n)_i})s_n$, with $\vec{p}(n)=\{p(n)_1,...,p(n)_{N_e}\}$ the n-permutation vector, and s_n its sign. I have also used the single particle Bloch eigenstate:

$$\phi_{\vec{k}_e}(\vec{r}_e)=\langle\vec{r}_e|\vec{k}_e\rangle=e^{i\vec{k}_e\vec{r}_e}u_{\vec{k}_e}(\vec{r}_e) \tag{E.7}$$

where $u_{\vec{k}_e}(\vec{r}_e)$ is periodic with respect to lattice translations (which includes the appropriate normalizing constant) and $\vec{k}_e$ is the electron (quasi) wave vector related to the quasi (or crystal) momentum $\vec{p}_e=\hbar\vec{k}_e$.

In the language of the second quantization, the Slater determinant of the electrons can be written as $\Phi_{\vec{k}}(\vec{r})\equiv\langle\vec{r}|\hat{c}^\dagger_{\vec{k}_1}...\hat{c}^\dagger_{\vec{k}_{N_e}}|0\rangle$. To explicitly write the dependence of $\Phi_{\vec{k}}(\vec{r})$ on $\vec{r}_e$, I expand the Slater determinant of electrons by minors as $\langle\vec{r}_e,\vec{z}_e|\hat{c}^\dagger_{\vec{k}_1}...\hat{c}^\dagger_{\vec{k}_{N_e}}|0\rangle=\sum_{w=1}^{N_e}\phi_{\vec{k}_w}(\vec{r}_e)s_{e,w}\langle\vec{z}_e|\hat{c}^\dagger_{\vec{k}_1}...c^\dagger_{\vec{k}_{w-1}}c^\dagger_{\vec{k}_{w+1}}...\hat{c}^\dagger_{\vec{k}_{N_e}}|0\rangle$, with $s_{e,w}$ the sign of the (e,w) cofactor. Then:

$$\Psi(\vec{r}_e,\vec{z}_e,\vec{R},t)=\sum_{\vec{k},\vec{q}} a(\vec{k},\vec{q},t)\Phi_{\vec{q}}(\vec{R})\sum_{\vec{k}_w}\phi_{\vec{k}_w}(\vec{r}_e)s_{e,w}\langle\vec{z}_e|\hat{c}^\dagger_{\vec{k}_1}..c^\dagger_{\vec{k}_{w-1}}c^\dagger_{\vec{k}_{w+1}}..\hat{c}^\dagger_{\vec{k}_N}|0\rangle \tag{E.8}$$

E.1.3 Evaluation of $H_{ep,\vec{u}}(\vec{r},\vec{R},t)\Psi(\vec{r},\vec{R},t)$:

The term $H_{ep,\vec{u}}=\sum_e H_{ep,\vec{u},\vec{r}_e}$ in Equation (E.5) is a sum over terms that depend on a unique $\vec{r}_e$, so that when conditioning $H_{ep,\vec{u}}(\vec{r},\vec{R},t)\Psi(\vec{r},\vec{R},t)$ to $\{\vec{z}^j_a[t],\vec{R}^j[t]\}$ all, except one term, do not depend on $\vec{r}_a$. Therefore, it is obtained:

$$H_{ep,\vec{u}}(\vec{r},\vec{R},t)\Psi(\vec{r}_a,\vec{z}_a,\vec{R},t)\Big|_{\vec{z}_a^j[t],\vec{R}^j[t]} = \left(\sum_e H_{ep,\vec{u},\vec{r}_e}(\vec{r}_e,\vec{R},t)\right)\Psi(\vec{r}_a,\vec{z}_a,\vec{R},t)\Big|_{\vec{z}_a^j[t],\vec{R}^j[t]} \quad \text{(E.9)}$$
$$= \left(\sum_{e\neq a} H_{ep,\vec{u},\vec{r}_e}(\vec{r}_e^j[t],\vec{R}^j[t],t)\right)\Psi(\vec{r}_a,\vec{z}_a^j[t],\vec{R}^j[t],t) + H_{ep,\vec{u},\vec{r}_a}(\vec{r}_a,\vec{R}^j[t],t)\Psi(\vec{r}_a,\vec{z}_a^j[t],\vec{R}^j[t],t)$$

The term $\sum_{e\neq a} H_{ep,\vec{u},\vec{r}_e}(\vec{r}_e^j[t],\vec{R}^j[t],t)$ is a constant value without dependence on $\vec{r}_a$. This pure time-dependent term only provides a global phase on the conditional wave function that can be omitted without any effect [72]. The only term that I have to compute explicitly is $H_{ep,\vec{u},\vec{r}_a}(\vec{r}_a,\vec{R},t)\Psi(\vec{r},\vec{R},t) = \langle\vec{r},\vec{R}|\hat{\mathcal{H}}_{ep,\vec{u},\vec{r}_a}|\Psi(t)\rangle$. Using the identities $\int_{\vec{r}} d\vec{r}|\vec{r}\rangle\langle\vec{r}| = \mathbb{1}$ and $\int_{\vec{R}} d\vec{R}|\vec{R}\rangle\langle\vec{R}| = \mathbb{1}$, the fact that $\hat{\mathcal{H}}_{ep,\vec{u},\vec{r}_a}$ is diagonal in the position representation, and the identity $\sum_{\vec{k}_a}|\vec{k}_a\rangle\langle\vec{k}_a| = \mathbb{1}$, I can write:

$$\begin{aligned}
&\langle\vec{r},\vec{R}|\hat{\mathcal{H}}_{ep,\vec{u},\vec{r}_a}|\Psi(t)\rangle = \langle\vec{r},\vec{R}|\hat{\mathcal{H}}_{ep,\vec{u},\vec{r}_a}|\vec{r},\vec{R}\rangle\langle\vec{r},\vec{R}|\Psi(t)\rangle \\
= &\sum_{\vec{k}_a}\sum_{\vec{k}_a''}\langle\vec{r}_a|\vec{k}_a''\rangle\langle\vec{k}_a'',\vec{z}_a,\vec{R}|\hat{\mathcal{H}}_{ep,\vec{u},\vec{r}_a}|\vec{k}_a,\vec{z}_a,\vec{R}\rangle\langle\vec{k}_a,\vec{z}_a,\vec{R}|\Psi(t)\rangle \\
&= \sum_{\vec{k}_a}\sum_{\vec{k}_a''}\mathcal{T}(\vec{k}_a'',\hat{\mathcal{H}}_{ep,\vec{u},\vec{r}_a},\vec{k}_a)\langle\vec{r}_a|\vec{k}_a''\rangle\langle\vec{k}_a,\vec{z}_a,\vec{R}|\Psi(t)\rangle \qquad \text{(E.10)}
\end{aligned}$$

where I have defined $\mathcal{T}(\vec{k}_a'',\hat{\mathcal{H}}_{ep,\vec{u},\vec{r}_a},\vec{k}_a) \equiv \langle\vec{k}_a'',\vec{z}_a,\vec{R}|\hat{\mathcal{H}}_{ep,\vec{u},\vec{r}_a}|\vec{k}_a,\vec{z}_a,\vec{R}\rangle$ as the electron-phonon Hamiltonian in the momentum (Bloch state) representation. This term can be rewritten as:

$$\mathcal{T}(\vec{k}_a'',\hat{\mathcal{H}}_{ep,\vec{u},\vec{r}_a},\vec{k}_a) = \int_{\vec{r}_a} d\vec{r}_a\langle\vec{k}_a''|\vec{r}_a\rangle\langle\vec{r}_a,\vec{z}_a,\vec{R}|\hat{\mathcal{H}}_{ep,\vec{u},\vec{r}_a}|\vec{r}_a,\vec{z}_a,\vec{R}\rangle\langle\vec{r}_a|\vec{k}_a\rangle \quad \text{(E.11)}$$

and using the final expression of the electron-phonon Hamiltonian in the position representation, Equation (E.5), I get:

$$\mathcal{T}(\vec{k}_a'',\hat{\mathcal{H}}_{ep,\vec{u},\vec{r}_a},\vec{k}_a) = \int_{\vec{r}_a} d\vec{r}_a e^{-i\vec{k}_a''\vec{r}_a}u_{\vec{k}_a''}(\vec{r}_a)e^{i\vec{k}_a\vec{r}_a}u_{\vec{k}_a}(\vec{r}_a)\langle\vec{r}_a,\vec{z}_a,\vec{R}|\hat{\mathcal{H}}_{ep,\vec{u},\vec{r}_a}|\vec{r}_a,\vec{z}_a,\vec{R}\rangle =$$
$$\int_{\vec{r}_a} d\vec{r}_a e^{-i\vec{k}_a''\vec{r}_a}u_{\vec{k}_a''}(\vec{r}_a)e^{i\vec{k}_a\vec{r}_a}u_{\vec{k}_a}(\vec{r}_a)\sum_h\sum_{\vec{q}_p}e^{i\vec{q}_p\vec{R}_{h,0}}\vec{Q}_{\vec{q}_p}\sum_{\vec{v}}(-i\vec{v})e^{i\vec{v}(\vec{r}_a-\vec{R}_{h,0})}U_{\vec{v}} \quad \text{(E.12)}$$

I take away from the integral those elements that do not depend on $\vec{r}_a$:

$$\mathcal{T}(\vec{k}''_a, \hat{\mathcal{H}}_{ep,\vec{u},\vec{r}_a}, \vec{k}_a) = \sum_h \sum_{\vec{q}_p} e^{i\vec{q}_p \vec{R}_{h,0}} \vec{Q}_{\vec{q}_p} \tag{E.13}$$
$$\sum_{\vec{v}} (-i\vec{v}) e^{-i\vec{v}\vec{R}_{h,0}} U_{\vec{v}} \int_{\vec{r}_a} d\vec{r}_a e^{-i\vec{k}''_a \vec{r}_a} u_{\vec{k}''_a}(\vec{r}_a) e^{i\vec{k}_a \vec{r}_a} u_{\vec{k}_a}(\vec{r}_a) e^{i\vec{v}\vec{r}_a}$$

Due to the periodicity of $u_{\vec{k}_a}(\vec{r}_a)$ I can use the change of variable $\vec{r}_a = \vec{r'}_a + \vec{R}_{m,0}$ where $\vec{r'}_a$ integrates only inside the first Brillouin zone. I get:

$$\mathcal{T}(\vec{k}''_a, \hat{\mathcal{H}}_{ep,\vec{u},\vec{r}_a}, \vec{k}_a) = \sum_h \sum_{\vec{q}_p} \vec{Q}_{\vec{q}_p} \sum_{\vec{v}} (-i\vec{v}) e^{i\vec{R}_{h,0}(\vec{q}_p - \vec{v})} U_{\vec{v}} \left(\sum_m e^{i\vec{R}_{m,0}(-\vec{k}''_a + \vec{v} + \vec{k}_a)} \right)$$
$$\int_{\vec{r'}_a} d\vec{r'}_a e^{-i\vec{k}''_a \vec{r'}_a} u_{\vec{k}''_a}(\vec{r'}_a) e^{i\vec{k}_a \vec{r'}_a} u_{\vec{k}_a}(\vec{r'}_a) e^{i\vec{v}\vec{r'}_a} \tag{E.14}$$

The sum over $\vec{R}_{h,0}$ in $\sum_h e^{i\vec{R}_{h,0}(\vec{q}_p - \vec{v})}$ imposes the condition $\vec{G} = \vec{q}_p - \vec{v}$ and the sum over $\vec{R}_{m,0}$ in $\sum_m e^{i\vec{R}_{m,0}(-\vec{k}''_a + \vec{v} + \vec{k}_a)}$ imposes that $\vec{G}' = -\vec{k}''_a + \vec{v} + \vec{k}_a$, with $\vec{G}$ and $\vec{G}'$ two vectors of the reciprocal lattice. For simplicity, although Umklapp scattering can also be considered, I assume that all momentum vectors can be considered in the first Brillouin zone, $\vec{G} = 0$ and $\vec{G}' = 0$, so that $\vec{k}''_a = \vec{q}_p + \vec{k}_a$. Therefore:

$$\mathcal{T}(\vec{k}''_a, \hat{\mathcal{H}}_{ep,\vec{u},\vec{r}_a}, \vec{k}_a) = \sum_{\vec{q}_p} \delta(\vec{k}''_a - \vec{q}_p - \vec{k}_a) g^{\vec{q}_p}_{\vec{k}_a} \tag{E.15}$$

All other terms in Equation (E.14) are included into the coupling constant $g^{\vec{q}_p}_{\vec{k}_a}$ defined as:

$$g^{\vec{q}_p}_{\vec{k}_a} = -i\vec{Q}_{\vec{q}_p}\ \vec{q}_p\ U_{\vec{q}_p} \int_{\vec{r'}_a} d\vec{r'}_a e^{-i(\vec{k}_a + \vec{q}_p)\vec{r'}_a} u_{\vec{k}_a + \vec{q}_p}(\vec{r'}_a) e^{i\vec{k}_a \vec{r'}_a} u_{\vec{k}_a}(\vec{r'}_a) e^{i\vec{v}\vec{r'}_a} \tag{E.16}$$

I emphasize that I did not include any dependence on the n band I are dealing with, since usually phonon energies are smaller than band gaps and then phonons cannot make band transitions. However, for materials with small band gaps these multi band transitions can be included straightforwardly. In fact, when dealing with graphene bispinors, I will include the dependence of the coupling constant on the energy branches. I introduce Equation (E.15) into Equation (E.10) and I conclude:

$$H_{ep,\vec{u},\vec{r}_a}(\vec{r}_a,\vec{z}_a,\vec{R},t)\Psi(\vec{r}_a,\vec{z}_a,\vec{R},t)=\sum_{\vec{k}_a}\sum_{\vec{k}''_a}\langle\vec{r}_a|\vec{k}''_a\rangle\mathcal{T}(\vec{k}''_a,\hat{\mathcal{H}}_{ep,\vec{u},\vec{r}_a},\vec{k}_a)\langle\vec{k}_a,\vec{z}^j_a[t],\vec{R}^j[t]|\Psi(t)\rangle$$
$$=\sum_{\vec{q}_p}\sum_{\vec{k}_a}g^{\vec{q}_p}_{\vec{k}_a}\langle\vec{r}_a|\vec{k}_a+\vec{q}_p\rangle\langle\vec{k}_a,\vec{z}_a,\vec{R}|\Psi(t)\rangle \tag{E.17}$$

E.1.4 Conditional (envelope) wave packet before the collision:

The conditional wave packet before the collision can be obtained from Equation (E.8) by fixing $\vec{z}_a=\vec{z}^j_a[t]$ and $\vec{R}=\vec{R}^j[t]$ where these positions correspond to one j experiment. Then:

$$\begin{aligned}&\Psi(\vec{r}_a,\vec{z}^j_e[t],\vec{R}^j[t],t) \\ =\;&\sum_{\vec{k},\vec{q}}a(\vec{k},\vec{q},t)\Phi_{\vec{q}}(\vec{R}^j[t])\sum_{\vec{k}_w}\phi_{\vec{k}_w}(\vec{r}_a)s_{a,w}\langle\vec{z}^j_a[t]|\hat{c}^\dagger_{\vec{k}_1}..c^\dagger_{\vec{k}_{w-1}}c^\dagger_{\vec{k}_{w+1}}..\hat{c}^\dagger_{\vec{k}_N}|0\rangle\end{aligned} \tag{E.18}$$

The dependence on $\vec{r}_a$ of the conditional wave packet in Equation (E.18) appears because of the Bloch state $\phi_{\vec{k}_w}(\vec{r}_a)\equiv\langle\vec{r}_a|\vec{k}_w\rangle$. Therefore, it can be compactly rewritten as:

$$\begin{aligned}&\psi_a(\vec{r}_a,t)\equiv\Psi(\vec{r}_a,\vec{z}^j_a[t],\vec{R}^j[t],t) \\ &=\sum_{\vec{k}_w}f_a(\vec{k}_w,\vec{z}^j_a[t],\vec{R}^j[t],t)\phi_{\vec{k}_w}(\vec{r}_a)=\sum_{\vec{k}_w}f_a(\vec{k}_w,t)\phi_{\vec{k}_w}(\vec{r}_a)\end{aligned} \tag{E.19}$$

where $f_a(\vec{k}_w,t)\equiv f_a(\vec{k}_w,\vec{z}^j_a[t],\vec{R}^j[t],t)\equiv\langle\vec{k}_w,\vec{z}^j_a[t],\vec{R}^j[t]|\Psi(t)\rangle$, appearing in Equation (5.55) and Equation (5.56) in the text, is defined here as:

$$f_a(\vec{k}_w,t)=\sum_{\vec{q}}\sum_{\vec{k},\vec{k}_e\neq\vec{k}_w}a(\vec{k},\vec{q},t)\Phi_{\vec{q}}(\vec{R}^j[t])s_{a,w}\langle\vec{z}^j_a[t]|\hat{c}^\dagger_{\vec{k}_1}..c^\dagger_{\vec{k}_{w-1}}c^\dagger_{\vec{k}_{w+1}}..\hat{c}^\dagger_{\vec{k}_N}|0\rangle \tag{E.20}$$

Under the standard envelope approximation in which the wave packet is centred around $\vec{k}_a\approx\vec{k}_{0a}$, I can rewrite the Bloch states as $\langle\vec{r}_a|\vec{k}_a\rangle=\phi_{\vec{k}_a}(\vec{r}_a)\approx e^{i\vec{k}_a\vec{r}_a}u_{\vec{k}_{0a}}(\vec{r}_a)$ and rewrite Equation (E.19) as:

$$\psi_a(\vec{r}_a,t) = u_{\vec{k}_{0a}}(\vec{r}_a)\sum_{\vec{k}_w} e^{i\vec{k}_w\vec{r}_a}\langle \vec{k}_w, \vec{z}_a^{\,j}[t], \vec{R}^j[t]|\Psi(t)\rangle$$
$$= u_{\vec{k}_{0a}}(\vec{r}_a)\sum_{\vec{k}_w} e^{i\vec{k}_w\vec{r}_a} f_a(\vec{k}_w,t) \tag{E.21}$$

I remark that $f(\vec{k}_a,t)$ includes now an (irrelevant) normalization constant. Finally, I notice that I will use the same symbol $\psi_a(\vec{r}_a,t)$ to refer to the conditional wave packet and to the envelope conditional wave function defined, by ignoring the atomic periodicity $u_{\vec{k}_{0a}}(\vec{r}_a)$, as:

$$\psi_a(\vec{r}_a,t) = \sum_{\vec{k}_w} e^{i\vec{k}_w\vec{r}_a}\langle \vec{k}_w, \vec{z}_a^{\,j}[t], \vec{R}^j[t]|\Psi(t)\rangle = \sum_{\vec{k}_w} e^{i\vec{k}_w\vec{r}_a} f_a(\vec{k}_w,t) \tag{E.22}$$

The ensemble momentum of the initial envelope wave packet $\psi_a(\vec{r}_a,t)$ in Equation (E.22), at $t = t_{c1}$ before the collision, can be written as:

$$\langle \vec{p}_a\rangle_{t_{c1}} = \sum_{\vec{k}_w} \hbar\vec{k}_w |f_a(\vec{k}_w,t)|^2 \tag{E.23}$$

E.1.5 Conditional (envelope) wave packet after the collision:

Conditioning the many-body wave function $\Psi(\vec{r}_a,\vec{z}_e,\vec{R},t)$ to the particular values of $\vec{z}_a^{\,j}[t]$ and $\vec{R}^j[t]$ belonging to the j experiment means that I am considering only one event of the many available in the wave function. In particular, from all phonon modes present in Equation (E.17), I consider that, in a particular j experiment, only one $\vec{q}_p^{\,j}[t]$ (or none) is relevant at each time t (if more than one phonon mode is relevant simultaneously then I can assume two single-phonon collisions simultaneously, each one with only one type of phonon mode). In addition, I consider that the involved wave packets are narrow enough in momentum space so that $g_{\vec{k}_a}^{\vec{q}_p,j}[t] \approx g_{\vec{k}_{0a}}^{\vec{q}_p,j}[t]$, with $\vec{k}_{0a}$ the central wave vector of the a wave packet. Then, Equation (E.17) conditioned to the value of $\vec{z}_a^{\,j}[t]$ and $\vec{R}^j[t]$ can be written as:

$$
\begin{aligned}
& H_{ep,\vec{u},\vec{r}_a}(\vec{r}_a,\vec{z}_a,\vec{R},t)\Psi(\vec{r}_a,\vec{z}_a,\vec{R},t)\big|_{\vec{z}_a^j[t]\vec{R}^j[t]} \\
= \; & g^{\vec{q}_p^j}_{\vec{k}_{0a}}[t]\sum_{\vec{k}_w}\langle\vec{r}_a|\vec{k}_w+\vec{q}_p\rangle\langle\vec{k}_w,\vec{z}_a^j[t],\vec{R}^j[t]|\Psi(t)\rangle
\end{aligned}
\tag{E.24}
$$

The coupling constant $g^{\vec{q}_p^j}_{\vec{k}_{0a}}[t]$ in the j experiment will imply an interaction of the $\vec{r}_a$ electron with the phonon mode $\vec{q}_p$ during a collision time interval, starting at t_{c1} and ending at t_{c2}. In a later time $g^{\vec{q}_p^j}_{\vec{k}_{0a}}[t]$ will indicate a collision with another phonon mode. The exact (deterministic) description of $g^{\vec{q}_p^j}_{\vec{k}_{0a}}[t]$ would require perfect knowledge of the dynamics of $\vec{R}^j[t]$. Since I do not explicitly simulate the dynamics of the ions (which are understood as the environment of the electrons), I can only introduce their effects in a stochastic way ensuring that the probabilities of different phonon modes given by $g^{\vec{q}_p^j}_{\vec{k}_{0a}}[t]$ satisfy some precomputed values. This is the origin of the stochasticity in Equation (3.11) due to the environment.

In one particular j experiment, during one collision, the term $g^{\vec{q}_q}_{\vec{k}_{0a}}[t]$ becomes irrelevant (the Bohmian velocity does only depends on the dependence of the phase on $\vec{r}_a$, not on the norm) and the final wave packet in Equation (E.24), at time $t > t_{c2}$ after the collision, can be written as:

$$
\begin{aligned}
& \psi_a(\vec{r}_a,t) \equiv \Psi(\vec{r}_a,\vec{z}_a^j[t],\vec{R}^j[t],t) = \sum_{\vec{k}_w} f_a(\vec{k}_w,\vec{z}_a^j[t],\vec{R}^j[t],t)\phi_{\vec{k}_w+\vec{q}_p}(\vec{r}_a) \\
& = \sum_{\vec{k}_w} f_a(\vec{k}_w,t)\phi_{\vec{k}_w+\vec{q}_p}(\vec{r}_a)
\end{aligned}
\tag{E.25}
$$

where $f_a(\vec{k}_w,t) = \langle\vec{k}_w,\vec{z}_a^j[t],\vec{R}^j[t]|\Psi(t)\rangle$ remains equal to the value in Equation (E.20) before the collision.

After the collision at $t = t_{c2}$, the (pseudo) momentum base changes from $|\vec{k}_e\rangle$ to $|\vec{k}_e + \vec{q}_p^j\rangle$, so that the final ensemble momentum of the envelope conditional wave packet in Equation (E.25) is:

$$
\langle\vec{p}_a\rangle_{t_{c2}} = \sum_{\vec{k}_w}\hbar(\vec{k}_w+\vec{q}_p^j)|f_a(\vec{k}_w,t)|^2 = \langle\vec{p}_a\rangle_{t_{c1}} + \hbar\vec{q}_p^j \tag{E.26}
$$

Let me emphasize that Equation (E.23) and Equation (E.26) provide the expected role of the electron-phonon interaction: Such collision generates a change of momentum $\hbar\vec{q}_p^{\,j}$ in the conditional wave packet during a time interval $t_{c2} - t_{c1}$. I remark that I am considering a collision with a finite duration. As it will be later explained, for simplicity in practical applications, I have considered instantaneous collisions in the text.

E.2 Evaluation of the term $\langle \vec{r}_a, \vec{z}_a, \vec{R}|\hat{\mathcal{H}}_c|\Psi(t)\rangle|_{\vec{z}_a^{\,j}[t],\vec{R}^j[t]}$ in Equation (5.50):

The term $\langle \vec{r}_a, \vec{z}_a, \vec{R}|\hat{\mathcal{H}}_c|\Psi(t)\rangle|_{\vec{z}_a^{\,j}[t],\vec{R}^j[t]} = \langle \vec{r}_a, \vec{z}_a, \vec{R}|K_e(\vec{r}) + K_h(\vec{R}) + V_{ee}(\vec{r}) + V_{hh}(\vec{R}) + H_{ep,\vec{R}_0}(\vec{r},\vec{R}_0)|\Psi(t)\rangle|_{\vec{z}_a^{\,j}[t],\vec{R}^j[t]}$ can be evaluated as follows. First, I divide $V_{ee}(\vec{r}) = V_{ee,\vec{r}_a}(\vec{r}_a) + V_{ee,\vec{z}_a}(\vec{z}_a)$ as the terms with an explicit dependence on $\vec{r}_a$, plus the terms without it. Similarly, $H_{ep,\vec{R}_0}(\vec{r},\vec{R}_0) = H_{ep,\vec{R}_0,\vec{r}_a}(\vec{r}_a,\vec{R}_0) + H_{ep,\vec{R}_0,\vec{z}_a}(\vec{z}_a,\vec{R}_0)$.

E.2.1 Evaluation of $\langle \vec{r}_a, \vec{z}_a, \vec{R}|\hat{\mathcal{V}}_{hh} + \hat{\mathcal{V}}_{ee,\vec{z}_a} + \hat{H}_{ep,\vec{R}_0,\vec{z}_a}|\Psi(t)\rangle|_{\vec{z}_a^{\,j}[t],\vec{R}^j[t]}$:

I have:

$$\langle \vec{r}_a, \vec{z}_a, \vec{R}|\hat{\mathcal{V}}_{hh} + \hat{\mathcal{V}}_{ee,\vec{z}_a} + \hat{H}_{ep,\vec{R}_0,\vec{z}_a}|\Psi(t)\rangle|_{\vec{z}_a^{\,j}[t],\vec{R}^j[t]} = \tag{E.27}$$
$$\left(V_{hh}(\vec{R}^j[t]) + V_{ee,\vec{z}_a}(\vec{z}_a^{\,j}[t]) + H_{ep,\vec{R}_0,\vec{z}_a}(\vec{z}_a^{\,j}[t],\vec{R}_0)\right)\Psi(\vec{r}_a,\vec{z}_a^{\,j}[t],\vec{R}^j[t],t)$$

where $V_{hh}(\vec{R}^j[t]) + V_{ee,\vec{z}_a}(\vec{z}_a^{\,j}[t]) + H_{ep,\vec{R}_0,\vec{z}_a}(\vec{z}_a^{\,j}[t],\vec{R}_0)$ are pure time-dependent terms, without $\vec{r}_a$ dependence and then it only contributes to an arbitrary pure time-dependent angle that can be directly ignored, see [72].

E.2.2 Evaluation of $\langle \vec{r}_a, \vec{z}_a, \vec{R}|\hat{\mathcal{V}}_{ee,\vec{r}_a}|\Psi(t)\rangle|_{\vec{z}_a^{\,j}[t],\vec{R}^j[t]}$:

Similarly, I write:

$$\langle \vec{r}_a, \vec{z}_a, \vec{R}|\hat{\mathcal{V}}_{ee,\vec{r}_a}\Psi(t)\rangle|_{\vec{z}_a^{\,j}[t],\vec{R}^j[t]} = V_{ee,\vec{r}_a}(\vec{r}_a,\vec{z}_a^{\,j}[t])|\Psi(\vec{r}_a,\vec{z}_a^{\,j}[t],\vec{R}^j[t],t)$$
$$= u_{\vec{k}_{0a}}(\vec{r}_a)V_{ee,\vec{r}_a}(\vec{r}_a,\vec{z}_a^{\,j}[t])\psi_a(\vec{r}_a,t) \tag{E.28}$$

where $V_{ee,\vec{r}_a}(\vec{r}_a,\vec{z}_a^{\,j}[t])$ can be easily known once the set of $\vec{r}^{\,j}[t]$ trajectories are known. Later I will use $V_a \equiv V_{ee,\vec{r}_a}(\vec{r}_a,\vec{z}_a^{\,j}[t])$.

E.2.3 Evaluation of $\langle \vec{r}_a, \vec{z}_a, \vec{R}|\hat{\mathcal{K}}_{e,\vec{z}_a} + \hat{\mathcal{K}}_h|\Psi(t)\rangle|_{\vec{z}_a^j[t],\vec{R}^j[t]}$:

The kinetic energy of ions $\hat{\mathcal{K}}_h$ and the kinetic energy of the rest of electrons, different from $\vec{r}_a$, defined as $\hat{\mathcal{K}}_{e,\vec{z}_a}$ with $\hat{\mathcal{K}}_e = \hat{\mathcal{K}}_{e,\vec{r}_a} + \hat{\mathcal{K}}_{e,\vec{z}_a}$, can be written as:

$$\begin{aligned}
&\langle \vec{r}_a, \vec{z}_a, \vec{R}|\hat{\mathcal{K}}_{e,\vec{z}_a} + \hat{\mathcal{K}}_h|\Psi(t)\rangle|_{\vec{z}_a^j[t],\vec{R}^j[t]} \qquad \text{(E.29)}\\
&= \sum_{e=1,e\neq a}^{N_e} K_{e,\vec{r}_a}\Psi(\vec{r}_a, \vec{z}_a, \vec{R}, t)\big|_{\vec{z}_a^j[t],\vec{R}^j[t]} + \sum_{h=1}^{N_h} \frac{-\hbar^2}{2m_h}\vec{\nabla}_h^2\Psi(\vec{r}_a, \vec{z}_a, \vec{R}, t)\big|_{\vec{z}_a^j[t],\vec{R}^j[t]}\\
&= A(\vec{r}_a, \vec{z}_a^j[t], \vec{R}^j[t], t)\Psi(\vec{r}_a, \vec{z}_a^j[t], \vec{R}^j[t], t) = u_{\vec{k}_{0a}}(\vec{r}_a)A_a(\vec{r}_a, \vec{z}_a^j[t], \vec{R}^j[t], t)\psi_a(\vec{r}_a, t)
\end{aligned}$$

where $K_{e,\vec{r}_a}$ is the kinetic energy of each $\vec{z}_a$ electron and where I have introduced the real potential A_a as:

$$\begin{aligned}
&A_a \equiv A_a(\vec{r}_a, \vec{z}_a^j[t], \vec{R}^j[t], t) \qquad \text{(E.30)}\\
&= \frac{\sum_{e=1,e\neq a}^{N_e} K_{e,\vec{r}_a}\Psi(\vec{r}_a, \vec{z}_a, \vec{R}, t)\big|_{\vec{z}_a^j[t],\vec{R}^j[t]}}{\Psi(\vec{r}_a, \vec{z}_a^j[t], \vec{R}^j[t], t)} + \frac{\sum_{h=1}^{N_h} \frac{-\hbar^2}{2m_h}\vec{\nabla}_h^2\Psi(\vec{r}_a, \vec{z}_a, \vec{R}, t)\big|_{\vec{z}_a^j[t],\vec{R}^j[t]}}{\Psi(\vec{r}_a, \vec{z}_a^j[t], \vec{R}^j[t], t)}
\end{aligned}$$

This constant A_a includes other correlations (different from the electron-lattice correlations that I treat exactly apart from the stochastic approximation for ions dynamics) and will be approximated later according to Ref.[72].

E.2.4 Evaluation of $\langle \vec{r}_a, \vec{z}_a, \vec{R}|\hat{\mathcal{K}}_{e,\vec{r}_a} + \hat{\mathcal{H}}_{ep,\vec{R}_0,\vec{r}_a}|\Psi(t)\rangle|_{\vec{z}_a^j[t],\vec{R}^j[t]}$:

The last terms that have to be evaluated from $\hat{\mathcal{H}}_c$ in Equation (5.49) are $\hat{\mathcal{K}}_{e,\vec{r}_a} + \hat{\mathcal{H}}_{ep,\vec{R}_0,\vec{r}_a}$. They determine the electronic band structure:

$$\begin{aligned}
&\langle \vec{r}_a, \vec{z}_a, \vec{R}|\hat{\mathcal{K}}_{e,\vec{r}_a} + \hat{\mathcal{H}}_{ep,\vec{R}_0,\vec{r}_a}|\Psi(t)\rangle|_{\vec{z}_a^j[t],\vec{R}^j[t]} \qquad \text{(E.31)}\\
&= \left(K_{e,\vec{r}_a} + \sum_h V_{ep}(\vec{r}_a - \vec{R}_{h,0})\right)\Psi(\vec{r}_a, \vec{z}_a^j[t], \vec{R}^j[t], t)
\end{aligned}$$

where $K_{e,\vec{r}_a}$ corresponds to the kinetic energy of the conditioned a electron and $H_{ep,\vec{R}_0,\vec{r}_a} = \sum_h V_{ep}(\vec{r}_a - \vec{R}_{h,0})$ is the periodic potential seen by this a electron. From here, and after a tight binding and the approximation for low energy excitations (small $\vec{k}$), depending

on the system I will end up with a band structure $E(\vec{p})$ either with linear or parabolic shape. Therefore:

$$\langle \vec{r}_a, \vec{z}_a, \vec{R}|\hat{\mathcal{K}}_{e,\vec{r}_a} + \hat{\mathcal{H}}_{ep,\vec{R}_0,\vec{r}_a}|\Psi(t)\rangle|_{\vec{z}_a^j[t],\vec{R}^j[t]} \approx u_{\vec{k}_{0a}}(\vec{r}_a)E(\vec{p})\psi_a(\vec{r}_a,t) \tag{E.32}$$

where $\psi_a(\vec{r}_a,t)$ is the (conditional) envelope wave packet already defined in Equation (E.21).

E.3 Schrödinger (parabolic band) equation

In the parabolic case, $E(\vec{p}_a)$ appearing in Equation (E.32) is $E(\vec{p}_a) = \frac{|\vec{p}_a|^2}{2m^*}$ with m^* an isotropic effective mass. After the collision, $t = t_{c2}$, regarding Equation (E.25) the state $|\vec{k}_e\rangle$ changes to $|\vec{k}_e + \vec{q}_p^j\rangle$. Under the mentioned envelope approximation, the Bloch states are $\langle \vec{r}_a|\vec{k}_a\rangle = \phi_{\vec{k}_a}(\vec{r}_a) \approx e^{i\vec{k}_a\vec{r}_a}u_{\vec{k}_{0a}}(\vec{r}_a)$. Then, the conditional wave packet at t_{c2} in Equation (E.25) can be related to the initial wave packet at t_{c1} given by Equation (E.22) as:

$$\begin{aligned}\psi_a(\vec{r}_a,t_{c2}) &= \sum_{\vec{k}_w} e^{i(\vec{k}_w+\vec{q}_p)\vec{r}_a}\langle \vec{k}_w, \vec{z}_a^j[t_{c2}], \vec{R}^j[t_{c2}]|\Psi(t_{c2})\rangle \\ &= \sum_{\vec{k}_w} e^{i(\vec{k}_w+\vec{q}_p)\vec{r}_a} f_a(\vec{k}_w,t_{c2}) = e^{i\vec{q}_p\vec{r}_a}\psi_a(\vec{r}_a,t_{c1})\end{aligned} \tag{E.33}$$

Therefore, since Bloch states are energy eigenstates, the ensemble energy before the collision $\langle E(\vec{k}_a)\rangle_{t_{c1}}$ changes to the value $\langle E(\vec{k}_a+\vec{q}_p)\rangle_{t_{c2}}$ after the collision. Putting together Equation (E.28), Equation (E.30) and Equation (E.32) into the original Equation (5.49), and removing $u_{\vec{k}_{0a}}(\vec{r}_a)$, I get:

$$i\hbar\frac{\partial\psi_a(\vec{r}_a,t)}{\partial t} = \left[\frac{1}{2m^*}(\vec{p}_a)^2 + V_a + A_a + iB_a\right]\psi_a(\vec{r}_a,t) \tag{E.34}$$

where the terms A_a and B_a in Equation (E.31) are approximated by a zero order Taylor expansion (i.e. no dependence on $\vec{r}_a$) so that they can be neglected when computing Bohmian velocities. See in [72] the discussion of such approximation. Therefore, the time evolution operator (propagator) from the initial time t_0 until a time before the

collision $t < t_{c1}$ is just $\hat{\mathcal{U}}_a(t,t_0) = e^{-\frac{i}{\hbar}\int_{t_0}^{t}\hat{\mathcal{H}}_{ca}(t')dt'}$, with $H_{ca} = \frac{1}{2m^*}(\vec{p}_a)^2 + V_a$, being H_c conditioned at $\vec{z}_a^{j}[t]$.

The time-evolution of the wave packet due to the collision with the phonon has to reproduce the condition given by Equation (E.33). The time evolution operator (propagator) from $t = t_0$ until a time $t > t_{c2}$ after the collision is then:

$$\begin{aligned}\hat{\mathcal{U}}_a(t,t_0) &= e^{-\frac{i}{\hbar}\int_{t_{c2}}^{t}\hat{\mathcal{H}}_{ca}(t')dt'}e^{-\frac{i}{\hbar}\int_{t_{c1}}^{t_{c2}}\hat{\mathcal{H}}_{epa}(t')dt'} \\ e^{-\frac{i}{\hbar}\int_{t_0}^{t_{c1}}\hat{\mathcal{H}}_{ca}(t')dt'} &= e^{-\frac{i}{\hbar}\int_{t_{c2}}^{t}\hat{\mathcal{H}}_{ca}(t')dt'}e^{i\frac{\vec{\lambda}_a\vec{r}_a}{\hbar}}e^{-\frac{i}{\hbar}\int_{t_0}^{t_{c1}}\hat{\mathcal{H}}_{ca}(t')dt'}\end{aligned} \tag{E.35}$$

where $\hat{\mathcal{H}}_{epa} = -\hbar\vec{\lambda}_a\vec{r}_a\delta(t-t_c)$ is the previously mentioned total electron-lattice interaction $\hat{\mathcal{H}}_{ep}$ conditioned at $\vec{z}_a^{j}[t]$.

For a small time interval, Δt, I have $\hat{\mathcal{U}}_a(t+\Delta t,t) = (1 - \frac{i}{\hbar}\Delta t\hat{\mathcal{H}}_{ca})$. Then, it can be proven that $(1 - \frac{i}{\hbar}\Delta t H_{ca})e^{i\frac{\vec{\lambda}_a\vec{r}_a}{\hbar}}\psi_a(\vec{r}_a,t_{c1}) = e^{i\frac{\vec{\lambda}_a\vec{r}_a}{\hbar}}(1 - \frac{i}{\hbar}\Delta t H_{ca+\lambda})\psi_a(\vec{r}_a,t_{c1})$, where $H_{ca+\lambda} = \frac{(\vec{p}_a+\vec{\lambda}_a)^2}{2m^*} + V_a$. The demonstration of this result just requires to show that:

$$\begin{aligned}&(\vec{p})^2 e^{i\frac{\vec{\lambda}_a\vec{r}_a}{\hbar}}\psi_a(\vec{r}_a,t) = -\hbar^2\vec{\nabla}^2 e^{-i\frac{\vec{\lambda}_a\vec{r}_a}{\hbar}}\psi_a(\vec{r}_a,t) \\ &= \vec{\lambda}_a^2 e^{i\frac{\vec{\lambda}_a\vec{r}_a}{\hbar}}\psi_a(\vec{r}_a,t) - 2i\hbar\vec{\lambda}_a e^{i\frac{\vec{\lambda}_a\vec{r}_a}{\hbar}}\vec{\nabla}\psi_a(\vec{r}_a,t) - \hbar^2 e^{i\frac{\vec{\lambda}_a\vec{r}_a}{\hbar}}\vec{\nabla}^2\psi_a(\vec{r}_a,t) = e^{i\frac{\vec{\lambda}_a\vec{r}_a}{\hbar}}(\vec{p}+\vec{\lambda}_a)^2\psi_a(\vec{r}_a,t)\end{aligned} \tag{E.36}$$

Therefore, the time evolution of the conditional wave packet at any time $t = t_{c2} + n\Delta t$ can be computed by applying the previous property n times and then:

$$\begin{aligned}&(1 - \frac{i}{\hbar}\Delta t H_{ca})...(1 - \frac{i}{\hbar}\Delta t H_{ca})e^{i\frac{\vec{\lambda}_a\vec{r}_a}{\hbar}}\psi_a(\vec{r}_a,t_{c1}) \\ &= e^{i\frac{\vec{\lambda}_a\vec{r}_a}{\hbar}}(1 - \frac{i}{\hbar}\Delta t H_{ca+\lambda})...(1 - \frac{i}{\hbar}\Delta t H_{ca+\lambda})\psi_a(\vec{r}_a,t_{c1})\end{aligned} \tag{E.37}$$

Finally, I can combine the time evolution of the envelope conditional wave packet $\psi_a(\vec{r}_a,t)$ before and after the collision in a unique equation of motion as:

$$i\hbar\frac{\partial\psi_a}{\partial t} = \left[\frac{1}{2m^*}\left(\vec{p}_a + \vec{\lambda}_a\Theta_t\right)^2 + V_a\right]\psi_a \tag{E.38}$$

where $\Theta_t(t)$ can be any function which accomplishes that $\Theta_t(t) = 0$ before the collision ($t < t_{c1}$) and $\Theta_t(t) = 1$ after the collision ($t > t_{c2}$). For practical purposes and to facilitate computations, in the numerical results I consider $\Theta_t \equiv \Theta_{t_c}$ to be the Heaviside step function, $t = t_c$ the time when the interaction occurs and t_{c2} a time infinitely small after t_c and t_{c1} a time infinitely small before t_c. Time interval $t_{c2} - t_{c1}$ can be roughly estimated from time-energy uncertainty relations and it gives a value on the order of few fs. If a more slow/adiabatic evolution of the collision is required in some practical implementations, the equation of motion in Equation (E.38) can be easily adapted to a slower or more adiabatic collision processes by just splitting the whole momentum exchange taking place during one time step of the simulation into more steps but with smaller momentum exchange. This equation of motion of the conditional wave function reproduces Equation (5.57) for the conditional wave packet suffering an electron-lattice interaction with parabolic energy bands. I emphasize that the stochasticity is introduced into Equation (E.38) because the exact (Bohmian) path of the ions $\vec{R}^j[t]$ is not explicitly simulated. Their effect is introduced into the dynamics of the electron $\vec{r}_a^j[t]$ through the random selection of collision times and phonon modes satisfying some *well-known* probability distributions.

By construction, the time evolution of $\psi(\vec{r}_a, t)$ before and after the collision is fully coherent. The main and important difference is the change of momentum. For example, in a double barrier, a collision adding and subtracting the momentum $\vec{\lambda}_a = \hbar\vec{q}_p$ in the wave function $\psi(\vec{r}_a, t)$ can convert a non resonant state into a resonant one or vice versa. Until here, only collisions within a unique band have been considered. The implementation in electron-phonon multibands models (already indicated below Equation (E.16)) or other types of collision could be straightforwardly done.

E.4 Dirac (linear band) equation

In the linear case, $E(\vec{p}_a) = \pm v_f|\vec{p}_a|$, with v_f the Fermi velocity. The same development done for the Schrödinger equation can be followed here for the evolution of the 2D bispinor solution of the Dirac equation, with a slight difference appearing because the wave function is a bispinor wave function Equation (4.39). The Bloch energy eigenstates $|\vec{k}_a\rangle$ defined in Equation (E.7) have to be substituted by $|\vec{k}_a, s_a\rangle$ defined as:

$$\phi_{\vec{k}_a,s_a} = \langle\vec{r}_a|\vec{k}_a, s_a\rangle = \frac{u_{\vec{k}_a} e^{i\vec{k}_a\vec{r}_a}}{\sqrt{2}} \begin{pmatrix} 1 \\ s_a e^{i\beta_{\vec{k}_a}} \end{pmatrix} \tag{E.39}$$

where s_a indicates if the electron is in the conduction ($s_a = 1$) or valence ($s_a = -1$) band, with positive or negative energies, respectively. I have defined $e^{i\beta_{\vec{k}_i}} = \frac{k_{ix}+ik_{iy}}{\sqrt{k_{ix}^2+k_{iy}^2}}$ and $\beta_{\vec{k}_i}$ the angle of the $\vec{k}_i$ wave vector.

All developments done previously for a parabolic band can be reproduced here by just introducing the appropriate index s_a and the bispinor. In particular, the initial conditional envelope wave packet before the collision in Equation (E.22) is rewritten here as:

$$\begin{aligned}\psi_a(\vec{r}_a,t) &= \begin{pmatrix}\psi_{a,1}(\vec{r}_a,t)\\ \psi_{a,2}(\vec{r}_a,t)\end{pmatrix} = \sum_{\vec{k}_w}\begin{pmatrix}1\\ s_a e^{i\beta_{\vec{k}_w}}\end{pmatrix} f_a(\vec{k}_w,t)e^{i\vec{k}_w\vec{r}_a}\\ &\approx \begin{pmatrix}1\\ s_{0a}e^{i\beta_{\vec{k}_{0a}}}\end{pmatrix}\sum_{\vec{k}_w} f_a(\vec{k}_w,t)e^{i\vec{k}_w\vec{r}_a}\end{aligned} \tag{E.40}$$

where I have assumed again that $\vec{k}_w \approx \vec{k}_{0a}$ and $s_a \approx s_{0a}$ with s_{0a} indicating that the initial wave packet belongs to the conduction ($s_{0a} = 1$) or valence ($s_{0a} = -1$) band. Identically, the coupling constant defined in Equation (E.16) has to be substituted by the new one:

$$\begin{aligned}g^{\vec{q}_p}_{\vec{k}_a,s_a,s'_a} =& -i\vec{Q}_{\vec{q}_p}\ \vec{q}_p\ U_{\vec{q}_p}\int_{\vec{r'}_a} d\vec{r'}_a e^{-i(\vec{k}_a+\vec{q}_p)\vec{r'}_a}\\ & u_{\vec{k}_a+\vec{q}_p}(\vec{r'}_a)e^{i\vec{k}_a\vec{r'}_a}u_{\vec{k}_a}(\vec{r'}_a)e^{i\vec{v}\vec{r'}_a}\left(\frac{1+s_a\ s'_a\ e^{i(\beta_{\vec{k}_a}-\beta_{\vec{k}_a+\vec{q}_p})}}{2}\right)\end{aligned} \tag{E.41}$$

which contains the information of the transition from the initial energy branch s_a to the final branch s'_a. It is assumed again that, in a particular experiment j, only one $\vec{q}_p[t]$ (or none) is relevant at each time and that $g^{\vec{q}_p,j}_{\vec{k}_a,s_a,s'_a}[t] \approx g^{\vec{q}_p,j}_{\vec{k}_{0a},s_{0a},s_{fa}}[t]$ where s_{fa} indicates that the final wave packet is in the conduction ($s_{fa} = 1$) or valence ($s_{fa} = -1$) band (more exotic collisions with final presence of the wave packet at both energy branches can be considered by two collisions with the one final-branch-collision process mentioned here). Then, the condition given in Equation (E.33) between the envelope conditional wave packet before and after the collision with parabolic energy bands can be straightforwardly rewritten here as:

$$\begin{aligned}\psi_a(\vec{r}_a,t_{c2}) &= \sum_{\vec{k}_w}\begin{pmatrix}1\\ s_{fa}\ e^{i\beta_{\vec{k}_w+\vec{q}_p}}\end{pmatrix} f_a(\vec{k}_w,t_{c1})e^{i\vec{k}_w\vec{r}_a}e^{i\vec{q}_p\vec{r}_a}\\ &= e^{i\frac{\vec{\lambda}_a\vec{r}_a}{\hbar}}\sum_{\vec{k}_w}\begin{pmatrix}1\\ s_{fa}s_{0a}e^{i(\beta_{\vec{k}_w+\vec{q}_p}-\beta_{\vec{k}_w})}s_{0a}e^{i\beta_{\vec{k}_w}}\end{pmatrix} f_a(\vec{k}_w,t_{c1})e^{i\vec{k}_w\vec{r}_a}\\ &\approx e^{i\frac{\vec{\lambda}_a\vec{r}_a}{\hbar}}\begin{pmatrix}1 & 0\\ 0 & e^{i\alpha_a}\end{pmatrix}\begin{pmatrix}1\\ s_{0a}e^{i\beta_{\vec{k}_w}}\end{pmatrix}\sum_{\vec{k}_w} f_a(\vec{k}_w,t_{c1})e^{i\vec{k}_w\vec{r}_a}\end{aligned} \tag{E.42}$$

where I have introduced $s_{0a}\ s_{0a}=1$ and $e^{-i\beta_{\vec{k}_w}}e^{i\beta_{\vec{k}_w}}=1$. I define $s_{fa}\ s_{0a}=e^{im\pi}$ where $m\pi$ reflects the changing from one branch to the other due to the absorption/emission of the phonon ($m=1$) or the collision without changing ($m=0$). I have finally defined $\alpha_a = m\pi+\beta_{\vec{k}_{fa}}-\beta_{\vec{k}_{0a}}$. I can then rewrite compactly Equation (E.42) as:

$$\psi_a(\vec{r}_a,t_{c2}) = \begin{pmatrix}\psi_{a,1}(\vec{r}_a,t_{c2})\\ \psi_{a,2}(\vec{r}_a,t_{c2})\end{pmatrix} \approx e^{i\frac{\vec{\lambda}_a\vec{r}_a}{\hbar}}\begin{pmatrix}\psi_{a,1}(\vec{r}_a,t_{c1})\\ e^{i\alpha_a}\psi_{a,2}(\vec{r}_a,t_{c1})\end{pmatrix} \tag{E.43}$$

With the same development done for the parabolic band, I know that the time-evolution of $\psi_a(\vec{r}_a,t)$ before the collision is given by the 2D Dirac equation as:

$$\begin{aligned} i\hbar\frac{\partial\psi_a}{\partial t} &= \left(v_f\hat{\sigma}_x p_{ax}+v_f\hat{\sigma}_y p_{ay}+(V_a+A_a+iB_a)\hat{I}\right)\psi_a\\ &= \begin{pmatrix}V_a+A_a+iB_a & v_f p_a^-\\ v_f p_a^+ & V_a+A_a+iB_a\end{pmatrix}\psi_a\end{aligned} \tag{E.44}$$

with $\hat{\sigma}_x=\begin{pmatrix}0&1\\1&0\end{pmatrix}$ and $\hat{\sigma}_y=\begin{pmatrix}0&-i\\i&0\end{pmatrix}$ the Pauli matrices, $\hat{I}=\begin{pmatrix}1&0\\0&1\end{pmatrix}$ the identity matrix, $\vec{p}=\{p_{ax},p_{ay}\}=\{-i\hbar\partial_x,-i\hbar\partial_y\}$ and $p_a^{\pm}=-i\hbar\partial_{x_a}\pm\hbar\partial_{y_a}$. With the same approximations used in Equation (E.34) for A_a and B_a based on Ref. [72], I get the following time evolution operator (propagator) from the initial time $t=t_0$ until a time before the collision $t<t_{c1}$ as $\hat{\mathcal{U}}_a(t,t_0)=e^{-\frac{i}{\hbar}\int_{t_0}^{t}\hat{\mathcal{H}}_{ca}(t')dt'}$ with $H_{ca}=v_f(\hat{\sigma}_x p_{ax}+\hat{\sigma}_y p_{ay})+V_a\hat{I}$. Again I can define the time evolution operator for any time larger than the collision $t>t_{c2}$ as:

$$\hat{\mathcal{U}}_a(t,t_0)=e^{-\frac{i}{\hbar}\int_{t_{c2}}^{t}\hat{\mathcal{H}}_{ca}(t')dt'}e^{-\frac{i}{\hbar}\int_{t_{c1}}^{t_{c2}}\hat{\mathcal{H}}_{epa}(t')dt'}e^{-\frac{i}{\hbar}\int_{t_{c1}}^{t_{c2}}\hat{\mathcal{H}}_{sa}(t')dt'}e^{-\frac{i}{\hbar}\int_{t_0}^{t_{c1}}\hat{\mathcal{H}}_{ca}(t')dt'} \tag{E.45}$$

with the interacting Hamiltonian given by $\mathcal{H}_{epa} = -\hbar\vec{\lambda}_a\vec{r}_a\delta(t-t_c)\hat{I}$ and $\mathcal{H}_{sa} = -\hbar\delta(t-t_c)\begin{pmatrix}1 & 0\\ 0 & \alpha_a\end{pmatrix}$. With this time-dependent Hamiltonian, it can be easily demonstrated that Equation (E.43) is satisfied:

$$\begin{aligned}\psi_a(\vec{r}_a,t_{c2}) &= \begin{pmatrix} e^{i\frac{\vec{\lambda}_a\vec{r}_a}{\hbar}}\psi_{a,1}(\vec{r}_a,t_{c1}) \\ e^{i\frac{\vec{\lambda}_a\vec{r}_a}{\hbar}}e^{i\alpha_a}\psi_{a,2}(\vec{r}_a,t_{c1})\end{pmatrix} \\ &= e^{-\frac{i}{\hbar}\int_{t_{c1}}^{t_{c2}}\hat{\mathcal{H}}_{epa}(t')dt'}e^{-\frac{i}{\hbar}\int_{t_{c1}}^{t_{c2}}\hat{\mathcal{H}}_{sa}(t')dt'}\psi_a(\vec{r}_a,t_{c1})\end{aligned} \tag{E.46}$$

It can also be demonstrated that $(p_a^+)e^{i\frac{\vec{\lambda}_a\vec{r}_a}{\hbar}}\psi_{a,1}(\vec{r}_a,t) = e^{i\frac{\vec{\lambda}_a\vec{r}_a}{\hbar}}(p_a^+ + \lambda_a^+)\psi_{a,1}(\vec{r}_a,t)$. Identically, $(p_a^-)e^{i\frac{\vec{\lambda}_a\vec{r}_a}{\hbar}}\psi_{a,2}(\vec{r}_a,t) = e^{i\frac{\vec{\lambda}_a\vec{r}_a}{\hbar}}(p_a^- + \lambda_a^-)\psi_{a,2}(\vec{r}_a,t)$, where I have defined $\lambda_a^\pm = \lambda_{ax} \pm i\lambda_{ay}$. Therefore, I have proved for the bispinor:

$$\begin{aligned}&(1-\frac{i}{\hbar}\Delta t\hat{\mathcal{H}}_{ca})....(1-\frac{i}{\hbar}\Delta t\hat{\mathcal{H}}_{ca})e^{i\frac{\vec{\lambda}_a\vec{r}_a}{\hbar}}\psi_a(\vec{r}_a,t_{c1}) \\ &= e^{i\frac{\vec{\lambda}_a\vec{r}_a}{\hbar}}(1-\frac{i}{\hbar}\Delta t\hat{\mathcal{H}}_{ca+\lambda})...(1-\frac{i}{\hbar}\Delta t\hat{\mathcal{H}}_{ca+\lambda})\psi_a(\vec{r}_a,t_{c1})\end{aligned} \tag{E.47}$$

with $\hat{H}_{ca+\lambda} = v_f(\hat{\sigma}_x(p_{ax}+\lambda_{ax}) + \hat{\sigma}_y(p_{ay}+\lambda_{ay})) + V_a\hat{I}$. Notice that I have still not considered the effect of the term $e^{-\frac{i}{\hbar}\int_{t_{c1}}^{t_{c2}}\hat{\mathcal{H}}_{sa}(t')dt'}$. It includes an angle $e^{i\alpha_a}$ in the second element of the bispinor at time $t = t_{c1}$. As discussed in Appendix C, in most practical applications, for simplicity, I assume an instantaneous collision. A slower or more adiabatic collision process is also easily implementable. Finally, the global equation of motion of the conditional bispinor that includes all mentioned dynamics and is valid for any time, either before or after the collision, is:

$$i\hbar\frac{\partial\psi_a(\vec{r}_a,t)}{\partial t} = v_f\begin{pmatrix} V_a/v_f & p_a^- + \lambda_a^-\Theta_{tc} \\ (p_a^+ + \lambda_a^+\Theta_{tc})\chi_{t_c} & V_a\chi_{t_c}/v_f\end{pmatrix}\psi_a(\vec{r}_a,t) \tag{E.48}$$

As I explained below the term $\chi_{t_c} = exp(i(m\pi + \beta_{\vec{k}_{fa}} - \beta_{\vec{k}_{0a}})\Lambda_{t_c})$ projects the general bispinor into positive or negative energy states, and for practical purposes in the numerical results I chose Θ_{tc} to be the Heaviside step function. This equation of motion exactly reproduces Equation (5.58). I emphasize again that the stochasticity is introduced into Equation (E.44) because the exact (Bohmian) path of the ions $\vec{R}^j[t]$ is not explicitly

simulated. Their effect is introduced into the dynamics of the electron $\vec{r}_a^{\,j}[t]$ through the random selection of collision times and phonon modes satisfying some *well-known* probability distributions.

I achieve the same conclusion as in the Schrödinger case: the time evolution of $\psi(\vec{r}_a, t)$ before and after the collision is fully coherent. For example, as it is shown in Section 5.3, if a collision occurs with an initial electron whose direction was not perpendicular to a potential barrier (and therefore will not suffer Klein tunneling) and that collision changes the electron direction appropriately, the electron can experience the full Klein tunnelling effect.

Appendix F

Number of electrons in a region of the phase space

F.1 Number of electrons in a region of the phase space

To simplify the discussion, I use a 1D phase-space and consider electrons (fermions) without spin. The spatial borders of the phase space are selected, arbitrarily, as $x = 0$ and $x = L$. The common argument used in the literature counts the number of Hamiltonian eigenstates fitting inside in the phase-space, when applying the well-known Born-von Karman periodic boundary conditions [90]. The result is that each electron requires a partial volume of 2π of the phase space, as indicated in Equation (6.24) in the text. After discussing the limitations of this procedure, the same result by imposing the exchange interaction among electrons associated to time-dependent wave packets is obtained.

F.1.1 Limitations of the Born-von Karman periodic boundary conditions

The single-particle Hamiltonian eigenstates of a semiconductor can be written as Bloch states $\Psi(x) \propto e^{ik_x x}$ so that, by imposing the Born-von Karman periodic boundary conditions on the spatial borders of the phase space, $\Psi(x + L) = \Psi(x)$, we require that $e^{ik_x L} = 1$. Thus, I conclude that the allowed wave vectors k_x have to take the discrete values:

$$k_x = 2\pi \frac{j}{L} = \Delta k_x \cdot j \tag{F.1}$$

for $j = 0, \pm 1, \pm 2, \ldots$ with $\Delta k_x = 2\pi/L$. Because of the Pauli exclusion principle, two electrons can not be associated to the same state $\Psi(x) \propto e^{ik_x x}$, i.e., to the same k_x. Therefore, the number of electrons in the $1D$ phase space, at zero temperature, is just $n_{1D} = k_f/\Delta k_x = k_f \cdot L/(2\pi)$ with k_f the wave vector associated to the Fermi energy. Thus, the well-known density of states in the $1D$ phase space (without spin or valley degeneracies) gives that each electron requires a volume of 2π of the phase space, in agreement with Equation (6.24) in the text.

In the above procedure, we give an unphysical definition of the values Δk_x and Δx mentioned in Eq.(1) in the manuscript. We assume that each electron described by $\Psi(x) \propto e^{ik_x x}$ has a spatial extension $\Delta x = L$, then, using $\Delta x \cdot \Delta k_x = 2\pi$ we get $\Delta k_x = 2\pi/L$. We argue here that a time dependent modeling of transport cannot be based on time-independent energy eigenstates $\Psi(x) \propto e^{ik_x x}$. We are interested in electrons moving from the left contact (i.e. with an initial probability located at the left), traveling along the active region, until the electron reach the right contact (i.e. with a final probability located at the right). Next, we discuss how the number of electrons in the phase space can be counted with time-dependent wave packets.

F.1.2 Exchange interaction among electrons in free space

I remark the wave nature of electrons in our 1D system using, for example, a Gaussian wave packet:

$$\psi_j(x) = \frac{1}{(\pi\sigma_x^2)^{1/4}} \exp\left(ik_{oj}\ (x - x_{oj})\right) \exp\left(-\frac{(x - x_{oj})^2}{2\sigma_x^2}\right) \tag{F.2}$$

where the electron wave function is located around the central position x_{oj} and central wave vector k_{oj}. The spatial dispersion in the position space is σ_x, and in the wave vector space $\sigma_k = 1/\sigma_x$. Strictly speaking, Equation (F.2) is the envelop of a wave function that varies smoothly in the atomistic resolution of a semiconductor. The normalization condition can be written as $\int_{-\infty}^{\infty} dx |\psi_j(x)|^2 = 1$.

I consider a first wave packet $\psi_1(x)$ located somewhere in the phase space and a second wave packet $\psi_2(x)$, initially far from the first wave packet, that approaches the first one, for example, because of the interaction with all other electrons. I simplify the many body dynamics by considering that the first wave packet has fixed the central position x_{01} and central wave vector k_{o1} and that the second one keeps the shape given by Equation (F.2) with values of the central position x_{02} and central wave vector k_{o2} varying to approach the location of the first wave packet in the phase space. Thus, I compute the probability

P of the antisymmetrical state $\Phi(x_1, x_2)$ of the two electrons from the Slater determinant, built from the single-particle wave packets in Equation (F.2), as:

$$P(\Phi) = \int_{-\infty}^{\infty}\int_{-\infty}^{\infty} dx_1\, dx_2 \frac{1}{2}|\psi_1(x_1)\psi_2(x_2) - \psi_1(x_2)\psi_2(x_1)|^2 \tag{F.3}$$
$$= \int_{-\infty}^{\infty}\int_{-\infty}^{\infty} dx_1\, dx_2 |\psi_1(x_1)|^2|\psi_2(x_2)|^2 - \int_{-\infty}^{\infty}\int_{-\infty}^{\infty} dx_1\, dx_2 \psi_1^*(x_1)\psi_2(x_1)\psi_2^*(x_2)\psi_1(x_2)$$

A straightforward computation of Equation (F.4), using Equation (F.2), gives [183]:

$$P(\Phi) = 1 - exp(-d_{1,2}^2) \tag{F.4}$$

where we have defined the distance $d_{1,2}$ between the wave packet 1 and 2 in the phase space as:

$$d_{1,2}^2 = \frac{(k_{o1} - k_{o2})^2}{2\sigma_k^2} + \frac{(x_{o1} - x_{o2})^2}{2\sigma_x^2} \tag{F.5}$$

The interpretation of Equation (F.4) is simple. When the wave packets are far away from each other in the phase space, i.e. $|x_{o1} - x_{o2}| >> \sigma_x$ or $|k_{o1} - k_{o2}| >> \sigma_k$, the norm of the two-electron wave function is equal to the unity. However, when the wave packets are approaching each other, the probability in Equation (F.4) decreases. In particular, for $x_{o1} = x_{o2}$ and $k_{o1} = k_{o2}$, we get $\psi_1(x) = \psi_2(x)$ and $\Phi(x_1, x_2) = \psi_1(x_1)\psi_1(x_2) - \psi_1(x_2)\psi_1(x_1) = 0$ with $P(\Phi) = 0$ in Equation (F.4). This is the time-dependent wave packet version of the Pauli exclusion principle (or exchange interaction) mentioned above for time-independent Hamiltonian eigenstates.

In Figure F.1, $1 - P(\Phi)$ is plotted as a function of k_{o2} and x_{02}. For large values of $d_{1,2}$, the probability of finding the second electron is equal to the unity, $P(\Phi) = 1$ (or $1 - P(\Phi) = 0$). However, for small $d_{1,2}$, the probability $P(\Phi)$ decreases. I now compute the area of the phase space forbidden for the second electron due to the presence of the first one. Not all points x_{o2} and k_{o2} are equally forbidden. The closer to x_{o1} and k_{o1}, the less probable such second electron. Thus, the computation of this forbidden *Area* has to be weighted by the probability $1 - P(\Phi)$ given by Equation (F.4) as:

$$Area = \int_{-\infty}^{\infty} dk_{o2} \int_{-\infty}^{\infty} dx_{o2}(1 - P(\Phi)) = \int_{-\infty}^{\infty} dk_{o2} \int_{-\infty}^{\infty} dx_{o2}\, exp(-d_{1,2}^2)$$
$$= \int_{-\infty}^{\infty} dx_{o2}\, e^{-\frac{(x_{o1}-x_{o2})^2}{2\sigma_x^2}} \int_{-\infty}^{\infty} dk_{o2}\, e^{-\frac{(k_{o1}-k_{o2})^2}{2\sigma_k^2}} = 2\pi \tag{F.6}$$

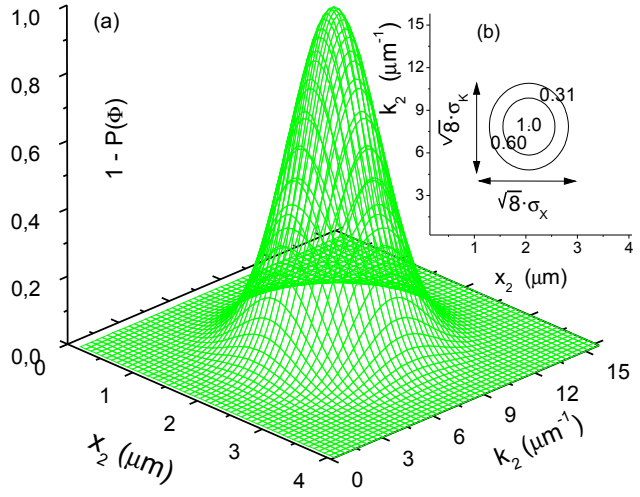

FIGURE F.1: (a) Probability of not finding a second electron in the central positions $x_{o2} = x_2$ and central wave vector $k_{o2} = k_2$ due to the presence of another electron in $x_{o1} = 2\ \mu m$ y $k_{o1} = 8\ \mu m^{-1}$. (b) Contour plot of figure (a). The line 0.31 corresponds to an ellipse (inside a rectangle with sides are $\sqrt{8}\sigma_x$ and $\sqrt{8}\sigma_k$) whose area is 2π. This surface corresponds to the volume of the phase-space needed for each electron. See the exact computation in Equation (F.6) in this appendix.

This $Area = 2\pi$ is universal and independent of the parameters of the Gaussian wave packets [183]. This result can also be extended to a many-particle wave function with a large number of particles. Again, we obtain that each electron requires a volume of 2π of the phase space, in agreement with Equation (6.24). The new important result that we get from this last wave-packet procedure is that the physical interpretation of Δx and Δk_x mentioned along the text can be defined as:

$$\Delta x = \sigma_x \sqrt{2\pi} \tag{F.7}$$

$$\Delta k_x = \sigma_k \sqrt{2\pi} \tag{F.8}$$

I remark that the condition $\sigma_x \cdot \sigma_k = 1$ implies the desired condition $\Delta x \cdot \Delta k_x = 2\pi$ as mentioned in Figure F.1.

Appendix G

Analytical two-particle probabilities for arbitrary wave packets

A general expression for the probabilities $\mathcal{P}_{\mathcal{LR}}$, $\mathcal{P}_{\mathcal{LL}}$ and $\mathcal{P}_{\mathcal{RR}}$ in Equation (6.40)-Equation (6.42) for an arbitrary normalized wave packet is developed in this appendix. I explicitly assume the conditions (i), (ii) and (iii) mentioned in Section 6.3. The solution of the time dependent Schrödinger equation with separable potentials can be found from two decoupled single-particle Schrödinger equations. After impinging with the barrier, at the time t_1 mentioned in the text, each initial one-particle wave function splits into (non-overlapping) transmitted (t) and reflected (r) components defined in Equation (6.44) and Equation (6.45).

From the set of four available reflected and transmitted components, I define the set of sixteen complex integrals:

$$I_{e,f}^{c,d} = \int_g^h dx\ \phi_e^c(x,t_1)\ \phi_f^{*d}(x,t_1) \tag{G.1}$$

where the upperindexes c and d are related to transmitted (t) and reflected (r) components, while the subindexes e and f to the initial position of the one-particle wave packets (a left and b right). The limits of the spatial integration, not explicitly indicated in $I_{e,f}^{c,d}$, are $g = -\infty, h = 0$ when both components are present at the left of the barrier, while $g = 0, h = \infty$ at the right. With the definitions of Equation (G.1), the transmission and reflection coefficients of the a-wave packet are rewritten as $T_a = I_{a,a}^{t,t}$ and

$R_a = I^{r,r}_{a,a}$, respectively. Identically, I define $T_b = I^{t,t}_{b,b}$ and $R_b = I^{r,r}_{b,b}$. By construction, $I^{c,d}_{e,f} = (I^{d,c}_{f,e})^*$.

Using the definitions in Equation (6.44)-Equation (6.45) and Equation (G.1), I get the property:

$$I^{r,t}_{a,b} + I^{t,r}_{a,b} = \int_{-\infty}^{\infty} dx\ \phi_a\ \phi_b^* = \int_{-\infty}^{\infty} dk g_a(k) g_b^*(k) \tag{G.2}$$

where I have defined

$$g_a(k) = \langle \phi_a(x,t_0)|\ \psi_k(x)\rangle = \int_{-\infty}^{\infty} \phi_a(x,t_0)\psi_k^*(x)dx \tag{G.3}$$

being $\psi_k(x)$ the scattering state (with k its wave vector). Accordingly, the wave packet $\phi_a(x,t)$ can be written by superposition as:

$$\phi_a(x,t) = \frac{1}{\sqrt{2\pi}} \int_{-\infty}^{\infty} g_a(k)\Delta e^{-\frac{iE_k\Delta t}{\hbar}} \psi_k(x)dk \tag{G.4}$$

Identical definition for $g_b(k)$. Let me notice that the scenario depicted in Figure 6.10 implies that there is no overlapping between $g_a(k)$ and $g_b(k)$ because they have opposite momenta at the initial time. This no overlapping condition is true initially and it also remains valid at any later time because $\psi_k(x)$ are Hamiltonian eigenstates. Then, I get $I^{r,t}_{a,b} + I^{t,r}_{a,b} = 0$.

Using $I^{c,d}_{e,f} = (I^{d,c}_{f,e})^*$, the probability of detecting two particles at the left of the barrier in equation Equation (6.41), at $t = t_1$, can be straightforwardly developed as:

$$\mathcal{P}_{\mathcal{LL}} = \int_{-\infty}^{0} dx_1 \int_{-\infty}^{0} dx_2\ \ |\Phi|^2 = R_a T_b \mp |I^{r,t}_{a,b}|^2 \tag{G.5}$$

Identically, the probability of detecting two particles at the right of the barrier is:

$$\mathcal{P}_{\mathcal{RR}} = T_a R_b \mp |I^{r,t}_{a,b}|^2 \tag{G.6}$$

Finally, using also the previous identity $I^{r,t}_{a,b} = -I^{t,r}_{a,b}$, the probability of one particle at each side is:

$$\begin{aligned}\mathcal{P}_{\mathcal{LR}} &= \frac{R_a R_b + T_a T_b}{2} \pm |I_{a,b}^{r,t}|^2 + \frac{R_a R_b + T_a T_b}{2} \pm |I_{a,b}^{r,t}|^2 = \\ &= R_a R_b + T_a T_b \pm 2|I_{a,b}^{r,t}|^2 \end{aligned} \tag{G.7}$$

Notice that the term $\pm|I_{a,b}^{r,t}|$ accounts for the difference between fermions and bosons. For these general conditions, one can check that $\mathcal{P}_{\mathcal{LL}} + \mathcal{P}_{\mathcal{RR}} + \mathcal{P}_{\mathcal{LR}} = R_a R_b + T_a T_b + 2T_a R_b$. Since $1 = R_a + T_a$ and $1 = R_b + T_b$, I finally get $\mathcal{P}_{\mathcal{LL}} + \mathcal{P}_{\mathcal{RR}} + \mathcal{P}_{\mathcal{LR}} = 1$, for either fermions or bosons.

Under the conditions (i), (ii) and (iii) mentioned in Section 6.3, the expression of $I_{a,b}^{r,t}$ can be further developed. I define a new wave packet $\Upsilon_a(x,t_1)$ as follows: $\Upsilon_a(x,t_1) = \phi_a^r(x,t_1)$ for all $x \in (-\infty, 0]$ and $\Upsilon_a(x,t_1) = 0$ elsewhere. This new wave packet can be written at t_1 as:

$$\Upsilon_a(x,t_1) = \frac{1}{\sqrt{2\pi}} \int_{-\infty}^{\infty} g_a(k) \Delta e^{-\frac{iE_k \Delta t_1}{\hbar}} r(k) e^{-ikx} dk \tag{G.8}$$

where $r(k)$ is the reflection (complex) amplitude of the scattering state $\psi_k(x)$. Notice that $\Upsilon_a(x,t_1)$ does not contain the incident plane wave $exp(ikx)$ included in $\psi_k(x)$. The reason is because, at time t_1, the superposition of these incident terms $exp(ikx)$ does not contribute to the wave function at the left of the barrier. Identically, I define $\Upsilon_b(x,t_1) = \phi_b^t(x,t_1)$ for all $x \in (-\infty, 0]$ and $\Upsilon_b(x,t_1) = 0$ elsewhere. At t_1:

$$\Upsilon_b(x,t_1) = \frac{1}{\sqrt{2\pi}} \int_{-\infty}^{\infty} g_b(k) \Delta e^{-\frac{iE_k \Delta t_1}{\hbar}} t(k) e^{-ikx} dk \tag{G.9}$$

where $t(k)$ is the transmission (complex) amplitude of the scattering state $\psi_k(x)$. Because of conditions (i), (ii) and (iii), I can consider $g(k) \equiv g_a(k) = g_b(-k)$. Then, using Equation (G.8) and Equation (G.9) I get:

$$I_{a,b}^{r,t} = \int_{-\infty}^{\infty} dx \Upsilon_a \Upsilon^*{}_b = \int_{-\infty}^{\infty} dk |g(k)|^2 r(k) t^*(k) \tag{G.10}$$

where the spatial integral in Equation (G.10) extends from $-\infty$ to ∞ because, by construction, $\Upsilon_a(x,t_1)$ and $\Upsilon_b^*(x,t_1)$ are zero at $x \in (0,\infty)$. I have also used the property of the scattering states $t(k) = t(-k)$. It is interesting to compare equation Equation (G.10)

with the well-known expression for the computation of the (one-particle) transmission coefficient:

$$T = T_b = T_a = I^{t,t}_{a,a} = \int_{-\infty}^{\infty} dk |g(k)|^2 |t(k)|^2 \tag{G.11}$$

and (one-particle) reflection coefficient:

$$R = R_b = R_a = I^{r,r}_{a,b} = \int_{-\infty}^{\infty} dk |g(k)|^2 |r(k)|^2 \tag{G.12}$$

Notice that, under the conditions (i), (ii) and (iii), the transmission $T = T_b = T_a$ and reflection $R = R_b = R_a$ coefficients are equal for the a and b wave packets. I notice that T and R take real values, while $I^{r,t}_{a,b}$ take complex ones.

From Equation (G.10), it is a straightforward procedure to deduce the maximum allowed value for $|I^{r,t}_{a,b}|^2$. The maximum value is $|I^{r,t}_{a,b}|^2 = RT$. It corresponds to an scenario where $r(k)$ and $t(k)$ are (almost) constant in the support of $g(k)$. Then, from Equation (G.10), I obtain $I^{r,t}_{a,b} \approx r(k^c)t^*(k^c)$ with k^c defined as the central wave vector of the wave packet. It can be straightforwardly demonstrated that this value implies that the shapes of the a-reflected $\phi^a_r(x,t)$ and b-transmitted $\phi^b_t(x,t)$ wave packets are identical up to an arbitrary (complex) constant:

$$\phi^r_a(x,t_1) = \phi^t_b(x,t_1)e^{\alpha+i\beta} \tag{G.13}$$

being α and β two real position-independent constants. For such scenarios, Equation (G.5)-Equation (G.7) can be rewritten as $\mathcal{P}^M_{\mathcal{LL}}$, $\mathcal{P}^M_{\mathcal{RR}}$ and $\mathcal{P}^M_{\mathcal{RR}}$ in Equation (6.47) and Equation (6.47). I use the upperindex M in Equation (6.47) and Equation (6.47) to indicate that the probabilities correspond to the maximum value of $|I^{r,t}_{a,b}|^2$. I repeat that Equation (6.47) and Equation (6.47) exactly reproduce the results found in the literature for scattering states in [79, 82, 170, 173].

However, the possibility of a minimum value $|I^{r,t}_{a,b}|^2 = 0$ in Equation (G.10) is in general ignored in the literature. This corresponds to an scenario where $r(k)$ and $t(k)$ vary very rapidly between 1 and 0 on the support of $g(k)$. For example, in a sharp resonance. Then, from Equation (G.10), I get $I^{r,t}_{a,b} \approx 0$. This value means that $\phi^a_r(x,t)$

and $\phi_t^b(x,t)$ in Equation (G.1) are orthogonal. In fact, the different schematic symbols of the wave packets in Figure 6.10 emphasize this point. When $|I_{a,b}^{r,t}|^2 = 0$, Equation (G.5)-Equation (G.7) can be rewritten as $\mathcal{P}_{\mathcal{LL}}^m$,$\mathcal{P}_{\mathcal{RR}}^m$ and $\mathcal{P}_{\mathcal{LR}}^m$ in Equation (6.48) and Equation (6.49). I use the upperindex m in Equation (6.48) and Equation (6.49) to indicate that these probabilities correspond to the minimum value of $|I_{a,b}^{r,t}|^2$. The probabilities in Equation (6.48)-Equation (6.49) show no difference between indistinguishable (fermions or bosons) or distinguishable particles.

Bibliography

[1] A. Corbin, *The Third Element: A Brief History of Electronics*, Bloomington, AuthorHouse (2006).

[2] ITRS, 2011 Edition; http://www.itrs.net/home.html

[3] P. A. Gargini, *Roadmap evolution: from NTRS to ITRS, from ITRS 2.0 to IRDS*, Proceedings of SPIE **10450**, 1045018 (2017).

[4] R. Eckhardt, *Stan Ulam, John von Neumann, and the Monte Carlo Method*, Los Alamos Science **15**, 131 (1987).

[5] J. D. Jackson, *Elettrodinamica Classica*, Bologna, Zanichelli (1984).

[6] J. Xu and L. Zikatanov, *A monotone finite element scheme for convection-diffusion equations*, Mathematics of Computation, **68** 1429 (1999).

[7] J. W. Jerome, *Mathematical Advances and Horizons for Classical and Quantum-Perturbed Drift-Diffusion Systems: Solid State Devices and Beyond*, J. Comput. Electron. **8**, 132 (2009).

[8] I. Rubinstein, *Electro-Diffusion of Ions*, Philadelphia, SIAM (1990).

[9] K. Blotekjaer, *Transport equations for electrons in two valley semiconductors*, IEEE Trans. Electron Devices **17**, 38 (1970).

[10] D. Chen, E. Kan, U. Ravaioli, C. Shu and R. Dutton, *An improved energy transport model including non-parabolic and non-Maxwellian distribution effects*, IEEE Elec. Dev. Lett. **13**, 26 (1992).

[11] J. W. Jerome and C. W. Shu, *Energy models for one-carrier transport in semiconductor devices*, Semiconductors, Part II. IMA Volumes in Mathematics and its Applications, **59**, New York, Springer, (1994).

[12] T.Kurosawa, J. Phys. Soc. Japan **21**, 424 (1966).

[13] C. Jacboni and L. Reggiani, *The Monte Carlo method for the solution of charge transport in semiconductors with application to covalent materials*", Rev. Mod. Phys., **55**, 645 (1983).

[14] C. Jacoboni and P. Lugli, *The Monte Carlo method for semiconductor device simulation*, Vienna-New York, Springer-Verlag, (1989).

[15] V. Sverdlov , E. Ungersboeck, H. Kosina and S. Selberherr, *Current transport models for nanoscale semiconductor devices*, Materials Science and Engineering **58** 228, (2008).

[16] D. F. Styer, et al., *Nine formulations of quantum mechanics*, Amer J Phys **70**, 3 (2002),

[17] G. Lindblad, *On the Generators of Quantum Dynamical Semigroups*, Communications in Mathematical Physics **48**, 119 (1976).

[18] E. Biolatti, R. C. Iotti, P. Zanardi, F. Rossi, *Quantum information processing with semiconductor macroatoms*, Phys. Rev. Lett. **85**, 5647 (2000).

[19] F. Castellano, R.C. Iotti, F. Rossi, J. Appl. Phys. 104, 123104 (2008).

[20] R.C. Iotti, F. Rossi, Rep. Prog. Phys. 68, 2533 (2005).

[21] C. Jacoboni and P. Bordone, *The Wigner-function approach to non-equilibrium electron transport*, Rep. Prog. Phys. **67**, 1033 (2004).

[22] C. Jacoboni and P. Bordone, *Wigner transport equation with finite coherence length*, J. Comput. Electron. **13** 257 (2014).

[23] H. Kosina and M. Nedjalkov, *Handbook of Theoretical and Computational Nanotechnology: Nanodevice Modeling and Nanoelectronics*, California, American Scientific Publ., (2006).

[24] R. K. Mains and G. I. Haddad, *Wigner Function Modeling of Resonant Tunneling Diodes With High Peak-to-Valley Ratios*, J. Appl. Phys. **64** 5041, (1988).

[25] D. Querlioz, et. al., *Wigner-Boltzmann Monte Carlo approach to nanodevice simulation: From quantum to semiclassical transport*", J. Comput. Electron. **8**, 324, (2009).

[26] D. Querlioz and P. Dollfus, *The Wigner Monte Carlo Method for Nanoelectronic Devices*, New York, John Wiley and Sons, (2010).

[27] D. Querlioz, J. Saint-Martin and P. Dollfus, *Implementation of the Wigner-Boltzmann transport equation within particle Monte Carlo*, J. Comput. Electron. **9** 224 (2010).

[28] J. Schwinger, *Brownian Motion of a Quantum Oscillator*, J. Math. Phys. **2**, 407 (1961).

[29] L. P. Kadanoff and G. Baym, *Quantum Statistical Mechanics: Green's Function Methods in Equilibrium and Non-Equilibrium Problems*, New York, W. A. Benjamin, (1962).

[30] S. Datta, *Nanoscale Device Modeling: the Green's Function Method*, Superlattices and Microstructures, **28** 253 (200).

[31] S. Datta, *Quantum Transport: From Atoms to Transistors*, New York, Cambridge University Press, (2005).

[32] http://vides.nanotcad.com/vides/

[33] Y. Yoon, G. Fiori, S. Hong, J. Guo and G. Iannaccone, *Performance Comparison of Graphene Nanoribbon FETs With Schottky Contacts and Doped Reservoirs*, IEEE Trans. on Electron Devices, **55**, 2314 (2008).

[34] G. Fiori, G. Iannaccone and G. Klimeck, *Coupled Mode Space Approach for the Simulation of Realistic Carbon Nanotube Field-Effect Transistors*, IEEE Trans. on Nanotechnology **6**, 475 (2007).

[35] G. Fiori, G. Iannaccone, *On the possibility of tunable-gap bilayer graphene FET*, IEEE Electron Dev. Lett. **30**, 261 (2009).

[36] M. Brandbyge, J. L. Mozos, P. Ordejón, J. Taylor, and K. Stokbro, *Density-functional method for nonequilibrium electron transport*, Phys. Rev. B **65**, 165401 (2002).

[37] J. M. Soler, E. Artacho, J. D. Gale, A. García, J. Junquera, P. Ordejón, and D. Sánchez-Portal, J. Phys. Condens. Matt. **14**, 2745 (2002).

[38] R. Landauer, *Spatial Variation of Currents and Fields Due to Localized Scatterers in Metallic Conduction*, IBM J. Res. Dev. **1**, 223 (1957).

[39] M. Büttiker, *Four-Terminal Phase-Coherent Conductance*, Phys. Rev. Lett. **57**, 1761 (1986).

[40] M. Büttiker, *Symmetry of electrical conduction*, IBM J. Res. Developm. **32**, 317 (1988).

[41] Y. M. Blanter and M. Büttiker, *Shot noise in mesoscopic conductors.* Phys. Rep. **336**, 1 (2000).

[42] P. Hohenberg and W. Kohn *Inhomogeneous electron gas* Phys. Rev. **136**, 864 (1964).

[43] Z. Merali, *What is really real?*, Nature **521**, 278 (2015).

[44] M. F. Pusey, J. Barrett and T. Rudolph, *On the reality of the quantum state*, Nat. Phys. **8**, 475 (2012).

[45] A. Einstein, *Autobiographical Notes, Albert Einstein: Philosopher-Scientist*, Illinois, Open Court Publishing (1949).

[46] P. McEvoy, *Niels Bohr: Reflections on Subject and Object*, MicroAnalytix (2001).

[47] T. Maudlin, *Three measurement problems*, Topoi **14**, 7 (1995).

[48] E. Schrödinger, *Die gegenwärtige Situation in der Quantenmechanik*, Naturwissenschaften **23**, 807 (1935).

[49] P. A. Schilpp, *Albert Einstein: Philosopher-Scientist. The Library of Living Philosophers*, Illinois, Open Court Publishing (1949).

[50] R. Feynman, *Feynman Lectures on Gravitation*, Cambridge, Perseus, (2002).

[51] Against Measurement John Bell August 1990 J. S. Bell, *Against "Measurement"*, NATO ASI Series (Series B: Physics), **226**, Boston, Springer (1990).

[52] P. A. M. Dirac, *The Principles of Quantum Mechanics*, Oxford, Oxford University Press, (1930).

[53] G. C. Ghirardi, A. Rimini, and T. Weber, *A Model for a Unified Quantum Description of Macroscopic and Microscopic Systems*, Berlin, Springer, (1985).

[54] G. C. Ghirardi, A. Rimini, and T. Weber, *Unified dynamics for microscopic and macroscopic systems*, Phys. Rev. D. **34** 470 (1986).

[55] A. Rimini, *Spontaneous Localization and Superconductivity*, New York, Plenum, (1995).

[56] H. Everett, *Theory of the Universal Wavefunction*, Thesis, Princeton University, (1956).

[57] H. Everett, *Relative State Formulation of Quantum Mechanics*, Rev. Mod. Phys. **29** 454 (1957).

[58] W. Heisenberg, *Über den anschaulichen Inhalt der quantentheoretischen Kinematik und Mechanik*, Zeitschrift für Physik, **43**, 172(1927).

[59] G. Bacciagaluppi and A. Valentini, *Quantum Theory at the Crossroads*, Cambridge, Cambridge University Press (2009).

[60] M. Planck, *On the Law of Distribution of Energy in the Normal Spectrum*, Annalen der Physik **4**, 553 (1901).

[61] N. Bohr, *On the Constitution of Atoms and Molecules*, Philosophical Magazine, **26** (1913).

[62] L. de Broglie, *Recherches sur la théorie des quantas*, Annalen de Physique **3**, 22 (1925).

[63] E. Schrodinger, **Quantisierung als Eigenwertproblem**, Annalen der Physik **79**, 361 (1926).

[64] J. S. Bell, *Speakable and Unspeakable in Quantum Mechanics*, Cambridge, Cambridge University Press (1987).

[65] D. Bohm, *Quantum Theory*, New York, Prentice-Hal (1951).

[66] D. Bohm, *A Suggested Interpretation of the Quantum Theory in Terms of "Hidden" Variables I*, Phys. Rev. **85**, 166 (1952).

[67] D. Bohm, *A Suggested Interpretation of the Quantum Theory in Terms of "Hidden" Variables II*, Phys. Rev. **85**, 180 (1952).

[68] D. Dürr, S. Goldstein and N. Zanghì, *Bohmian mechanics and quantum equilibrium*, Stochastic Processes, Physics and Geometry II World Scientific, (1995).

[69] P. A. M. Dirac, *Quantum mechanics of many-electron systems*, Proc. Roy. Soc. A **213**, 714 (1929).

[70] M. Born, *The Classical Mechanics of Atoms*, New York, Ungar (1960).

[71] C. Cohen-Tanoudji, B. Diu and F. Laloë, *Quantum Mechanics*, New York, Wiley (1977).

[72] X. Oriols, *Quantum trajectory approach to time dependent transport in mesoscopic systems with electron-electron interactions*, Phys. Rev. Lett. **98**, 066803 (2007).

[73] N. Bohr, *Atomic Theory and the Description of Nature*, Cambridge, Cambridge University Press (1934).

[74] W. Heisenberg, *The Physical Principles of the Quantum Theory*, New York, Dover (1930).

[75] X. Oriols and J. Mompart, *Applied Bohmian Mechanics: From Nanoscale Systems to Cosmology*, Singapore, Pan Stanford Publishing (2012).

[76] D. Dürr, S. Goldstein and Zanghì, *Quantum theory without quantum philosophy*, Berlin, Springer (2013).

[77] N. D. Mermin, *What's Wrong with this Pillow?* Phys. Today **42**, 9 (1989).

[78] M. J. M., De Jong and C. W. J. Beenakker, *Shot noise in mesoscopic systems*, NATO ASI Series E **345**, Dordrecht, Kluwer Academic Publishing (1997).

[79] M. Büttiker, *Scattering theory of thermal and excess noise in open conductors*, Phys. Rev. Lett. **65**, 2901 (1990).

[80] T. Martin and R. Landauer, *Wave-packet approach to noise in multichannel mesoscopic systems*, Phys. Rev. B **45**, 1742 (1992).

[81] C. Beenakker and C. Schönenberger, *Quantum Shot Noise*, Phys. Today **56**, 37 (2003).

[82] M. Büttiker, *Scattering theory of current and intensity noise correlations in conductors and wave guides*, Phys. Rev. B **46**, 12485 (1992).

[83] L. S. Levitov, H. Lee, G. B. Lesovik, *Electron Counting Statistics and Coherent States of Electric Current*, J. Math. Phys. **37**, 4845 (1996).

[84] G. Albareda, D. Marian, A. Benali, S. Yaro, N. Zanghì and X. Oriols, *Time-resolved electron transport with quantum trajectories*, J. Comput. Electron, Special Issue on Quantum Trasport Beyond DC, **12**, 405 (2013).

[85] D. Dürr, S. Goldstein and N. Zanghì, *Quantum equilibrium and the origin of absolute uncertainty*, J. Stat. Phys. **67**, 843 (1992).

[86] I. Vega and D. Alonso, *Dynamics of non-Markovian open quantum systems*, Rev. Mod. Phys., **89** 015001 (2017).

[87] E. Colomés, Z. Zhan, D. Marian, X. Oriols, *Quantum dissipation with conditional wave functions: Application to the realistic simulation of nanoscale electron devices*, Phys. Rev. B, **96** 075135 (2017).

[88] S. Das Sarma, A. Shaffique, E.H. Hwang and E. Rossi, *Electronic transport in two-dimensional graphene*, Rev. Mod. Phys. **83**, 407 (2011).

[89] A. H. Castro, F. Guinea, N.M.R. Peres, K.S. Novoselov and A.K. Geim, *The electronic properties of graphene*, Rev. of Mod. Phys., **81**, 109 (2009).

[90] N. W. Ashcroft and N. Mermin, *Solid State of Physics*, New York, Cengage Learning, 1976

[91] P. E. Allain and J. N. Fuchs, *Klein Tunneling in graphene: optics with massless electrons*, Eur. Phys. J. B **83**, 301 (2011).

[92] U. Becker, N. Grün and W. Scheid, *Solution of the time-dependent Dirac equation by the finite difference method and application for* $Ca^{20+}+U^{91+}$, J. Phys. B **16**, 1967(1983).

[93] R. Stacey, *Eliminating lattice fermion doubling*, Phys. Rev. D **26**, 468 (1982).

[94] K. Momberger, A. Belkacem and A. H. Sorensen, *Numerical treatment of the time-dependent Dirac equation in momentum space for atomic processes in relativistic heavy-ion collisions*, Phys. Rev. A **53**, 1605 (1996).

[95] G. R. Mocken and C. H. Keitel, *Quantum dynamics of relativistic electrons*, J. Comp. Phys. **199**, 558 (2004).

[96] F. F. Gourdeau, E. Lorin and A. D. Bandrauk, *Numerical solution of the time-dependent Dirac equation in coordinate space without fermion-doubling*, Comp. Phys. Comm. **183**, 1403 (2012).

[97] L. Susskind, *Lattice fermions* Phys. Rev. D **16**, 3031 (1977).

[98] R. Hammer and W. Pötz, *Staggered grid leap-frog scheme for the (2+ 1) D Dirac equation*, Comp. Phys. Comm. **185**, 40 (2014).

[99] R. Hammer, W. Pötz, and A. Arnold J. Comp. Phys. **265**, 50 (2014).

[100] F. L. Traversa, Z. Zhan and X. Oriols, *Absorption and injection models for open time-dependent quantum systems*, Phys. Rev. E **90**, 23304 (2014).

[101] M. I. Katsnelson, K.S. Novoselov and A. K. Geim, *Chiral tunnelling and the Klein paradox in gaphene*, Nat. Phys. **2**, 620 (2006).

[102] G. Albareda, J. Suné and X. Oriols, *May-particle Hamiltonian for open systems with full Coulomb interaction: Application to classical and quantum time-dependent simulations of nanoscale electron devices*, Phys. Rev. B. **79**, 75315, (2009).

[103] H. P. Breuer and F. Petruccione, *Theory of Open Quantum Systems*, Oxford, Oxford University Press (2002).

[104] B. Vacchini, *Completely Positive Quantum Dissipation*, Phys. Rev. Lett. **84**, 1374 (2000).

[105] J. M. Dominy, A. Shabani, and D. A. Lidar, *Reduced dynamical maps in the presence of initial correlations*, Quantum Inf. Proc. **15**, 1349 (2016).

[106] G. Stefanucci, Y. Pavlyukh, A. M. Uimonen, and R. van Leeuwen, *Diagrammatic expansion for positive density-response spectra: Application to the electron gas*, Phys. Rev. B **90**, 115134 (2014).

[107] L. Diósi, *Quantum Master Equation of a Particle in a Gas Environment*, Europhys. Lett. **30**, 63 (1995).

[108] B. Vacchini and K. Hornberger, *Quantum linear Boltzmann equation*, Phys. Rep. **478**, 71 (2009).

[109] K. Kraus, *States, Effects and Operations: Fundamental Notions of Quantum Theory* **190**, Berlin, Springer (1983).

[110] M. D. Choi, *Completely Positive Linear Maps on Complex Matrices*, Linear Algebra Appl. **10**, 285 (1975).

[111] I. Bengtsson and K. Zyczkowski, *Geometry of Quantum States*, Cambridge, Cambridge University Press (2006).

[112] C. Wood, *Non-Completely Positive Maps: Properties and Applications*, Thesis, Macquarie University (2009).

[113] A. O. Caldeira and A. Leggett, *Path integral approach to quantum Brownian motion*, Physica A **121**, 587 (1983).

[114] V. Sverdlov, T. Grasser, H. Kosina and S. Selberherr, *Scattering and space-charge effects in Wigner Monte Carlo simulations of single and double barrier devices*, J. Comput. Electron. **5**, 447 (2006).

[115] V. Sverdlov a, A. Gehring, H. Kosina and S. Selberherr, *Quantum transport in ultra-scaled double-gate MOSFETs: A Wigner function-based Monte Carlo approach*, Solid-State Electronics **49**, 1510 (2005).

[116] V. Sverdlov, H. Kosina and S. Selberherr, *Modeling current transport in ultra-scaled field-effect transistors*, Microelectronics Reliability **47**, 11 (2007).

[117] L. Demeio, L. Barletti, A. Bertoni, P. Bordone and C. Jacoboni, *Wigner-function approach to multibandtransport in semiconductors*, Physica B **314**, 104 (2002).

[118] E. Cancellieri, P. Bordone and C. Jacoboni, *Effect of symmetry in the many-particle Wigner function*, Phys. Rev. B **76**, 214301 (2007).

[119] L. E. Ballentine, *Quantum mechanics: a modern development* **15**, Singapore, World Scientific (1988).

[120] L. Boltzmann, *Weitere Studien über das Wärmegleichgewicht unter Gasmolekülen*, Wien, Wiener Berichte, **66** (1872).

[121] D. Querlioz and P. Dollfus, *The Wigner Monte-Carlo Method for Nanoelectronic Devices: A Particle Description of Quantum Transport and Decoherence*, New Jersey, Wiley-ISTE, (2010).

[122] B. R. Nag, *Electron Transport in Compound Semiconductors*, Berlin, Springer (1980).

[123] R. Shankar, *Principles of Quantum Mechanics*, US, Springer (2013).

[124] E. Wigner, *On the Quantum Correction For Thermodynamic Equilibrium*, Phys. Rev. **40**, 749 (1932) .

[125] W. B. Case, *Wigner functions and Weyl transforms for pedestrians*, Am. J. Phys. **76**, 937 (2008).

[126] D. Querlioz, J. Saint-Martin, A. Bournel, and P. Dollfus, *Wigner Monte Carlo simulation of phonon-induced electron decoherence in semiconductor nanodevices*, Phys. Rev. B **78**, 165306 (2008).

[127] M. Nedjalkov, et. al., *Physical scales in the Wigner-Boltzmann equation*, Ann. Phys. **328**, 220 (2013).

[128] A. Alarcón, X. Cartoixà, and X. Oriols, *Towards the explicit computation of bohm velocities associated to n-electron wavefunctions with arbitrary spin-orientations*, Phys. Status Solidi. **7**, 2636 (2010).

[129] A. Alarcón, S. Yaro, X. Cartoixà, and X. Oriols, *Computation of many-particle quantum trajectories with exchange interaction: Application to the simulation of nanoelectronic devices*, Journal of Physics: Condensed Matter **25**, 325601 (2013).

[130] A. Kossakowski, *On quantum statistical mechanics of non-Hamiltonian systems*, Rep. Math. Phys. **3**, 247 (1972).

[131] G. Lindblad, *On the generators of quantum dynamical semigroups*, Commun. Math. Phys. **48**, 119 (1976).

[132] V. Gorini, K. Kossakowski and E. Sudarshan, J. Math. Phys. **17**, 821 (1976).

[133] L. Ferialdi, *Exact Closed Master Equation for Gaussian Non-Markovian Dynamics*, Phys. Rev. Lett. **116**, 120402 (2016).

[134] L. Ferialdi, *Dissipation in the Caldeira-Leggett model*, Phys. Rev. A **95**, 052109 (2017).

[135] A. Bassi, K. Lochan, S. Satin, T. P. Singh and H. Ulbricht, *Models of wave-function collapse, underlying theories, and experimental tests*, Rev. Mod. Phys. **85**, 471 (2013).

[136] L. Diósi, N. Gisin and W. T. Strunz, *Non-Markovian quantum state diffusion*, Phys. Rev. A **58**, 1699 (1998).

[137] W. T. Strunz, L. Diósi and N. Gisin, *Open System Dynamics with Non-Markovian Quantum Trajectories*, Phys. Rev. Lett. **82**, 1801 (1999).

[138] W. T. Strunz, *The Brownian motion stochastic Schrödinger equation*, Chem. Phys. **268**, 237 (2001).

[139] L. Ferialdi and A. Bassi, *Exact solution for a non-Markovian dissipative quantum dynamics.*, Phys. Rev Lett. **108**, 170404 (2012).

[140] L. Diósi, *Exact solution for a non-Markovian dissipative quantum dynamics*, Phys. Rev. Lett. **100**, 080401 (2008).

[141] H. M. Wiseman and J. M. Gambetta, *Pure-State Quantum Trajectories for General Non-Markovian Systems Do Not Exist*, Phys. Rev. Lett. **101**, 140401 (2008).

[142] L. Diósi, *Non-markovian continuous quantum measurement of retarded observables*, Phys. Rev. Lett. **101**, 149902 (2008).

[143] J. Gambetta and H. M. Wiseman, *Non-Markovian stochastic Schrödinger equations: Generalization to real-valued noise using quantum-measurement theory*, Phys. Rev. A **66**, 012108 (2002).

[144] J. Gambetta and H. M. Wiseman, *Interpretation of non-Markovian stochastic Schrödinger equations as a hidden-variable theory*, Phys. Rev. A. **68**, 062104 (2003).

[145] L. Diósi, and L. Ferialdi, *General Non-Markovian Structure of Gaussian Master and Stochastic Schrödinger Equations*, Phys. Rev. Lett. **113**, 200403 (2014).

[146] D. Dürr, S. Goldstein, R. Tumulka, and N. Zanghì, *On the Role of Density Matrices in Bohmian Mechanics*, Found. Phys. **35**, 449 (2005).

[147] I. Christov, *Time-dependent quantum Monte Carlo*, New J. Phys. **9**, 70 (2007).

[148] R. E. Wyatt, *Quantum Dynamics with Trajectories: Introduction to Quantum Hydrodynamics*, New York, Springer, (2005).

[149] Y. Goldfarb, I. Degani and D. J. Tannor, *Interference in Bohmian mechanics with complex action*, J. Chem. Phys. **125** 231103 (2006).

[150] E. Gindensperger, C. Meier and J. A. Beswick, *Quantum-classical description of rotational diffractive scattering using Bohmian trajectories: Comparison with full quantum wave packet results*, J. Chem. Phys. **116** 8 (2002).

[151] B. D'Espagnat, *Conceptual Foundations of Quantum Mechanics*, Advanced Book Program, New York, Perseus Books, (1976).

[152] C. Jacoboni and L. Paolo, *The Monte Carlo Method for Semiconductor Device Simulation*, Berlin, Springer, (1989).

[153] K. L. Jensen and F. A. Buot, *The effects of scattering on current-voltage characteristics, transient response, and particle trajectories in the numerical simulation of resonant tunneling diodes*, J. Appl. Phys. **67**, 7602 (1990).

[154] W. R. Frensley, *Quantum Transport Modeling of Resonant-Tunneling Devices*, Solid State Electron. **31**, 739 (1988).

[155] T. Fang, A. Konar, H. Xing and D. Jena, *High-field transport in two-dimensional graphene*, Phys. Rev. B, **84** 125450 (2011).

[156] R.C. Iotti and F. Rossi, *Electronic phase coherence vs. dissipation in solid-state quantum devices: Two approximations are better than one*, EPL **112**, 67005 (2015).

[157] F. Rossi, *Theory of Semiconductor Quantum Devices* , Berlin , Springer-Verlag (2011).

[158] R. G. Lake, G. Klimeck, M. P. Anantram and S. Datta, *Rate equations for the phonon peak in resonant-tunneling structures*, Phys. Rev. B **48**, 15132 (1993).

[159] S. Datta, *Steady-state quantum kinetic equation*, Phys. Rev. B **40**, 5830 (1989).

[160] Y. Aharonov, D. Z. Albert and L. Vaidman, *How the result of a measurement of a component of the spin of a spin-1/2 particle can turn out to be 100*, Phys. Rev. Lett. **60**, 1351 (1988).

[161] A. G. Kofman, S. Ashhab and F. Nori, *Nonperturbative theory of weak pre- and post-selected measurements*, Phys. Rep. **520**, 43 (2012).

[162] B. Braverman and C. Simon, *Proposal to Observe the Nonlocality of Bohmian Trajectories with Entangled Photons*, Phys. Rev. Lett. **110**, 060406 (2013).

[163] J. Dressel, M. Malik, F. M. Miatto, A. N. Jordan and R. W. Boyd, *Understanding quantum weak values: Basics and applications*, Rev. Mod. Phys. **86**, 307 (2014).

[164] S. Kocsis, B. Braverman, S. Ravets, M. J. Stevens, R. P. Mirin, L. K. Shalm and A. M. Steinberg, *Observing the average trajectories of single photons in a two-slit interferometer.*, Science 332, 1170 (2011).

[165] D. Marian, N. Zanghì and X. Oriols, *Weak Values from Displacement Currents in Multiterminal Electron Devices*, Phys. Rev. Lett. **116**, 110404 (2016).

[166] D. Marian, *Application of Bohmian Mechanics to Quantum Transport: the Conditional Wave Function*, Thesis, Università degli Studi di Genova, (2015).

[167] S. Ramo, *Currents induced by electron motion*, Proceedings of the IRE, **27**, 584 (1939).

[168] W. Shockley, *Currents to conductors induced by a moving point charge*, J. Appl. Phys. **9**, 635 (1938).

[169] B. Pellegrini, *Electric charge motion, induced current, energy balance, and noise*, Phys. Rev. B, **34**, 5921 (1986).

[170] R. Landauer, *The noise is the signal*, Nature **392**, 658 (1998).

[171] P. J. Price, *Fluctuations of hot electrons*, New York, Academic Press, (1965).

[172] S. Goldstein, J. L. Lebowitz, C. Mastrodonato, R. Tumulka, N. Zanghì, *Normal typicality and von Neumann's quantum ergodic theorem*, Proc. R. Soc. A **466**, 3203 (2010).

[173] R. Landauer, Solid-State shot noise. Phys. Rev. B **47**, 16427 (1993).

[174] W. R. Frensley, *Boundary conditions for open quantum systems driven far from equilibrium*, Rev. Mod. Phys. **62**, 745 (1990).

[175] F. Rossi, *Theory of semiconductor quantum devices: microscopic modeling and simulation strategies*, Berlin, Springer-Verlag, Berlin (2011).

[176] D. Marian, E. Colomés and X. Oriols, *Time-dependent exchange and tunneling: detection at the same place of two electrons emitted simultaneously from different sources*, J. Phys. Condens. Matter **27**, 245302 (2015).

[177] T. Gonzalez, J. Mateos, D. Pardo, L. Varani and L. Reggiani, *Injection statistics simulator for dynamic analysis of noise in mesoscopic devices*, Semicond. Sci. Technol. **14**, 371999 (1999).

[178] X. Oriols, E. Fernandez-Diaz, A. Alvarez and A. Alarcón, *An electron injection model for time-dependent simulators of nanoscale devices with electron confinement: Application to the comparison of the intrinsic noise of 3D-, 2D-and 1D-ballistic transistors, Solid State Electronics*, **51**, 306 (2007).

[179] R. Landauer, and T. Martin, *Equilibrium and Shot Noise in Mesoscopic Systems*, Physica B **175**, 167 (1991).

[180] C. M. Zener, *Elasticity and anelasticity of metals*, Chicago, University of Chicago Press, (1948).

[181] A. Paussa, G. Fiori, P. Palestri, M. Geromel, D. Esseni, G. Iannaccone and L. Selmi, *Simulation of the performance of graphene FETs with a semiclassical model, including band-to-band tunneling*, IEEE Trans. Electron Devices, **61**, 5 (2014).

[182] F. Schwierz, J. Pezoldt and R. Granzner, *Combination of Equilibrium and Nonequilibrium Carrier Statistics Into an Atomistic Quantum Transport Model for Tunneling Heterojunctions*, IEEE Trans. Electron Dev. **64**, (2017).

[183] X. Oriols, *Non-universal conductance quantization for long quantum wires: the role of the exchange interaction*, Nanotechnology **15**, 167 (2004).

[184] Z.Zhan, E. Colomés and X. Oriols, *Limitations of the Intrinsic Cutoff Frequency to Correctly Quantify the Speed of Nanoscale Transistors*, IEEE Trans. Electron Dev., **64**, 2617 (2017).

[185] A. Beggi, P. Bordone, F. Buscemi and A. Bertoni, *Time-dependent Simulation and Analytical Modelling of Electronic Mach-Zehnder Interferometry with Edge-states wave packets*, Journal of Physics: Condensed Matter, **27**, 47 (2015).

[186] E. Bocquillon, V. Freulon, J. M. Berroir, P. Degiovanni, B. Plaçais, A. Cavanna, Y. Jin, and G. Feve, *Coherence and Indistinguishability of Single Electrons Emitted by Independent Sources*. Science **339**, 1054 (2013).

[187] J. Dubois, et. al., *Minimal-excitation states for electron quantum optics using levitons*, Nature **502**, 659 (2013).

[188] W. Pauli, *Über den Geschwindigkeitsabhängigkeit der Elektronenmasse auf den Zeemaneffekt*, Z. Physik **31**, 373 (1925).

[189] M. Lanzagorta, *Quantum radar*, California, Morgan and Claypool (2011).

[190] H. Nyquist, *Thermal Agitation of Electric Charge in Conductors*, Phys. Rev. **32**, 110 (1928).

[191] J. Johnson, *Thermal Agitation of Electricity in Conductors*, Phys. Rev. **32**, 97 (1928).

[192] R. Venugopal, S. Goasguen, S. Datta and M. Lundstrom, *Quantum mechanical analysis of channel access geometry and series resistance in nanoscale transistors*, J. Appl. Phys **95**, 292 (2004).

[193] V. Freulon, A. Marguerite, A. Berroir, B. Plaçais B, A. Cavanna, Y. Jin and G. Fève, *Hong-Ou-Mandel experiment for temporal investigation of single-electron fractionalization*, Nat. Commun. **6**, 6854 (2015).

[194] C. Wahl, J. Rech, T. Jonckheere and T. Martin, *Interactions and Charge Fractionalization in an Electronic Hong-Ou-Mandel Interferometer*, Phys. Rev. Lett. **112**, 046802 (2014).

[195] G. Fève, P. Degiovanni and T. Jolicoeur, Phys. Rev. B **77**, 035308 (2008).

[196] R. C. Liu, B. Odom, Y. Yamamoto and S. Tarucha, *Quantum interference in electron collision*, Nature **391**, 263 (1988).

[197] M. Moskalets, *Floquet scattering matrix approach to the phase noise of a single-electron source in the adiabatic regime*, J. Comput. Electron. **12**, 397 (2013).

[198] G. Platero and R. Aguado, *Photon-assisted transport in semiconductor nanostructures*, Phys. Rep. **395** 1 (2004).

[199] L. B. Kish, *End of Moore's law: thermal (noise) death of integration in micro and. nano electronics*, Phys. Rev. A **305**, 144 (2002).

[200] J. Singh, *Semiconductor Devices: Basic Principles*, New York, Wiley (2001).

[201] K. Rais, G. Ghibaudo, F. Balestra and M. Dutoit, *Study of saturation velocity overshoot in deep submicron silicon MOSFETS from liquid helium up to room temperature*, J. Phys. IV **C6**, 19 (1994).